Kontrolle einfacher quantenmechanischer Systeme durch Laserstrahlung

DISSERTATION

zur Erlangung des Doktorgrades
der Naturwissenschaften
(Dr. rer. nat.)

dem Fachbereich Physik
der Philipps-Universität Marburg
vorgelegt

von

Klaus Stefan Drese
aus Hünfeld

Marburg/Lahn 1998

Vom Fachbereich Physik der
Philipps–Universität als
Dissertation angenommen am: 20.07.1998

Erstgutachter: Priv.-Doz. Dr. Martin Holthaus

Zweitgutachter: Prof. Dr. Siegfried Großmann

Tag der mündlichen Prüfung: 29.07.1998

Inhaltsverzeichnis

Abbildungsverzeichnis

1 Zusammenfassung

Mit Hilfe von Laserstrahlung können quantenmechanische Systeme gezielt manipuliert werden. Zum einen kann starke cw-Laserstrahlung benutzt werden, um das Spektrum des bestrahlten Systems und dadurch auch seine Eigenschaften zu verändern. Zum anderen können Laserpulse mit einer genau definierten Einhüllenden und möglicherweise auch einem „Frequenzchirp“ eingesetzt werden, um einen quantenmechanischen Populationstransfer von einem Anfangszustand in einen gewünschten Zielzustand zu erreichen.

In der vorliegenden Arbeit werden diese beiden Möglichkeiten quantenmechanischer Kontrolle anhand einfacher Modellsysteme theoretisch untersucht. Im ersten Teil, der sich aus den Kapiteln 2 und 3 zusammensetzt, wird die Kontrolle durch einen streng periodischen Antrieb behandelt, und zwar speziell für Teilchen, die sich in räumlich periodischen Potentialen bewegen. Der zweite Teil, bestehend aus den Kapiteln 4 und 5, widmet sich dem gezielten Populationstransfer durch Laserpulse. Da in beiden Fällen die Laserfelder aus der Sicht des ungestörten Systems sehr stark sein können, ist die übliche Störungstheorie unzureichend. Aus diesem Grund baut diese Arbeit auf dem Floquet-Theorem auf, welches die zeitliche Periodizität des Laserfeldes konsequent ausnutzt: Für einen zeitlich periodischen Hamilton-Operator garantiert das Floquet-Theorem die Existenz von Lösungen der zeitabhängigen Schrödinger-Gleichung, die sich aus einer periodischen Funktion („Floquet-Funktion“) und einem Phasenfaktor zusammensetzen; die Phase wird durch die „Quasienergie“ bestimmt. Diese Floquet-Zustände übernehmen in periodisch zeitabhängigen Systemen die Rolle stationärer Zustände.

1.1 Kontrolle durch cw-Laserstrahlung

In Kapitel 2 wird ein Tight-Binding-System untersucht, welches zwei Energiebänder besitzt und periodisch angetrieben wird. Dieses System kann als ein stark vereinfachtes Modell für ein Halbleiter-Übergitter angesehen werden, welches mit starker THz-Strahlung wechselwirkt. Es zeigt sich, daß selbst, wenn die ungestörten Bänder durch die Interbandwechselwirkung stark miteinander gekoppelt werden, „Quasienergiebänder“ des angetriebenen Systems existieren. Diese Quasienergiebänder spielen eine ähnliche Rolle wie die Energiebänder im antriebsfreien Fall. Wenn insbesondere das Tight-Binding-Gitter durch ein Zufallspotential gestört wird, tritt Anderson-Lokalisierung auf, wobei der Quotient aus Unordnungsstärke

und Quasienergiebandbreite den Grad der Lokalisierung bestimmt. Da nun die Quasienergiebandbreite von der Antriebsstärke abhängt, kann der Grad der Anderson-Lokalisierung durch die Antriebsstärke kontrolliert werden. Dieser Zusammenhang zeigt sich sehr deutlich in Abbildung 2.5.

Während bei realen Halbleiter-Übergittern noch eine Reihe konkurrierender Effekte zu berücksichtigen sind, bilden ultrakalte Atome in modulierten optischen Gittern eine vergleichsweise saubere Realisierung von zeitlich periodisch angetriebenen Teilchen in räumlich periodischen Potentialen. Kapitel 3 behandelt solche ultrakalte Atome in eindimensionalen Lichtgittern, wobei zwei verschiedene Fälle diskutiert werden. Ist das optische Gitter so tief, daß seine einzelnen Mulden viele quantenmechanische Energieniveaus tragen, dann ist der Tunneleffekt zwischen den Mulden vernachlässigbar und man findet in den einzelnen Mulden semiklassische Dynamik. Insbesondere wird in den Abbildungen 3.4 und 3.6 gezeigt, daß der periodische Antrieb das ungestörte Spektrum völlig umordnet und zur Ausbildung eines „neuen Grundzustandes“ führt. Ist dagegen das optische Potential so schwach, daß es nur ein einziges Band unterhalb der Potentialoberkante zuläßt, so wird es durch ein Tight-Binding-System mit nur einem Band beschrieben. Da flache optische Gitter fast ideale, dissipationsfreie Systeme sind, ergibt sich hier die Möglichkeit, einen Kollaps des Quasienergiebandes zu untersuchen, der bei bestimmten Antriebsstärken auftritt und zur sogenannten dynamischen Lokalisierung führt. Tatsächlich ist es kürzlich gelungen, diese Voraussage experimentell zu bestätigen (M.G. Raizen, private Mitteilung, Juni 1998). Daher scheint es möglich, daß auch ein zweiter Vorschlag, der in diesem dritten Kapitel gemacht wird, experimentell umgesetzt werden kann: Es wird gezeigt, daß bichromatische optische Potentiale im Tight-Binding-Fall auf das Harper-Modell führen, welches sonst aus der Beschreibung zweidimensionaler Bloch-Elektronen in einem Magnetfeld bekannt ist und einen Metall-Isolator-Übergang aufweist. Dieser Übergang läßt sich in angetriebenen quasiperiodischen optischen Gittern kontrollieren; je nach Antriebsstärke befindet man sich in der „metallischen“ oder in der „isolierenden“ Phase.

Bei einer etwas genaueren Modellierung quasiperiodischer optischer Potentiale wird man zu einem leicht modifizierten Harper-Modell geführt. In Anhang A wird gezeigt, daß dieses modifizierte Modell den gleichen Metall-Isolator-Übergang aufweist wie das ursprüngliche Harper-Modell, zusätzlich jedoch in seinem Parameterraum einen ausgedehnten Bereich von kritischen Zuständen besitzt (d.h. von Zuständen, die weder ausgedehnt noch exponentiell lokalisiert sind).

1.2 Kontrolle durch Laserpulse

In der Atom- und Molekülphysik, aber auch in der Physikalischen Chemie, ist man häufig daran interessiert, ein Atom oder Molekül durch Laserpulse schnell in einem gewünschten Zustand zu präparieren. Da die Einhüllende der Pulse im allgemeinen langsam im Vergleich zur Laserperiode variiert, ist es naheliegend, adiabatische Prozesse auszunutzen. In der Tat beruht eines der erfolgreichsten praktisch eingesetzten Verfahren, nämlich das STIRAP-Verfahren — die Abkürzung bedeutet STImulated Raman Adiabatic Passage — ausschließlich auf adiabatischem Folgen. Es ergibt sich daher die Aufgabe, adiabatische und nicht-adiabatische Prozesse, die bei der Wechselwirkung mit starken Laserpulsen auftreten, möglichst allgemein zu beschreiben.

In Kapitel 4 werden Abweichungen vom adiabatischen Verhalten zunächst unter einem allgemeinen Gesichtspunkt untersucht. Es wird gezeigt, daß sich nicht-adiabatische Übergangsamplituden aus einem universell beschreibbaren und einem störungstheoretisch leicht zugänglichen Anteil zusammensetzen. Durch die Interferenz beider Anteile läßt sich etwa die Dynamik des Landau-Zener-Übergangs im Detail erklären, wie es durch Abbildung 4.7 besonders gut verdeutlicht wird. Der universelle Anteil kann durch sogenannte superadiabatische Transformation erhalten werden. Neben dem von M.V. Berry [10] untersuchten Transformationsschema wird in diesem Kapitel ein iteratives Schema betrachtet, welches auch zu einer „Renormierung“ der adiabatischen Eigenwerte führt. Mit Hilfe dieser renormierten Eigenwerte können Phasenfaktoren, welche bei nicht-adiabatischer Prozeßführung auftreten, systematisch berechnet werden, wie es exemplarisch in den Gleichungen (4.27) und (4.28) bei der Berechnung der Stueckelberg-Phase im Falle des Landau-Zener-Übergangs vorgeführt wird. Eine erste konkrete Anwendung finden diese allgemeinen Überlegungen bei der Erklärung des Zusammenbruchs der sogenannten Dykhne-Davis-Pechukas-Formel bei STIRAP-Systemen, der kürzlich unter Verwendung der Drehwellennäherung (RWA; „Rotating Wave Approximation“) von T.A. Laine und S. Stenholm [79] gefunden wurde.

Um jedoch die Reaktion von Atomen und Molekülen auf Laserpulse auch ohne Verwendung der Drehwellennäherung beschreiben zu können, muß die adiabatische Beschreibung mit dem Floquet-Bild kombiniert werden. Ein theoretischer Rahmen, mit dem sich diese Kombination erreichen läßt, wird in Kapitel 5 vorgestellt. Hier wird die zeitabhängige Schrödinger-Gleichung durch Einführung einer zweiten Zeitvariablen in einen erweiterten Hilbert-Raum „geliftet“. Nachdem auf diese Weise eine explizite Trennung der schnellen Laserfeld-Oszillationen von den langsamen Parametervariationen erreicht wurde, lassen sich nun in diesem erweiterten Raum die im vorherigen Kapitel erklärten Techniken der adiabatischen Störungstheorie anwenden. Im letzten Schritt erhält man die Lösung der ursprüngli-

chen Schrödinger-Gleichung, indem man aus dem erweiterten in den physikalischen Raum zurückprojiziert. Dieser „Zwei-Zeiten-Formalismus“ läßt sich in folgendem Diagramm zusammenfassen:

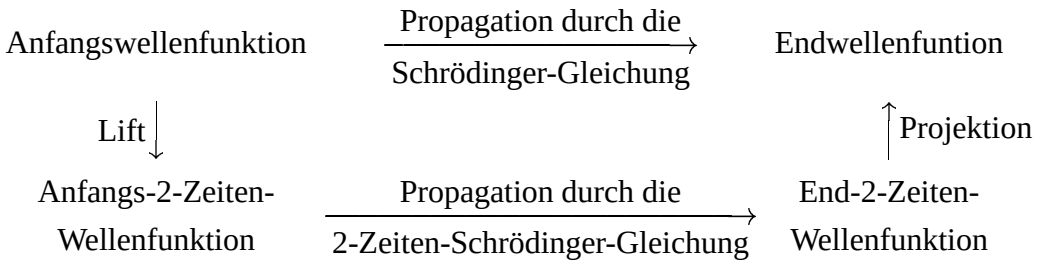

Dieser auf den ersten Blick kompliziert aussehende Formalismus erweist sich als überaus schlagkräftig. Er erklärt Oszillationen, die während eines Laserpulses in den Besetzungen der adiabatischen Floquet-Zustände auftreten, durch einen Interferenzeffekt, der in Abbildung 5.2 verdeutlicht wird. Ferner erlaubt diese Technik die Konstruktion von superadiabatischen Floquet-Basen, die eine wesentlich bessere Beurteilung der Pulsdynamik ermöglichen als die übliche adiabatische Basis, vgl. Abbildung 5.8. Das detaillierte Verständnis der Pulsdynamik wiederum ist Voraussetzung für das Aufstellen von Pulsstrategien, die den gewünschten Populationstransfer mit möglichst geringen Verlusten erlauben. Das Erstellen solcher Strategien wird beispielhaft für einen angetrieben Morse-Oszillator verdeutlicht, der die Streckschwingungen eines HF-Moleküls in Gegenwart starker Laserfelder modelliert. Es können sowohl „gechirpte“ Laserpulse als auch zweifarbige Laserfelder, wie sie beim STIRAP-Prozeß auftreten, behandelt werden.

Zusammenfassend läßt sich das Zusammenspiel der verschiedenen Techniken für die theoretische Untersuchung der Kontrolle quantenmechanischer Systeme durch Laserstrahlung wie folgt darstellen:

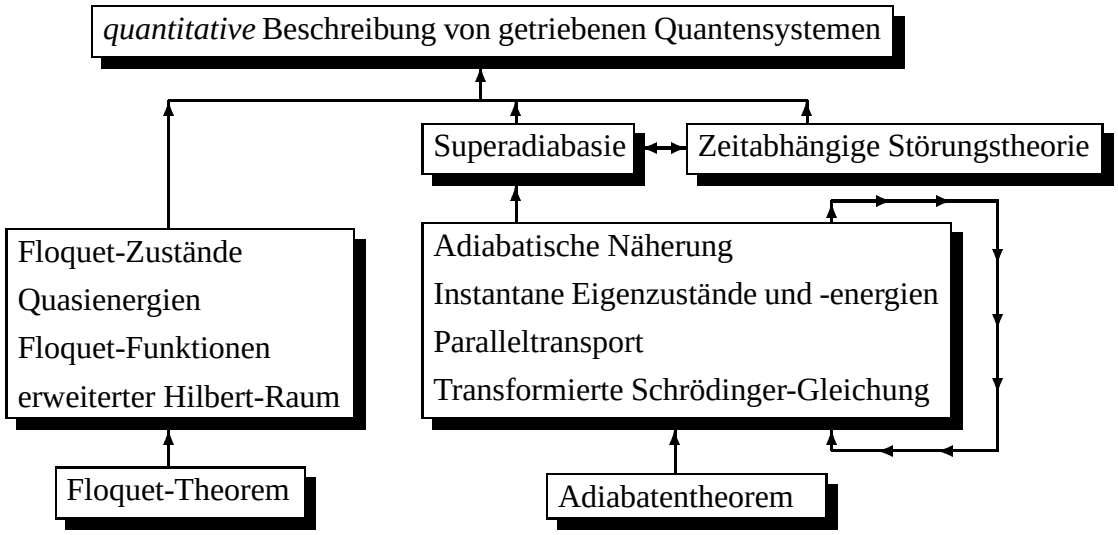

Auf der einen Seite steht das Floquet-Theorem, welches die Grundlage für die Beschreibung von Systemen mit streng periodischem Antrieb liefert und die Kontrollaspekte erfaßt, die

allein auf den Eigenschaften des Quasienergiespektrums bzw. der Floquet-Zustände bei festen Systemparametern beruhen. Auf der anderen Seite steht das Adiabatentheorem, welches das Floquet-Bild auch auf Situationen mit „langsam“ veränderlichen Parametern, wie eben Laserpulse, anzuwenden gestattet. Abweichungen vom adiabatischen Verhalten können systematisch berechnet werden. Das Zusammenführen dieser beiden Konzepte ermöglicht ein quantitatives Verständnis des Verhaltens quantenmechanischer Systeme unter dem Einfluß starker Laserstrahlung und, darauf aufbauend, die Entwicklung effizienter Kontrollstrategien.

2 Anderson localisation in an ac-driven two-band model

Random disorder in periodic potentials causes Anderson localisation of the electronic energy eigenstates [3, 71, 90, 113]. In one-dimensional disordered lattices, in particular, all eigenstates are localised even for arbitrarily weak disorder. The localisation lengths are determined by the ratio of disorder strength and energy band width [114]. For *finite*, weakly disordered lattices the localisation lengths can exceed the size of the whole lattice, so that localisation is negligible and the eigenstates can be regarded as effectively extended.

Semiconductor superlattices are important examples of effectively one-dimensional, finite periodic structures. These artificially grown mesoscopic systems typically consist of about 100 lattice periods, often even less, and they inevitably contain a certain amount of disorder. Usually one is interested in high-quality superlattice samples for studying, e.g., Bloch oscillations, but it is well possible to fabricate also intentionally disordered superlattices [84], and to investigate the effects of layer thickness fluctuations on electronic transport properties.

For a systematic experimental study of localisation effects in superlattices, it would be desirable to manipulate the localisation lengths within an individual sample. One could then explore the crossover effects that occur when the localisation lengths are comparable to the sample size. However, since both the amount of disorder and the energy (mini-)bandwidths are sample-specific properties, such a tunability of localisation lengths appears impossible.

The situation is quite different if the superlattice is exposed to a spatially homogeneous ac electric field. Then the total Hamiltonian is periodically time-dependent, and Floquet states and quasienergy bands take over the role that Bloch waves and energy bands had played in the static case [52, 101, 122]. The widths of the quasienergy bands depend strongly on the ac amplitude, and can even approach zero under certain conditions. In the presence of ac fields, it is the ratio width that determines the degree of localisation [54–56]. Hence, in principle it is possible to change the localisation lengths by suitably adjusting the amplitude of the ac field.

In this chapter we extend the previous theoretical studies on ac-field-controlled Anderson localisation [54–56] to include interband effects. To this end, we explore the dynamics of a single electron in a two-band tight-binding model [32, 101] driven simultaneously by a static and a resonant, oscillating field. Needless to say, this simple model can not give a one-to-one

description of all processes in real superlattices. For example, an electron in a semiconductor never experiences only the external field, but also a field from induced polarisation [18]. However, it has been shown recently by Meier et al. [86–88] that consequences of the band collapse found in the ideal single band tight-binding model [52], such as dynamic localisation [28, 63, 97, 107], survive even in the presence of Coulomb interactions, and should be experimentally observable. We may therefore assume that the idealised tight-binding model still captures a significant part of the physics of real superlattice samples. In any case, this model provides a paradigmatically clear example for the influence of interband effects on Anderson localisation in ac fields. Since successful experiments with semiconductor superlattices in strong terahertz fields have already been carried out [45, 62, 72, 73, 115], it might be of interest to search for signatures of ac-field-controlled Anderson localisation in these systems.

This chapter is organised as follows: Section 2.1 contains a brief description of the model, as well as analytical and numerical results for its quasienergy band structure in the absence of disorder. Since the numerical computation of quasienergy bands is a straightforward matter, particular emphasis is put on a transparent explanation of the physics that leads to the emergence of these bands. Section 2.2 then discusses the relation between quasienergy band width and localisation in the randomly disordered model, and typical effects caused by interband transitions. Some conclusions are drawn in the final section 2.3.

2.1 Quasienergy bands for the ideal two-band model

We consider the standard two-band tight-binding Hamiltonian for a lattice electron driven by an electric field [32, 101]:

$$H(t) = H_{0,1} + H_{F,1}(t) + H_{0,2} + H_{F,2}(t) + H_{IB}(t) \ . \tag{2.1}$$

For either $j = 1$ or $j = 2$ the Hamiltonian $H_{0,j}$ describes the dynamics within a single band of width Δ_j,

$$H_{0,j} = (-1)^j \frac{D}{2} \sum_\ell |\ell, j\rangle\langle \ell, j| + \ (-1)^j \frac{\Delta_j}{4} \sum_\ell \Big(|\ell+1, j\rangle\langle \ell, j| + |\ell, j\rangle\langle \ell+1, j| \Big) \ ,$$

and $H_{F,j}(t)$ models the interaction with an external electric field $F(t)$:

$$H_{F,j}(t) = eF(t)\, d \sum_\ell |\ell, j\rangle \ell \langle \ell, j| \ .$$

The centres of the two unperturbed bands are separated by the energy distance D. The interaction between them is given by $H_{IB}(t)$,

$$H_{IB}(t) = eF(t) X \sum_\ell \Big(|\ell, 1\rangle\langle \ell, 2| + |\ell, 2\rangle\langle \ell, 1| \Big) \ .$$

We have denoted the Wannier state at the ℓ-th site in the j-th band ($j = 1, 2$) by $|\ell, j\rangle$; e is the electronic charge, d the lattice constant, and X the interband matrix element. The electric field consists of a static part of strength F_0 and an oscillating part with amplitude F_1 and frequency ω:

$$F(t) = F_0 + F_1 \cos(\omega t) \ .$$

If the ac amplitude F_1 vanishes, then the energy spectrum of the dc-driven two-band model consists of two interspaced Wannier-Stark ladders, i.e., of two sequences of energy eigenvalues with constant spacing $\Delta E = e F_0 d$ between adjacent members of each sequence [32].

On the other hand, if the amplitude F_1 of the ac field is so high that standard low-order perturbation theory ceases to be applicable, it is no longer practical to analyse the dynamics in terms of energy eigenstates and energy eigenvalues. Rather, one can resort to Floquet theory: given a quantum system governed by a Hamiltonian $H(t)$ that is periodic in time, with period $T = 2\pi/\omega$, there should be a complete set $\{|\psi_r(t)\rangle\}$ of solutions to the Schrödinger equation $i\hbar\partial_t|\psi(t)\rangle = H(t)|\psi(t)\rangle$ of the particular form [98, 123]

$$|\psi_r(t)\rangle = |u_r(t)\rangle \exp\left(-i\frac{\varepsilon_r t}{\hbar}\right) \ ,$$

where the functions $|u_r(t)\rangle$ inherit the T-periodicity of the Hamiltonian:

$$|u_r(t)\rangle = |u_r(t+T)\rangle \ .$$

A wave function $|\psi_r(t)\rangle$ is called Floquet state, with quasienergy ε_r. Inserting such a Floquet state into the Schrödinger equation, one obtains

$$\left[H(t) - i\hbar\partial_t\right] |u_r(t)\rangle = \varepsilon_r |u_r(t)\rangle \ . \tag{2.2}$$

Hence, the periodic functions $|u_r(t)\rangle$ and the quasienergies ε_r can be computed by solving the eigenvalue problem associated with the operator $[H\,(t) - i\hbar\partial_t]$ in an extended Hilbert space consisting of T-periodic functions [103]. The scalar product in that space,

$$\langle\langle \cdot \,|\, \cdot \rangle\rangle \ := \ \frac{1}{T}\int_0^T \mathrm{d}t \, \langle \cdot \,|\, \cdot \rangle \ ,$$

is the usual scalar product combined with time-averaging. The conceptual advantage of the Floquet states lies in the fact that an arbitrary solution $|\psi(t)\rangle$ to the Schrödinger equation can be expanded as

$$|\psi(t)\rangle = \sum_r a_r |u_r(t)\rangle \exp\left(-i\frac{\varepsilon_r t}{\hbar}\right) \ , \tag{2.3}$$

with time-independent coefficients a_r.

Exactly as a quasimomentum in a periodic lattice is defined up to an integer multiple of the reciprocal lattice vector, a quasienergy is defined up to an integer multiple of $\hbar\omega$: if $|u_r(t)\rangle$ is a T-periodic solution to the eigenvalue equation (2.2) with quasienergy ε_r, and if m is an arbitrary, positive or negative integer, then also $|u_r(t)\exp(im\omega t)\rangle$ is a T-periodic eigensolution, with quasienergy $\varepsilon_r + m\hbar\omega$. All of these replica are physically equivalent, because

$$|u_r(t)\, e^{im\omega t}\rangle \cdot \exp\left(-i\frac{(\varepsilon_r + m\hbar\omega)t}{\hbar}\right) = |u_r(t)\rangle \cdot \exp\left(-i\frac{\varepsilon_r t}{\hbar}\right) \ .$$

Nevertheless, *all* solutions to (2.2) are required for the completeness relation in the extended Hilbert space.

If one applies this Floquet theory to the lattice Hamiltonian (2.1), one accounts for the T-periodicity induced by the ac field. It must be recognised, however, that also the dc field induces time-periodic wave packet motion, namely, Bloch oscillations [125]. If the Bloch frequency $\omega_{\text{Bloch}} = eF_0\, d/\hbar$ is different from the ac frequency ω, then the Floquet states, which mark out *one* type of periodicity, might not provide the optimal basis. The problem becomes obvious by changing the gauge: the Hamiltonian (2.1) is unitarily equivalent to

$$\begin{aligned}\widetilde{H}(t) = &\sum_{j=1,2}\sum_{\ell}(-1)^j\frac{D}{2}|\ell,j\rangle\langle\ell,j| \ + \ \sum_{j=1,2}\sum_{\ell}(-1)^j\frac{\Delta_j}{4} \\ &\times\left[\exp\left(-i\frac{eA(t)d}{\hbar}\right)|\ell+1,j\rangle\langle\ell,j| + |\ell,j\rangle\langle\ell+1,j|\exp\left(+i\frac{eA(t)d}{\hbar}\right)\right] \\ &+ eF(t)X\sum_{\ell}\Big(|\ell,1\rangle\langle\ell,2| + |\ell,2\rangle\langle\ell,1|\Big)\ , \end{aligned} \tag{2.4}$$

where

$$A(t) = -F_0\, t - \frac{F_1}{\hbar\omega}\,\sin(\omega t)$$

is the gauge potential. Unless the Bloch frequency $\omega_{\text{Bloch}} = eF_0\, d/\hbar$ and the ac frequency ω are rationally related, the phase factors $\exp(\pm ie\,A(t)\,d/\hbar)$ are quasiperiodic functions of time. In order to account for this type of time-dependence, one should apply two-mode Floquet theory to $\widetilde{H}\,(t)$. There is, however, an important case where T-periodicity is not affected by the gauge transformation: if ω_{Bloch} is a multiple of ω, then both (2.1) and (2.4) are T-periodic, and the Floquet states can incorporate the effects of both the ac and the dc field in an optimal way.

With this caveat in mind, we now turn to the eigenvalue problem (2.2) for the two-band tight-binding Hamiltonian (2.1). We proceed in several steps. First we rewrite $H(t)$ as

$$H(t) = H_0 + \sum_{\ell} H_{IB}^{(\ell)}(t) + \sum_{\ell} H_F^{(\ell)}(t)\ ,$$

where

$$H_0 = H_{0,1} + H_{0,2}$$

is the time-independent part. Field-induced transitions between the two Wannier states at the ℓ-th site are described by

$$H_{IB}^{(\ell)}(t) = \Big(|\ell,2\rangle\langle\ell,1| + |\ell,1\rangle\langle\ell,2| \Big)\, eX \left[F_0 + F_1 \cos(\omega t) \right] ,$$

and

$$H_F^{(\ell)}(t) = \Big(|\ell,1\rangle\langle\ell,1| + |\ell,2\rangle\langle\ell,2| \Big)\, e\ell d \left[F_0 + F_1 \cos(\omega t) \right]$$

is the diagonal part of the interaction with the electric field. In order to compute the quasienergy bands for the model (2.1), i.e., the spectrum of $[H(t) - i\hbar\partial_t]$, we will first derive the exact Floquet states for the operator $[H(t) - H_0 - i\hbar\partial_t]$, and then treat H_0 perturbatively.

Solutions to the Schrödinger equations

$$\left[H_{IB}^{(\ell)}(t) + H_F^{(\ell)}(t) - i\hbar\partial_t \right] |\varphi^{(\ell)}(t)\rangle = 0$$

are given by

$$|\varphi_\pm^{(\ell)}(t)\rangle = \frac{1}{\sqrt{2}} \Big(|\ell,1\rangle \pm |\ell,2\rangle \Big) \exp\left\{ -i \Big[\pm eX + e\ell d \Big] \left[\frac{F_0\, t}{\hbar} + F_1 \frac{\sin(\omega t)}{\hbar\omega} \right] \right\} .$$

Evidently, these are Floquet states with quasienergies

$$\varepsilon_\pm^{(\ell)} = \pm e F_0\, X + \ell \cdot e F_0\, d \mod \hbar\omega .$$

The individual on-site Floquet states $|\varphi_\pm^{(\ell)}(t)\rangle$ are coupled by the hopping terms in H_0. They can hybridise and form quasienergy bands of finite width *only* if they are quasienergetically degenerate with their nearest neighbours, — i.e., if there exists an integer n such that

$$e F_0\, d = n\hbar\omega . \tag{2.5}$$

This condition for quasienergetic alignment simply means that the energy of n photons matches the energy difference between adjacent rungs of the Wannier-Stark ladders. As noted before, this is also the condition for the Floquet states to constitute an optimal basis. In the following we will therefore assume that the ac frequency is tuned such that (2.5) is satisfied.

We then form linear superpositions

$$\begin{aligned} |\psi_\pm(k;t)\rangle &= \sum_\ell e^{-ik\ell d}\, |\varphi_\pm^{(\ell)}(t)\rangle \\ &\equiv |u_\pm(k;t)\rangle \exp\left(-i \frac{\varepsilon_\pm\, t}{\hbar} \right) . \end{aligned}$$

By construction, the T-periodic functions $|u_\pm(k;t)\rangle$,

$$|u_\pm(k;t)\rangle = \sum_\ell \frac{|\ell,1\rangle \pm |\ell,2\rangle}{\sqrt{2}} \exp\left[-ik\ell d - i\ell n\omega t - i(\ell d \pm X)\frac{eF_1}{\hbar\omega}\sin(\omega t)\right] , \quad (2.6)$$

are extended quasienergy eigenfunctions of the operator $[H(t) - H_0 - i\hbar\partial_t]$, provided (2.5) holds. Their quasienergy eigenvalues, $\varepsilon_\pm = \pm eF_0X \mod \hbar\omega$, are degenerate with respect to the wave vector k.

In general, this degeneracy will be removed as a consequence of the hopping between nearest neighbours as described by H_0. If both the hopping strengths and the unperturbed energy band separation are small, i.e., if $\Delta_1/(\hbar\omega) \ll 1$, $\Delta_2/(\hbar\omega) \ll 1$, and $D/(\hbar\omega) \ll 1$, we can treat the effect of H_0 on the spectrum by low-order perturbation theory in the extended Hilbert space [103]. Since H_0 has nonvanishing matrix elements only between Floquet eigenfunctions (2.6) that are characterised by the same wave vector, k is a good quantum number. We have to distinguish two cases: if there is no integer m such that

$$2eF_0X = m\hbar\omega , \quad (2.7)$$

then ε_+ and ε_- do not coincide ($\mathrm{mod}\,\hbar\omega$), and we can resort to nondegenerate perturbation theory. Since

$$\langle u_\pm(k';t)|H_0|u_\pm(k;t)\rangle \;=\; \frac{\Delta_2-\Delta_1}{4}\cos\left(kd + n\omega t + \frac{eF_1d}{\hbar\omega}\sin(\omega t)\right)\,\delta_{k,k'} ,$$

the required matrix elements in the extended Hilbert space are

$$\langle\langle u_\pm(k';t)|H_0|u_\pm(k;t)\rangle\rangle \;=\; \frac{\Delta_2-\Delta_1}{4}\,J_{-n}\left(\frac{eF_1d}{\hbar\omega}\right)\cos(kd)\,\delta_{k,k'} . \quad (2.8)$$

Hence, we obtain the quasienergy-quasimomentum dispersion relations

$$\varepsilon_\pm(k) = \pm eF_0X + (-1)^n\frac{\Delta_2-\Delta_1}{4}\,J_n\left(\frac{eF_1d}{\hbar\omega}\right)\cos(kd) \mod \hbar\omega . \quad (2.9)$$

Within this first-order approximation, the two quasienergy bands are simple cosine bands with identical widths, and they both collapse when the dimensionless ac amplitude $e\,F_1\,d/(\hbar\omega)$ equals a zero $j_{n,s}$ of the ordinary Bessel function J_n, exactly as in the case of a single band [52, 56, 122].

The approximate spectrum (2.9) does not contain the original energy band separation D. If D is not small compared to the photon energy $\hbar\omega$, but still $\Delta_j/(\hbar\omega) \ll 1$ for $j = 1, 2$, one can consider first the limiting case $\Delta_1/(\hbar\omega) = \Delta_2/(\hbar\omega) = 0$. Then the Hamiltonian (2.1) still reduces to a system of uncoupled two-level systems $H_{tls}^{(\ell)}(t)$ that are labelled by the site index ℓ :

$$H_{tls}^{(\ell)}(t) = \frac{D}{2}\sigma_z + eF(t)\,\ell d\,\mathbf{1} + eF(t)\,X\sigma_x , \quad (2.10)$$

where σ_x and σ_z are the usual Pauli matrices. The quasienergy spectra of all these systems coincide, provided the resonance condition (2.5) is satisfied. If then $\Delta_1/(\hbar\omega) \neq 0$ and $\Delta_2/(\hbar\omega) \neq 0$, so that different sites communicate with each other, this ℓ-degeneracy is again removed, and quasienergy bands emerge. The centres of these bands tend to follow the quasienergies of the associated two-level systems (2.10), and their widths tend to oscillate proportional to $J_n(eF_1 d/(\hbar\omega))$, as in the case $D/(\hbar\omega) \ll 1$.

Figure 2.1 depicts such a scenario for a finite lattice with $N = 41$ sites; the wave functions

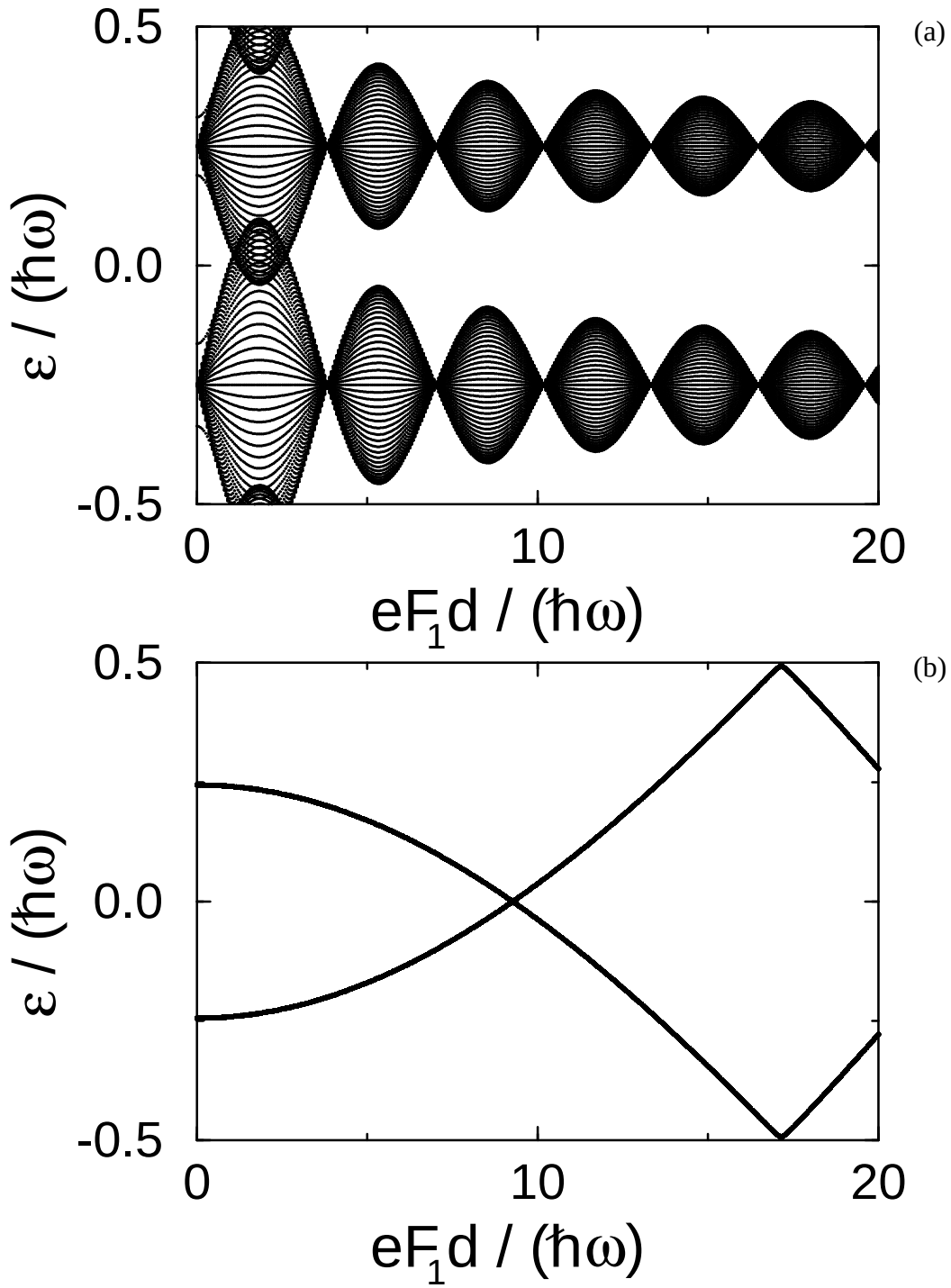

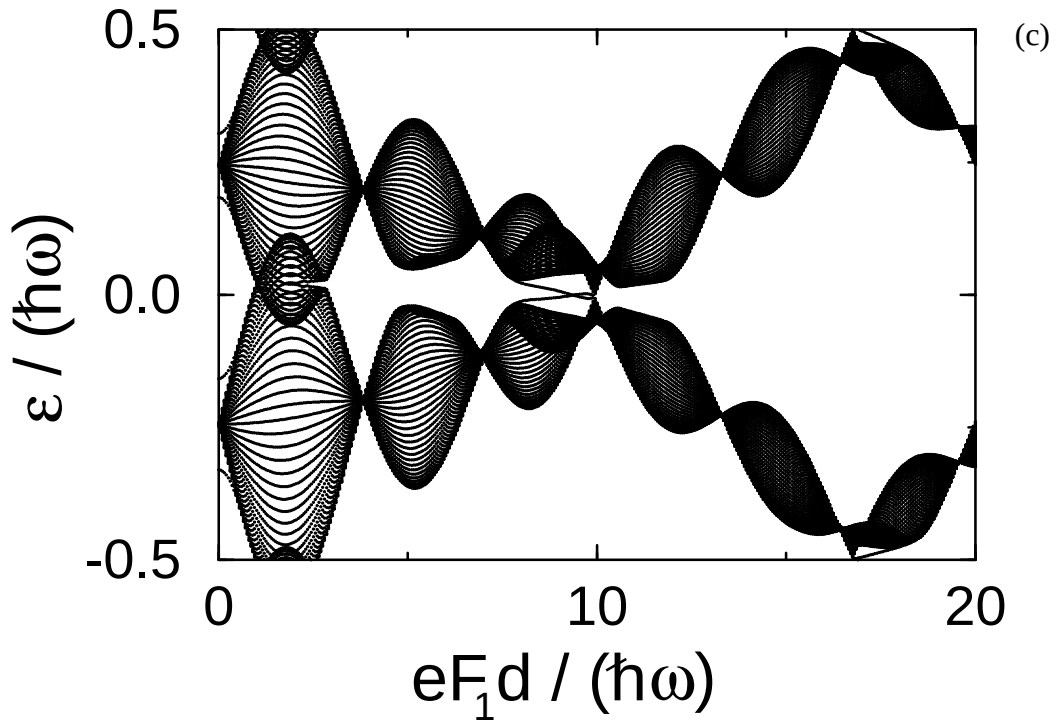

Figure 2.1: Quasienergy bands for the two-band model (2.1) with 41 sites, versus the scaled ac amplitude $eF_1d/(\hbar\omega)$. The case considered here is a one-photon resonance, $eF_0d = 1\cdot\hbar\omega$. (a): vanishing interband interaction, $X/d = 0$. The energy band widths are $\Delta_1/(\hbar\omega) = 1.0$, $\Delta_2/(\hbar\omega) = 1.2$; the energy band separation is $D/(\hbar\omega) = 5.5$. Both quasienergy bands collapse at the zeros of J_1. (b): $X/d = -16/(9\pi^2)$, but $\Delta_j/(\hbar\omega) = 0$ ($j = 1, 2$). (c): quasienergy bands with $\Delta_j/(\hbar\omega)$ as in (a), and X/d as in (b). Note that the band collapses are hardly affected by the interband interaction.

are assumed to vanish at the chain ends. Plot 2.1 (a) shows the two quasienergy bands without interaction $(X/d = 0)$, versus the scaled ac amplitude $eF_1d/(\hbar\omega)$. The parameters chosen are $n = 1$ (that is, we have a one-photon resonance, $eF_0d = 1\cdot\hbar\omega$), $\Delta_1/(\hbar\omega) = 1.0$, $\Delta_2/(\hbar\omega) = 1.2$, and $D/(\hbar\omega) = 5.5$. Plot 2.1 (b) shows the quasienergies for the two-level systems (2.10). The value of the interband matrix element is $X/d = -16/(9\pi^2)$ [101], so that the second resonance (2.7) is not met. Plot 2.1 (c) shows the quasienergy bands for the full system, with $\Delta_j/(\hbar\omega)$ as in (a) and X/d as in (b). The band collapses are hardly affected by the interband interaction; they occur at the same ac amplitudes as in the case $X/d = 0$.

The quasienergy spectrum becomes more complicated if, besides the basic condition (2.5) required for the emergence of quasienergy bands, also the second resonance condition (2.7) is satisfied. Then the quasienergies $\varepsilon^{(\ell)}_{tls,\pm}$ of the two-level systems (2.10) show the strongest dependency on the ac amplitude. A standard calculation [106] readily yields a strong-field

approximation:

$$\varepsilon^{(\ell)}_{tls,\pm} = \frac{m\omega}{2} \pm (-1)^m \frac{D}{2}\, J_m\!\left(\frac{2eF_1X}{\hbar\omega}\right) \qquad \mathrm{mod}\ \hbar\omega\ ,$$

which shows that the already familiar Bessel function $J_n(e\,F_1\,d/[\hbar\omega])$ resulting from the coupling of adjacent sites now has to compete with the Bessel function $J_m(2e\,F_1\,X/[\hbar\omega])$ originating from the coupling of the two Wannier-Stark ladders.

The calculation of the approximate quasienergy band structure for the case $\Delta_j/(\hbar\omega) \ll 1$ $(j = 1, 2)$, $D/(\hbar\omega) \ll 1$ requires degenerate perturbation theory, since, by virtue of of (2.7), the quasienergy eigenfunctions $|u_+(k;t)\rangle$ and $|u_-(k;t)\rangle\, e^{im\omega t}$ belong to the same quasienergy. Hence, besides the matrix elements (2.8) we also need

$$\begin{aligned}\langle\langle u_+(k;t)|H_0|u_-(k;t)\, e^{im\omega t}\rangle\rangle \;&=\; -(-1)^m \frac{D}{2}\, J_m\!\left(\frac{2eF_1X}{\hbar\omega}\right) \\ &- \frac{\Delta_1+\Delta_2}{8}\left[\, e^{ikd}\, J_{-n-m}\!\left(\frac{(2X+d)\,eF_1}{\hbar\omega}\right) + e^{-ikd}\, J_{n-m}\!\left(\frac{(2X-d)\,eF_1}{\hbar\omega}\right)\right] .\end{aligned}$$

Defining the dimensionless parameters

$$\alpha = \frac{eF_1d}{\hbar\omega} \qquad \text{and} \qquad \beta = \frac{2eF_1X}{\hbar\omega}\ ,$$

we then obtain the approximate quasienergy bands for the case where both resonance conditions (2.5) and (2.7) are satisfied:

$$\begin{aligned}\varepsilon_\pm(k) \;&=\; \frac{m\omega}{2} + (-1)^n \frac{\Delta_2-\Delta_1}{4}\, J_n(\alpha)\cos(kd) \;\pm\Bigg\{ \frac{D^2}{4}\, J_m^2(\beta) + \left(\frac{\Delta_1+\Delta_2}{8}\right)^2 \\ &\times \left[J^2_{m+n}(\beta+\alpha) + J^2_{m-n}(\beta-\alpha) + 2\, J_{m+n}(\beta+\alpha)\, J_{m-n}(\beta-\alpha)\cos(2kd)\right] \\ &+ (-1)^n D\frac{\Delta_1+\Delta_2}{8} J_m(\beta)\cos(kd)\Big[J_{m+n}(\beta+\alpha)+J_{m-n}(\beta-\alpha)\Big]\Bigg\}^{1/2} \mathrm{mod}\ \hbar\omega\,.\end{aligned} \tag{2.11}$$

These are no longer simple cosine bands. Depending on the respective values of the integers n and m, up to four different Bessel functions appear. The widths of the quasienergy bands still depend strongly on the ac amplitude, but there are no perfect band collapses.

Figure 2.2 (a) depicts the numerically computed quasienergy bands for a finite lattice with 41 sites, for $\Delta_1/(\hbar\omega) = 0.4$, $\Delta_2/(\hbar\omega) = 0.8$, and $D/(\hbar\omega) = 1.2$. We have chosen $n = 5$ and $X/d = -0.2$, which gives $m = -2$. Figure 2.2 (b) shows the evaluation of (2.11) for these parameters. Since $D/(\hbar\omega)$ is not really small, the approximation fails at low ac amplitudes. For high amplitudes, however, the agreement is quite good, thus indicating the correctness of our line of reasoning.

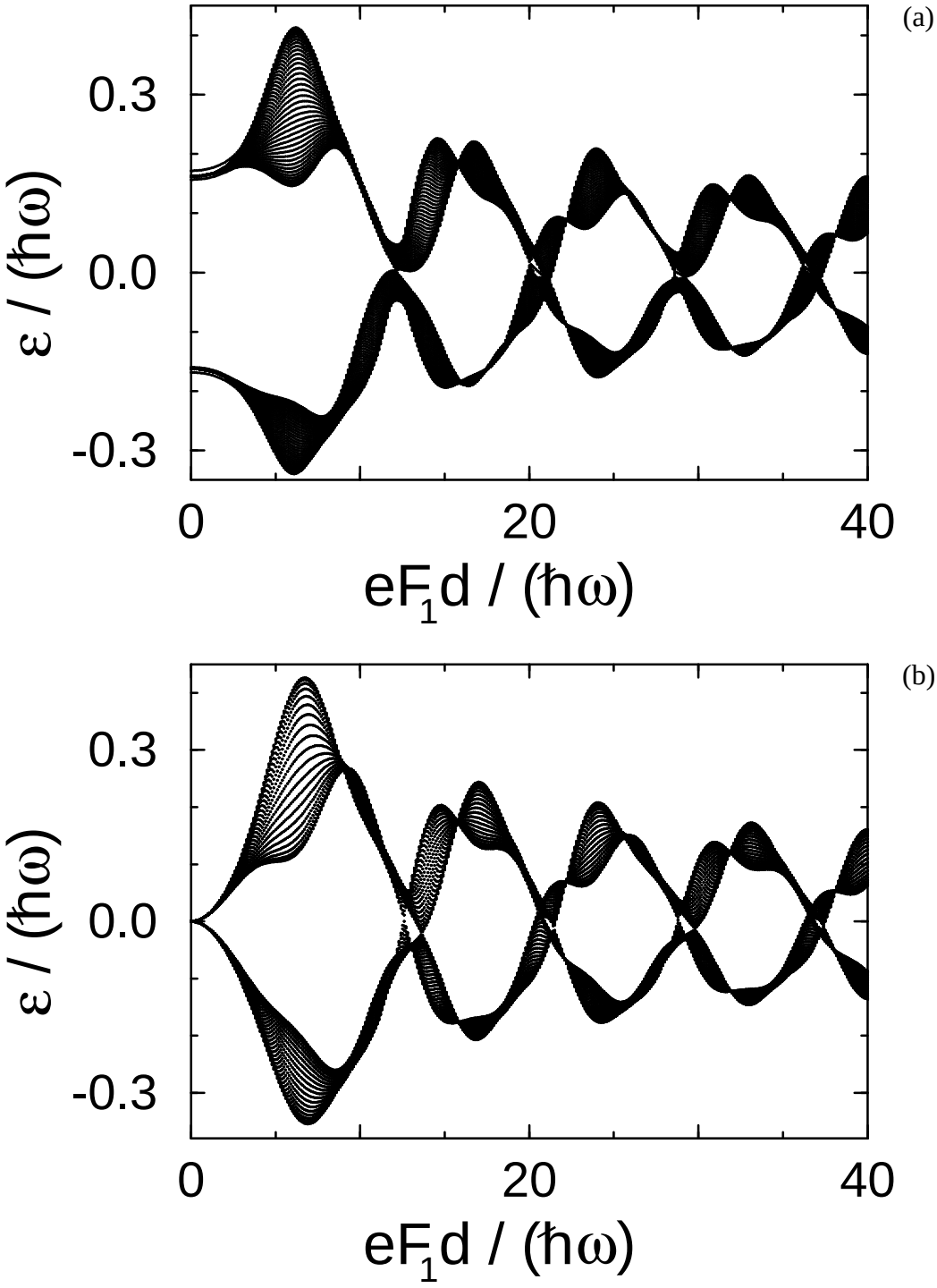

Figure 2.2: Quasienergy bands for a case of double resonance. (a): numerically computed quasienergy bands for a finite lattice with 41 sites, for $n = 5$ and $m = -2$ ($X/d = -0.2$). The other parameters are $D/(\hbar\omega) = 1.2$, $\Delta_1/(\hbar\omega) = 0.4$, and $\Delta_2/(\hbar\omega) = 0.8$. (b): evaluation of the approximate formula (2.11) for these parameters.

It should be pointed out that for nonvanishing dc fields both resonance conditions (2.5) and (2.7) can be satisfied simultaneously only if $2X/d = m/n$ is a ratio of two integers. Of course, any given ratio $2X/d$ could be approximated arbitrarily well by rational numbers, but the resonances will be physically meaningful only if both n and m are small. However, if there is no dc field at all, then both conditions are satisfied automatically, with $n = m = 0$. In that case the analytical formula (2.11) shows that the quasienergy bands do no longer collapse perfectly when α equals a zero of J_0, as has recently been observed in numerical studies by Rotvig et al. [101]. Whether or not an approximate collapse occurs depends on the values of both α and β.

2.2 Amplitude-controlled Anderson localisation

We now introduce site-diagonal random disorder into the tight-binding model by adding to $H(t)$ the Hamiltonian

$$H_{\text{random}} = \sum_{\ell} \nu_\ell \Big(|\ell,1\rangle\langle\ell,1| + |\ell,2\rangle\langle\ell,2| \Big) \; .$$

We assume that the random energies ν_ℓ are distributed uniformly in the interval $[-\nu_{\max}, +\nu_{\max}]$, so that their probability distribution $\rho(\nu)$ is given by

$$\rho(\nu) = \begin{cases} 1/(2\nu_{\max}) & \text{for } |\nu| \le \nu_{\max} \\ 0 & \text{otherwise} \end{cases}$$

Figure 2.3 (a) shows an example for the effect of disorder on the quasienergy spectrum. The parameters chosen are the same as in figure 2.1 (c); the disorder strength is $\nu_{\max}/(\hbar\omega) = 0.05$.

The random disorder leads to localisation of the quasienergy band states. To investigate this localisation we expand the numerically computed quasienergy states $|u_r(t)\rangle$ in the basis of the Wannier states,

$$|u_r(t)\rangle = \sum_{\ell=1}^{N} \Big(c_{\ell,1}^{(r)}(t)|\ell,1\rangle + c_{\ell,2}^{(r)}(t)|\ell,2\rangle \Big) \; ,$$

and compute the inverse participation ratios

$$P^{(r)}(t) = \sum_{\ell=1}^{N} \Big(|c_{\ell,1}^{(r)}(t)|^2 + |c_{\ell,2}^{(r)}(t)|^2 \Big)^2 \; .$$

These quantities measure the spatial extension of the quasienergy states. $P^{(r)}(t)$ approaches unity when $|u_r(t)\rangle$ is localised entirely at a single site, and vanishes as N^{-1} when $|u_r(t)\rangle$ is uniformly extended. The time-dependence of $P^{(r)}(t)$, $r = 1, \ldots, 2N$, becomes weak when the ac photon energy $\hbar\omega$ is larger than the energy band widths Δ_1 and Δ_2 [56, 57]. It then

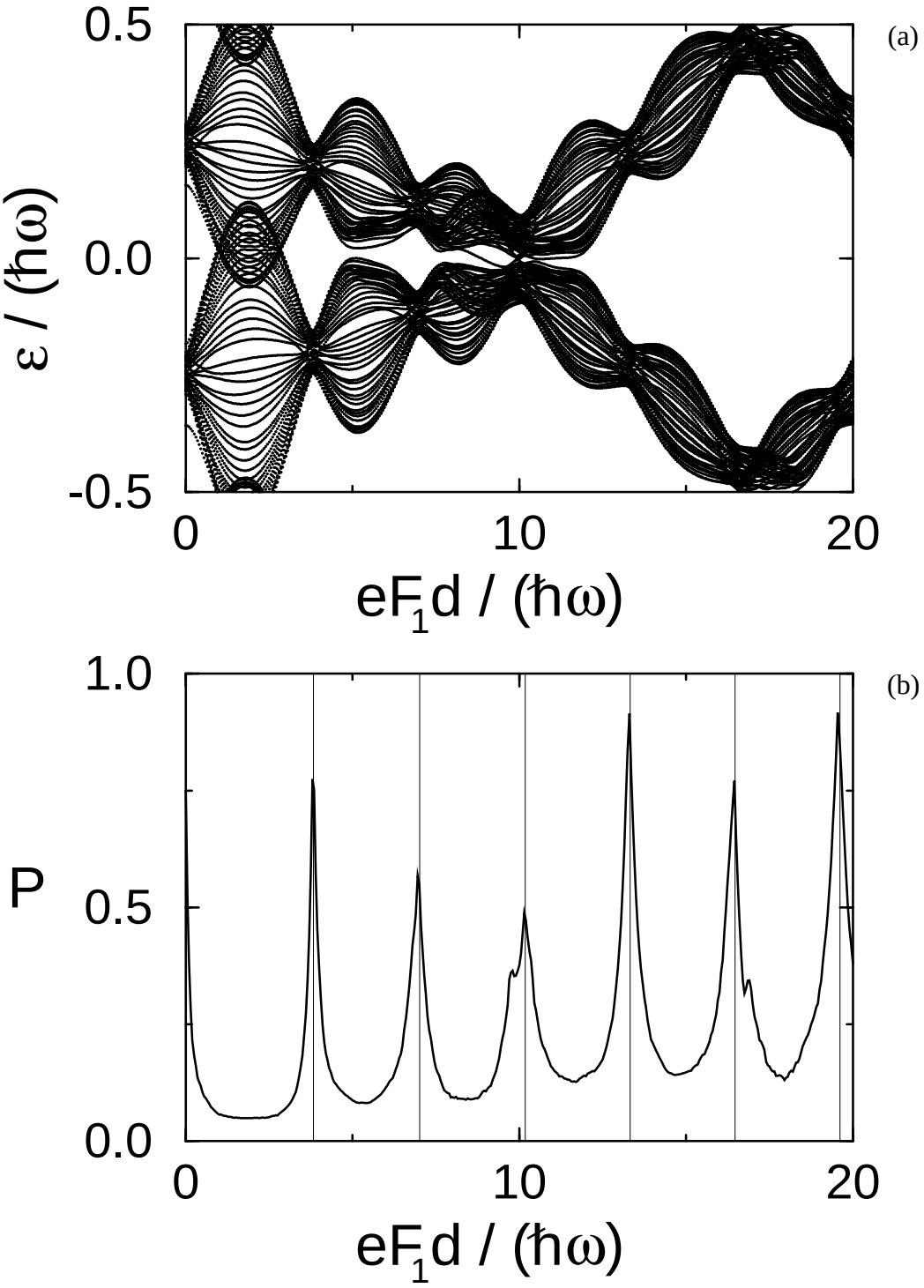

Figure 2.3: (a): Quasienergy spectrum for a randomly disordered two-band model with parameters as in figure 2.1 (c). The disorder strength is $\nu_{\max}/(\hbar\omega) = 0.05$. (b): corresponding averaged inverse participation ratio P, see (2.12). The vertical lines indicate dimensionless amplitudes $e\ F_1\ d/(\hbar\omega)$ that correspond to zeros of the Bessel function J_1, where the quasienergy bands of the ideal lattice collapse.

suffices to represent the functions $P^{(r)}(t)$ by their value at some arbitrary moment t_0. For numerical convenience we choose $t_0 = 3T/4$, where the ac field vanishes. However, this particular choice is without principal significance for the results that follow.

A measure for the degree of disorder-induced localisation now is the averaged inverse participation ratio

$$P := \frac{1}{2N} \sum_{r=1}^{2N} P^{(r)}\left(\frac{3T}{4}\right) \ . \tag{2.12}$$

Figure 2.3 (b) shows P as function of the scaled ac amplitude $eF_1 d/(\hbar\omega)$ for the situation considered in figure 2.3 (a). Localisation is most strongly pronounced at the zeros of J_1, where the widths of the quasienergy bands are minimum, and comparatively weak in between. This result is not trivial. The Hamiltonian $H(t)$ for the ideal lattice describes Bloch oscillations, Zener-tunnelling, and Rabi-oscillations between the unperturbed energy bands. The quasienergy band states that reflect the dynamics in resonant ac fields incorporate these phenomena. Nevertheless, in the presence of disorder they behave just like energy band states in the static case: the degree of localisation is determined by the ratio of disorder strength and band width. Since now the band widths depend on the ac amplitude, changing the amplitude means changing the localisation lengths.

The situation studied in figures 2.3 (a),(b) is still comparatively simple, since the second resonance condition (2.7) is not met, and the behaviour of the two bands is not too different from the noninteracting case $(X/d = 0)$. If (2.7) is satisfied, the dynamics is richer and, as a consequence, the dependency of P on the ac amplitude more complicated. We display in

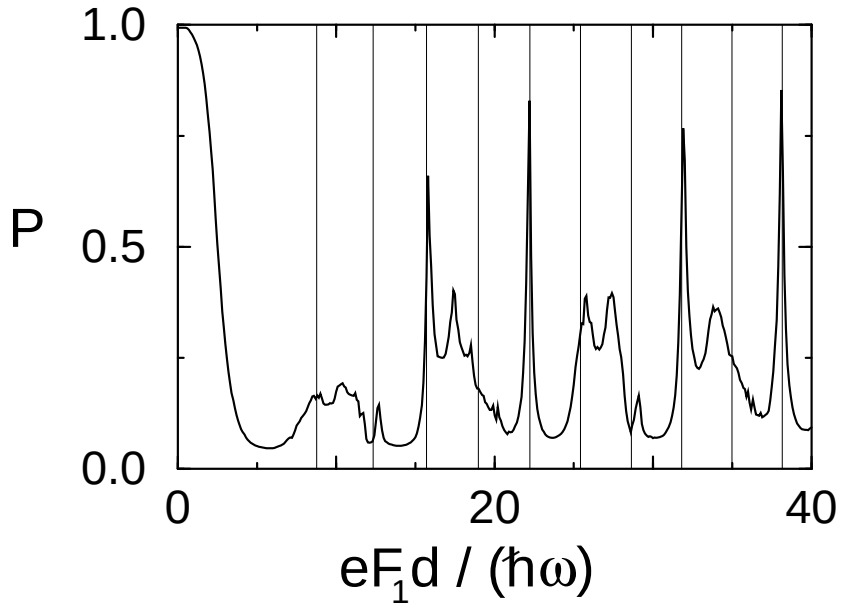

Figure 2.4: Inverse participation ratio for the model with parameters as in figure 2.2 (a), and additional disorder of strength $\nu_{\max}/(\hbar\omega) = 0.01$. The vertical lines indicate zeros of J_5.

figure 2.4 the averaged inverse participation ratio for such a situation. The system parameters are as in figure 2.2 (a), and there is additional disorder of strength $\nu_{\max}/(\hbar\omega) = 0.01$ (so that $\nu_{\max}/\Delta_1 = 0.025$, $\nu_{\max}/\Delta_2 = 0.0125$). Since we now have a five-photon resonance between the rungs of the Wannier-Stark ladders, vertical lines are drawn to indicate the zeros of J_5. There still is pronounced localisation at *some* of the zeros, but the fluctuations of P between the spikes are apparently unrelated to the other zeros. A glance at figure 2.2 (a) shows the reason: the two quasienergy bands exhibit avoided crossings when $2eF_1X/(\hbar\omega)$ is approximately equal to a zero of J_2. Then the single-band dynamics is strongly modified, and the band widths do not follow the simple J_5-pattern. The very connection between quasienergy band width and degree of localisation, however, remains valid.

To further substantiate this statement, we also compute the band-resolved participation ratios

$$P_{\text{br}} := \frac{1}{N} \sum_{\text{one band}} P^{(r)}\left(\frac{3T}{4}\right) , \tag{2.13}$$

where the summation extends only over indices r pertaining to one of the two quasienergy bands. The upper parts of figures 2.5 (a),(b),(c) show results of such calculations; the lower parts depict the corresponding quasienergy bands for the *ideal* model ($\nu_{\max}/(\hbar\omega) = 0$). The parameters are as in figure 2.4. In all three cases, the dashed curve belongs to the upper band and the full curve to the lower one; vertical lines are drawn at zeros of J_5. The behaviour of P_{br} reflects even fine details visible in the quasienergy bands, such as slight shifts of the collapse points away from the zeros of J_5, or the appearance of additional band narrowings in only one of the bands.

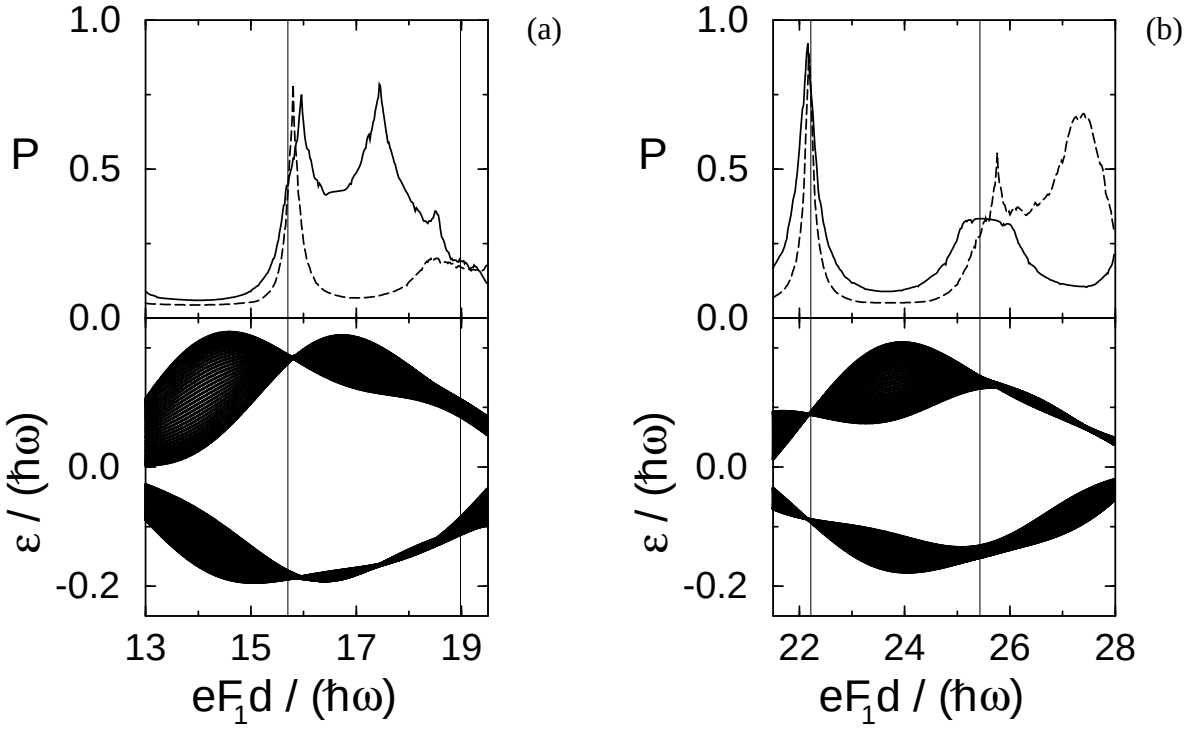

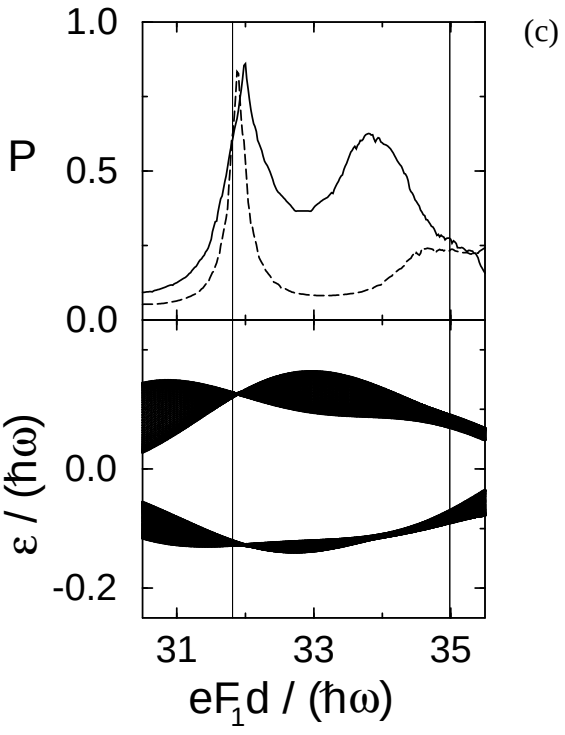

Figure 2.5: Band-resolved inverse participation ratios (2.13) for parameters as in figure 2.4; compared to the the quasienergy bands of the ideal lattice ($\nu_{\max}/(\hbar\omega) = 0$). The dashed curves belong the the upper bands, the full curves to the lower. Note that the points of collapse are slightly shifted from the zeros of J_5 (vertical lines), and that additional band narrowings occur.

2.3 Conclusions

The original energy bands of the two-band model are coupled by Rabi oscillations and Zener tunnelling. An arbitrary wave packet, initially prepared in one of the bands, will soon acquire components in the other. The introduction of quasienergy states corresponds to a transformation from these interacting bands to *noninteracting* quasienergy bands: a wave packet can be characterised by its expansion coefficients with respect to the quasienergy states, and these coefficients remain constant in time, see (2.3). Since the quasienergy states already incorporate both the ac and the dc field, they serve as a basis which allows us to describe the time evolution in complete analogy to the field-free case.

It is remarkable that this analogy extends even further. When there is random lattice disorder, the quasienergy band states localise in space. The dimensionless parameter that determines the degree of localisation is the ratio of disorder strength and band width, exactly as in the well known case of Anderson localisation of energy eigenstates in random lattices without external fields. But now there is an important new feature: the quasienergy bands reflect

both the spatial lattice periodicity and the temporal periodicity induced by the driving fields. Varying the amplitude of the ac field means changing the properties of the spatio-temporal lattice, and, hence, changing its quasienergy band structure. For disordered lattices, varying the band widths means controlling the degree of localisation. In principle, therefore, there exists a possibility to control Anderson localisation by spatially homogeneous ac fields.

Even though there is still a long way to go from our idealised model to an actual superlattice sample, it is tempting to speculate about possible implications of the results outlined in this chapter for current experiments that probe the dynamics of semiconductor superlattices under the influence of strong terahertz radiation [45, 62, 72, 73, 115]. At parameters where the quasienergy bands are sufficiently wide, the inevitable disorder in these mesoscopic systems might play only a minor role, so that electronic transport should proceed via the effectively extended states. In that case, phonon scattering would *impede* the flow of electrons. On the other hand, there exist only localised states at field parameters where the quasienergy bands (almost) collapse, so that phonon scattering now would be a mechanism that *helps* the electrons to hop from one site to another. That could result in a conductivity that *decreases* with temperature when the quasienergy bands are wide, but *increases* with temperature when they are collapsed. The observation of a strongly amplitude-dependent conductivity-temperature relation would, therefore, be an indication for Anderson localisation of quasienergy states. It might also be attractive to perform experiments with intentionally disordered superlattices. In any case, the further exploration of the concept of ac-field-controlled Anderson localisation presents a new challenge to both theorists and experimentalists.

3 Ultracold atoms in standing light waves

There are many situations where it would be of substantial interest to *control*, rather than merely observe, the time evolution of a quantum system. One example has been given in the last chapter, another one is laser chemistry, where the ultimate goal is to steer a chemical reaction along a desired path by means of judiciously designed, strong laser pulses [85].

The experimental study of the question just how effective an active control by external fields might be depends on the availability of test systems that can be subjected to time-dependent forces under precisely defined and reproducible conditions — which is not an easy task with molecules in strong laser fields. One test system that fulfils this criterion is the highly excited hydrogen atom in a microwave field. During the last decade this system has given numerous insights into the dependency of quantum dynamics on strength, frequency, and temporal variation of the amplitude of an oscillating force, and the research is still continuing [75, 76].

A second test system, consisting of a dilute cloud of ultracold atoms in a modulated standing light wave, has emerged only recently. This system is particular in so far as it has two entirely different faces. When the optical potential is deep — some hundred atomic single-photon recoil energies, say — and the temperature of the atom cloud is somewhat higher than the recoil temperature — but still low enough for the atoms to be trapped in the potential wells — then the dynamics in the individual wells are essentially independent, and one obtains multiple realisations of driven, anharmonic oscillators. On the other hand, when the depth of the potential is just a few recoil energies, and the atoms are at about recoil temperature, then the spatial periodicity of the optical potential gives rise to effects that have previously been linked exclusively with quantum dynamics in crystal lattices. The wide ranges within which the relevant parameters can be adjusted makes ultracold atoms in modulated standing light waves most attractive for the further exploration of the possibilities of active quantum control.

In the present chapter we sketch, from a theoretician's viewpoint, the above two aspects of the dynamics of ultracold atoms in standing light waves. We first collect some basic material, in order to familiarise with recent experimental achievements. In section 3.1 we will then study the role of classical resonances for the dynamics in modulated, i.e., periodically driven, deep optical lattices, whereas section 3.3 treats the effect of an oscillating force on atoms in comparatively shallow optical potentials. In that section we also suggest to realise Harper's

model with ultracold atoms, and thus to study a metal-insulator transition with atomic matter waves. The final section 3.4 then briefly summarises this chapter.

3.1 One-dimensional optical lattices: basic facts

The starting point for what follows is a two-level atom with ground state $|g\rangle$ and excited state $|e\rangle$ that experiences the electric field $\mathcal{E}\cos(k_L x)\cos(\omega_L t)$ of a classical standing light wave with wave number k_L and frequency ω_L. We assume that the spatial variation of the light field in the plane orthogonal to the x-direction can be neglected, which means that the waists of the laser beams generating the standing wave have to be sufficiently wide, and consider the atomic motion in this direction only. Within the dipole approximation, we then have the Hamiltonian [40]

$$H = \frac{P^2}{2M}\mathbf{1} + \hbar\omega_0|e\rangle\langle e| + \mu\mathcal{E}\cos(k_L x)\cos(\omega_L t)\Big(|g\rangle\langle e| + |e\rangle\langle g|\Big)\ , \tag{3.1}$$

where M denotes the mass of the atom, P the x-component of its momentum, $\mathbf{1} = |g\rangle\langle g| + |e\rangle\langle e|$, the spacing between the two energy levels is $\hbar\omega_0$, and μ is the dipole matrix element for the transition. We stipulate further that the detuning δ_L of the laser frequency ω_L from the transition frequency ω_0 be sufficiently large so that spontaneous transitions from the upper level can be safely neglected [37, 68], but small compared to the transition frequency itself,

$$\delta_L \equiv \omega_0 - \omega_L \ll \omega_0\ .$$

Then a reasonable ansatz for the atomic wave function is given by

$$|\Psi(x,t)\rangle = |\psi_g(x,t)|g\rangle\rangle + |\psi_e(x,t)\,e^{-i\omega_L t}|e\rangle\rangle\ . \tag{3.2}$$

Inserting (3.2) into the Schrödinger equation and employing the rotating wave approximation, i.e., neglecting the oscillating terms proportional to $\exp(\pm 2i\omega_L t)$, one obtains the equations

$$\begin{aligned} i\hbar\frac{\partial}{\partial t}|\psi_g(x,t)\rangle &= -\frac{\hbar^2}{2M}\frac{\partial^2}{\partial x^2}|\psi_g(x,t)\rangle + \frac{\mu\mathcal{E}}{2}\cos(k_L x)|\psi_e(x,t)\rangle \\ i\hbar\frac{\partial}{\partial t}|\psi_e(x,t)\rangle &= -\frac{\hbar^2}{2M}\frac{\partial^2}{\partial x^2}|\psi_e(x,t)\rangle + \hbar\delta_L|\psi_e(x,t)\rangle + \frac{\mu\mathcal{E}}{2}\cos(k_L x)|\psi_g(x,t)\rangle\ . \end{aligned}$$

If the atom is initially in its ground state, and provided that the detuning is large compared to the excited-state kinetic energy and to the Rabi frequency Ω,

$$\delta_L \gg \frac{\mu\mathcal{E}}{\hbar} \equiv \Omega\ ,$$

then the excited-state amplitude $|\psi_e(x,t)\rangle$ can be adiabatically eliminated to yield

$$i\hbar\frac{\partial}{\partial t}|\psi_g(x,t)\rangle = -\frac{\hbar^2}{2M}\frac{\partial^2}{\partial x^2}|\psi_g(x,t)\rangle - \frac{\hbar\Omega^2}{8\delta_L}\left[\cos(2k_L x) + 1\right]|\psi_g(x,t)\rangle\ .$$

(A more refined discussion of this adiabatic elimination can be found in reference [41] Dropping the overall energy shift, we thus obtain an effective Hamiltonian

$$H_{\text{eff}}(x) = -\frac{\hbar^2}{2M}\frac{\mathrm{d}^2}{\mathrm{d}x^2} + \frac{V_0}{2}\cos(2k_L x) \tag{3.3}$$

for a particle that moves in a one-dimensional cosine potential. From now on we will suppress the subscript g, so that $|\psi(x,t)\rangle$ will denote the ground-state amplitude, with the tacit understanding that the excited-state amplitude remain negligible. A more detailed discussion of the extended Harper model is given in the appendix A.

The depth of the potential wells is

$$V_0 = -\frac{\hbar\Omega^2}{4\delta_L}\ . \tag{3.4}$$

Hence, V_0 is negative if the laser is detuned to the red side of the atomic transition ($\delta_L > 0$), so that the locations of the potential minima coincide with the locations of maximum laser intensity. In the opposite case of blue detuning, the atoms are attracted to the intensity minima.

The lattice constant d of the optical potential is half the laser wavelength,

$$d = \frac{\pi}{k_L} = \frac{\lambda_L}{2}\ .$$

Quantum mechanical effects caused by the spatial periodicity of the optical lattice, like the formation of Bloch waves, become important once the atomic de Broglie wavelength $2\pi\hbar/P$ significantly exceeds the lattice constant, which gives the condition

$$\frac{P^2}{2M} \ll 4\,\frac{\hbar^2 k_L^2}{2M} \equiv 4E_R\ .$$

The spatial periodicity can make itself felt if the kinetic energy associated with the motion in the direction of the standing light wave is less than or at most comparable to the single-photon recoil energy E_R. When investigating Bloch dynamics, the atoms have to be "ultracold" in this sense.

The band structure pertaining to the optical potential is then determined by the stationary eigenvalue equation

$$\Big(-\frac{\hbar^2}{2M}\frac{\mathrm{d}^2}{\mathrm{d}x^2} + \frac{V_0}{2}\cos(2k_L x) - E\Big)|\varphi(x)\rangle = 0\ ,$$

which, in terms of the dimensionless coordinate $z = k_L x$ and $\widetilde{\varphi}(z) \equiv |\varphi(z/k_L)\rangle$, is nothing but the well-known Mathieu equation [1]

$$\widetilde{\varphi}''(z) + \Big[a - 2q\cos(2z)\Big]\widetilde{\varphi}(z) = 0 \tag{3.5}$$

with parameters

$$q = \frac{V_0}{4E_R} \qquad \text{and} \qquad a = \frac{E}{E_R} \,.$$

Therefore, a Bloch wave $|\varphi_k(x)\rangle = |u_k(x)\exp(ikx)\rangle$ with a periodic function $|u_k(x)\rangle = |u_k(x+d)\rangle$ and a quasimomentum k corresponds directly to a Floquet solution $\widetilde{\varphi}_\nu(z) = P_\nu(z)\exp(i\nu z)$ of the Mathieu equation, where $P_\nu(z) = P_\nu(z+\pi)$ and the characteristic exponent $\nu = k/k_L$ is real. In particular, the energies at the band edges $k/k_L = 0$ are given by the characteristic values [1] of the Mathieu equation that are associated with π-periodic Mathieu functions; the energies at the edges $k/k_L = \pm 1$ are given by characteristic values associated with 2π-periodic functions. Following standard notation [1], we denote those characteristic values that belong to the even Mathieu functions $ce_n(z,q)$ by $a_n(q)$ (with $n = 0, 1, 2, \ldots$), and those belonging to the odd functions $se_{n+1}(z,q)$ by $b_{n+1}(q)$. Defining

$$\alpha_n^{(0)}(q) \equiv \begin{cases} a_n(q) & , \quad n = 0, 2, 4, \ldots \\ b_{n+1}(q) & , \quad n = 1, 3, 5, \ldots \end{cases} \tag{3.6}$$

and

$$\alpha_n^{(1)}(q) \equiv \begin{cases} b_{n+1}(q) & , \quad n = 0, 2, 4, \ldots \\ a_n(q) & , \quad n = 1, 3, 5, \ldots \end{cases} \,,$$

we then have

$$E_n\left(\frac{k}{k_L} = 0\right) = \alpha_n^{(0)}(q)\, E_R \qquad \text{and} \qquad E_n\left(\frac{k}{k_L} = 1\right) = \alpha_n^{(1)}(q)\, E_R \,,$$

where n is the band index. Thus, given the strength $q = V_0/(4E_R) = -\hbar\Omega^2/(16\delta_L E_R)$ of the optical potential, the band structure can be read off the stability chart of the Mathieu equation.

Figure 3.1 shows the characteristic values as functions of q, as computed efficiently by the method suggested in reference [83]. It is obvious from the Mathieu equation itself that the parameter combination $a = 2q$ has special significance: classically speaking, it separates unbound motion with total energy exceeding the top of the barriers ($a > 2q$) from motion bound in the individual wells ($a < 2q$). The upwards-sloped line in figure 3.1 indicates this borderline between the almost free particle regime (thick bands) and the tight binding regime (thin bands). We will encounter a similar crossover in section 3.2, albeit in a quite different setting.

Figure 3.2 depicts the dispersion relations $E_n(k)$ for the lowest three bands in an optical potential with $q = 1.25$ (corresponding to $V_0/E_R = 5.0$). In this case, the second band ($n = 1$) lies already above the potential ridges, whereas the dispersion relation of

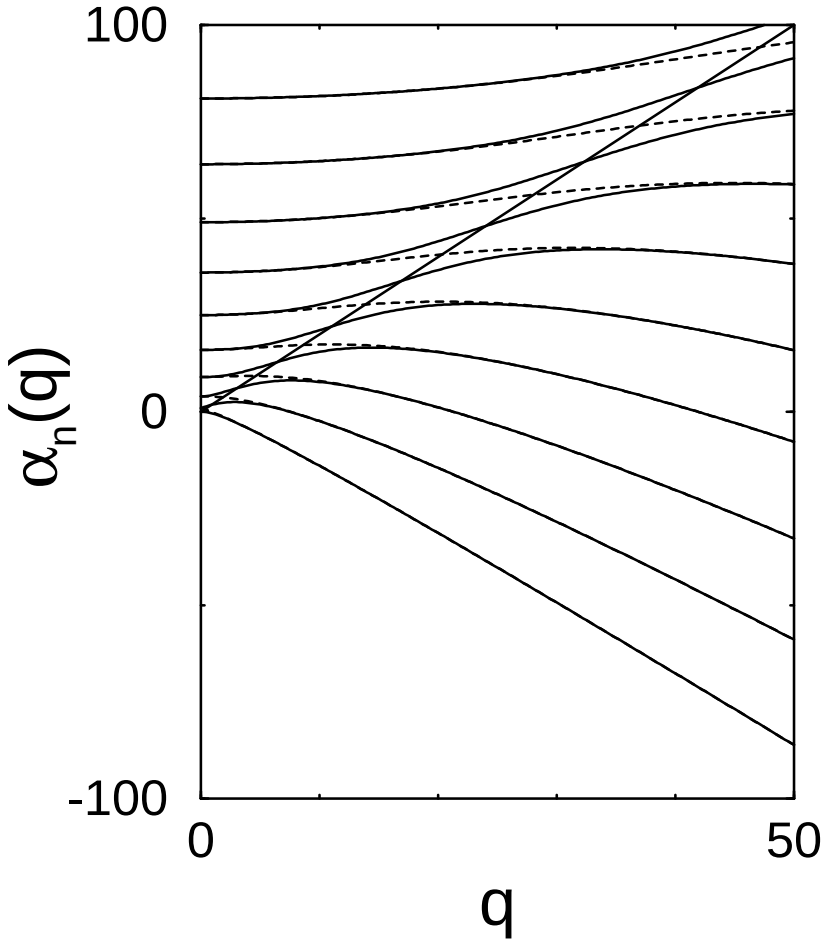

Figure 3.1: Characteristic values $a_n(q)$ (full lines) and $b_{n+1}(q)$ (dashed) for the Mathieu equation (3.5), cf. reference [1]. The intervals between $a_n(q)$ and $b_{n+1}(q)$ correspond to energy bands of the optical potential, in multiples of the recoil energy E_R. The upwards-sloped straight line separates the regime of almost free motion from the tight-binding regime.

the lowest band, the width Δ_0 of which is merely $0.264\ E_R$, is determined almost entirely by nearest neighbour hopping. Hence, it can be well approximated by a cosine function, $E_0(k) \approx -(\Delta_0/2)\cos(kd)$. We will use this system in section 3.3 to illustrate the possibility of realising Harper's model with matter waves.

Ultracold atoms in standing light waves provide an almost ideal testing ground to study fundamental effects of solid state physics in their purest form [7, 92, 120]. The initial momentum distribution of an atom cloud can be tailored as desired, during the experiment there is practically no dissipation or scattering from lattice defects, and the potential can be switched off in the end, giving access to the momentum distribution of the final states. Moreover, typical atom samples in optical lattices are so dilute that atom-atom interactions are negligible, which means that one can actually probe single-particle wave functions, although the measurements are performed on an ensemble. But there are even more attractive features.

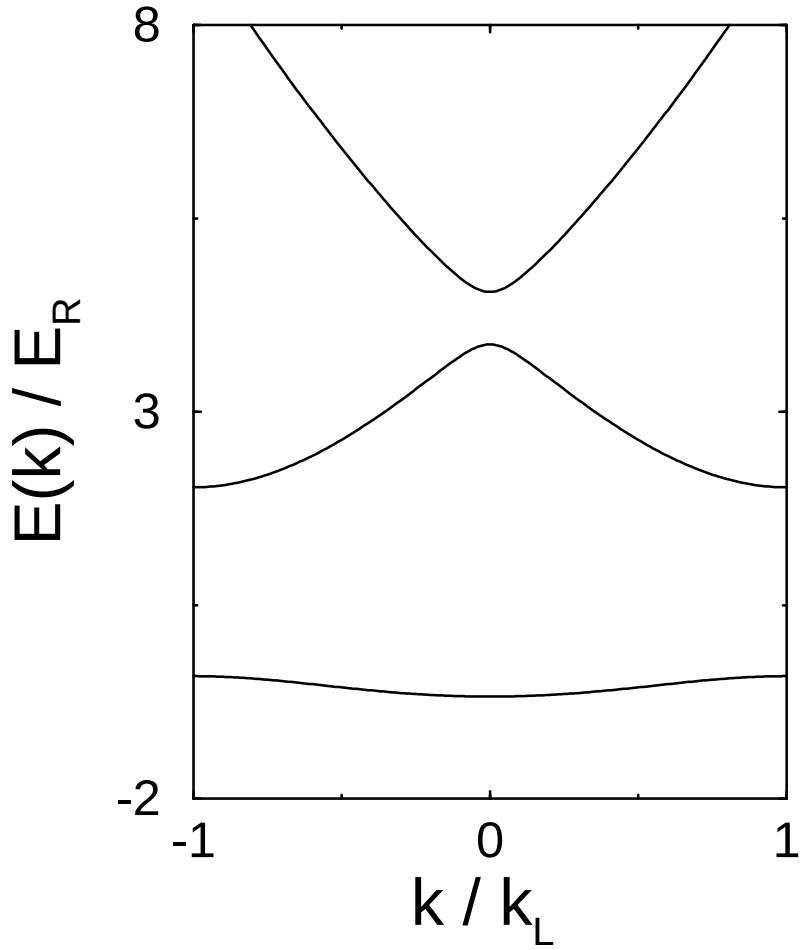

Figure 3.2: Dispersion relations $E_n(k)$ for the lowest three bands of an optical potential with $q = 1.25$, i.e., $V_0/E_R = 5.0$.

Above all, ultracold atoms in standing light waves can be subjected to external forces in a very well-controlled manner. If the standing wave is generated by directing a laser beam against a mirror, one can modulate the position of the mirror periodically by means of a piezoelectric crystal [40]. Denoting the amplitude and frequency of the mirror oscillation by ΔL and ω, respectively, and neglecting retardation effects, the electric field is then given by $\mathcal{E}\cos(k_L[x + \Delta L\cos(\omega t)])\cos(\omega_L t)$, so that the effective Hamiltonian (3.3) is replaced by

$$H_{\text{eff}}^{(1)}(x,t) = \frac{p^2}{2M} + \frac{V_0}{2}\cos(2k_L[x + \Delta L\cos(\omega t)]) \tag{3.7}$$

with $p = (\hbar/i)\mathrm{d}/\mathrm{d}x$. There are two other, unitarily equivalent forms of this Hamiltonian that are of interest. If one transforms the wave functions $|\psi^{(1)}(x,t)\rangle$ that correspond to $H_{\text{eff}}^{(1)}(x,t)$ according to

$$|\psi^{(1)}(x,t)\rangle = \exp\left(\frac{i}{\hbar}\Delta L\cos(\omega t)\,p - \frac{i}{8\hbar}M\,\Delta L^2\omega\sin(2\omega t)\right)|\psi^{(2)}(x,t)\rangle\ , \tag{3.8}$$

then the dynamics of the new wave functions $|\psi^{(2)}(x,t)\rangle$ are governed by

$$H^{(2)}_{\text{eff}}(x,t) = \frac{1}{2M}\Big[p - M\,\Delta L\,\omega\sin(\omega t)\Big]^2 + \frac{V_0}{2}\cos(2k_L x) - \frac{1}{4}M\,(\Delta L\,\omega)^2\,, \tag{3.9}$$

and the further transformation

$$|\psi^{(2)}(x,t)\rangle = \exp\left(\frac{i}{\hbar}M\,\Delta L\,\omega\,\sin(\omega t)x\right)|\psi^{(3)}(x,t)\rangle \tag{3.10}$$

yields

$$H^{(3)}_{\text{eff}}(x,t) = \frac{p^2}{2M} + \frac{V_0}{2}\cos(2k_L x) + K_1 x\cos(\omega t) - \frac{1}{4}M\,(\Delta L\,\omega)^2\,. \tag{3.11}$$

Hamiltonian operators of these types are usually encountered when studying laser-atom interaction within the dipole approximation [35]. The Hamiltonian $H^{(3)}_{\text{eff}}(x,t)$ describes a particle driven by a monochromatic force of frequency ω and strength

$$K_1 = M\,\Delta L\,\omega^2$$

that is coupled to the particle in the "length gauge"; $H^{(2)}_{\text{eff}}(x,t)$ describes the same situation in the "velocity gauge" (i.e., by minimum coupling). The term $M\,(\Delta L\,\omega)^2/4$ is exactly the "ponderomotive energy" [31] of the particle, i.e., the mean kinetic energy associated with its quiver motion due to the oscillating force. The original Hamiltonian $H^{(1)}_{\text{eff}}(x,t)$ with its oscillating potential describes the dynamics in the Kramers-Henneberger frame [36].

It should be pointed out that there are other ways of exerting forces on the atoms than to modulate the position of a mirror. If one splits the output of a laser into two beams, lets them counterpropagate against each other, and introduces a small time-dependent frequency difference $\delta\nu(t)$ between the two travelling light waves that now create the optical potential, then the reference frame in which the potential is stationary moves with velocity $\delta\nu(t)\lambda_L/2$, so that the atoms experience in that frame an inertial force $-Ma(t) = -M\lambda_L\frac{\mathrm{d}}{\mathrm{d}t}\delta\nu(t)/2$. For instance, if the frequency difference is ramped up at a constant rate, one obtains a uniformly accelerated potential $V_0/2\cdot\cos(2k_L[x - at^2/2])$, which, by transformations analogous to those leading from (3.7) to (3.11), translates into $V_0/2\cdot\cos(2k_L x) + axM$ in the stationary frame. "Accelerated standing light waves" thus provide a means to investigate the effect of a *constant*, spatially homogeneous force field on Bloch particles. This is the principle that has been exploited recently to study Wannier-Stark ladders [92, 120] and Bloch oscillations [7] of ultracold atoms in optical potentials.

Likewise, ultracold atoms in *periodically* modulated standing light waves mimic particles in spatially periodic potentials under the influence of a periodically oscillating force and can therefore be employed to investigate the effects of a strong external periodic drive on the Bloch dynamics. Experiments with this goal are presently also being performed

with electrons in semiconductor superlattices that are exposed to strong far-infrared laser fields [45, 62, 72, 73, 115]. But whereas these experiments are plagued by dissipation, lattice defects, and the Coulomb interaction among the electrons, ultracold atoms can be expected to show the basic effects with paradigmatic clarity. Hence, it appears not unlikely that solid state physics and atom optics will develop a common branch in the near future.

Before examining the dynamics of periodically driven ultracold atoms in optical potentials in more detail, it will be useful to express the underlying Hamiltonian (3.7) in terms of dimensionless quantities. We introduce again the spatial coordinate $z = k_L x$ that occurs already in the Mathieu equation (3.5), together with the time variable $\tau = \omega t$. Then, defining $|\widetilde{\psi}\,(z,\tau)\rangle \equiv |\psi^{(1)}\,(x,t)\rangle$ and multiplying the Schrödinger equation by $2\omega_R/(\hbar\omega^2)$, where $\omega_R = E_R/\hbar$ is the atomic single-photon recoil frequency, one arrives at the equation [1]

$$i\hbar_{\text{eff}}\frac{\partial}{\partial\tau}|\widetilde{\psi}(z,\tau)\rangle = \left(-\frac{\hbar_{\text{eff}}^2}{2}\frac{\partial^2}{\partial z^2} + \frac{\gamma}{2}\cos(2[z+\beta\cos(\tau)])\right)|\widetilde{\psi}(z,\tau)\rangle$$

that contains only three parameters:

$$\begin{aligned}
&\text{effective Planck constant} : \quad \hbar_{\text{eff}} = 2\frac{\omega_R}{\omega} \\
&\text{driving strength} \quad : \quad \beta \;\; = k_L\,\Delta L \\
&\text{well depth} \quad : \quad \gamma \;\; = \frac{2V_0\,\omega_R}{\hbar\omega^2}
\end{aligned}$$

Note that γ is related to the Mathieu parameter q by

$$q = \frac{\gamma}{2\hbar_{\text{eff}}^2}\,.$$

Large values of q, which imply that there are at least several tightly bound energy bands for $\beta = 0$, correspond to small values of $\hbar_{\text{eff}}$, which characterise the regime of semiclassical dynamics. Moderate values of q, on the other hand, can be obtained with an effective Planck constant of order unity, indicating the deep quantum regime. In that case the driving frequency ω is not too different from the recoil frequency ω_R.

Since q is proportional to the intensity of the laser field and inversely proportional to the detuning δ_L, one has to work with small detunings in order to achieve large q with readily available intensities. However, the value of the detuning governs the time scale τ_{sp} for spontaneous emission, i.e., the time scale during which the effective Hamiltonian (3.7) retains its validity [41] — the larger δ_L, the longer τ_{sp}. To give the reader an impression of the range of parameters that is presently accessible, we quote the relevant numbers

[1] The scaling employed here differs slightly from that in reference [40], since we use the coordinate $z = k_L x$ (rather than $2k_L x$) in order to stay close to the Mathieu equation (3.5).

from two recent milestone experiments. In a set-up that led to the direct observation of the quantum mechanical suppression of classical diffusive motion, Moore et al. [91] employed the $(3S_{1/2}, F = 2) \rightarrow (3P_{3/2}, F = 3)$ transition at 589 nm in sodium, so that $\omega_0/2\pi = 5.09 \cdot 10^{14}$ Hz. The authors worked with the detuning $\delta_L/2\pi = 5.4 \cdot 10^9$ Hz and the Rabi frequency $\Omega/2\pi = 3.45 \cdot 10^8$ Hz. The separations of time scales required to establish the effective Hamiltonian, $\Omega \ll \delta_L \ll \omega_0$, are thus guaranteed. Since the recoil frequency of the sodium atoms amounts to $\omega_R/2\pi = 25 \cdot 10^3$ Hz for the chosen laser frequency and since the driving frequency $\omega/2\pi$ was $1.3 \cdot 10^6$ Hz, the remaining parameters are $\hbar_{\text{eff}} = 0.038$ and $q = 55$ (or $\gamma = 0.16$). This experiment clearly falls into the semiclassical regime; the authors estimate that probabilities for spontaneous emission ranged between 10% and 20% during the 10 μs that the modulated standing wave was turned on [91]. In a different experiment designed to observe Bloch oscillations of ultracold atoms, Ben Dahan et al. [7] worked with the $6S_{1/2} \rightarrow 6P_{3/2}$ transition in cesium at $\lambda_L = 852$ nm, hence $\omega_0/2\pi = 3.52 \cdot 10^{14}$ Hz. The detuning was $\delta_L/2\pi = 3 \cdot 10^{10}$ Hz; the Rabi frequencies $\Omega/2\pi$ ranged from 0 to about $4 \cdot 10^7$ Hz, giving values of q up to 1.5. The recoil frequency now is $\omega_R/2\pi = 2.07 \cdot 10^3$ Hz, so that a driving frequency $\omega/2\pi$ of 10^3 Hz — 3 orders of magnitude lower than in the former experiment! — would give $\hbar_{\text{eff}} \approx 4$, pushing the dynamics into the deep quantum regime. Since the spontaneous emission rate is at most $4\ \text{s}^{-1}$ for this situation [7], one could follow the time evolution for about hundred cycles of the external drive under almost ideal conditions.

3.2 Driven deep optical lattices: semiclassical dynamics

We now fix the potential strength $q = 100$ (or $V_0 = 400\, E_R$), which means that the undriven lattice admits 13 energy bands below the maxima of the potential barriers. The driving frequency is then chosen such that the band edge $k/k_L = 0$ of the sixth band is exactly resonant, i.e.,

$$\frac{E_5'(0)}{E_R} \equiv \frac{E_6(0) - E_4(0)}{2E_R} = \frac{\omega}{\omega_R}\ , \tag{3.12}$$

which yields the parameters

$$\hbar_{\text{eff}} = 0.0593 \qquad \text{and} \qquad |\gamma| = 0.704\ . \tag{3.13}$$

In this case the tunnelling between the individual wells, i.e., the band aspect of the problem, will play only a minor role. Since $\hbar_{\text{eff}} \ll 1$, a first glimpse of the dynamics can be obtained by studying the purely classical Hamiltonian

$$H_{\text{class}} = \frac{p_z^2}{2} + \frac{\gamma}{2}\cos(2[z + \beta\cos(\tau)])\ , \tag{3.14}$$

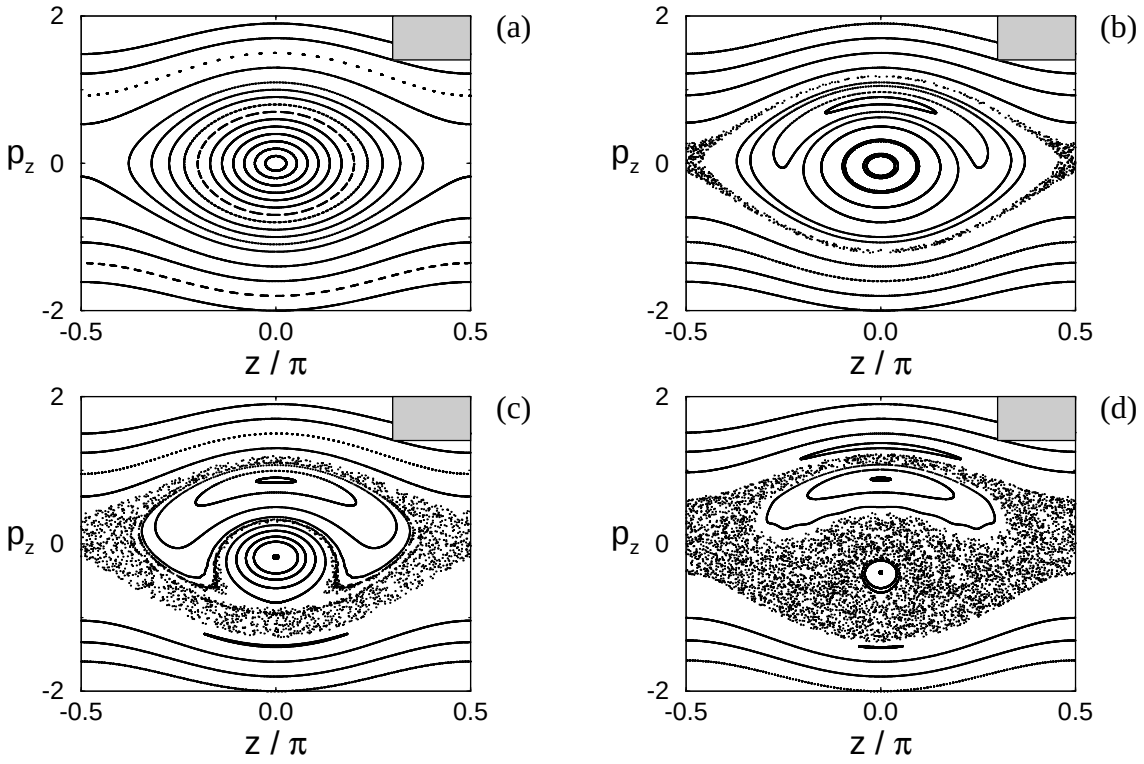

Figure 3.3: Poincaré sections for the classical driven pendulum (3.14) with $\gamma = -0.704$, taken at $\tau = 3\pi/2 \bmod 2\pi$ for $\beta = 0.0$ (a), 0.01 (b), 0.05 (c), and 0.10 (d). The area of the box in the upper right corners is $2\pi\hbar_{\text{eff}}$ with $\hbar_{\text{eff}}$ as given by (3.13), corresponding to the area "occupied" by a Floquet state.

where the coordinate $z \equiv z + \pi$ is taken modulo π, and p_z is the canonically conjugate momentum. Then (3.14) describes a periodically driven pendulum [39]. The figures 3.3 a–d show Poincaré sections for this system with $\beta = 0$ (a), 0.01 (b), 0.05 (c), and 0.10 (d). Whereas figure 3.3 a depicts simply the familiar phase space portrait of an unperturbed pendulum, one sees the emergence of a $1:1$ resonance zone [82] for $\beta > 0$: when the energy of the particle is such that the period of unperturbed motion coincides with the period of the external driving force, there is a stable (elliptic) periodic orbit with the same period as the drive. This orbit is circumvented in phase space by a zone of predominantly regular resonant motion, so that most of the trajectories starting close to the stable periodic orbit are confined to invariant periodic vortex tubes surrounding the orbit. This zone is visible as the banana-shaped region in figure 3.3 b. The second main effect of the periodic drive, the separatrix splitting [82], leads to the appearance of a stochastic layer close to the separatrix curve of the original pendulum. Both the stochastic layer and the regular resonance zone grow when β is enhanced (figure 3.3 c), at the expense of that part of phase space that still supports motion of the same type as prevailing in the unperturbed pendulum. At $\beta = 0.1$ this latter part has become much smaller than the resonance zone, both being embedded in a stochastic sea.

What is the effect of such a restructuring of the classical phase space on quantum mechanics? The scale of classical phase space structures that can still be resolved by quantum mechanical wave functions is determined by the magnitude of $\hbar_{\text{eff}}$, i.e., by the ratio of the atomic recoil frequency and the driving frequency. In our case, the choice (3.13) corresponds to the area $2\pi\hbar_{\text{eff}}$ that is indicated in the upper right corners of the Poincaré sections: the newly emerging classical resonance zone should influence several quantum states already for $\beta \approx 0.05$.

Since the Hamiltonian (3.7) is periodic in both space and time,

$$H^{(1)}_{\text{eff}}(x,t) = H^{(1)}_{\text{eff}}(x+d,t) = H^{(1)}_{\text{eff}}(x,t+T)$$

(where $T = 2\pi/\omega$), there is a distinguished set of solutions to the time-dependent Schrödinger equation of the Floquet form

$$|\psi^{(1)}_{n,k}(x,t)\rangle = |w_{n,k}(x,t)\rangle \exp\left(ikx - i\frac{\varepsilon_n(k)\,t}{\hbar}\right) .$$

Because of the spatial periodicity the quasimomentum k remains a good quantum number, and because of the temporal periodicity there are quasienergies $\varepsilon_n(k)$, where again n is the band index. The functions $|w_{n,k}(x,t)\rangle$ inherit the symmetries of $H^{(1)}_{\text{eff}}(x,t)$, so that $|w_{n,k}(x,t)\rangle = |w_{n,k}(x+d,t)\rangle = |w_{n,k}(x,t+T)\rangle$.

Imposing the periodic boundary condition $z \equiv z + \pi$ on the classical Hamiltonian (3.14) is tantamount to considering only the band edges with $k/k_L = 0$ in the quantum case, which is justified as long as the bands remain sufficiently thin. Figure 3.4 depicts the quasienergies $\varepsilon_n(0)$ that emerge from the unperturbed bands $n = 0$ to 18. Because quasienergies are defined modulo $\hbar\omega$ (just as the quasimomenta are defined modulo $\hbar \cdot 2\pi/d$), this spectrum appears a bit complicated on the first glance, but it actually shows the effect of the classical resonance in great clarity. To see this, consider an arbitrary one-dimensional anharmonic oscillator H_0 with energy eigenvalues E_n and eigenstates $|n\rangle$, so that $H_0|n\rangle = E_n|n\rangle$. Assume that the anharmonicity is weak, i.e., that the level spacing varies sufficiently slowly so that the formal derivative E'_n of the eigenvalues with respect to the quantum number n (defined in analogy to equation (3.12)) is meaningful. Assume further that this system is driven by an external force, so that the total Hamiltonian is $H_0 + K_1 x\cos(\omega t)$, and that the frequency ω is chosen such that $E'_r = \hbar\omega$ for a certain resonant level r (as we have $r = 5$ in (3.12)). Expanding the energy eigenvalues up to second order around E_r, and employing the rotating wave approximation, the ansatz

$$|\psi(x,t)\rangle = \sum_n c_n(t)|n\rangle \exp\left(-i\left[(n-r)\omega + \frac{E_r}{\hbar}\right]t\right) \tag{3.15}$$

for the wave functions then yields

$$i\hbar\dot{c}_n(t) = \frac{1}{2}(n-r)^2 E''_r c_n(t) + \frac{K_1}{2}\Big[\langle n|x|n-1\rangle c_{n-1}(t) + \langle n|x|n+1\rangle c_{n+1}(t)\Big] .$$

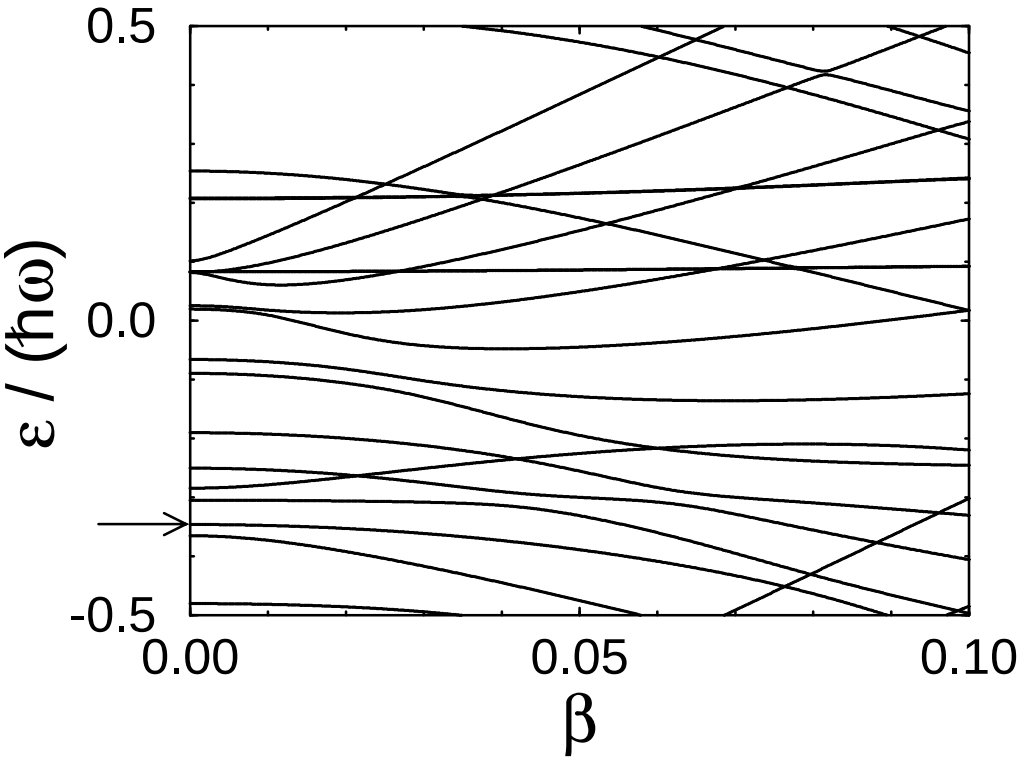

Figure 3.4: One Brillouin zone of quasienergies (ranging from $-\hbar\omega/2$ to $+\hbar\omega/2$) for ultracold atoms in a modulated standing light wave with $\hbar_{\text{eff}} = 0.0593$ and $\gamma = 0.704$. The quasienergies shown are those for the band edge $k/k_L = 0$, with $n = 0, \ldots, 18$. The arrow indicates the quasienergy originating from the $n = 0$–ground state of the undriven system.

When all the matrix elements $K_1\langle n|x|n \pm 1\rangle/2$ are approximated by a constant V that is independent of n, and neglecting the fact that $n \geq 0$ in (3.15), this is just the Fourier transform of a Mathieu equation: setting

$$c_n(t) = \frac{1}{\pi}\int_0^{\pi} \mathrm{d}Z\, \chi(Z) \exp\left(i \left[2(n-r)Z - \frac{Wt}{\hbar} \right] \right)$$

with a π-periodic function $\chi(Z) = \chi(Z + \pi)$, one obtains

$$\chi''(Z) + [A - 2Q\cos(2Z)]\,\chi(Z) = 0 \tag{3.16}$$

with

$$A = \frac{8W}{E_r''} \qquad \text{and} \qquad Q = \frac{8V}{E_r''}\ .$$

Since the required π-periodic Mathieu functions $\chi(Z)$ exist only if $A = A_N$ equals one of the characteristic values $\alpha_N^{(0)}(Q)$ defined in equation (3.6), the functions $\chi(Z) = \chi_N(Z)$ and the energies $W = W_N$ carry a discrete label $N = 0, 1, 2, \ldots$. Starting now from a particular,

normalised Mathieu function $\chi_N(Z)$, one finds the coefficients

$$\begin{aligned} c_n^{(N)}(t) &= \frac{1}{\pi}\int_0^\pi \mathrm{d}Z\, \chi_N(Z)\exp\!\left(i\left[2(n-r)Z - \frac{W_N\, t}{\hbar}\right]\right) \\ &\equiv \chi_{n-r}^{(N)}\, \exp\!\left(-i\frac{W_N\, t}{\hbar}\right)\ , \end{aligned}$$

which, in turn, yield the wave functions

$$\begin{aligned} |\psi_N(x,t)\rangle &= \left(\sum_n \chi_{n-r}^{(N)}\, |n\rangle e^{-i(n-r)\omega t}\right)\exp\!\left(-i\frac{[E_r + W_N]\, t}{\hbar}\right) \\ &\equiv |u_N(x,t)\rangle\exp\!\left(-i\frac{\varepsilon_N t}{\hbar}\right)\ . \end{aligned} \tag{3.17}$$

In order to be consistent, this approximation requires that the Fourier coefficients $\chi_{n-r}^{(N)}$ be negligibly small for $n < 0$. Since the functions $|u_N(x,t)\rangle$ defined in (3.17) are T-periodic, each $|\psi_N(x,t)\rangle$ is a Floquet state with quasienergy [53]

$$\begin{aligned} \varepsilon_N &= E_r + W_N \quad \mod \hbar\omega \\ &= E_r + \frac{1}{8}E_r''\,\alpha_N^{(0)}(Q) \quad \mod \hbar\omega\ . \end{aligned} \tag{3.18}$$

Note that the above analysis refers to the Hamiltonian (3.11), so that one has to subtract the ponderomotive energy from the quasienergies (3.18) before comparing them to the numerically computed data.[2]

In order to apply this approximation to the situation considered in figure 3.4, we first have to estimate the Mathieu parameter Q. Approximating the dipole matrix elements of the pendulum by those of a harmonic oscillator, one obtains

$$Q \approx \frac{4\sqrt{r+1}\,\beta}{\sqrt[4]{q}\,\hbar_{\mathrm{eff}}^2\,(E_r''/E_R)}\ ,$$

which gives

$$Q \approx -664\,\beta \tag{3.19}$$

for the present parameters. Figure 3.5 then shows the approximate quasienergies (3.18), corrected for the ponderomotive energy, for $N = 0, \ldots, 9$. This spectrum appears upside down as compared to the characteristic values in figure 3.1, since $E_5''/E_R < 0$, so that the effective mass of the excitations described by (3.16) is negative. Obviously the approximation compares reasonably well with the exact quasienergies in figure 3.4, in spite of the somewhat crude assumptions in its derivation.

[2]The transformations (3.8) and (3.10) are not only unitary but also T-periodic, and thus preserve the quasienergy spectrum.

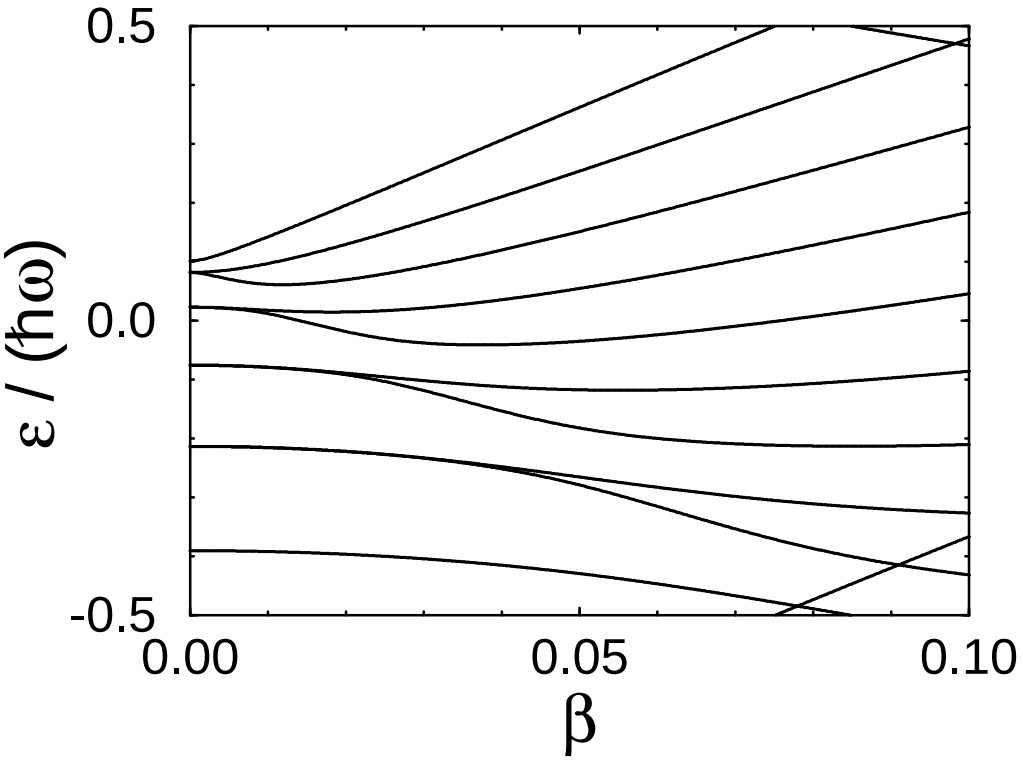

Figure 3.5: Evaluation of the approximation (3.18) for the situation considered in figure 3.4, corrected for the ponderomotive energy shift. Note that the spectrum appears upside down as compared to the characteristic values shown in figure 3.1, since the effective mass of the excitations described by equation (3.16) is negative.

The key point to observe is that the reorganisation of the classical phase space corresponds to a reorganisation of the quantum mechanical level structure. Whereas the undriven optical lattice is described by the Mathieu equation (3.5) (with lowercase parameters), the dynamics under the influence of a weak, resonant periodic force are governed by another Mathieu equation (3.16) (with uppercase parameters). This reorganisation is expressed formally by the appearance of a new quantum number: the "resonant" state with $n = r$ becomes a "ground state" with $N = 0$; the unperturbed states with $n = r \pm 1$ become states with $N = 1, 2$; and so on. The new quantum number, in turn, is reflected in the nodal structure of the wave functions. As an example we display in figure 3.6 the metamorphosis of the unperturbed state $n = r = 5$ into the ground state $N = 0$, at the edge $k/k_L = 0$.

The appearance of the new quantum number can easily be understood from a semiclassical point of view. The semiclassical construction of Floquet states [16] relies on the quantisation of temporally periodic vortex tubes in the extended phase space spanned by position, momentum, and time. In our case there are two types of such vortex tubes: those surrounding the stable periodic orbit that originates from the stable equilibrium of the undriven pendulum,

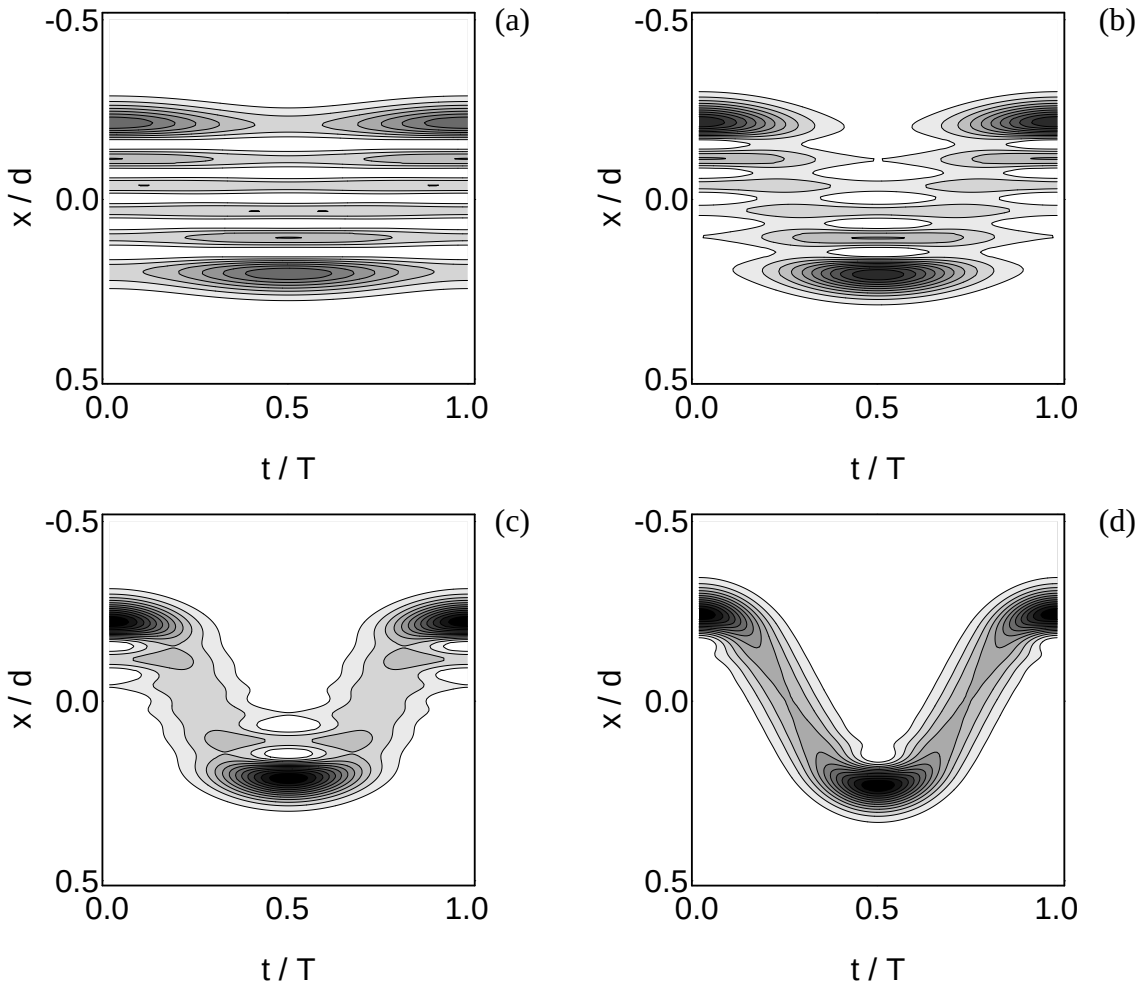

Figure 3.6: Contour plots of the density of a Floquet state with $k/k_L = 0$ in a driven optical lattice, showing the metamorphosis from an unperturbed state with $n = r = 5$ to a driven ground state with $N = 0$. The frame of reference chosen for this calculation corresponds to the Hamiltonian $H^{(2)}_{\text{eff}}$, see (3.9). The driving amplitudes are $\beta = 0.001$ (a), 0.003 (b), 0.01 (c), and 0.05 (d).

and those surrounding the stable periodic orbit brought about by the $1:1$ resonance. The former are associated with the original quantum number n, the latter with the new quantum number N. Intersections of both types of tubes with the plane $\tau = 3\pi/2$ appear as closed contours in figures 3.3 b–d. The phase space area associated with the N-type states (and, hence, the total number of Floquet states accessible to the Mathieu approximation (3.16)) grows when the driving amplitude β (and hence Q) is increased, whereas the phase space area associated with *bound* n-type states decreases, until at $\beta \approx 0.1$, when the magnitude of the new Mathieu parameter Q has become comparable to that of the old q (see (3.19)), the old quantum number n becomes meaningless, as far as bound ("below barrier"-) states are concerned. Mathematically, the crossover from n- to N-type Floquet states, as illustrated in

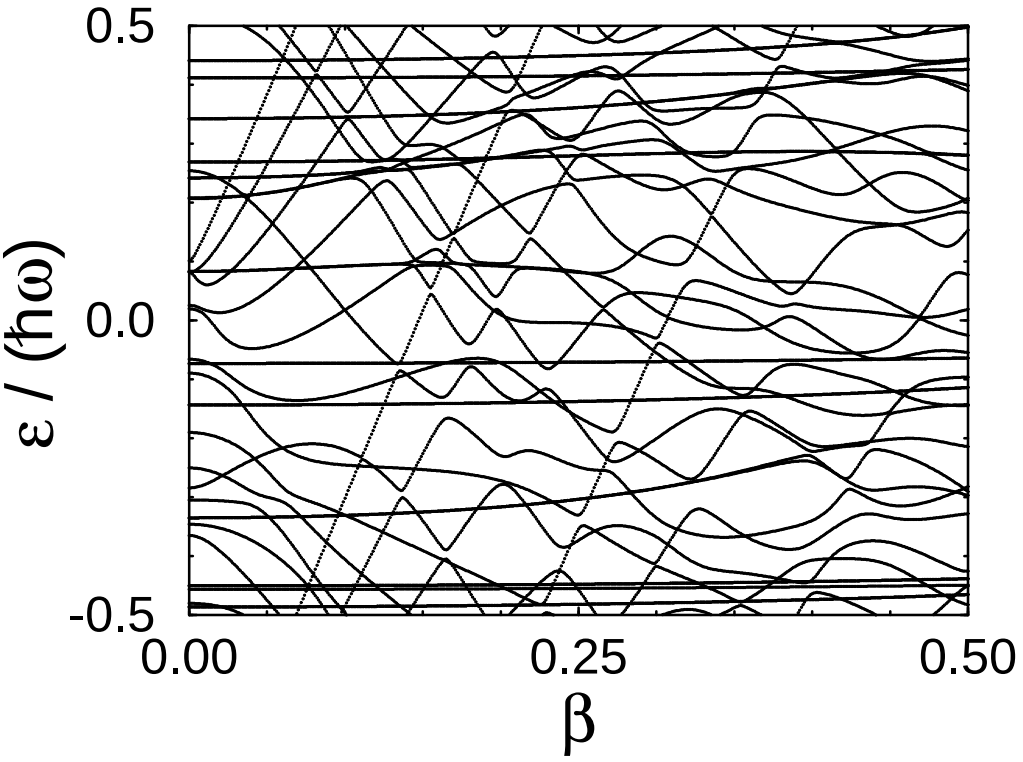

Figure 3.7: Behaviour of the quasienergies for larger driving strengths β; the values of $\hbar_{\text{eff}}$ and γ are the same as in figure 3.4. Note the gradual breakdown of the Mathieu approximation.

figure 3.6, is closely related to crossing the "$a = 2q$"-line in figure 3.1 (though it is "$A = 2Q$" here).

But this qualitative reasoning, although it clearly captures a good deal of truth, has serious drawbacks. On the one hand, it ignores the destruction of invariant vortex tubes and the appearance of chaotic motion in the classical system, on the other, the assumptions made to derive the second, approximate Mathieu equation (3.16) can not be justified for large β. Whereas this equation can describe the actual level structure reasonably well up to $\beta \approx 0.1$ (cf. figures 3.4 and 3.5), even though for $\beta = 0.1$ a major fraction of phase space is already occupied by chaotic motion (cf. figure 3.3 d), the character of the spectrum changes gradually when β is enhanced beyond 0.1, as shown in figure 3.7. The destruction of the classical islands of regular motion is reflected by the appearance of more and more avoided crossings in the quantum spectrum, until there is no discernible regularity left. It is precisely the ability to control the two relevant parameters β — which determines the degree of classical nonintegrability — and $\hbar_{\text{eff}}$ — which determines the magnitude of those phase space structures that can still be resolved in quantum mechanics — that makes ultracold atoms in deep, driven optical lattices most promising for the further study of how the classical transition from regular

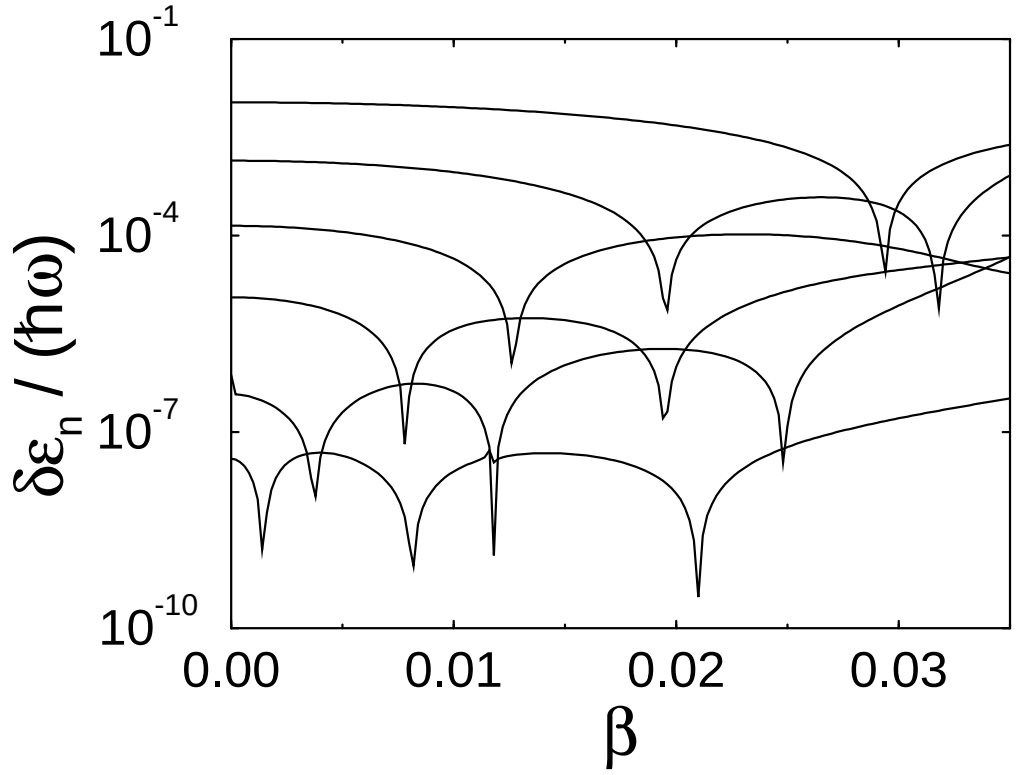

Figure 3.8: Width of the quasienergy bands $n = 5$ to $n = 10$ in the presence of weak driving forces. The values of $\hbar_{\text{eff}}$ and γ are the same as in figure 3.4.

to chaotic motion reflects itself in quantum mechanics [6, 91, 99, 100]. Many aspects of this question are still only improperly understood. For example, the little regular n-type island that is still visible in the Poincaré section at $\beta = 0.1$ has an area that is clearly smaller than $1/2 \cdot 2\pi\hbar_{\text{eff}}$, which means that the vortex tube associated with the original $n = 0$-ground state has already been destroyed — but the inspection of the quasienergy $\varepsilon_{n=0}$ in figure 3.4 reveals no sign of this destruction. What, then, determines the perturbation strength at which a particular quantum state is "visibly" affected by the chaotic motion in the corresponding classical system?

The considerations so far have entirely neglected quantum tunnelling. Strictly speaking, Floquet states that can be constructed semiclassically by vortex-tube quantisation in the individual wells correspond to Wannier states of the lattice, from which bands are formed by well-to-well hopping. Defining the relevant tunnelling time scale T_n for the n-th band by $\delta\varepsilon_n T_n/\hbar = 2\pi$, where $\delta\varepsilon_n = |\varepsilon_n(0) - \varepsilon_n(k_L)|$ is the quasienergy bandwidth, one obtains $T_n/T = (\delta\varepsilon_n/(\hbar\omega))^{-1}$. Figure 3.8 displays the bandwidths for small β, and $n = 5, \ldots, 10$. Obviously quantum tunnelling will not be important for the parameters considered here, if the experiment lasts only some ten cycles T of the driving force [91]. Nevertheless, figure 3.8 reveals an important fact: the quasienergy bandwidths depend strongly on the driving

amplitude; at certain values of β the quasienergy bands are by orders of magnitude thinner than the original energy bands. This effect will play a major role in the following section.

3.3 Driven far-detuned lattices: dynamic localisation and the Harper model

We now consider a quite different situation: the Mathieu parameter q is assumed to be of order unity, so that there are only one or two tightly bound energy bands, and the driving frequency is assumed to be small in comparison with the gap between the two lowest bands, so that interband transitions can be neglected and the dynamics remain restricted to the lowest band, provided the atoms are sufficiently cold. Such low-q, large-$\hbar_{\text{eff}}$ lattices can be realised with lasers detuned far from the atomic resonance, thus guaranteing large spontaneous emission times. Denoting the lowest-band Wannier state that is centred around the ℓ-th site of the optical lattice by $|\ell\rangle$, taking into account only nearest-neighbour hopping matrix elements, and omitting the ponderomotive energy shift, the single-band tight-binding approximation to the Hamiltonian (3.11) reads

$$H_{\text{tb}}^{(3)}(t) = -\frac{\Delta_0}{4}\sum_{\ell}\Big(|\ell+1\rangle\langle\ell| + |\ell\rangle\langle\ell+1|\Big) + K(t)\sum_{\ell}|\ell\rangle\ell d\langle\ell| \;, \tag{3.20}$$

where Δ_0 is the width of the unperturbed lowest energy band, and we have admitted a force

$$K(t) = K_0 + K_1\cos(\omega t)$$

containing both a static and an oscillating component. The energy eigenstates for the undriven lattice, i.e., the Bloch waves, take the form

$$|\varphi_k\rangle = \sum_{\ell} e^{ik\ell d}|\ell\rangle \;; \tag{3.21}$$

their dispersion relation is

$$E_0(k) = -\frac{\Delta_0}{2}\cos(kd) \;. \tag{3.22}$$

Because there is no coupling to other bands, it is not difficult to solve the time-dependent Schrödinger equation with the Hamiltonian (3.20). Introducing the potential $A(t) = -K_0 t - K_1\sin(\omega t)/\omega$ and transforming $|\psi^{(3)}(t)\rangle = \exp(iA(t)x/\hbar)\,|\psi^{(2)}(t)\rangle$, where $x \equiv \sum_\ell |\ell\rangle\ell d\langle\ell|$, one obtains

$$H_{\text{tb}}^{(2)}(t) = -\frac{\Delta_0}{4}\sum_{\ell}\left[\exp\left(-i\frac{A(t)\,d}{\hbar}\right)|\ell+1\rangle\langle\ell| + |\ell\rangle\langle\ell+1|\exp\left(+i\frac{A(t)\,d}{\hbar}\right)\right] . \tag{3.23}$$

Since the Bloch waves (3.21) obey the equation $H_{\rm tb}^{(2)}(t)\,|\varphi_k\rangle = E(\kappa_k(t))\,|\varphi_k\rangle$, where

$$\kappa_k(t) = k + \frac{A(t)}{\hbar}\ ,$$

it follows immediately that a complete set of solutions to the Schrödinger equation with the Hamiltonian (3.23) is provided by the wave functions

$$|\psi_k^{(2)}(t)\rangle = \sum_\ell |\ell\rangle \exp\!\left(ik\ell d - \frac{i}{\hbar}\int_0^t \mathrm{d}\tau\, E(\kappa_k(\tau))\right)\ .$$

In the frame of reference pertaining to the Hamiltonian (3.20), they correspond to the functions

$$|\psi_k^{(3)}(t)\rangle = \sum_\ell |\ell\rangle \exp\!\left(i\kappa_k(t)\ell d - \frac{i}{\hbar}\int_0^t \mathrm{d}\tau\, E(\kappa_k(\tau))\right)\ . \tag{3.24}$$

These simple transformations emphasise an important fact. If K_1 vanishes, so that there is only a *constant* force K_0, then $H_{\rm tb}^{(2)}(t)$ is *periodic in time* with the Bloch period $T_{\rm Bloch} = 2\pi\hbar/(K_0 d)$. Hence the Hamiltonian (3.20) actually describes a two-frequency problem; besides the directly apparent ac driving frequency $\omega = 2\pi/T$ there is also the hidden Bloch frequency $\omega_{\rm Bloch} = K_0 d/\hbar$. While the general case should therefore be handled with the tools of the two-colour Floquet theory, the most important special case is quite simple. When the Bloch frequency is an integral multiple of the ac frequency ω, so that

$$\omega_{\rm Bloch} = m\,\omega\ , \tag{3.25}$$

then both (3.20) and (3.23) are merely T-periodic, as is the transformation connecting them. In this case the Floquet states of the Hamiltonian (3.20) coincide with the wave functions (3.24), i.e., we have $|\psi_k^{(3)}\,(t)\rangle = |u_k\,(t)\rangle \exp(-i\varepsilon(k)t/\hbar)$ with T-periodic functions $|u_k(t)\rangle = |u_k(t+T)\rangle$ that are extended over all the lattice, and characterised by a quasimomentum k. The ensuing quasienergy-quasimomentum dispersion relation is [122]

$$\begin{aligned}\varepsilon(k) &= \frac{1}{T}\int_0^T \mathrm{d}t\, E_0(\kappa_k(t)) \quad \mod \hbar\omega \\ &= (-1)^m J_m\!\left(\frac{K_1 d}{\hbar\omega}\right) E_0(k) \quad \mod \hbar\omega\ ,\end{aligned} \tag{3.26}$$

where $J_m(z)$ is an ordinary Bessel function, the order m of which is determined by (3.25) . What is the meaning of this relation? If one considers a Gaussian wave packet

$$|\psi(t)\rangle = \sum_\ell f_\ell(t)|\ell\rangle \tag{3.27}$$

initially centred around the site $\ell = 0$ with momentum $\hbar k_0$, so that

$$f_\ell(0) = \left(\frac{1}{2\pi\sigma_0^2}\right)^{1/4} \exp\!\left(-\frac{\ell^2}{4\sigma_0^2} + ik_0\ell d\right)\ ,$$

and if the width of the packet is large compared to the lattice constant d, so that $\sigma_0 \gg 1$, then a Gaussian approximation shows that the *average* group velocity of the packet is given by

$$\bar{v} = (-1)^m \frac{\Delta_0\, d}{2\hbar}\, J_m\!\left(\frac{K_1 d}{\hbar\omega}\right) \sin(k_0\, d) = \frac{1}{\hbar}\, \frac{\mathrm{d}\varepsilon(k)}{\mathrm{d}\,k}\bigg|_{k_0} . \tag{3.28}$$

Just as the group velocity was determined by the derivative of the unperturbed dispersion relation $E_0(k)$ with respect to k in the undriven case, it is now determined by the derivative of $\varepsilon(k)$. This new dispersion relation also determines the spreading of the wave packet: on the average, i.e., neglecting T-periodic oscillations, the width of the packet develops in time according to

$$\bar{\sigma}(t) = \sigma_0 \left(1 + \left[\frac{\Delta_0\, t}{4\hbar\sigma_0^2}\, J_m\!\left(\frac{K_1 d}{\hbar\omega}\right) \cos(k_0 d)\right]^2\right)^{1/2} . \tag{3.29}$$

Hence, if the ratio $K_1 d/(\hbar\omega)$ equals a zero of the Bessel function J_m, any wave packet becomes dispersionless: it can, on the average, neither move nor spread. This phenomenon has been termed "dynamic localisation" [28, 97]; some indications for its occurrence in terahertz-driven semiconductor superlattices have been reported only recently [73]. But it has to be reemphasised that a proper theory of dynamic localisation in semiconductor superlattices requires a full treatment of the Coulomb interaction among the electrons [86–88], whereas dynamic localisation of ultracold atoms in periodically driven optical lattices would be a genuine single-particle effect.

But is it possible to realise the idealised Hamiltonian (3.20) with sufficient accuracy? To answer this question, we return to the situation considered in figure 3.2, so that $q = 1.25$, $\Delta_0 = 0.264\, E_R$, and the gap between the lowest two bands is $2.44\, E_R$. We then choose the driving frequency $\omega = \omega_R/2$, or $\hbar_{\text{eff}} = 4$, which means that $\hbar\omega$ is almost twice as large as the bandwidth Δ_0, but still almost five times smaller than the band gap. For cesium atoms in far-detuned optical lattices with $\lambda_L = 852$ nm, as used in the recent Bloch-oscillation experiments [7], this choice corresponds to $\omega/2\pi \approx 1$ kHz. We assume a purely sinusoidal drive, $K(t) = K_1 \cos(\omega t)$, so that $m = 0$ and dynamic localisation is expected to occur when the parameter $K_1 d/(\hbar\omega)$ approaches a zero $j_{0,s}$ of J_0, where the band (3.26) collapses. Since $j_{0,1} \approx 2.405$, and since

$$\frac{K_1 d}{\hbar\omega} = \frac{\pi}{\hbar_{\text{eff}}}\, \beta ,$$

the driving amplitude required for the first band collapse corresponds to $\beta \approx 3$, which does not appear to be unrealistically high. Figure 3.9 now shows quasienergies computed from the *full* Hamiltonian (3.7) for $q = 1.25$, $\hbar_{\text{eff}} = 4$ and $k/k_L = 0.0, 0.1, \ldots, 1.0$. The arrows in the left margin indicate the edges of the quasienergy band that originates from the unperturbed

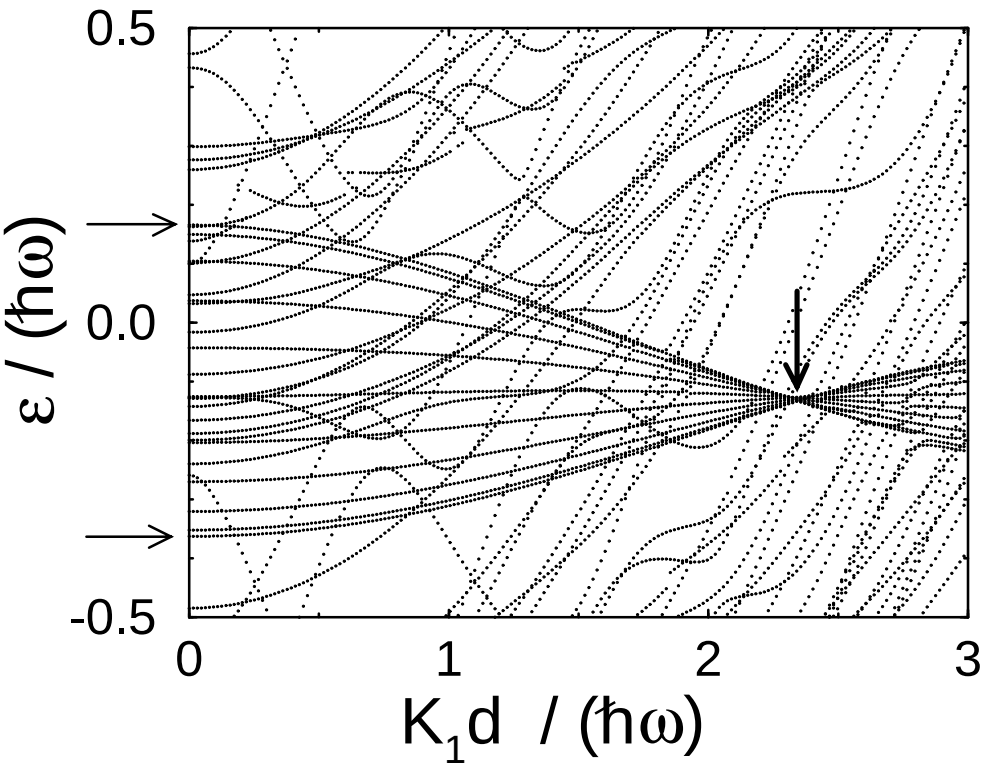

Figure 3.9: Quasienergies computed from the full Hamiltonian (3.7) for $V_0 = 5\,E_R$ and $\omega = \omega_R/2$. The values of k/k_L range from 0.0 to 1.0, in steps of 0.1. Arrows in the left margin indicate the edges of the quasienergy band that originates from the unperturbed ground-state band; a further arrow indicates the approximate collapse of this band at $K_1 d/(\hbar\omega) \approx 2.35$. If the tight-binding approximation (3.20) had been exact, the collapse would have occurred at $K_1 d/(\hbar\omega) = j_{0,1} \approx 2.405$.

ground-state energy band. This quasienergy band is clearly very well described by the tight-binding approximation (3.26) with $m = 0$; in particular, it collapses for $K_1 d/(\hbar\omega) \approx 2.35$, quite close to $j_{0,1}$. It should be noted that this collapse is actually imperfect, i.e., not all band states are exactly degenerate, not only because of residual interband effects, but also because there actually are small next-to-nearest neighbour hopping elements. Hence, the true dispersion relation $E_0(k)$ contains, besides the leading term (3.22), a small correction proportional to $\cos(2kd)$, so that the quasienergy dispersion relation (3.26) acquires a correction proportional to $J_m(2K_1 d/(\hbar\omega))\cos(2kd)$. But a mere glance at figure 3.9 is sufficient to show that the simple Hamiltonian (3.20) catches the main features. Note that the tight-binding approximation applies only to the ground-state band $n = 0$; quasienergies originating from the bands $n = 1$ and $n = 2$ merely form a more or less irregular "background" in figure 3.9.

The possibility to control the bandwidth in optical lattices by a periodic modulation has some interesting consequences. If a wave packet moves in lattice driven by an oscillating

force $K_1 \cos(\omega t)$, one can adjust K_1 such that it stops almost completely, or even *reverses its direction*. The future will show whether this effect can be fruitfully exploited. But even more intriguing phenomena occur if we consider three-level atoms with states $|g\rangle$, $|e_1\rangle$, and $|e_2\rangle$ that are connected by dipole-allowed transitions $|g\rangle \to |e_1\rangle$ and $|g\rangle \to |e_2\rangle$. If these atoms are placed in the field of *two* standing light waves (with wave numbers $k_L^{(1)}$ and $k_L^{(2)}$) that are superimposed along the x-axis, each of them being suitably detuned from one of the transitions, then the generalisation of the steps that led to the effective Hamiltonian (3.3) yields [25]

$$H_{\text{eff}}(x) = -\frac{\hbar^2}{2M}\frac{\mathrm{d}^2}{\mathrm{d}x^2} + \frac{V_0^{(1)}}{2}\cos(2k_L^{(1)}x) + \frac{V_0^{(2)}}{2}\cos(2k_L^{(2)}x + \eta) \;, \tag{3.30}$$

where η is a relative phase. Let us now arrange this set-up such that the first light wave creates a tight-binding system $-(\Delta_0/4)\sum_\ell(|\ell+1\rangle\langle\ell| + |\ell\rangle\langle\ell+1|)$ as before, and that the second light wave is just a weak perturbation. If we then approximate the Wannier functions $|\ell\rangle$ by harmonic-oscillator ground-state functions, we can estimate that the additional potential generated by the second, weak light wave alters the on-site energies by the amounts

$$\nu(\ell) = \nu_0 \cos(2\pi g\ell + \eta) \;,$$

where

$$g = \frac{k_L^{(2)}}{k_L^{(1)}} \qquad \text{and} \qquad \nu_0 = \frac{V_0^{(2)}}{2}\exp\left(-\frac{g^2}{\sqrt{V_0^{(1)}/E_R}}\right) \;,$$

so that the single-band approximation to (3.30) becomes

$$H_{\text{Harper}} = -\frac{\Delta_0}{4}\sum_\ell\Big(|\ell+1\rangle\langle\ell| + |\ell\rangle\langle\ell+1|\Big) + \nu_0\sum_\ell \cos(2\pi g\ell+\eta)|\ell\rangle\langle\ell| \;. \tag{3.31}$$

This is exactly the Harper model, which had originally been designed to describe Bloch electrons in magnetic fields [48, 109, 111]. The most conspicuous feature of this model is that it exhibits a metal-insulator transition: for irrational values of g, all eigenstates are extended for $\nu_0/\Delta_0 < 1/2$, but localised for $\nu_0/\Delta_0 > 1/2$ [111]. To realise the Harper model along the lines we have just indicated, and thus to study a metal-insulator transition with ultracold atoms in standing light waves, should be a most rewarding experiment.

Let us estimate the required magnitude of $V_0^{(2)}$. If we start again with $V_0^{(1)}/E_R = 5$, so that we obtain a tight-binding Hamiltonian with $\Delta_0/E_R = 0.264$ as before, and if g is chosen as the most irrational number, namely as the golden mean, $g = (\sqrt{5}+1)/2$, then the equation $\nu_0/\Delta_0 = 1/2$ fixing the perturbation strength required for the metal-insulator transition yields $V_0^{(2)}/V_0^{(1)} \approx 0.17$: under these conditions, the strength of the second potential should be about 17% of that of the first. This is not really small, and one might wonder whether the

approximation (3.31) that takes into account only the on-site effects of the second potential is really sufficient [25]. We therefore also change the hopping integral connecting $|\ell\rangle$ and $|\ell+1\rangle$ from $\Delta_0/4$ to $\Delta_0/4+\delta(\ell)$, where

$$\delta(\ell) = f\,\nu_0 \cos\left(2\pi g\left[\ell+\frac{1}{2}\right]+\eta\right)\ . \tag{3.32}$$

The parameter f is a dimensionless perturbation strength. We then compute the eigenstates $|\varphi_n\rangle = \sum_\ell a_\ell^{(n)}|\ell\rangle$ numerically for a lattice with 1500 sites, and calculate for each state the standard deviation $\sigma^{(n)}$ of the site-occupation probabilities $|a_\ell^{(n)}|^2$. The average value $\bar\sigma$, normalised by the standard deviation σ_0 for a uniformly extended state, provides a measure for the degree of localisation. Figure 3.10 shows $\bar\sigma/\sigma_0$ as function of ν_0/Δ_0, for $f = 0.0$, 0.2, 0.49, and 0.5. The curves for $f < 0.5$ almost coincide; a violent change of behaviour occurs only for $f = 0.5$, which is by far larger than realistic. This result is quite important: the modulation of the hopping integrals does not destroy the self-duality of the Harper model, which is a crucial ingredient for the explanation of its metal-insulator transition [109, 111]. Hence this transition remains clearly visible even under conditions where the modulation of the hopping integrals is not negligible. A detailed discussion of the extended Harper model is given in the appendix A.

One can, of course, reduce the required strength $V_0^{(2)}$ by enhancing $V_0^{(1)}$ (and thereby reducing Δ_0). But enhancing $V_0^{(1)}$ means employing a more intense laser and thus reducing the spontaneous emission times, which might not be desirable. There is, however, a possible way out of this dilemma. As equations (3.28) and (3.29) have already shown, a tight-binding system (3.20) with bandwidth Δ_0 that is *driven* by a dc force of strength K_0 and an ac force of strength K_1 becomes practically equivalent to an *undriven* system with renormalised bandwidth $(-1)^m J_m\left(K_1 d/[\hbar\omega]\right)\Delta_0$, provided the resonance condition (3.25) is satisfied [56]. This means that one can employ the effect visualised in figure 3.9 to decrease the bandwidth by adding an oscillating force to the system, rather than by increasing the intensity of the laser creating the lattice. For the resonantly driven Harper model, the metal-insulator transition is expected to occur when

$$\left|\frac{\nu_0}{\Delta_0}\right| \approx \frac{1}{2}\left|J_m\left(\frac{K_1 d}{\hbar\omega}\right)\right|\ , \tag{3.33}$$

provided $\hbar\omega$ is large compared to Δ_0 [25]. In general, the time-evolution operator $U(t,0)$ for a periodically driven quantum system can be written as $P(t)\exp(-iGt/\hbar)$ with $P(t) = P(t+T)$; the eigenvalues of the time-independent operator G are the quasienergies. For the driven tight-binding system (3.20), this operator G is just the undriven part of the Hamiltonian (3.20) with renormalised hopping integrals. But for the driven Harper model, the renormalised, undriven Harper Hamiltonian appears only as the dominant term in a high-

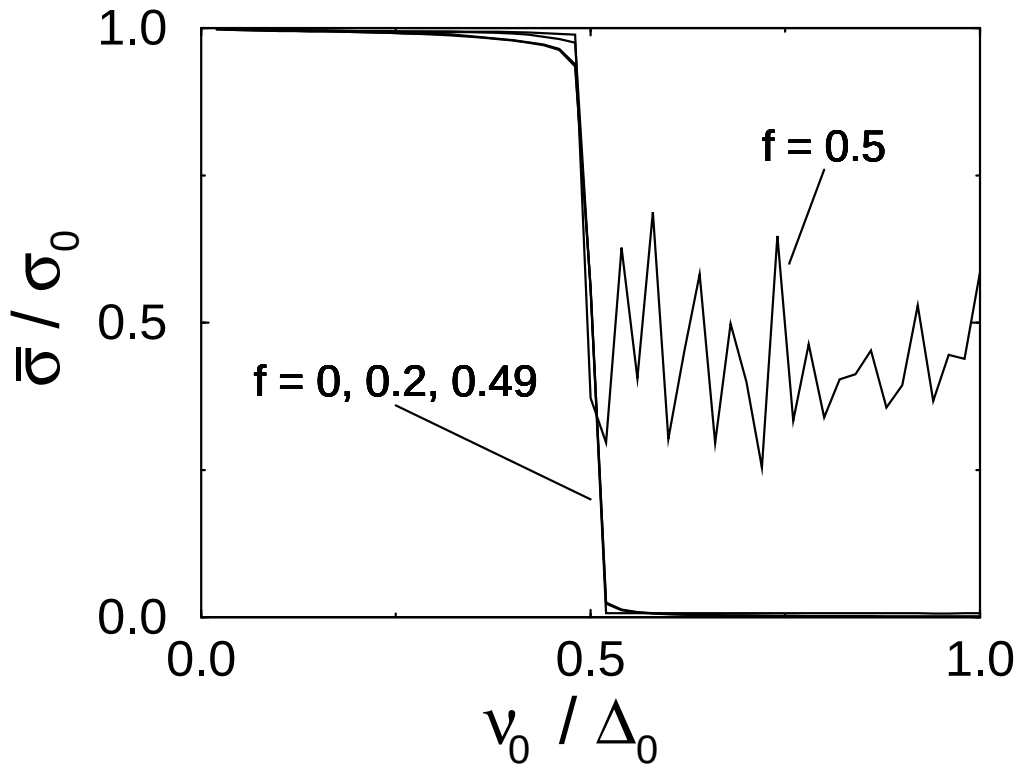

Figure 3.10: Average, normalised standard deviation for the squared expansion coefficients of eigenstates of Harper's model with hopping integrals modified according to (3.32); $\bar{\sigma}/\sigma_0 = 1$ indicates completely delocalised states. Note that curves for $f < 0.5$ fall almost on top of each other.

frequency expansion of G; the leading corrections are of second order in $\Delta_0/(\hbar\omega)$. Therefore, (3.33) can be valid only when $\hbar\omega \gg \Delta_0$. This places an experiment right between Skylla and Charybdis: too small a driving frequency might not work as desired, since G would not be close enough to Harper's Hamiltonian, and too large a frequency will entail undesired interband effects. To indicate that there is viable territory in between, we compare in figure 3.11 the second moments $M_2(t) = \sum_\ell \ell^2 |f_\ell(t)|^2$ of wave functions (3.27) for a Harper model (3.31) sinusoidally driven by $K(t) = K_1 \cos(\omega t)$ to the moments of wave functions for the corresponding undriven models with renormalised hopping elements $\Delta_0\, J_0(K_1 d/(\hbar\omega))/4$. In both cases, lattices with 1001 sites have been employed in the numerical calculations ($\ell_{min} = -500$, $\ell_{\max} = +500$), η has been set to zero, $g = (\sqrt{5}+1)/2$, and the wave functions were initially concentrated on a single site, $f_\ell(0) = \delta_{\ell,0}$. The parameters are $\Delta_0/(\hbar\omega) = 0.385$ and $\nu_0/(\hbar\omega) = 0.1$. Since $\nu_0/\Delta_0 \approx 1/2 \cdot J_0(1.5)$, a change of behaviour is expected for $K_1 d/(\hbar\omega)$ close to 1.5: a wave packet made up of localised states only will stay localised, but otherwise spread indefinitely. Figure 3.11 a shows the evolution of $M_2(t)$ for the driven system with $K_1 d/(\hbar\omega) = 1.3, 1.4, \ldots, 1.9$, whereas figure 3.11 b shows $M_2(t)$ for the corresponding undriven, renormalised systems. Figure 3.12

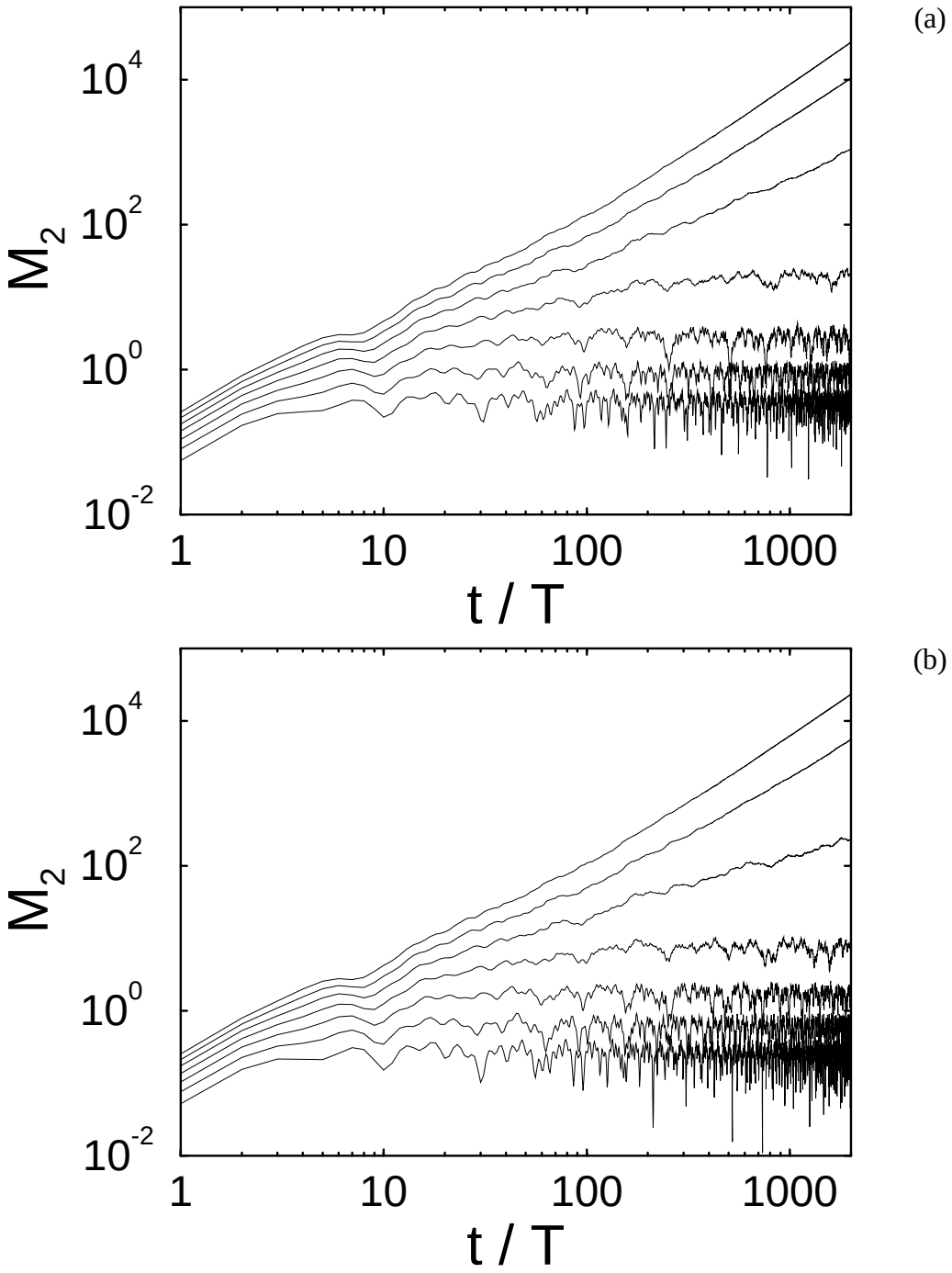

Figure 3.11: Second moments $M_2(t) = \sum_\ell \ell^2 |f_\ell(t)|^2$ for wave functions $|\psi\ (t)\rangle = \sum_\ell f_\ell(t)|\ell\rangle$ of the Harper model (3.31) sinusoidally driven by $K(t) = K_1 \cos(\omega t)$ (a), and for the corresponding undriven Harper models with renormalised hopping elements (b). The parameters are $g = (\sqrt{5}+1)/2$, $\eta = 0$, $\Delta_0/(\hbar\omega) = 0.385$, and $\nu_0/(\hbar\omega) = 0.1$. The driving strength $K_1 d/(\hbar\omega)$ varies from 1.3 to 1.9 (top to bottom), in steps of 0.1. The initial conditions were $f_\ell(0) = \delta_{\ell,0}$; the time t is measured in units of $T = 2\pi/\omega$. The crossover from unbounded to bounded $M_2(t)$ for $K_1 d/(\hbar\omega) \approx 1.5$ signals the metal-insulator transition.

shows the wave functions for the driven system after 2000 cycles, for $K_1 d/(\hbar\omega) = 1.4$ (thin line) and 1.6 (heavy line). In the first case the wave function spreads over all the lattice, but in the second case it stays localised. The almost perfect exponential decay, clearly developed over no less than 25 orders of magnitude, leaves no doubt that we are dealing with a genuine, amplitude-controlled localisation effect. The agreement between the figures 3.11 a

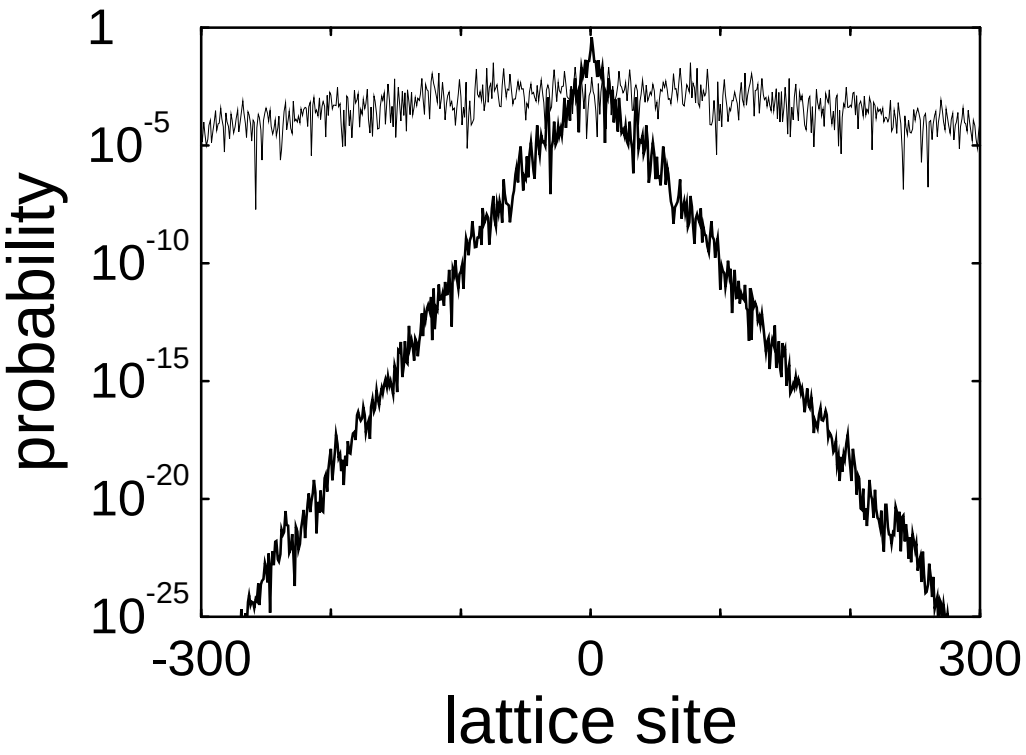

Figure 3.12: Occupation probabilities $|c_\ell(t_0)|^2$ of lattice sites for the periodically driven Harper model (cf. figure 3.11 a) with $K_1 d/\hbar\omega = 1.4$ (thin line) and 1.6 (heavy), at $t_0 = 2000\,T$.

and 3.11 b speaks for itself, fully confirming the above line of reasoning: the metal-insulator transition of the Harper model can be controlled by varying the amplitude of an additional oscillating force.

This finding is certainly interesting for its own sake, but an experimental confirmation might not be easy. Ideally, one would like to prepare a well localised, minimum-uncertainty atomic wave packet, subject it to modulated standing light waves, and finally measure its width after the interaction. Preferably such an experiment should be done with light atoms, such as lithium [4]. However, even in the "metallic phase" an appreciable (and detectable) spreading of the wave packet requires some time, during which the quantum evolution has to remain coherent — which conflicts not only with spontaneous emission, but also with the inevitable laser noise. But in view of the recent experimental progress [7, 120], and considering the

speed at which quantum optics is developing, there seems room for some optimism.

3.4 Conclusions

Ultracold atoms in standing light waves are a rare example of a system that allows us to vary the effective Planck constant, $\hbar_{\text{eff}}$, over about two orders of magnitude, thus bridging the semiclassical and the deep quantum regime. In either regime, a periodic force has major effects. If $\hbar_{\text{eff}} \ll 1$, periodic forcing yields a test system for studying how the classical transition from regular to chaotic motion manifests itself in quantum mechanics. Varying $\hbar_{\text{eff}}$ then enables one to vary the scale at which the quantum system "sees" the classical phase space. In the deep quantum regime, i.e., for $\hbar_{\text{eff}} \approx 1$, one obtains the possibility to investigate the dynamic localisation that accompanies a quasienergy band collapse, under conditions that are perhaps more apt to the original proposal [28, 97] than they could be in a semiconductor superlattice.

One of the most fascinating prospects for future research is the chance to obtain an approximate realisation of Harper's model with ultracold atoms in bichromatic standing light waves. This prospect implies nothing less than the possibility to explore a metal-insulator transition with atomic de Broglie waves — and this transition can even be controlled by an oscillating force, since the amplitude of that force determines the effective nearest neighbour hopping elements. If the rather high coherence demands can be met, quantum optics could thus furnish a major contribution to the experimental study of quasiperiodic systems.

4 Perturbative and nonperturbative processes in adiabatic population transfer

The adiabatic theorem of quantum mechanics [13, 17, 89] states that the wave function of a system governed by a slowly changing Hamiltonian follows the instantaneous eigenstates. With the advent of modern lasers capable of delivering pulses with controllable and reproducible shapes, this concept has gained enormous practical importance for the coherent manipulation of atoms or molecules. For instance, the STIRAP mechanism, which allows one to accomplish highly efficient population transfer in effective three-level systems [19, 78, 105, 108], is based entirely on adiabatic following induced by two partially overlapping laser pulses. It is then of interest to study not only how the system behaves in the adiabatic limit, but also how this limit is approached, that is, how the system responds to parameter variations that do *not* occur "infinitely slowly".

For two-level systems with instantaneous energy eigenvalues that remain nondegenerate for all times, a classic result due to Dykhne [29] and Davis and Pechukas [22] states that deviations from the adiabatic limit are beyond any power of the adiabaticity parameter ε, namely exponentially small in $1/\varepsilon$; an extension of this treatment to N-level systems has been formulated in reference [61]. However, it has recently been discovered by Laine and Stenholm [79] and Vitanov and Stenholm [116] that this exponential dependence breaks down and gives way to a power-law dependence in the case of typical STIRAP models, where the instantaneous eigenvalues become degenerate in both the distant past and distant future. It is now a conceptually important question just how this breakdown of the Dykhne-Davis-Pechukas exponential behaviour comes about, since it is *not* related to any nonsmoothness of the parameter variation. Is there a possibility to compute the deviations from the adiabatic limit in a simple, yet accurate way, even for models that are not analytically solvable?

The answer to this question, which will be given in section 4.5, turns out to be affirmative, and surprisingly simple, but to get to this answer in a systematic fashion requires quite some work. We start in the following section by outlining an iterative scheme [9] that yields superadiabatic bases, i.e., bases which in some sense take over the role which the usual adiabatic basis plays in the limit $\varepsilon \to 0$, so that they are particularly well suited for describing the dynamics for finite ε. In section 4.2 we apply this scheme to the Landau-Zener transition, and show that it behaves quite similar to another superadiabatic scheme investigated in great

detail by Berry [10]: Both schemes yield an optimal basis with respect to which the transition amplitude acquires a universal, error-function-like form. In section 4.3 we then collect the necessary prerequisites of STIRAP, and apply the superadiabatic techniques to a generic three-level system.

The following, more technical section 4.4 then demonstrates that the total transition amplitude, tracked in time in the customary adiabatic basis, can be uniquely decomposed into a nonperturbative component — that is, a component beyond all powers of the adiabaticity parameter ε —, which equals just Berry's universal error function previously met in the optimal superadiabatic basis, and a perturbative component with terms proportional to powers of ε. The fast oscillations that accompany, e.g., the Landau-Zener transition in the adiabatic basis can hence be understood as resulting from the interference of these two parts.

In most cases considered so far, the perturbative component dies out when merely the final transition amplitude is considered, leaving only the nonperturbative component corresponding to the Dykhne-Davis-Pechukas result. This is what is different in the case of STIRAP: As elaborated in section 4.5, the behaviour of the nonadiabatic coupling at infinite times effectuates the survival of the perturbative component. Evaluating this component to lowest nonvanishing order in ε and adding the nonperturbative contribution gives a total transition probability that agrees very favourably with exact numerical data.

This chapter builds on the seminal papers by Davis and Pechukas [22] and by Berry [10], but we have tried to explain all the required technical details, in order to make the key ideas accessible.

4.1 Beyond the adiabatic basis

We consider a Hamiltonian $H^{(0)}$ that describes an N-level system depending slowly on time t, i.e., $H^{(0)} = H^{(0)}(t/T_0)$, where T_0 is some long time scale. $H^{(0)}$ is assumed to be analytic. Transforming to the dimensionless time variable $\tau = t/T_0$, the Schrödinger equation can be written in the form

$$\left(H^{(0)}(\tau) - i\varepsilon\partial_\tau\right)|\psi^{(0)}(\tau)\rangle = 0\,, \tag{4.1}$$

where the small adiabaticity parameter ε is given by the ratio $\hbar/T_0$, scaled by a suitable characteristic energy. For ease of notation, we will often suppress the argument τ in the following.

At each moment τ there are instantaneous eigenstates $|u_j^{(0)}\rangle$ and eigenvalues $E_j^{(0)}$:

$$H^{(0)}|u_j^{(0)}\rangle = E_j^{(0)}|u_j^{(0)}\rangle \tag{4.2}$$

with

$$\langle u_j^{(0)} | u_k^{(0)} \rangle = \delta_{jk} \ .$$

These equations still leave the phases of the eigenstates $|u_j^{(0)}\rangle$ unspecified at each instant τ. We fix these phases by requiring parallel transport [110]

$$\langle u_j^{(0)} | \partial_\tau | u_j^{(0)} \rangle = 0 \tag{4.3}$$

for each state j. Taken together, the instantaneous eigenstates now form the columns of a unitary matrix $U^{(0)}$. Applying the unitary transformation defined by $U^{(0)}$ to the Schrödinger equation, one obtains

$$U^{(0)\dagger} \left(H^{(0)} - i\varepsilon\partial_\tau \right) U^{(0)} \, U^{(0)\dagger} |\psi^{(0)}\rangle \equiv \left(H^{(1)} - i\varepsilon\partial_\tau \right) |\psi^{(1)}\rangle = 0 \ , \tag{4.4}$$

with the transformed wave function

$$|\psi^{(1)}\rangle = U^{(0)\dagger} |\psi^{(0)}\rangle$$

and the new Hamiltonian

$$H^{(1)} = U^{(0)\dagger} H^{(0)} U^{(0)} - i\varepsilon U^{(0)\dagger} \left(\partial_\tau U^{(0)} \right) \ .$$

By construction, the first term on the r.h.s. is a diagonal matrix with elements $E_j^{(0)}$, while the diagonal elements of $U^{(0)\dagger}\partial_\tau U^{(0)}$ are zero, as a consequence of the parallel transport (4.3). Note that the off-diagonal elements of $H^{(1)}$ carry a prefactor ε.

The usual adiabatic approximation [17, 89] now consists in neglecting the off-diagonal elements of $H^{(1)}$ altogether. Assuming that the system was prepared in the j-th eigenstate of $H^{(0)}$ in the infinite past, and denoting the solution to the Schrödinger equation (4.1) that evolves from this initial condition as $|\psi_j^{(0)}\rangle$, one finds the familiar approximate "adiabatic" wave functions

$$\begin{aligned} |\psi_j^{(0)}(\tau)\rangle &\approx U^{(0)}(\tau) \, |e_j\rangle \exp\left(-\frac{i}{\varepsilon} \int_0^\tau \mathrm{d}\tau' E_j^{(0)}(\tau') \right) \\ &= |u_j^{(0)}(\tau)\rangle \exp\left(-\frac{i}{\varepsilon} \int_0^\tau \mathrm{d}\tau' \, E_j^{(0)}(\tau') \right) \ , \end{aligned} \tag{4.5}$$

where $|e_j\rangle$ is the j-th unit vector.

Instead of adopting this adiabatic approximation, one can also iterate the whole scheme [9]: the new Schrödinger equation (4.4) has the same form as the original equation (4.1), with $H^{(0)}$ replaced by $H^{(1)}$, and $U^{(0)\dagger}|\psi^{(0)}\rangle$ appears instead of $|\psi^{(0)}\rangle$. We fix the phases of the orthonormal eigenstates $|u_j^{(1)}\rangle$ of $H^{(1)}$ again by parallel transport; these eigenstates yield a

matrix $U^{(1)}$ that defines a further unitary transformation. Proceeding in this manner, one obtains after $(n+1)$ steps a Schrödinger equation

$$\left(H^{(n+1)} - i\varepsilon\partial_\tau\right)|\psi^{(n+1)}\rangle = 0\ ,$$

where

$$|\psi^{(n+1)}\rangle = U^{(n)\dagger}\ldots U^{(0)\dagger}|\psi^{(0)}\rangle$$

and

$$H^{(n+1)} = U^{(n)\dagger}H^{(n)}U^{(n)} - i\varepsilon U^{(n)\dagger}\left(\partial_\tau U^{(n)}\right)\ . \tag{4.6}$$

By induction, the off-diagonal elements of $H^{(n+1)}$ are of order ε^{n+1}. Hence it is tempting to neglect these elements and to construct, in strict analogy to equation (4.5), improved adiabatic approximations to the true solutions of equation (4.1):

$$\begin{aligned}|\psi_j^{(0)}(\tau)\rangle &\approx U^{(0)}(\tau)\ldots U^{(n)}(\tau)\,|e_j\rangle\,\exp\left(-\frac{i}{\varepsilon}\int_0^\tau \mathrm{d}\tau' E_j^{(n)}(\tau')\right)\\ &\equiv |\varphi_j^{(n)}(\tau)\rangle_I\ .\end{aligned} \tag{4.7}$$

It should be noted that the eigenvalues $E_j^{(n)}$ pertaining to different steps are approximately equal. In particular, they coincide in those time intervals where $H^{(0)}$ remains constant, as follows from the parallel transport (4.3).

The above construction tries to exploit the idea of parallel transport as consistently as possible even beyond the adiabatic limit $\varepsilon \to 0$. Hence, the approximation (4.7) follows the true j-th evolving state, but cannot describe transitions to other states. Because such nonadiabatic transitions do become important beyond the adiabatic limit, even if they are only of order $e^{-\mathrm{const.}/\varepsilon}$ [22, 29], the procedure is bound to diverge for $n \to \infty$, and thus has an asymptotic meaning. One has to expect that the off-diagonal elements of $H^{(n)}$ first become rapidly smaller from step to step, but then start to blow up, since the decrease of ε^n is eventually overcompensated by the growth of the time-derivative that enters into $U^{(n)\dagger}\partial_\tau U^{(n)}$. When terminating the procedure at that step $n = n_c$ where the off-diagonal elements are smallest, one should obtain an optimal description of the "transition-free component" of the total wave function. In other words, we are seeking an asymptotic representation of the adiabatic part [1] of the solution to Schrödinger's equation. When expanding the full wave function with respect to the basis $\{|\varphi_j^{(n_c)}(\tau)\rangle_I \mid j = 1,\ldots,N\}$, the characteristic features of nonadiabatic transitions will stand out most clearly.

There is a closely related concept that aims in the same direction, namely the series of superadiabatic bases introduced by Berry in his study of histories of quantum transitions in

[1] Actually, "transition-free" is an almost literal translation of the greek root of "adiabatic".

two-level systems [10]. Applying Berry's ideas to N-level systems, we write $|\psi_j^{(0)}\rangle$ as a formal power series in ε,

$$|\psi_j^{(0)}(\tau)\rangle = \exp\left(-\frac{i}{\varepsilon}\int_0^\tau \mathrm{d}\tau'\, E_j^{(0)}(\tau')\right) \sum_{m=0}^{\infty} \varepsilon^m\, |v_j^{(m)}(\tau)\rangle\ , \tag{4.8}$$

where the vectors $|v_j^{(m)}\rangle$ defined here are expressed as linear combinations of the instantaneous eigenstates (4.2):

$$|v_j^{(m)}(\tau)\rangle = \sum_{k=1}^{N} a_{jk}^{(m)}(\tau)\, |u_k^{(0)}(\tau)\rangle\ .$$

Stipulating again that the system occupies the j-th state for $\tau \to -\infty$, the determination of the coefficients $a_{jk}^{(m)}$ starts from the initial conditions

$$\begin{aligned} a_{jk}^{(0)}(\tau) &= \delta_{j,k} \\ a_{jk}^{(m)}(-\infty) &= 0 \qquad \text{for } m > 0\ . \end{aligned} \tag{4.9}$$

Inserting the formal series (4.8) into the Schrödinger equation (4.1) and comparing coefficients of equal powers of ε, we obtain the recursion relations

$$a_{jk}^{(m)} = \frac{-i}{E_j^{(0)} - E_k^{(0)}} \left\{ \partial_\tau a_{jk}^{(m-1)} + \sum_{l=1}^{N} a_{jl}^{(m-1)} \gamma_{lk}^* \right\} \qquad (j \neq k) \tag{4.10}$$

$$\partial_\tau a_{jj}^{(m)} = -\sum_{l=1}^{N} a_{jl}^{(m)} \gamma_{lj}^*\ , \tag{4.11}$$

where the quantities γ_{lk} denote the coupling matrix elements

$$\gamma_{lk} = -\langle u_l^{(0)} | \partial_\tau | u_k^{(0)} \rangle\ .$$

Note that $\gamma_{jj} = 0$, by virtue of equation (4.3). Having computed the coefficients $a_{jk}^{(m)}$ for $j \neq k$ from the coefficients $a_{jk}^{(m-1)}$ by means of equation (4.10), the diagonal elements $a_{jj}^{(m)}$ can be obtained by solving the first-order differential equation (4.11). As shown in more detail in appendix B, the evaluation of this recursive scheme can be reduced to the computation of the matrix elements of $\partial_\tau^n H^{(0)}$, combined with the integration required by equation (4.11).

Since nonadiabatic transitions are of order $e^{-(\text{const.}/\varepsilon)}$, that is, beyond any power of ε, the series (4.8) cannot describe these transitions and therefore must diverge [10], as does the previous iterative scheme. However, by terminating the series at some finite order n one gets the superadiabatic basis states [10]

$$|\varphi_j^{(n)}(\tau)\rangle_S \ \equiv\ \exp\left(-\frac{i}{\varepsilon}\int_0^\tau \mathrm{d}\tau'\, E_j^{(0)}(\tau')\right) \sum_{m=0}^{n} \varepsilon^m \sum_{k=1}^{N} a_{jk}^{(m)}(\tau)\, |u_k^{(0)}(\tau)\rangle \tag{4.12}$$

that can be employed to expand the wave function $|\psi_l^{(0)}\rangle$ evolving from the initially occupied l-th eigenstate of $H^{(0)}$. As shown by Berry for the two-level case $N = 2$, there is an optimal order $n = n_c$ that provides a distinguished, "natural" basis for the description of the dynamics (see section 4.2).

The superadiabatic scheme based on the series (4.8) will be labelled by "S" in the following; the previous iterative scheme by "I". In the next section we will show with the help of a typical example that both schemes are in a certain sense complementary, but lead to very similar physical results.

4.2 The Landau-Zener transition

For a two-level system with a Hamiltonian $H^{(0)}$ given by a traceless real symmetric matrix, the iterative scheme produces after $n+1$ steps a Hamiltonian matrix of the form

$$H^{(n+1)} = \begin{pmatrix} E^{(n)} & -i\varepsilon\gamma^{(n)*} \\ i\varepsilon\gamma^{(n)} & -E^{(n)} \end{pmatrix} , \tag{4.13}$$

with diagonal elements given by

$$\begin{aligned} E^{(n)} &= \sqrt{E^{(n-1)2} + \left(\varepsilon|\gamma^{(n-1)}|\right)^2} \\ &= E^{(0)} \sqrt{1 + \varepsilon^2 \sum_{k=0}^{n-1} \left(\frac{|\gamma^{(k)}|}{E^{(0)}}\right)^2} \end{aligned} \tag{4.14}$$

and off-diagonal elements determined by the recursion relation

$$\begin{aligned} \gamma^{(n)} &= i\varepsilon \frac{\gamma^{(n-1)}\partial_\tau E^{(n-1)} - E^{(n-1)}\partial_\tau \gamma^{(n-1)}}{2E^{(n)2}} \\ &= -i\varepsilon \, \frac{1}{2} \left(\frac{E^{(n-1)}}{E^{(n)}}\right)^2 \partial_\tau \left(\frac{\gamma^{(n-1)}}{E^{(n-1)}}\right) . \end{aligned} \tag{4.15}$$

Hence, $E^{(n+1)} - E^{(n)}$ is of order ε^{2n+2}.

As an archetypal example [34], we consider in this section the Landau-Zener Hamiltonian

$$H^{(0)} = \begin{pmatrix} \tau & 1 \\ 1 & -\tau \end{pmatrix} . \tag{4.16}$$

In this case one finds

$$E^{(0)} = \sqrt{\tau^2 + 1} \tag{4.17}$$

$$\gamma^{(0)} = \frac{i}{4(\tau + i)} - \frac{i}{4(\tau - i)} . \tag{4.18}$$

Expanding the the wave function $|\psi_1^{(0)}(\tau)\rangle$ in the n-th order superadiabatic bases, either in the bases (4.7) corresponding to the scheme I or in the bases (4.12) provided by S,

$$|\psi_1^{(0)}(\tau)\rangle = \sum_{k=1}^{2} c_{1k}^{(n)}(\tau)\, |\varphi_k^{(n)}(\tau)\rangle \;,$$

the coefficients $c_{12}^{(n)}$ denote the transition amplitudes with respect to these bases. These amplitudes can approximately be obtained from first-order time-dependent perturbation theory in the nonadiabatic coupling [22]. For the iterative scheme, this yields

$$c_{12}^{(n)}(\tau) = \int_{-\infty}^{\tau} \mathrm{d}\tau'\, \gamma^{(n)}(\tau')\, \exp\left(-2\,\frac{i}{\varepsilon}\int_0^{\tau'} \mathrm{d}\tau''\, E^{(n)}(\tau'')\right) \;. \tag{4.19}$$

To elucidate the flaw of this perturbative treatment, let us first compute the final transition amplitude $c_{12}^{(0)}(+\infty)$ in the usual adiabatic basis $n = 0$. In this case it is useful to introduce the new variable [10]

$$w(\tau) = 2\int_0^{\tau} \mathrm{d}\tau'\, E^{(0)}(\tau') \tag{4.20}$$

and to close the path of integration along the real axis by a semicircle in the lower half of the complex w-plane:

$$c_{12}^{(0)}(\infty) = \frac{1}{2}\oint \mathrm{d}w\, \frac{\gamma^{(0)}(w)}{E^{(0)}(w)}\, \exp\left(-\frac{iw}{\varepsilon}\right) \;.$$

According to equation (4.15), a (complex) degeneracy of the two eigenvalues $E^{(n)}$ and $-E^{(n)}$ is generally accompanied by a pole of the nonadiabatic coupling $\gamma^{(n)}$. For the Landau-Zener system, the equations (4.17) and (4.18) show that there are degeneracies of $\pm E^{(0)}$ and poles of $\gamma^{(0)}$ at $\tau = \pm i$; for the computation of $c_{12}^{(0)}(\infty)$ we only need to know $\gamma^{(0)}/E^{(0)}$ close to $w_c \equiv w(\tau_c)$, with $\tau_c = -i$. From the definition (4.20) one readily finds

$$w \approx w_c + \frac{1}{3}\, E^{(0)}(\tau)\, 4(\tau + i)$$

with

$$w_c = -\frac{i\pi}{2} \;,$$

hence we have

$$\frac{\gamma^{(0)}(w)}{E^{(0)}(w)} \approx \frac{i}{3(w - w_c)} \tag{4.21}$$

for w close to w_c. Contour integration then gives

$$c_{12}^{(0)}(\infty) = \frac{\pi}{3}\exp\left(-\frac{|w_c|}{\varepsilon}\right) \;. \tag{4.22}$$

It is well known that the prefactor $\pi/3$ is wrong. The error is an artifact of first-order perturbation theory in the adiabatic basis; adding the contributions from all orders renormalises the prefactor to unity [22]. We shall repeatedly come back to this "$\pi/3$-problem" [10]. The corrected formula $c_{12}^{(0)}(\infty) = \exp(-|w_c|/\varepsilon)$, which shows that the transition amplitude is simply determined by the value of w at the point of degeneracy, is often referred to as the Dykhne-Davis-Pechukas formula ("DDP-formula"; see references [22, 29]).

We now turn to the transition histories $c_{12}^{(n)}$ pertaining to the iterative scheme I. The computation runs parallel to Berry's calculation for the scheme S [10], but there is an interesting difference, since for S the iterated energies $E^{(n)}$ with $n \geq 1$ do not appear. We briefly sketch the line of reasoning: Aiming at the amplitudes $c_{12}^{(n)}(\tau)$ for finite τ, we cannot close the path of integration as before, and have to remain on the real axis. The approximation (4.21) is valid only in the vicinity of the pole at w_c. However, if we tentatively approximate $E^{(n)}$ by $E^{(0)}$ for all n, the recursion relation (4.15) becomes

$$\frac{\gamma^{(n)}(w)}{E^{(0)}(w)} = -i\varepsilon\,\partial_w\left(\frac{\gamma^{(n-1)}(w)}{E^{(0)}(w)}\right) \tag{4.23}$$

and thus produces, with increasing n, poles of successively higher order at w_c. The "domain of influence" of these higher-order poles eventually reaches the real axis for sufficiently large n [10]. Hence, we can then evaluate the transition integral (4.19) with the approximation

$$\frac{\gamma^{(n)}(w)}{E^{(0)}(w)} \approx \frac{i(i\varepsilon)^n n!}{3}\left(\frac{1}{(w-w_c)^{n+1}} - \frac{1}{(w+w_c)^{n+1}}\right)$$

that results from plugging (4.21) into equation (4.15) with all $E^{(n)}$ replaced by $E^{(0)}$, and we have also added the contribution from the pole in the upper half-plane. Expanding to second order in $w/|w_c|$ then gives

$$\begin{aligned}\frac{\gamma^{(n)}(w)}{2E^{(0)}(w)} \approx & \frac{\pi}{3}\frac{\varepsilon^n n^{n+\frac{1}{2}}e^{-n}}{\sqrt{2\pi}|w_c|^{n+1}}\exp\left(-\frac{(n+1)w^2}{2|w_c|^2}\right) \\ & \times\left[\exp\left(i\frac{(n+1)w}{|w_c|}\right) + (-1)^n\exp\left(-i\frac{(n+1)w}{|w_c|}\right)\right] .\end{aligned} \tag{4.24}$$

Approximating $E^{(n)}$ by $E^{(0)}$ also in the exponential of the integrand (4.19), and changing to the variable w, the factor $\exp(-iw/\varepsilon)$ counteracts the oscillation of the first term in the square brackets of (4.24), but enhances the oscillations of the second term, which is therefore neglected. Setting [10]

$$n = n_c \equiv \mathrm{Int}\frac{|w_c|}{\varepsilon} \tag{4.25}$$

eliminates even the slow oscillations and thus defines the order of the optimal superadiabatic basis. In this way, one finally arrives at

$$c_{12}^{(n_c)}(\tau) = \frac{\pi}{3}\exp\left(-\frac{|w_c|}{\varepsilon}\right)\int_{-\infty}^{w(\tau)} \mathrm{d}w' \frac{1}{\sqrt{2\pi\varepsilon|w_c|}}\exp\left(-\frac{w'^2}{2\varepsilon|w_c|}\right)$$
$$= \frac{\pi}{3}\frac{1}{2}\left[1+\mathrm{erf}\left(\frac{w(\tau)}{\sqrt{2\varepsilon|w_c|}}\right)\right]\exp\left(-\frac{|w_c|}{\varepsilon}\right) \quad . \tag{4.26}$$

This error-function transition history is universal in the sense that it does not depend on the details of the Hamiltonian [10]. Unfortunately, the replacement of all $E^{(n)}$ by $E^{(0)}$ in equation (4.15) causes the result (4.26) to be too large, since on the real axis we have $E^{(n)} \geq E^{(n-1)}$. This is the reason why the incorrect prefactor $\pi/3$ remains present here. As shown by Berry [10] and Berry and Lim [11] for the scheme S, first-order perturbation theory in the optimal basis $n = n_c$ does indeed produce the correct transition amplitude when n_c goes to infinity. In the present case I this superadiabatic renormalisation is destroyed by the approximation $E^{(n)} \approx E^{(0)}$, and the recovery of the correct prefactor appears to be difficult. However, as sketched in appendix C, already for $n = 1$ the prefactor is reduced from $\pi/3 \approx 1.047$ to $\pi\sin(1/3) \approx 1.028$.

Even though the iterative scheme appears to be more difficult to handle analytically than the scheme S it has its merits, in particular when ε is *not* small. Then S becomes problematic because the bases (4.12) are not properly orthonormalised, whereas I remains sound. This allows one to use the iterative scheme even when nonadiabatic effects become sizeable. In the n-th I-basis (4.7) the "transition-free component" of the wave function acquires a total phase $(1/\varepsilon)\int_{-\infty}^{\infty}\mathrm{d}\tau\, E_1^{(n)} + \Phi_1^{(n)}$, measured with respect to the parallel-transported basis state $|u_1^{(n)}\rangle$, and the magnitude of $\Phi_1^{(n)}$ characterises the deviation from ideal parallel transport. In the adiabatic basis one meets the familiar dynamical phase $(1/\varepsilon)\int_{-\infty}^{\infty}\mathrm{d}\tau\, E_1^{(0)}$ for $\varepsilon \to 0$, whereas for finite ε the additional piece $\Phi_1^{(0)}$ does not vanish. The optimal superadiabatic basis $n = n_c$, on the other hand, is by its very construction just that basis which describes the actual quantum evolution as closely as possible by parallel transport even for finite ε, hence $\Phi_1^{(n_c)} \approx 0$. If we now restrict ourselves to systems for which the unitary transformations $U^{(1)}, \ldots, U^{(n_c)}$ connecting the optimal and the adiabatic bases at $\tau = \pm\infty$ reduce to the identity operation, as is the case for the Landau-Zener model, then we have

$$\frac{1}{\varepsilon}\int_{-\infty}^{+\infty}\mathrm{d}\tau\, E_1^{(n_c)}(\tau) = \frac{1}{\varepsilon}\int_{-\infty}^{+\infty}\mathrm{d}\tau\, E_1^{(0)}(\tau) + \Phi_1^{(0)}\,, \tag{4.27}$$

so that there appears the correction

$$\Phi_1^{(0)} = \frac{1}{\varepsilon}\int_{-\infty}^{+\infty}\mathrm{d}\tau\left[E_1^{(n_c)}(\tau) - E_1^{(0)}(\tau)\right]$$

to the dynamical phase of the transition-free component [27]. The argument employed here is similar to the reasoning used by Berry [9] for computing quantum phase corrections for cyclic evolution. In particular, for the Landau-Zener model itself we obtain

$$\begin{aligned}\Phi_1^{(0)} &= \frac{\varepsilon}{6} + \frac{\varepsilon^3}{45} + \frac{8\,\varepsilon^5}{315} + \frac{8\,\varepsilon^7}{105} + \frac{128\,\varepsilon^9}{297} + \dots \\ &= \sum_{k=1}^{n_c} \frac{(-1)^{k-1}\mathrm{B}_{2k}\,(2\varepsilon)^{2k-1}}{2k(2k-1)} + O(\varepsilon^{2n_c+1})\;, \end{aligned} \tag{4.28}$$

with B_{2k} denoting the Bernoulli numbers. For $n_c \to \infty$ this gives [1]

$$\sum_{k=1}^{\infty} \frac{(-1)^{k-1}\mathrm{B}_{2k}\,(2\varepsilon)^{2k-1}}{2k(2k-1)} \sim \frac{\pi}{4} + \frac{1}{2\varepsilon}\ln\left(\frac{1}{2\varepsilon}\right) - \frac{1}{2\varepsilon} + \arg(\Gamma[1 - i/(2\varepsilon)])\;, \tag{4.29}$$

which is precisely the asymptotic series for the Stueckelberg phase that accompanies the Landau-Zener transition [20]. This phase is unimportant for small ε, when the evolution is mostly adiabatic, but it has to be taken into account when the Landau-Zener transition probability becomes large. It should also be observed that approximating the exponential $\exp(-2i/\varepsilon \int_0^\tau \mathrm{d}\tau' E^{(n)})$ in the transition integral (4.19) by $\exp(-2i/\varepsilon \int_0^\tau \mathrm{d}\tau' E^{(0)})$ means neglecting a phase factor $\exp[-2i/\varepsilon \int_0^\tau \mathrm{d}\tau'(E^{(n)} - E^{(0)})]$ in the derivation of equation (4.26), so that, strictly speaking, the error function should be equipped with a Stueckelberg-like phase in the optimal superadiabatic basis, whereas there is no such phase for the transition amplitude in the adiabatic basis. In the following we will neglect the Stueckelberg phase, since it is quite small in the examples considered. However, the fact that the iterative scheme yields this phase in an appealingly simple manner appears to be noteworthy.

Apart from their different performance for large ε, the schemes I and S match well. In both cases the optimal orders are given by equation (4.25), and both schemes provide, if properly executed, a superadiabatic basis in which the transition amplitude takes the universal form

$$c_{12}^{(\mathrm{np})}(\tau) = \frac{1}{2}\left[1 + \mathrm{erf}\left(\frac{w(\tau)}{\sqrt{2\varepsilon|w_c|}}\right)\right]\exp\left(-\frac{|w_c|}{\varepsilon}\right)\;. \tag{4.30}$$

As will be shown in section 4.4, this expression has a clear-cut meaning also in the adiabatic basis.

To demonstrate the range of applicability of the above concepts, we display in figure 4.1 transition histories for $\varepsilon = 1$, which is clearly *not* asymptotically small. According to equation (4.25), the optimal superadiabatic order then is $n_c = 2$. We have plotted the probabilities $|c_{12}^{(n)}|^2$ in the adiabatic basis $n = 0$ (figure 4.1 a), and in the superadiabatic bases $n = 2$ (figure 4.1 b) and $n = 4$ (figure 4.1 c). Full lines refer to the iterative scheme I, dashed lines to S. For $n = 0$ both schemes give the same amplitudes; the final value is approached after significant overshooting. For $n = n_c = 2$ both schemes yield a history that already

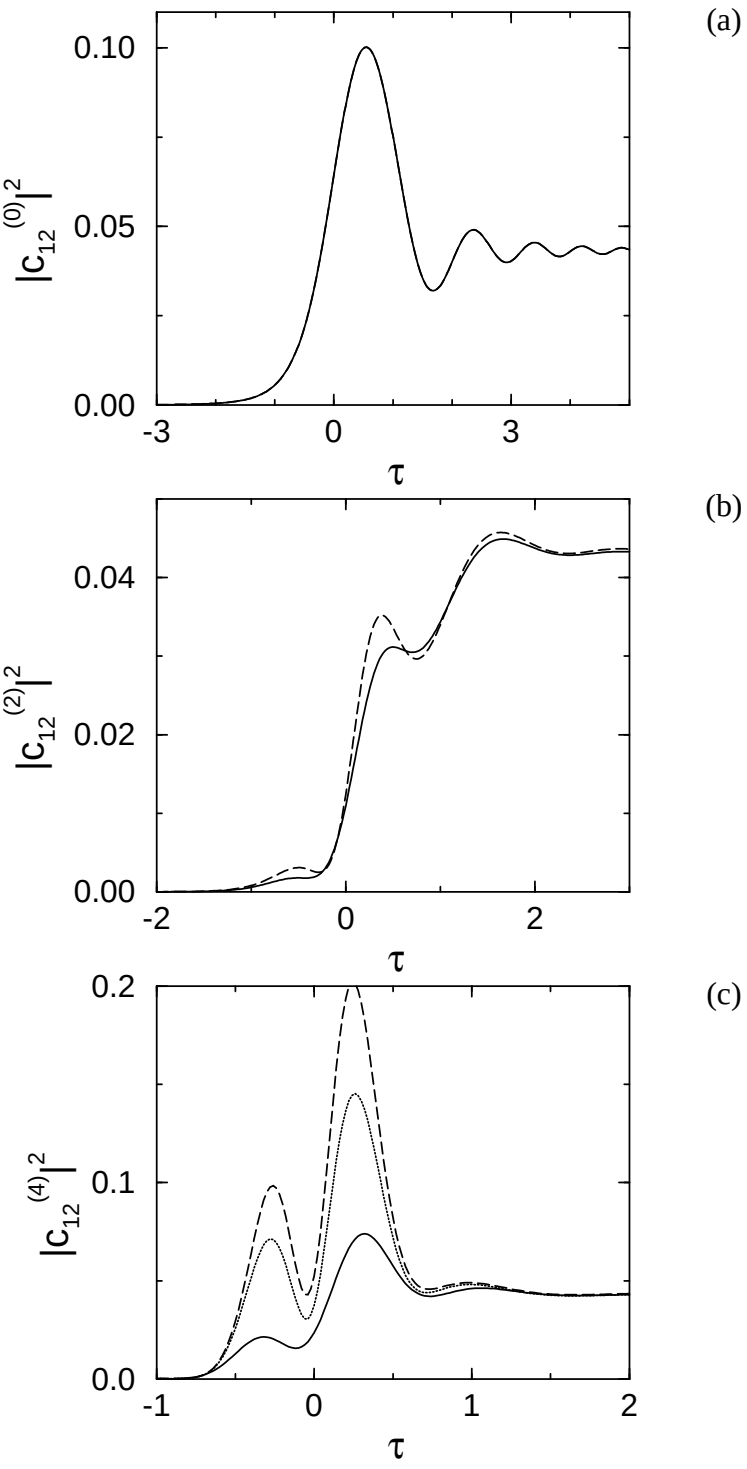

Figure 4.1: Transition histories $|c_{12}^{(n)}(\tau)|^2$ in the n-th order superadiabatic basis corresponding to the iterative scheme I (full line) and to the series scheme S (dashed), for the Landau-Zener Hamiltonian (4.16) with $\varepsilon = 1$ and $n = 0$ (a), $n = n_c = 2$ (b), and $n = 4$ (c). The dotted line in figure 4.1 c has been obtained from S after normalising the basis (4.12).

resembles the ideal error function; the remaining wiggles can be traced to the neglected fast-oscillating exponential [81]. For $n = 4$, beyond the optimal order, the scheme I is more well behaved than S, which then produces rather large values. This is partly due to the fact that

the bases (4.12) are not normalised exactly, but even normalising the basis vectors (dotted line) does not bring the two schemes into agreement.

Figure 4.2 shows the histories for $\varepsilon = 1/3$ and $n = 0$ (a), $n = 2$ (b), and $n = n_c = 5$ (c). The overshooting for $n = 0$ is now even more pronounced. For $n > 0$ the two schemes

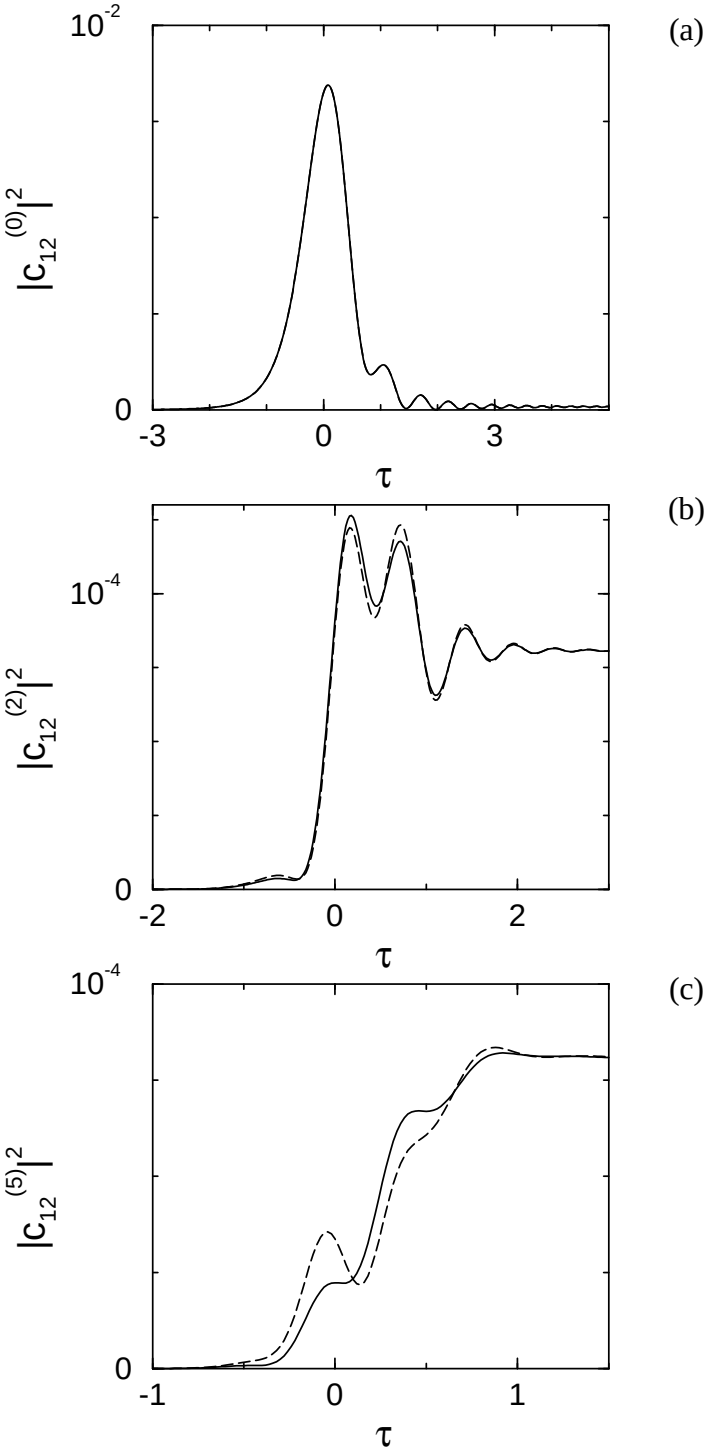

Figure 4.2: As figure 4.1, with $\varepsilon = 1/3$ for $n = 0$ (a), $n = 2$ (b), and $n = n_c = 5$ (c). The scales of the ordinates are linear.

behave fairly similar up to the optimal order; the histories provided by I tend, in general, to be smoother.

Figure 4.3 demonstrates that transition dynamics viewed in the optimal superadiabatic basis looks profoundly different from the dynamics in the adiabatic basis: the upper line (exhibiting unresolved fast oscillations at large τ) is the history $|c_{12}^{(0)}|^2$ for $\varepsilon = 1/6$; the lower line is $|c_{12}^{(n_c)}|^2$ for the same process ($n_c = 10$; computed within scheme S). The physical signifi-

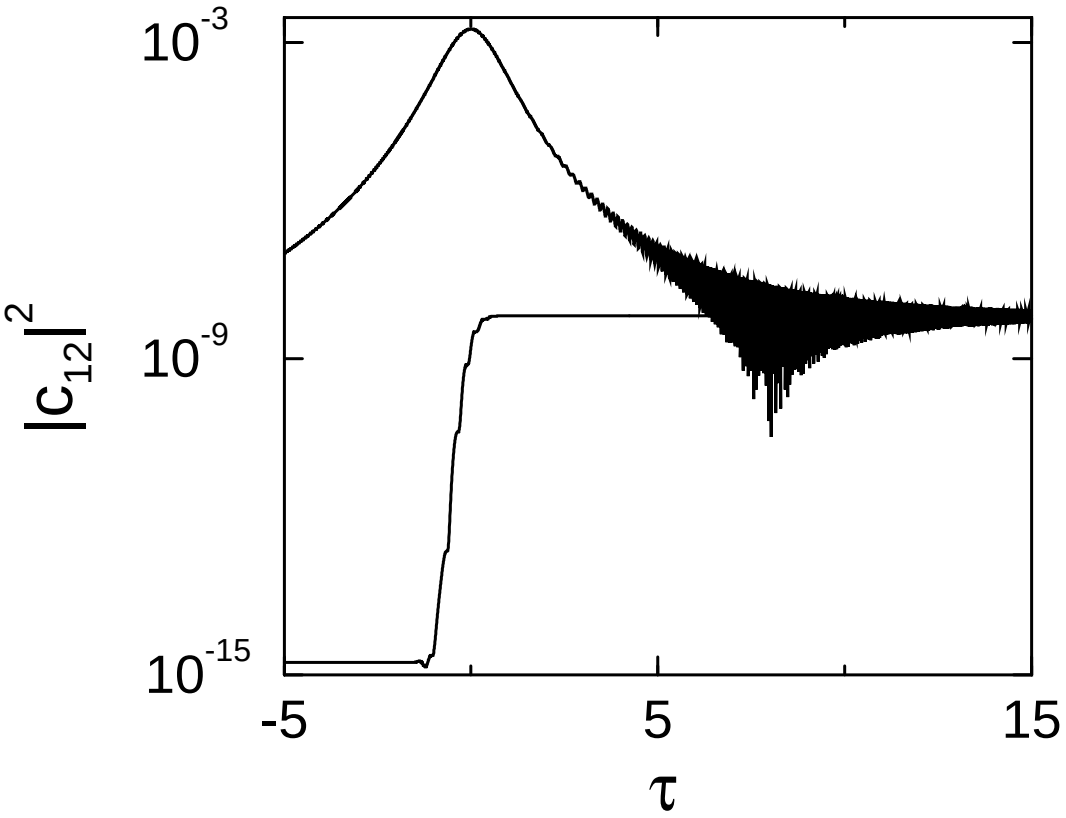

Figure 4.3: Landau-Zener transition history for $\varepsilon = 1/6$ in the adiabatic basis (upper line), and in the optimal superadiabatic basis ($n_c = 10$, computed within scheme S). The black area is caused by unresolved fast oscillations.

cance of the "optimal" transition amplitude will become obvious in section 4.4, where it will reappear as part of the total amplitude in the adiabatic basis.

4.3 Application to three-level systems

A particularly important example for adiabatic population transfer is provided by the STIRAP mechanism (see, e.g., references [19, 78, 105, 108]; the acronym stands for "Stimulated Raman Adiabatic Passage"): Taking a three-level Λ-system, the initially populated bare level 1 is coupled to the intermediate bare level 2 by a pump laser with Rabi frequency $\Omega_1(\tau)$, while level 2 is coupled to the final bare level 3 by a Stokes laser with Rabi frequency $\Omega_2(\tau)$.

The laser frequencies are chosen such that levels 1 and 3 are on two-photon resonance, whereas the intermediate level can be off-resonant by a detuning Δ. Within the rotating wave approximation, the Hamiltonian then reads

$$H^{(0)}(\tau) = \begin{pmatrix} 0 & \Omega_1(\tau) & 0 \\ \Omega_1(\tau) & \Delta & \Omega_2(\tau) \\ 0 & \Omega_2(\tau) & 0 \end{pmatrix} . \tag{4.31}$$

Usually the two laser pulses are applied in counterintuitive order, so that the Stokes pulse $\Omega_2(\tau)$, coupling initially unpopulated levels, *precedes* the pump pulse $\Omega_1(\tau)$, but both pulses have to overlap sufficiently [19].

The instantaneous ("dressed") energies $E_j^{(0)}$ of $H^{(0)}$ are

$$\begin{aligned} E_1^{(0)} &= \frac{1}{2}\left(\Delta + \sqrt{\Delta^2 + 4(\Omega_1^2 + \Omega_2^2)}\right) \\ E_2^{(0)} &= 0 \\ E_3^{(0)} &= \frac{1}{2}\left(\Delta - \sqrt{\Delta^2 + 4(\Omega_1^2 + \Omega_2^2)}\right) , \end{aligned}$$

so that $E_2^{(0)}$ does not depend on the laser parameters. The working principle of the STIRAP mechanism relies on the fact that the corresponding instantaneous eigenstate $|u_2^{(0)}\rangle$,

$$|u_2^{(0)}\rangle = \frac{\Omega_2}{\sqrt{\Omega_1^2 + \Omega_2^2}}\,|1\rangle - \frac{\Omega_1}{\sqrt{\Omega_1^2 + \Omega_2^2}}\,|3\rangle ,$$

is a linear combination of the bare levels 1 and 3 only, without admixture of the intermediate level 2. For $\tau = -\infty$, when Ω_1/Ω_2 vanishes, $|u_2^{(0)}\rangle$ coincides with the initially populated bare state $|1\rangle$; for $\tau = +\infty$, when Ω_2/Ω_1 becomes negligible, $|u_2^{(0)}\rangle$ coincides with the bare target state $-|3\rangle$. Hence, *in the adiabatic limit* the counterintuitive pulse sequence leads to complete population transfer from the bare level 1 to 3, irrespective of the detuning Δ.

Going beyond the adiabatic limit, i.e., considering the actually relevant case of pulses that change on a finite time scale, there must be nonadiabatic corrections to the ideal population transfer [79, 116] resembling the ones encountered in the Landau-Zener transition. A mathematically most appealing way of studying the emergence of these corrections is to follow the STIRAP dynamics in the superadiabatic bases. For $\Delta = 0$, when the STIRAP Hamiltonian can be reduced exactly to an effective two-level system [19], this type of superadiabatic analysis has been initiated by Elk [30], resulting in transition histories very similar to those shown in figures 4.1 and 4.2. For $\Delta \neq 0$ an exact reduction to a two-level system is not possible, so that we resort to the N-level scheme outlined in appendix B. Following Elk [30], we investigate "ramp pulses" [79] and parametrise the time dependence of the Rabi frequencies

as

$$\Omega_2(\tau) = \cos(\theta(\tau))$$
$$\Omega_1(\tau) = \sin(\theta(\tau)) \ , \tag{4.32}$$

with

$$\theta(\tau) = \frac{1}{2}\arctan(\tau) + \frac{\pi}{4} \tag{4.33}$$

and τ varying from $-\infty$ to $+\infty$, so that Ω_2 decreases monotonically from unity to zero, while Ω_1 increases from zero to one. We set $\varepsilon = 1/6$ and plot in figure 4.4 the histories $|c_{21}|^2$ and $|c_{23}|^2$ of the transitions from the initially occupied state $|u_2^{(0)}\rangle$; the detuning is $\Delta = 1/2$. The

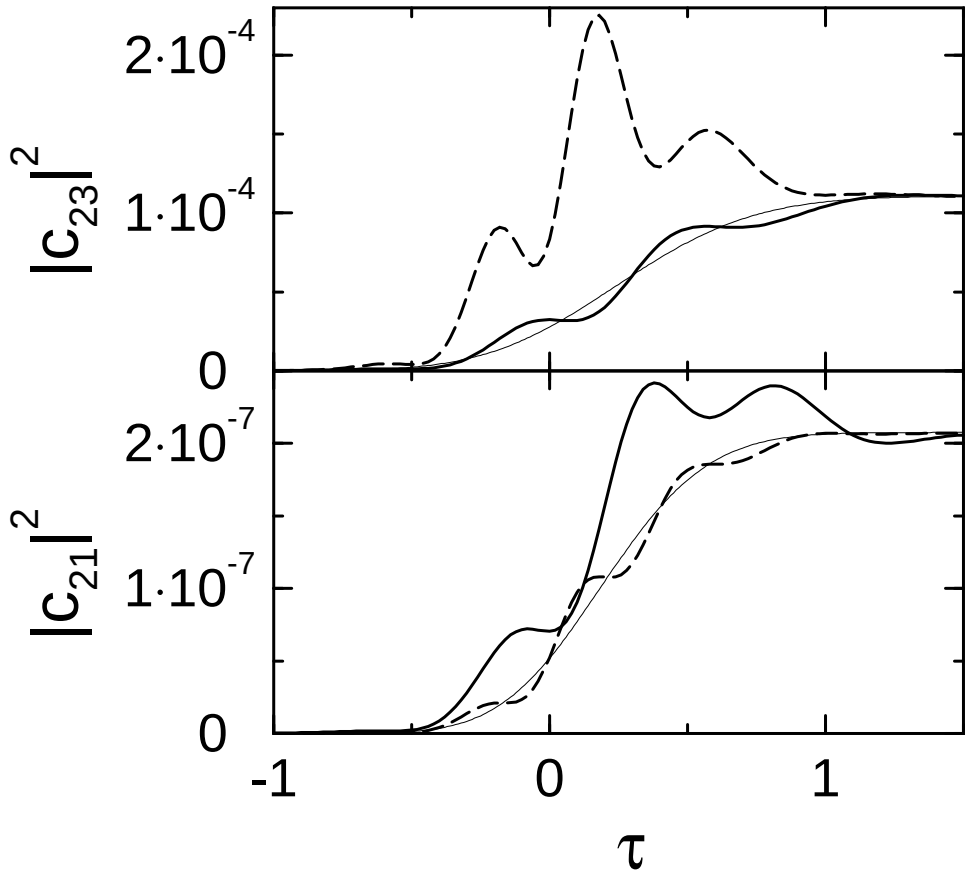

Figure 4.4: Transition histories for the STIRAP Hamiltonian (4.31) with $\Delta = 1/2$ and Rabi frequencies (4.32); the adiabaticity parameter is $\varepsilon = 1/6$. These histories have been calculated in the scheme S according to appendix B, with normalised basis functions. The superadiabatic orders are $n = 5$ (heavy full line) and $n = 8$ (dashed). The thin lines indicate the ideal error functions.

superadiabatic orders considered here are $n = 5$ (heavy full lines) and $n = 8$ (dashed); these are the optimal superadiabatic orders for the two transitions. It can be seen that (i) also in this

generic multilevel case the population losses reach their final values in an errorfunction-like manner in the optimal bases (the ideal error-function histories are indicated by the thin lines), and (ii) the order n_c of the optimal basis depends on the transition in the expected way: the smaller the nonadiabatic population loss, the larger n_c.

Figure 4.5 shows histories of the total population loss $|c_{21}|^2 + |c_{23}|^2$, again for $\varepsilon = 1/6$. The

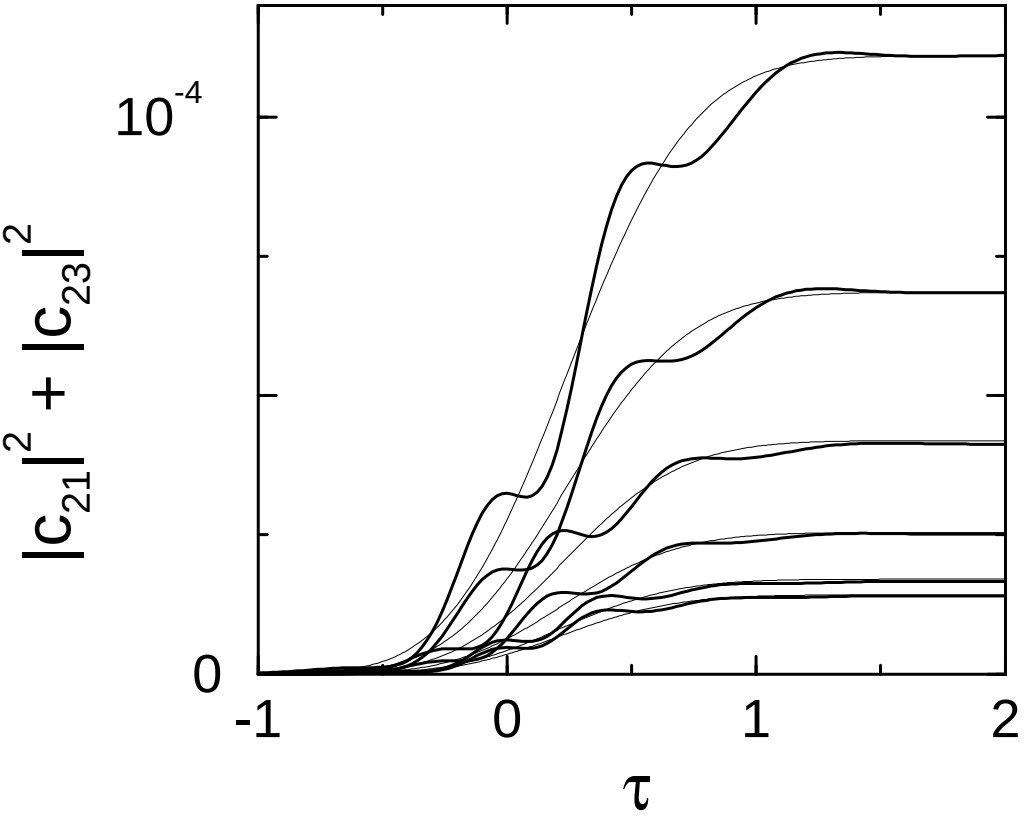

Figure 4.5: Adiabaticity defect for STIRAP with $\varepsilon = 1/6$, and detunings Δ ranging from 0.0 to 0.5, in steps of 0.1 (bottom to top). The thin lines are fits to error functions. The scale of the ordinate is linear.

detuning Δ is varied between 0 to 0.5; each history refers to its respective optimal basis. Evidently, the larger Δ, the larger the population loss, so that $\Delta = 0$ is the best choice for minimising this adiabaticity defect [117]. We stress that the transition dynamics have been reduced to their essentials in this figure, whereas the same dynamics appears much more complicated in the usual adiabatic basis. In that basis there is strong "overshooting", similar to the one depicted in figures 4.1 a and 4.2 a, and the final transition probability is attained much later, in an oscillatory manner.

4.4 Summing the perturbation series in the adiabatic basis

With respect to the optimal superadiabatic bases (4.7) and (4.12), the transition amplitudes acquire the simple error-function form (4.30). In this section we will discuss the transition dynamics exclusively in the customary adiabatic basis $(n = 0)$. We will focus on the two-level case for simplicity, and omit the superscript (0).

To begin with, we consider the first-order approximation (4.19) to the transition amplitude,

$$c_{12}(\tau) = \frac{1}{2}\int_{-\infty}^{w(\tau)} \mathrm{d}w' \, \frac{\gamma(w')}{E(w')} \exp\left(-\frac{i}{\varepsilon}w'\right) \ . \tag{4.34}$$

Integrating n times by parts, which constitutes a standard technique for constructing asymptotic series [24], and assuming that γ/E and all its derivatives vanish for $w \to -\infty$, we find

$$\begin{aligned} c_{12}(\tau) = &-\frac{1}{2}\sum_{k=1}^{n}(-i\varepsilon)^k \, \partial_w^{k-1}\left(\frac{\gamma(w)}{E(w)}\right)\exp\left(-\frac{i}{\varepsilon}w\right) \\ &+\frac{1}{2}\int_{-\infty}^{w(\tau)} \mathrm{d}w' \, (-i\varepsilon)^n \, \partial_{w'}^{n}\left(\frac{\gamma(w')}{E(w')}\right)\exp\left(-\frac{i}{\varepsilon}w'\right) \ . \end{aligned} \tag{4.35}$$

Provided that $\partial_w^n(\gamma/E)$ is absolutely integrable, the integral goes to zero for $\varepsilon \to 0$, as a consequence of the Riemann-Lebesgue lemma [22], so that the remaining sum, which is merely a power series in ε, has to account for the main contribution to the exact transition amplitude at *finite* τ. This series, of course, does *not* contribute to the factor $\exp(-|w_c|/\varepsilon)$ that appears in the final transition amplitude; this factor is contained in the integral.

The integral, on the other hand, coincides exactly with the expression (4.19) for the transition amplitude *in the n-th order superadiabatic basis*, when the latter is evaluated within scheme I, making use of the approximation (4.23). Hence, it becomes the universal error function for $n = n_c$. This observation suggests a fairly intuitive interpretation of the superadiabatic schemes: Performing the unitary transformations to the successive superadiabatic bases amounts to removing from the total transition amplitude the terms proportional to powers of ε, the sum of which we will denote as the perturbative contribution $c_{12}^{(\mathrm{pt})}$. The universal error function that remains after this removal then has a well-defined meaning also in the adiabatic basis: it provides the nonperturbative contribution $c_{12}^{(\mathrm{np})}$.

This interpretation is based on first-order perturbation theory in the nonadiabatic coupling, and therefore still faces the $\pi/3$-problem. However, it can actually be made water-tight by adapting an argument due to Davis and Pechukas [22] that aims at summing the entire perturbation series. For later use, we first slightly generalise the pole approximation (4.21) to the nonadiabatic coupling of the Landau-Zener model, and consider instead

$$\frac{\gamma(w)}{E(w)} \approx \frac{ir}{w - w_c} \ , \tag{4.36}$$

from which the Landau-Zener case can be recovered by setting $r = 1/3$ [2] ; w_c now indicates the pole of γ/E in the lower half of the complex w-plane that lies closest to the real axis. Then, defining

$$b_1 = c_{11}$$
$$b_2 = c_{12} \exp(i w_c/\varepsilon) \ ,$$

introducing the variable

$$x = \frac{w - w_c}{\varepsilon} \ ,$$

utilising the approximation (4.36), and keeping only the leading singularities, the integral form of the Schrödinger equation for the two-level system becomes (see also references [22, 65])

$$\begin{aligned} b_2(x) &= -\frac{r}{2} \int_{-\infty}^{x} \mathrm{d}x' \, \frac{e^{-ix'}}{ix'} \, b_1(x') \\ b_1(x) &= 1 + \frac{r}{2} \int_{-\infty}^{x} \mathrm{d}x' \, \frac{e^{ix'}}{ix'} \, b_2(x') \\ &= 1 - \frac{r^2}{4} \int_{-\infty}^{x} \mathrm{d}x' \, \frac{e^{ix'}}{ix'} \int_{-\infty}^{x'} \mathrm{d}x'' \, \frac{e^{-ix''}}{ix''} \, b_1(x'') \ , \end{aligned} \tag{4.37}$$

where the integrations for b_2 and b_1 have to pass above $x' = 0$. For computing the transition amplitude b_2, we first formally evaluate the amplitude b_1 for staying in the initially occupied state with the help of the ansatz

$$b_1(x) \sim \sum_{n=0} \alpha_n \frac{n!}{(ix)^n} \tag{4.38}$$

with $\alpha_0 = 1$; this ansatz features the typical "factorial by power"-terms characteristic of asymptotic series. By means of successive integration by parts one obtains

$$b_1(x) \sim 1 + \frac{r^2}{4} \sum_{n=0} \alpha_n \sum_{m=0} (-1)^m \frac{(n+m)!}{n+m+1} \, \frac{1}{(ix)^{n+m+1}} \ .$$

Equating this expression with the ansatz (4.38), comparing powers of x, and solving the resulting recursion relation then yields

$$\sum_{m=0}^{n-1} (-1)^m \alpha_m = \prod_{m=1}^{n-1} \left(1 - \frac{r^2}{4m^2} \right) \equiv g_{n-1} \ . \tag{4.39}$$

[2] The case $r = 1/3$ is generic; it occurs when $E^2(\tau)$ has a simple zero at the degeneracy point τ_c. See, e.g., appendix C in reference [10].

So far, this calculation follows the argument that Davis and Pechukas have designed for computing $b_2(\infty)$ [22]. Now comes the essential difference: Inserting the ansatz (4.38) into equation (4.37), we sum the resulting series only up to $n = n_c$,

$$b_2(x) \sim -\frac{r}{2} \sum_{n=0}^{n_c} \alpha_n n! \int_{-\infty}^{x} \mathrm{d}x' \, \frac{e^{-ix'}}{(ix')^{n+1}} \ ,$$

and integrate each term by parts until the exponent $n_c + 1$ appears in the denominator:

$$\begin{aligned} b_2(x) \sim & -\frac{ir}{2} \sum_{n=0}^{n_c} \alpha_n \sum_{m=0}^{n_c-n-1} (-1)^m (n+m)! \, \frac{e^{-ix}}{(ix)^{n+m+1}} \\ & -\frac{r}{2} \sum_{n=0}^{n_c} (-1)^{n_c-n} \alpha_n \, n_c! \int_{-\infty}^{x} \mathrm{d}x' \, \frac{e^{-ix'}}{(ix')^{n_c+1}} \ . \end{aligned}$$

Interchanging the order of summation over n and m, and exploiting the equation (4.39) that embodies the knowledge about $b_1(x)$, we arrive at

$$\begin{aligned} b_2(x) \sim & -\frac{ir}{2} \sum_{m=0}^{n_c-1} (-1)^m g_m m! \frac{e^{-ix}}{(ix)^{m+1}} \\ & -\frac{r}{2} \, (-1)^{n_c} g_{n_c} n_c! \int_{-\infty}^{x} \mathrm{d}x' \, \frac{e^{-ix'}}{(ix')^{n_c+1}} \end{aligned} \tag{4.40}$$

Upon resubstituting w for x, the sum corresponds term by term to the sum obtained in the first order-calculation (4.35), except for the factor g_m that now multiplies the m-th term, with $g_0 = 1$ denoting the empty product. The integral gives precisely the error function (4.26), with the prefactor $\pi/3$ replaced by πr, and with the additional factor g_{n_c}. Since

$$g_\infty = \prod_{m=1}^{\infty} \left(1 - \frac{r^2}{4m^2} \right) = 2 \, \frac{\sin(r\pi/2)}{r\pi} \ ,$$

the previous formula (4.30) now generalises for $\varepsilon \to 0$ (that is, for large n_c) to

$$c_{12}^{(\mathrm{np})}(\tau) = \sin\!\left(\frac{r\pi}{2}\right) \left[1 + \mathrm{erf}\left(\frac{w(\tau)}{\sqrt{2\varepsilon |w_c|}} \right) \right] \exp\!\left(-\frac{|\mathrm{Im}\, w_c|}{\varepsilon} \right) \ , \tag{4.41}$$

and the DDP-formula becomes

$$c_{12}(+\infty) = 2 \sin\!\left(\frac{r\pi}{2}\right) \exp\!\left(-\frac{|\mathrm{Im}\, w_c|}{\varepsilon} \right) \ , \tag{4.42}$$

in agreement with a result obtained first by Joye [65] with the help of a rigorous comparison-equation technique and by Berry and Lim [11] from first-order perturbation theory in the superadiabatic bases. In particular, in the Landau-Zener case one now finds the correct prefactor unity, so that the representation (4.40) is no longer plagued by the remnants of the $\pi/3$-problem.

The value of these deliberations lies in the fact that they reveal just how to decompose the adiabatic transition amplitude into a universal, nonperturbative part — the error function $c_{12}^{(\mathrm{np})}$ — and a power series in the adiabaticity parameter ε, truncated at $n = n_c$, that gives the perturbative contribution $c_{12}^{(\mathrm{pt})}$. The total transition probability, tracked in time, can be written as a phase-coherent superposition of both parts:

$$|c_{12}(\tau)|^2 = |c_{12}^{(\mathrm{pt})}(\tau) + c_{12}^{(\mathrm{np})}(\tau)|^2 \; . \tag{4.43}$$

Since the first contribution is universal, and the second is usually well approximated by the lowest nonvanishing order in ε, the complicated transition dynamics can be understood as resulting from the interference of two easily accessible parts.

To substantiate this claim, we return once more to the Landau-Zener transition. The lowest-order perturbative part

$$c_{12}^{(\mathrm{pt})}(\tau) = \frac{i\varepsilon}{2}\,\frac{\gamma(\tau)}{E(\tau)}\exp\!\left(-\frac{i}{\varepsilon}w(\tau)\right) \tag{4.44}$$

then becomes

$$c_{12}^{(\mathrm{pt})}(\tau) = \frac{i\varepsilon}{4(\tau^2+1)^{3/2}}\exp\!\left(-\frac{i}{\varepsilon}\left[\tau\sqrt{\tau^2+1} + \operatorname{arsinh}(\tau)\right]\right) \; . \tag{4.45}$$

In figure 4.6 we compare $|c_{12}^{(\mathrm{pt})}|^2$ with the exact transition probabilities $|c_{12}|^2$, for $\varepsilon = 1/2$, $1/4$, $1/6$, and $1/8$. Even for $\varepsilon = 1/2$ the perturbative part alone gives a good description of the actual probability for $\tau < 0$; naturally, the agreement has to break down when the nonperturbative part $c_{12}^{(\mathrm{np})}$ becomes significant. For the smaller values of ε the performance of the perturbation theory is impressive: for $\varepsilon = 1/4$, the first-order approximation yields 90% of the exact maximum transition probability; summing the perturbation series up to $n = n_c = 6$ gives 100.7%. For $\varepsilon = 1/8$, the first-order contribution is 98%. Of course, this trend reflects the fact that already the perturbative part alone is asymptotic to the exact amplitude, as long as τ remains finite [22].

Figure 4.7 demonstrates the striking accuracy with which the composition formula (4.43) can describe the full dynamics even when it is evaluated approximately; the adiabaticity parameter here is $\varepsilon = 1/4$. We have plotted the numerically computed, exact probability $|c_{12}|^2$ (full line), together with the perturbative part given by equation (4.45) (dashed) and the nonperturbative part computed from the series scheme S (dashed-dotted; optimal superadiabatic order $n_c = 6$). The curve resulting from the addition of both parts has been plotted as a dotted line — but it is practically indistinguishable from the exact data; the only visible difference is close to the maximum at $\tau \approx 0$. Even in the inset exact and approximate data (full and dotted line) lie on top of each other. This figure nicely illustrates the essentials of nonadiabatic transitions: The final, exponentially small transition probability is already born when it is still

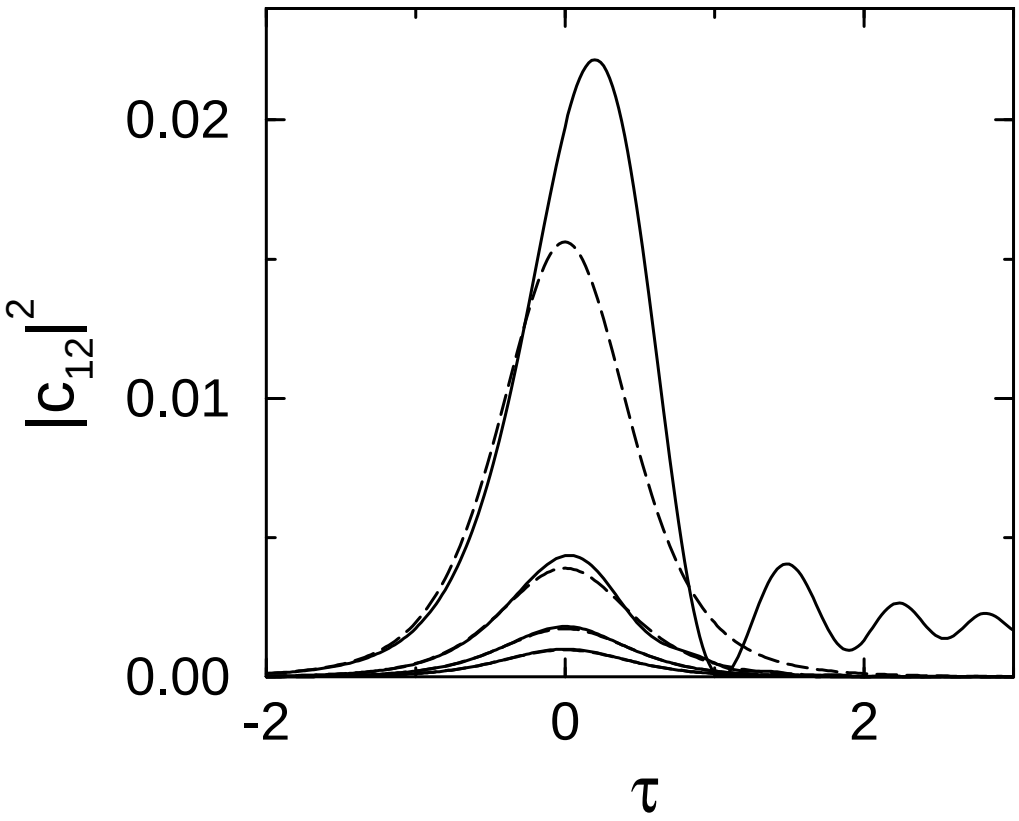

Figure 4.6: Exact histories for the Landau-Zener transition in the adiabatic basis (full lines), compared with the prediction (4.45) of first-order perturbation theory (dashed), for $\varepsilon = 1/2$, $1/4$, $1/6$, and $1/8$ (top to bottom). The corresponding ratios of perturbative and exact peak heights are 0.69, 0.90, 0.96, and 0.98. For $\varepsilon = 1/8$ the graphs of the perturbative and the exact history cannot be distinguished.

overwhelmed by a perturbative overshooting. Lowest-order perturbation theory describes the exact amplitude well up to the point where the perturbative prediction crosses the graph of the error function. The crossover from the perturbative to the nonperturbative dynamics is accompanied by fast oscillations that stem from the interference of both components, so that their amplitude is largest right in the vicinity of the crossing point. Since the perturbative overshooting decreases merely as a power of ε, whereas the final transition amplitude decreases exponentially in $1/\varepsilon$, the relative mismatch between the maximum overshooting and the final value of $|c_{12}|^2$ *grows* substantially with decreasing ε.

4.5 Adiabatic perturbation theory for STIRAP

In the previous section it has been assumed that the ratio γ/E and all its w-derivatives vanish for $w \to \pm\infty$, so that, for example, the integrations by parts leading to equation (4.35) did not pick up contributions from $w = -\infty$, and the final transition amplitude was given

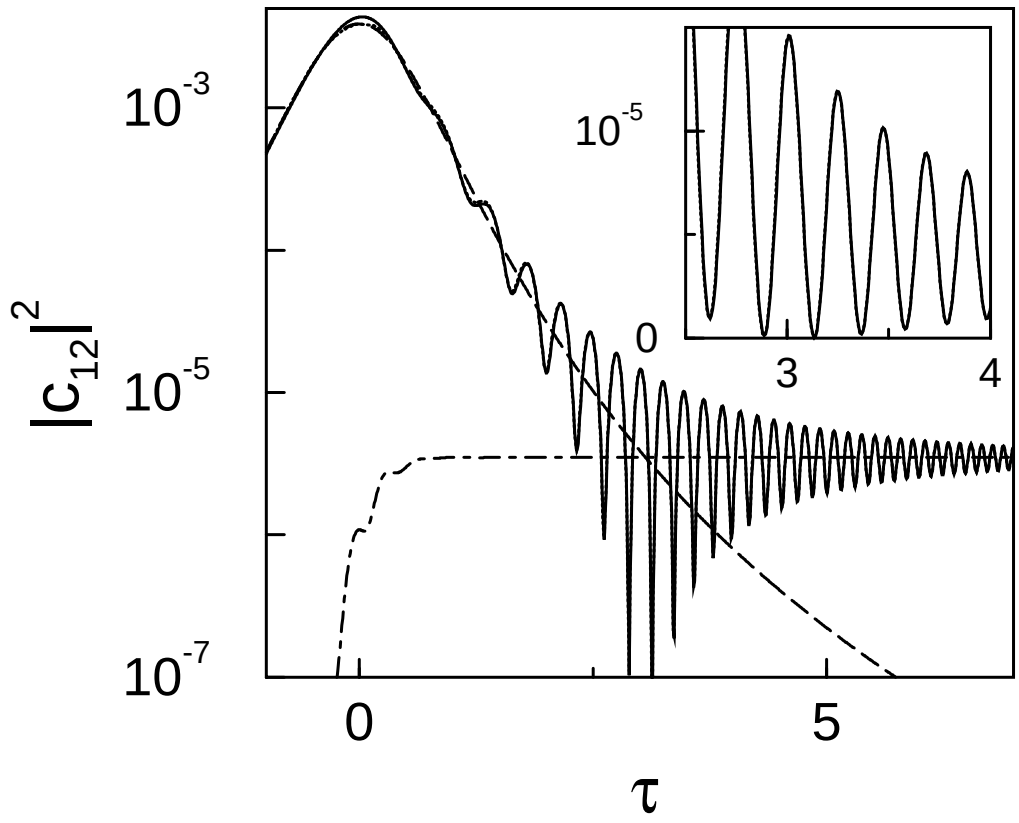

Figure 4.7: Exact history for the Landau-Zener transition with $\varepsilon = 1/4$ (full line), together with the prediction of perturbation theory (dashed) and the history in the optimal superadiabatic basis (dashed-dotted). The phase-coherent superposition (4.43) of the two latter parts is also plotted as a dotted line, but is practically indistinguishable from the exact data (except for the vicinity of the peak). The inset shows the oscillations on a linear scale. Even here the exact results are indistinguishable from the superposition.

entirely by the DDP-formula (4.42). The STIRAP mechanism, however, provides important examples where this assumption fails [79, 116, 117]. For discussing the consequences of this failure from the perturbative point of view, we restrict ourselves to the case $\Delta = 0$, where the three-level system (4.31) is exactly equivalent to a two-level system [19]. Sticking to the notation employed in equation (4.13), and again omitting the superscripts as we will be working in the adiabatic basis only, the effective two-level system has instantaneous energies [79]

$$E(\tau) = \frac{1}{2}\sqrt{\Omega_1^2(\tau) + \Omega_2^2(\tau)}\ .$$

The nonadiabatic coupling

$$\gamma(\tau) = \frac{1}{2}\partial_\tau \theta(\tau)$$

is given by the derivative of the "mixing angle"

$$\theta(\tau) = \arctan\left(\frac{\Omega_1(\tau)}{\Omega_2(\tau)}\right)\ , \tag{4.46}$$

which varies from 0 to $\pi/2$ in STIRAP systems with counterintuitive pulse sequence, as in the previous example (4.33).

Instead of considering "ramp pulses" [79] like those defined by equations (4.32) and (4.33), which mimic the actual pulse shapes only during the phase where both pulses overlap, we now treat models incorporating realistic pulses that vanish properly for $\tau \to -\infty$, increase smoothly and monotonically to maximum strength, then decrease and finally vanish for $\tau \to +\infty$. As a consequence, the instantaneous energies $\pm E$ of the effective two-level system become degenerate for $\tau \to \pm\infty$. However, it has to be kept in mind that it is not E but rather the ratio γ/E that matters.

As a first example of how adiabatic perturbation theory works for such STIRAP configurations, we investigate an analytically solvable model introduced by Vitanov and Stenholm [116]. It is defined by

$$\begin{aligned} E(\tau) &= \frac{1}{2}\operatorname{sech}^2(\tau) \\ \gamma(\tau) &= \frac{b}{2}\operatorname{sech}^2(\tau)\operatorname{sech}[\sigma\tanh(\tau)] \ , \end{aligned} \tag{4.47}$$

with constants b and σ that determine the relative strength and shape of the nonadiabatic coupling, respectively. This describes a genuine STIRAP system, i.e., the mixing angle (4.46) varies from 0 to $\pi/2$, provided these parameters obey [116]

$$\frac{b}{\sigma} = \frac{\pi}{4\arctan(\sinh\sigma)} \ . \tag{4.48}$$

However, the techniques discussed here are valid for an arbitrary system of the type (4.47), so that we need not consider this restriction (4.48) in the following.

Since now the ratio γ/E does not vanish for $\tau \to \pm\infty$, but rather approaches $b\operatorname{sech}(\sigma)$, there is a perturbative contribution to the final transition amplitude that can easily be obtained by adapting equation (4.44):

$$\begin{aligned} c_{12}^{(\mathrm{pt})}(+\infty) &= \frac{i\varepsilon}{2}\,\frac{\gamma(\tau)}{E(\tau)}\exp\left(-\frac{i}{\varepsilon}w(\tau)\right)\Bigg|_{-\infty}^{+\infty} \\ &= \varepsilon b\operatorname{sech}(\sigma)\sin\left(\frac{1}{\varepsilon}\right) \ . \end{aligned} \tag{4.49}$$

Since, moreover,

$$\frac{\gamma(w)}{E(w)} = b\operatorname{sech}(\sigma w) \approx \frac{b}{\sigma}\frac{i}{w - w_c}$$

close to $w_c = -i\pi/(2\sigma)$, the nonperturbative contribution

$$c_{12}^{(\mathrm{np})}(+\infty) = 2\sin\left(\frac{\pi b}{2\sigma}\right)\exp\left(-\frac{\pi}{2\varepsilon\sigma}\right) \tag{4.50}$$

follows from the DDP-formula (4.42) by setting $r = b/\sigma$.

The exact analytical result [116], which can be calculated the by relating the model (4.47) to the Rosen-Zener model [34], acquires for moderately large values of σ the form [3]

$$|c_{12}(+\infty)|^2 \approx \left| 2\varepsilon b \exp(-\sigma) \sin(1/\varepsilon) + \sin\left(\frac{\pi b}{2\sigma}\right) \operatorname{sech}\left(\frac{\pi}{2\varepsilon\sigma}\right) \right|^2 ,$$

in beautiful agreement with what follows by adding our approximations (4.49) and (4.50). In figure 4.8 we compare the total transition probability $|c_{12}^{(\mathrm{pt})}(+\infty) + c_{12}^{(\mathrm{np})}(+\infty)|^2$, as given by equations (4.49) and (4.50) and plotted as the dashed line, to the exact data (full line), for $b = 1$ and $\sigma = 6$. The agreement is close to perfect. Thus, our analysis explains the

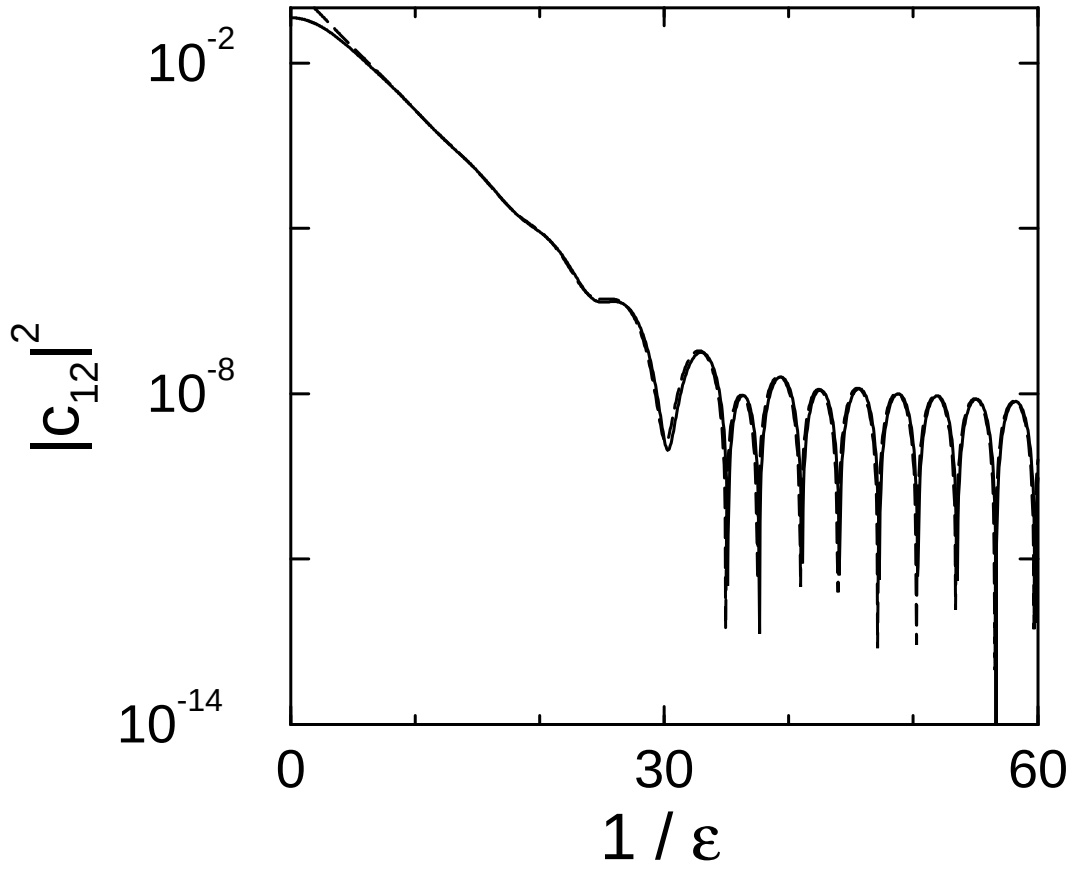

Figure 4.8: Full line: Exact final transition probability for the STIRAP system (4.47) with $b = 1$ and $\sigma = 6$; dashed line: coherent superposition of the perturbative and the nonperturbative component, as approximated by equations (4.49) and (4.50).

breakdown of the Dykhne-Davis-Pechukas exponential behaviour that is observed for large values of $1/\varepsilon$, without having to recourse to specific properties of the model.

[3] See equation (33) in reference [116]. The parameter α used by Vitanov and Stenholm corresponds to $1/(\varepsilon\sigma)$ in our notation; their β is our b/σ. Their parameter σ has the same meaning as ours.

The actual strength of the perturbative approach, however, stems from the fact that it lends itself, with equal accuracy and simplicity, also to models that can *not* be treated exactly, such as the following STIRAP-like model considered by Laine and Stenholm [79]:

$$E(\tau) = \frac{1}{2}\left[\operatorname{sech}^2(\tau+\delta) + \operatorname{sech}^2(\tau-\delta)\right]^{1/2}$$
$$\gamma(\tau) = \frac{b}{2}\,\frac{\sinh(2\delta)}{\cosh^2(\tau+\delta) + \cosh^2(\tau-\delta)}\ . \tag{4.51}$$

Again, this describes an actual STIRAP process if the parameters b and δ are chosen such that

$$\theta(\infty) = 2\int_{-\infty}^{+\infty} \mathrm{d}\tau\,\gamma(\tau) = \frac{\pi}{2}\ ,$$

but our results for the system (4.51) are valid even without this restriction. Now the perturbative part of the final transition amplitude becomes

$$c_{12}^{(\mathrm{pt})}(+\infty) = \frac{i\varepsilon}{2}\,\frac{\gamma(\tau)}{E(\tau)}\exp\left(-\frac{i}{\varepsilon}w(\tau)\right)\Bigg|_{-\infty}^{+\infty}$$
$$+\ \frac{\varepsilon^2}{4E(\tau)}\,\partial_\tau\left(\frac{\gamma(\tau)}{E(\tau)}\right)\exp\left(-\frac{i}{\varepsilon}w(\tau)\right)\Bigg|_{-\infty}^{+\infty} + O(\varepsilon^3)\ .$$

Since γ/E vanishes for $\tau \to \pm\infty$, but $(1/E)\partial_\tau(\gamma/E)$ does not, the leading term of the perturbative amplitude is proportional to ε^2:

$$c_{12}^{(\mathrm{pt})}(+\infty) = -\frac{\varepsilon^2}{4}\,b\,\sinh(2\delta)\operatorname{sech}^2(2\delta)\,\cos\left(\frac{w(+\infty)}{\varepsilon}\right)\ . \tag{4.52}$$

The approximate calculation of the nonperturbative amplitude starts from the degeneracy of the eigenvalues $\pm E(\tau)$ at [79]

$$\tau_c = -i\arctan[\coth(\delta)]\ .$$

After some elementary steps, one finds

$$\frac{\gamma(w)}{E(w)} \approx \frac{b}{3}\frac{i}{w-w_c}$$

in the vicinity of $w_c = w(\tau_c)$, hence

$$c_{12}^{(\mathrm{np})}(+\infty) = 2\sin\left(\frac{\pi b}{6}\right)\exp\left(-\frac{|w_c|}{\varepsilon}\right)\ . \tag{4.53}$$

Figure 4.9 confirms the accuracy of this reasoning for $b = 1$ and $\delta = 0.5$; the integrals w_c and $w(+\infty)$ have been computed numerically. In the adiabatic regime, i.e., for $1/\varepsilon \gg 1$, there is perfect agreement between the exact final transition probability (full line) and the

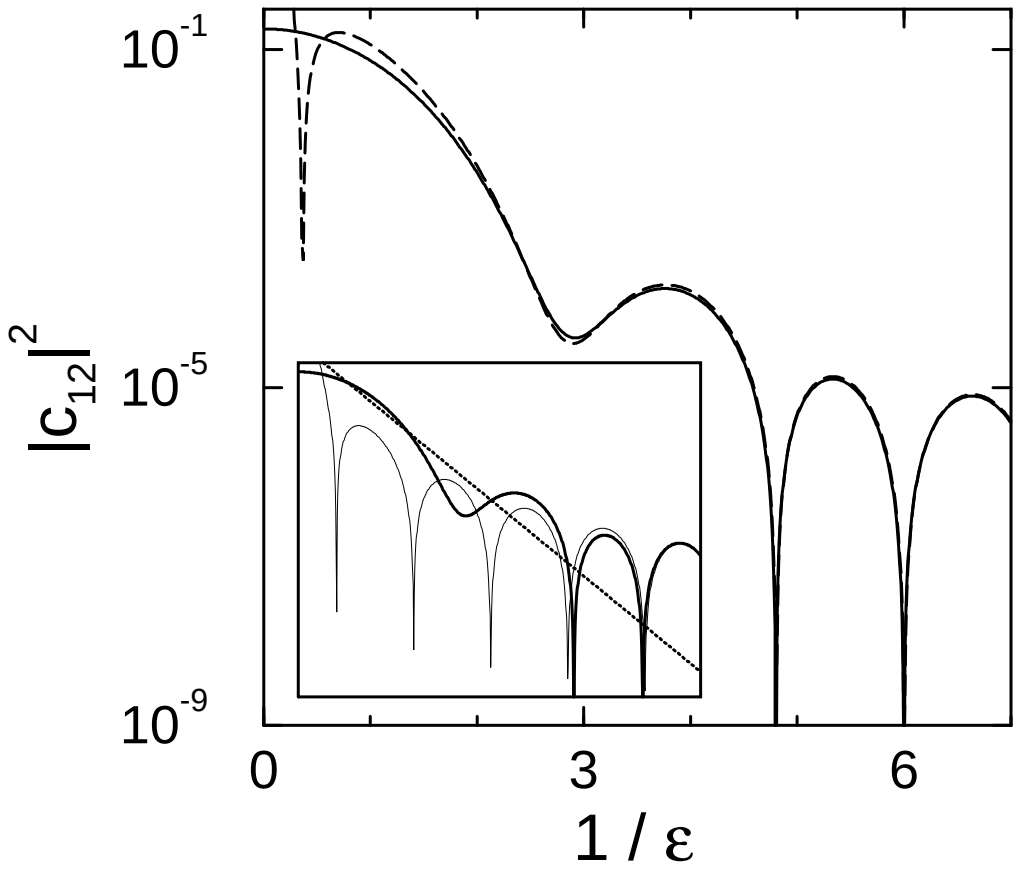

Figure 4.9: Full line: Exact final transition probability for the STIRAP system (4.51) with $b = 1$ and $\delta = 0.5$; dashed line: coherent superposition of the perturbative and the nonperturbative component, as approximated by equations (4.52) and (4.53). The inset shows the exact probability (full line), the nonperturbative part $|c_{12}^{(\mathrm{np})}|^2$ alone (dotted), and the perturbative part $|c_{12}^{(\mathrm{pt})}|^2$ alone (thin line).

prediction derived by summing and squaring equations (4.52) and (4.53). The inset shows, on the same scale, the exact data (full line) in comparison with the DDP exponential decay alone (dotted) and the perturbative component alone (thin line). Evidently, the perturbative component dominates for large $1/\varepsilon$, while the nonperturbative DDP component alone does not suffice to give a satisfactory description of the exact result for any ε, at least not for the values of b and δ chosen here. It is only when the interference of both components is taken into account that one gets a complete understanding of the dynamics.

Quite a particular example emerges if one chooses [118]

$$\begin{aligned} E(\tau) &= \frac{1}{2}\mathrm{sech}^2(\tau) \\ \theta(\tau) &= \frac{\pi}{4}\left(\tanh(\tau)+1\right) \ , \end{aligned} \tag{4.54}$$

which implies that the crucial ratio γ/E has no poles at all,

$$\frac{\gamma(\tau)}{E(\tau)} = \frac{\pi}{4} \, .$$

Hence, there is no nonperturbative contribution to the final transition amplitude, and one finds to lowest order

$$\begin{aligned} c_{12}(+\infty) &= \frac{i\varepsilon}{2} \, \frac{\pi}{4} \, \exp\left(-\frac{i}{\varepsilon} \tanh(\tau) \right) \Big|_{-\infty}^{+\infty} \\ &= \frac{\varepsilon\pi}{4} \sin\left(\frac{1}{\varepsilon} \right) \, . \end{aligned} \tag{4.55}$$

Moreover, equation (4.15) shows that the first superadiabatic transformation produces a diagonal Hamiltonian, so that even the exact solution to Schrödinger's equation can easily be found:

$$|c_{12}(+\infty)|^2 = \left(\frac{\varepsilon\pi}{4} \right)^2 \frac{1}{1 + (\varepsilon\pi/4)^2} \sin^2\left(\frac{1}{\varepsilon} \sqrt{1 + \left(\frac{\varepsilon\pi}{4} \right)^2} \right) \, ,$$

which confirms that the perturbative result (4.55) merges into the exact one for $\varepsilon \to 0$. Thus, the exact solution to the system (4.54), first stated in reference [118], follows from the general framework in a remarkably transparent manner. From the viewpoint of laser-induced population transfer, it is noteworthy that one can design γ/E such that the nonperturbative losses are avoided altogether.

4.6 Conclusions

The superadiabatic schemes have a twofold interpretation: On the one hand, they provide a basis with respect to which the transition amplitude acquires a simple and universal form, namely Berry's error function (4.41); on the other, they isolate from the total transition amplitude that part which cannot be represented by terms proportional to powers of the adiabaticity parameter ε. This part has been denoted as the nonperturbative component. Figure 4.3 can thus be read as showing *either* the same process in two different bases, *or* the evolution of the total transition probability and of its nonperturbative component. Both schemes I and S considered in this chapter behave quite similar up to the optimal order, and the scheme S may be a bit more tractable in practice, but I is distinguished by the explicit appearance of the eigenvalues of the iterated Hamiltonian. Since quantum evolution at finite ε corresponds, as closely as possible, to parallel transport in the optimal superadiabatic basis, phase corrections that appear in the adiabatic basis can be directly related to these eigenvalues, as shown explicitly in section 4.2 for the Stueckelberg phase emerging in the Landau-Zener transition.

The decomposition of the total transition amplitude into a "perturbative" and a "nonperturbative" component allows one, first of all, to get a simple physical picture for the large

oscillations that characterise the transition amplitude in the adiabatic basis: These oscillations stem from the interference of both components, and are largest in amplitude just at the point of crossover from the perturbative to the nonperturbative dynamics, see figure 4.7.

Whereas in "classic" systems covered by the Dykhne-Davis-Pechukas formula only the nonperturbative component survives in the final transition amplitude, the description of the STIRAP process within the rotating wave approximation has led to models where this is no longer true [79, 116]. In such cases even the final outcome is determined by the interference of the perturbative and the nonperturbative part, but already low-order approximations to the perturbative part, together with the DDP-approximation for the nonperturbative component, suffice to give a very satisfactory description of the exact transition probability. It is this combination of simplicity and accuracy that makes the present approach interesting also for the analysis of more involved systems occurring in laser-controlled population transfer.

5 Floquet theory for short laser pulses

Laser pulses with well-controlled temporal characteristics of amplitude and frequency have a high potential for selective manipulation of the internal state of atoms and molecules [85]. The theoretical analysis of such processes is quite demanding, since it requires the solution of the time-dependent Schrödinger equation for systems with several variable or adjustable parameters. Provided the pulse's envelope and frequency do not vary too rapidly, adiabatic techniques are of great value. However, an adiabatic analysis should be accompanied by the description of nonadiabatic processes that occur inevitably when the pulses are short.

In this chapter we develop such an adiabatic description of laser-pulsed N-level systems, based on the adiabatic response of Floquet states. We start in section 5.1 by formulating the adiabatic principle for Floquet states, in a manner that is particularly useful when the laser frequency is chirped. This yields the necessary prerequisites for section 5.2, where we quantify the deviations from the ideal adiabatic behaviour by elaborating and testing adiabatic perturbation theory for Floquet states, and the Landau-Zener description of multiphoton transitions among Floquet states. An appealing way of investigating quantum evolution beyond the adiabatic limit, relying on the use of superadiabatic bases, is adapted to the Floquet picture in section 5.3. After these theoretical developments, we compare in section 5.4 two mechanisms for the selective excitation of molecular vibrational states: A sequential chirp around successive single-photon resonances, and a multiphoton chirp. In section 5.5 we show how STIRAP-like population transfer schemes fit into our framework. Finally, we discuss our results in section 5.6.

5.1 Adiabatic response of Floquet states

We consider an N-level quantum system, described by a Hamiltonian matrix H_0 with eigenstates $|n\rangle$ ($n = 1, \ldots, N$), which interacts with a classical radiation pulse. The total Hamiltonian then is of the form

$$H(t) = H_0 + \widehat{\mu} F(t) \sin(\phi(t)) \;, \tag{5.1}$$

where $\widehat{\mu}$ is the dipole matrix, $F(t)$ describes the envelope of the pulse's electric field, and the phase $\phi(t)$ is a strictly monotonically increasing, smooth function of time. Its derivative,

$$\frac{\mathrm{d}\phi(t)}{\mathrm{d}t} \equiv \omega(t) \;, \tag{5.2}$$

is the instantaneous radiation frequency. We assume that the time interval during which ω changes significantly is large compared to the instantaneous oscillation period $T = 2\pi/\omega$, as is the case for conventionally chirped laser pulses. Likewise, it is understood that during the entire pulse the envelope $F(t)$ varies only slightly and smoothly on the time scale set by T.

We wish to understand, from an analytical point of view, the principles that determine the response of the system H_0 to the pulse. Given some initial state $|\psi(t_i)\rangle$, usually an eigenstate of H_0, and assuming that the pulse is fired in the time interval between t_i and t_f, we have to solve the time-dependent Schrödinger equation

$$i\hbar\frac{\mathrm{d}}{\mathrm{d}t}|\psi(t)\rangle = H(t)|\psi(t)\rangle \tag{5.3}$$

for $t_i \leq t \leq t_f$, and explain the distribution of the final wave function $|\psi(t_f)\rangle$ over the H_0-eigenstates. The goal is to extract guidelines for robust, selective population transfer from the initial state to a certain prescribed target state, to identify obstacles that might prohibit an efficient transfer, and, if possible, to develop strategies for overcoming them.

Although this problem is too wide in scope to be solved in full generality, even in cases where H_0 comprises just two or three levels, it is certainly possible to pin down its most decisive features. This is due to the fact that the Hamiltonian (5.1) becomes strictly periodic in time if both F and ω are kept fixed at any value that is met during the pulse. Each $T(\omega)$-periodic Hamiltonian obtained in this way has a complete set of Floquet states [106, 123], and the adiabatic theorem of quantum mechanics allows us to relate the solution of the Schrödinger equation (5.3) to these states [14, 15, 121], at least if the parameters vary sufficiently slowly. Utilising the adiabatic principle for developing optimal pulse strategies then requires to find out what "sufficiently slowly" means in practice, and to control, or deliberately exploit, deviations from the rigidly adiabatic evolution.

5.1.1 Instantaneous Floquet states

For carrying through this program in detail, we first switch from the time t to the phase ϕ as the independent variable. This is always possible, since $\phi(t)$ is strictly monotonically increasing. Writing $F(\phi)$, $\omega(\phi)$ and $|\psi(\phi)\rangle$ instead of $F(t(\phi))$, $\omega(t(\phi))$ and $|\psi(t(\phi))\rangle$, the Schrödinger equation becomes

$$i\hbar\omega(\phi)\frac{\mathrm{d}}{\mathrm{d}\phi}|\psi(\phi)\rangle = \left(H_0 + \widehat{\mu}F(\phi)\sin(\phi)\right)|\psi(\phi)\rangle \ .$$

Next, we collect the pulse parameters in a formal vector $R \equiv (F, \omega)$. Keeping R *fixed*, instead of considering pulses $R(\phi)$, each particular choice of R then yields an instantaneous scaled Hamiltonian

$$K^R(\phi) \equiv \frac{H_0 + \widehat{\mu}F\sin(\phi)}{\hbar\omega} \ , \tag{5.4}$$

which satisfies

$$K^R(\phi) = K^R(\phi + 2\pi) \; .$$

As a consequence of going from t to ϕ, the scaled Hamiltonian is always 2π-periodic, whereas the instantaneous period of the original Hamiltonian (5.1) varies when the frequency is chirped.

The Floquet theorem now provides [106, 123] for each fixed R a set of *Floquet states* $|\psi_\alpha^R(\phi)\rangle$,

$$|\psi_\alpha^R(\phi)\rangle = |u_\alpha^R(\phi)\rangle \exp\left(-i\,\frac{\varepsilon_\alpha^R}{\hbar\omega}\,\phi\right) \; , \tag{5.5}$$

with *quasienergies* ε_α^R and functions $|u_\alpha^R(\phi)\rangle$ that inherit the 2π-periodicity of $K^R(\phi)$,

$$|u_\alpha^R(\phi)\rangle = |u_\alpha^R(\phi + 2\pi)\rangle \; .$$

We briefly recollect some properties of the Floquet states that will be indispensable in the following [21]. Since each such state solves the time-dependent Schrödinger equation with the fixed-parameter Hamiltonian $K^R(\phi)$, i.e.,

$$i\frac{\mathrm{d}}{\mathrm{d}\phi}|\psi_\alpha^R(\phi)\rangle = K^R(\phi)|\psi_\alpha^R(\phi)\rangle \; , \tag{5.6}$$

one immediately gets

$$\left(K^R(\phi) - i\frac{\mathrm{d}}{\mathrm{d}\phi}\right)|u_\alpha^R(\phi)\rangle = \frac{\varepsilon_\alpha^R}{\hbar\omega}\,|u_\alpha^R(\phi)\rangle \; . \tag{5.7}$$

These are eigenvalue equations for quasienergies and Floquet functions at the respective parameters R, posed in an *extended Hilbert space* consisting of 2π-periodic functions [103]. This Hilbert space is naturally equipped with the scalar product

$$\langle\langle u_\alpha^R|v_\beta^R\rangle\rangle = \frac{1}{2\pi}\int_0^{2\pi}\mathrm{d}\phi\;\langle u_\alpha^R(\phi)|v_\beta^R(\phi)\rangle \; , \tag{5.8}$$

where $\langle\,\cdot\,|\,\cdot\,\rangle$ denotes the usual scalar product in the space spanned by the eigenstates of H_0.

An important point to be noted here is the Brillouin-zone structure of the solutions to these eigenvalue problems (5.7): If $|u_n^R(\phi)\rangle$ is an eigenfunction with quasienergy ε_n^R, then also $|u_n^R(\phi)e^{im\phi}\rangle$ is an eigenfunction, with quasienergy $\varepsilon_n^R + m\hbar\omega$. The requirement that the eigenfunctions are 2π-periodic restricts m to (positive or negative) integer numbers. However, all eigenfunctions that can be obtained by multiplying a given $|u_n^R(\phi)\rangle$ by a factor $e^{im\phi}$ belong to the *same* Floquet state, since obviously

$$|u_n^R(\phi)e^{im\phi}\rangle \exp\left(-i\,\frac{\varepsilon_n^R + m\hbar\omega}{\hbar\omega}\,\phi\right) = |u_n^R(\phi)\rangle \exp\left(-i\,\frac{\varepsilon_n^R}{\hbar\omega}\,\phi\right) \; .$$

Hence, the index α that labels the solutions to the eigenvalue problem (5.7) has to be understood as a double-index:

$$\alpha = (n, m) \ , \qquad n = 1, \ldots, N \ ; \ \ m = 0, \pm 1, \pm 2, \ldots \ ,$$

with n counting the N Floquet states to the 2π-periodic N-level Hamiltonian (5.4), and m accounting for the $\mathrm{mod}\,\hbar\omega$-multiplicity of the quasienergies that is introduced by factorising a Floquet state (5.5) into a 2π-periodic eigenfunction to the problem (5.7) and an exponential. In other words, there is a whole *class* of eigensolutions to (5.7), labelled by n, that corresponds to a single physical Floquet state; the individual members of this class are distinguished by the second quantum number m. Correspondingly, the quasienergy of a Floquet state is determined only up to an integer multiple of $\hbar\omega$.

This observation gives rise to two different notions of completeness, both of which will become important in the following. On the one hand, the N linearly independent Floquet states are complete, at each instant ϕ, in the N-dimensional Hilbert space spanned by the eigenstates of H_0,

$$\sum_{n=1}^{N} |u_n^R(\phi)\rangle\langle u_n^R(\phi)| = \mathbf{1} \ .$$

Hence, each solution $|\psi(\phi)\rangle$ to the fixed-parameter Schrödinger equation (5.6) can be expanded, with ϕ-independent coefficients a_n, according to

$$|\psi(\phi)\rangle = \sum_{n=1}^{N} a_n \, |u_n^R(\phi)\rangle \exp\!\left(-i \, \frac{\varepsilon_n^R}{\hbar\omega} \, \phi\right) \ , \tag{5.9}$$

where we have used the index n as a shorthand for $(n, 0)$, indicating that *only one* representative from each class of eigensolutions to (5.7) is needed here. On the other hand, *all* solutions to (5.7) are required for the completeness relation in the extended Hilbert space,

$$\sum_{n=1}^{N} \sum_{m=-\infty}^{+\infty} |u_n^R(\phi)\rangle\langle u_n^R(\phi')| \, e^{im(\phi-\phi')} = \mathbf{1} \cdot 2\pi\delta_{2\pi}(\phi - \phi') \ , \tag{5.10}$$

where $\delta_{2\pi}(\phi)$ denotes the 2π-periodic δ-function.

5.1.2 The adiabatic principle

The fact that the expansion coefficients a_n in equation (5.9) are ϕ– (i.e., time–) independent underlies the usefulness of the Floquet states for the analysis of the dynamics induced by a strictly time-periodic Hamiltonian. When expanding the same wave function (5.9) with respect to the eigenstates of H_0, the expansion coefficients vary with time in a complicated

manner. In contrast, once the Floquet states have been computed, and the initial wave function has been expanded in the Floquet basis, the wave function (5.9) is known for all times.

However, we are not primarily interested in the dynamics governed by a 2π-periodic Hamiltonian $K^R(\phi)$, but rather in the solutions to the Schrödinger equation (5.3) with the "slowly" varying Hamiltonian $H(t) = \hbar\omega(t)\, K^{R(\phi(t))}(\phi(t))$, where the curve $R(\phi)$ in parameter space specifies the laser pulse. To connect this pulse problem to the set of all Floquet eigenvalue problems that emerge by "freezing" $R(\phi)$ at some instantaneous value, we introduce a further phase variable p, formally independent of ϕ, and construct an "extended" Hamiltonian $K^{R(p)}(\phi)$:

$$K^{R(p)}(\phi) = \frac{H_0 + \widehat{\mu} F(p)\sin(\phi)}{\hbar\omega(p)} \,,$$

which has the important properties that it is 2π-periodic in ϕ for each fixed p, and that changing p accounts for the parameter variation during the pulse.

Next, we introduce a wave function $|\Psi(\phi,p)\rangle$ which equals the physical wave function $|\psi(\phi)\rangle$ on the diagonal $p=\phi$ [59, 60],

$$|\Psi(\phi,\phi)\rangle = |\psi(\phi)\rangle \,.$$

The Schrödinger equation with moving parameters,

$$i\frac{\mathrm{d}}{\mathrm{d}\phi}|\psi(\phi)\rangle = K^{R(\phi)}(\phi)|\psi(\phi)\rangle \,,$$

then translates into

$$\left[i\frac{\partial}{\partial\phi}|\Psi(\phi,p)\rangle + i\frac{\partial}{\partial p}|\Psi(\phi,p)\rangle\right]_{p=\phi} = K^{R(p)}(\phi)|\Psi(\phi,p)\rangle\big|_{p=\phi} \,.$$

Requiring the validity of this equation even for $p \neq \phi$, one obtains the evolution equation [14, 15]

$$i\frac{\partial}{\partial p}|\Psi(\phi,p)\rangle = \mathcal{K}(\phi,p)|\Psi(\phi,p)\rangle \,, \tag{5.11}$$

where we have introduced the operator

$$\mathcal{K}(\phi,p) \equiv K^{R(p)}(\phi) - i\frac{\partial}{\partial\phi} \,. \tag{5.12}$$

This evolution equation distinguishes the short time scale $T = 2\pi/\omega$, associated with ϕ, from the comparatively long time scale that characterises the change of the pulse parameters R, associated with p. We remark that also the so-called $(t{-}t')$ method, which has been designed for the numerical solution of the Schrödinger equation [94], makes similar use of two time variables.

We are now in a position to apply the adiabatic theorem of quantum mechanics [13, 17, 67, 89] to this equation (5.11). To this end, we first have to find the eigenstates and eigenvalues of the operator $\mathcal{K}(\phi, p)$ for each fixed parameter combination R that lies on the curve $R(p)$. This means nothing but solving all the eigenvalue problems (5.7), i.e., determining the instantaneous Floquet states. We require that these states be properly normalised with respect to the scalar product (5.8). This requirement still leaves the phases of the instantaneous Floquet states unspecified at each R. We fix these phases, up to an overall phase for each state, by demanding

$$\langle\langle u_\alpha^{R(p)} | \nabla_R \, u_\alpha^{R(p)} \rangle\rangle \cdot \dot{R}(p) = 0 \; . \tag{5.13}$$

This is where the change from the original time variable t to the phase ϕ becomes crucial. When working with t, one encounters extended Hilbert spaces spanned by the sets $\{|n\rangle e^{im\omega t}\}$, which means that a frequency chirp affects the basis vectors. In contrast, when working with ϕ, there is just a single extended Hilbert space spanned by $\{|n\rangle e^{im\phi}\}$, and the requirement (5.13) — paralleling directly the fixing of the instantaneous eigenstates' phases in the familiar formulations of the adiabatic theorem [13, 17, 67, 89] — corresponds to parallel transport [110] in this extended space. Moreover, we stipulate that different Floquet eigenfunctions belonging to the same Floquet state (i.e., eigenfunctions labelled by the same index n, but different m), differ merely by the phase factor $e^{im\phi}$, thus excluding an additional constant phase. It is then clear that all members of a class of Floquet functions respect equation (5.13), if one does.

For convenience, we now set $\phi(t_i) = 0$. The adiabatic theorem [13, 17, 67, 89], applied to the evolution equation (5.11), then states that given an initial function

$$|\Psi(\phi, p = 0)\rangle = \sum_\alpha c_\alpha |u_\alpha^{R(0)}(\phi)\rangle \; , \tag{5.14}$$

this function will evolve with p according to

$$|\Psi(\phi, p)\rangle = \sum_\alpha c_\alpha |u_\alpha^{R(p)}(\phi)\rangle \exp\left(-i \int_0^p \mathrm{d}p' \, \frac{\varepsilon_\alpha^{R(p')}}{\hbar\omega(p')} \right) \tag{5.15}$$

in the adiabatic limit of "infinitely slow" parameter variation, so that the expansion coefficients c_α remain constant, provided the instantaneous quasienergies ε_α^R remain nondegenerate along the path $R(p)$. Note that this application of the adiabatic theorem involves *all* solutions to the eigenvalue equation (5.7), as expressed by the appearance of the double index α.

In order to exploit this adiabatic principle for the solution of the original Schrödinger equation (5.3) that one is actually interested in, we first have to "lift" the initial state

$$|\psi(\phi = 0)\rangle = \sum_{n=1}^{N} a_n |u_n^{R(0)}(0)\rangle$$

to the extended Hilbert space. This procedure is *not unique*: All functions

$$|\Psi(\phi, p=0)\rangle = \sum_{\alpha} c_\alpha |u_\alpha^{R(0)}(\phi)\rangle$$
$$= \sum_{n=1}^{N} \sum_{m=-\infty}^{+\infty} c_{(n,m)} |u_{(n,0)}^{R(0)}(\phi) e^{im\phi}\rangle$$

correspond to $|\psi(\phi=0)\rangle$, if only

$$\sum_{m=-\infty}^{+\infty} c_{(n,m)} = a_n \tag{5.16}$$

for $n = 1, \ldots, N$. Therefore, it has to be guaranteed that the final wave function $|\psi(\phi_f))\rangle$ that results from lifting the initial state, adiabatically transporting in the extended Hilbert space, and back-projecting by setting $p = \phi_f$, does not depend on the particular choice of the coefficients $c_{(n,m)}$, provided they comply with (5.16). But this can easily be seen: Resolving the double index α, the transported wave function (5.15) becomes

$$|\Psi(\phi, p)\rangle = \sum_{n=1}^{N} \sum_{m=-\infty}^{+\infty} c_{(n,m)} |u_{(n,0)}^{R(p)}(\phi) e^{im\phi}\rangle \exp\left(-i \int_0^p \mathrm{d}p' \, \frac{\varepsilon_{(n,0)}^{R(p')}}{\hbar\omega(p')} - imp \right) .$$

After projection, this gives the *unique* adiabatic approximation

$$|\psi(\phi_f)\rangle = \sum_{n=1}^{N} a_n |u_n^{R(\phi_f)}(\phi_f)\rangle \exp\left(-i \int_0^{\phi_f} \mathrm{d}\phi \, \frac{\varepsilon_n^{R(\phi)}}{\hbar\omega(\phi)} \right)$$

to the Schrödinger wave function, using equation (5.16) and again writing n for $(n, 0)$. The simplicity of this consistency check rests once more on the use of the variable ϕ instead of t.

5.2 Adiabatic perturbation theory for Floquet states

The tool for understanding the deviations from strictly adiabatic motion that will necessarily emerge when the pulse parameters do *not* vary "infinitely slowly" is time-dependent perturbation theory in the adiabatic basis. We split the treatment into three parts, and consider deviations that occur during the pulse, when there are no near-degeneracies of instantaneous quasienergies, deviations that stem from the way the pulse is switched on and off and remain visible at the end of the pulse, and Landau-Zener transitions of Floquet states at avoided crossings of quasienergies.

5.2.1 Transition probabilities during the pulse

We assume that at the beginning of the pulse (when the pulse's amplitude still vanishes, so that the Floquet states coincide with the eigenstates of the unperturbed Hamiltonian H_0) only

a single eigenstate of H_0 is populated,

$$|\psi(\phi=0)\rangle = |u_1^{R(0)}(0)\rangle \ ,$$

lift this wave function to the extended Hilbert space,

$$|\Psi(\phi, p=0)\rangle = |u_{(1,0)}^{R(0)}(\phi)\rangle \ ,$$

and consider the *exact* wave function

$$|\Psi(\phi,p)\rangle = \sum_\alpha c_\alpha(p)|u_\alpha^{R(p)}(\phi)\rangle \exp\left(-i\int_0^p \mathrm{d}p' \, \frac{\varepsilon_\alpha^{R(p')}}{\hbar\omega(p')}\right) \tag{5.17}$$

that evolves from this initial state under the influence of the pulse. Note that we have done the lifting, without loss of generality, by going from $a_n(0) = \delta_{n,1}$ to $c_{(n,m)}(0) = \delta_{n,1}\delta_{m,0}$ (i.e., we have not spread the initial amplitude over more than one mode belonging to the Floquet state $n = 1$), but that, nonetheless, *all* indices α are needed in the expansion (5.17), since we now rely on the completeness (5.10) in the extended Hilbert space.

The expansion coefficients then obey the infinite system of equations

$$\partial_p c_\alpha(p) = -\sum_\beta c_\beta(p)\langle\langle u_\alpha^{R(p)}|\partial_p|u_\beta^{R(p)}\rangle\rangle \exp\left(-i\int_0^p \mathrm{d}p' \, \frac{\varepsilon_\beta^{R(p')} - \varepsilon_\alpha^{R(p')}}{\hbar\omega(p')}\right) \ , \tag{5.18}$$

where we have used the symbol ∂_p to indicate the derivative with respect to the evolution variable p, and the double brackets indicate the scalar product (5.8). First-order perturbation theory amounts to replacing $c_\beta(p)$ by the initial values $c_{(n,m)}(0) = \delta_{n,1}\delta_{m,0}$, hence

$$c_\alpha(p) = -\int_0^p \mathrm{d}p' \, \langle\langle u_\alpha^{R(p')}|\partial_{p'}|u_{(1,0)}^{R(p')}\rangle\rangle \exp\left(-i\int_0^{p'} \mathrm{d}p'' \, \frac{\varepsilon_{(1,0)}^{R(p'')} - \varepsilon_\alpha^{R(p'')}}{\hbar\omega(p'')}\right) \tag{5.19}$$

for $\alpha \neq (1,0)$. This integral, with its fast-oscillating integrand, is difficult to evaluate as it stands, but successive partial integrations yield a systematic expansion in powers of $\hbar$ [22, 24, 61]. The first such step results in

$$\begin{aligned} c_\alpha(p) = \ & -i\hbar\omega(p')\frac{\langle\langle u_\alpha^{R(p')}|\partial_{p'}|u_{(1,0)}^{R(p')}\rangle\rangle}{\varepsilon_{(1,0)}^{R(p')} - \varepsilon_\alpha^{R(p')}} \exp\left(-i\int_0^{p'} \mathrm{d}p'' \, \frac{\varepsilon_{(1,0)}^{R(p'')} - \varepsilon_\alpha^{R(p'')}}{\hbar\omega(p'')}\right)\Bigg|_0^p \\ & + \int_0^p \mathrm{d}p' \, \left(\partial_{p'}\left[i\hbar\omega(p')\frac{\langle\langle u_\alpha^{R(p')}|\partial_{p'}|u_{(1,0)}^{R(p')}\rangle\rangle}{\varepsilon_{(1,0)}^{R(p')} - \varepsilon_\alpha^{R(p')}}\right]\right) \exp\left(-i\int_0^{p'} \mathrm{d}p'' \, \frac{\varepsilon_{(1,0)}^{R(p'')} - \varepsilon_\alpha^{R(p'')}}{\hbar\omega(p'')}\right) \ . \end{aligned} \tag{5.20}$$

Upon further partial integration, the remaining integral then produces terms proportional to $\hbar^2$ and another integral, and so on. However, since the expression (5.20) has been obtained

within first-order perturbation theory from equation (5.18), only the $O(\hbar)$-term is consistent here; computing higher-order terms requires higher-order perturbation theory right from the outset.

Within the first-order approximation, we therefore keep only the $O(\hbar)$-term in equation (5.20). For calculating the amplitudes $a_n(\phi)$ in the expansion

$$|\psi(\phi)\rangle = \sum_{n=1}^{N} a_n(\phi)|u_n^{R(\phi)}(\phi)\rangle \exp\left(-i\int_0^\phi \mathrm{d}\phi' \, \frac{\varepsilon_n^{R(\phi')}}{\hbar\omega(\phi')}\right) ,$$

and hence the occupation probabilities $|a_n(\phi)|^2$ of the instantaneous Floquet states during the pulse, subject to the initial condition $a_n(0) = \delta_{n,1}$, we have to return to the physical Hilbert space by setting $p = \phi$, and to sum over all the modes that make up the n-th Floquet state. Assuming that there is no contribution from $p = 0$ (which is the case, e.g., if the envelope function $F(p)$ is continuously differentiable at $p = 0$, see following subsection), we find

$$\begin{aligned} |a_n(\phi)|^2 &= \hbar^2\omega^2(\phi) \left| \sum_{m=-\infty}^{+\infty} \frac{\langle\langle u_{(n,m)}^{R(p)}|\partial_p|u_{(1,0)}^{R(p)}\rangle\rangle_{p=\phi}}{\varepsilon_{(1,0)}^{R(\phi)} - \varepsilon_{(n,m)}^{R(\phi)}} \exp\left(-i\int_0^\phi \mathrm{d}\phi' \, \frac{\varepsilon_{(1,0)}^{R(\phi')} - \varepsilon_{(n,m)}^{R(\phi')}}{\hbar\omega(\phi')}\right) \right|^2 \\ &= \hbar^2\omega^2(\phi) \left| \sum_{m=-\infty}^{+\infty} \frac{\langle\langle u_{(n,m)}^{R(p)}|\partial_p|u_{(1,0)}^{R(p)}\rangle\rangle_{p=\phi}}{\varepsilon_{(1,0)}^{R(\phi)} - \varepsilon_{(n,m)}^{R(\phi)})} \, e^{im\phi} \right|^2 \end{aligned} \tag{5.21}$$

for $n \neq 1$. Hence, even when tracked in the adiabatic basis, the instantaneous occupation probabilities exhibit oscillations that result from the periodic driving. At this point the Brillouin-zone structure of the eigenvalue problem (5.7), which remained invisible as long as the parameters were kept fixed, manifests itself: It is the interference of different modes belonging to the same Floquet state that is responsible for the oscillations of the transition probabilities.

To see what this means in practice, we consider a pulsed two-level system with separation ΔE between the unperturbed energy levels:

$$H(t) = \frac{\Delta E}{2}\sigma_z + \mu F(t)\sin(\phi(t))\sigma_x \,, \tag{5.22}$$

where σ_x and σ_z denote the usual Pauli matrices; $\mu\sigma_x = \widehat{\mu}$ is the dipole operator. We set $\phi(t) = \omega t$, i.e., we keep the frequency ω fixed, and study the response to pulses of the form

$$F(t) = F_{\max}\sin^2\left(\frac{\pi t}{T_{\text{pulse}}}\right) \tag{5.23}$$

for $0 = t_i \leq t \leq T_{\text{pulse}} = t_f$. Figure 5.1 shows the quasienergies for $\Delta E/(\hbar\omega) = 2.2$ as functions of the instantaneous field strength F. There is an avoided crossing at $\mu F/(\hbar\omega) \approx 1.33$, where the two levels are ac-Stark-shifted into a three-photon resonance.

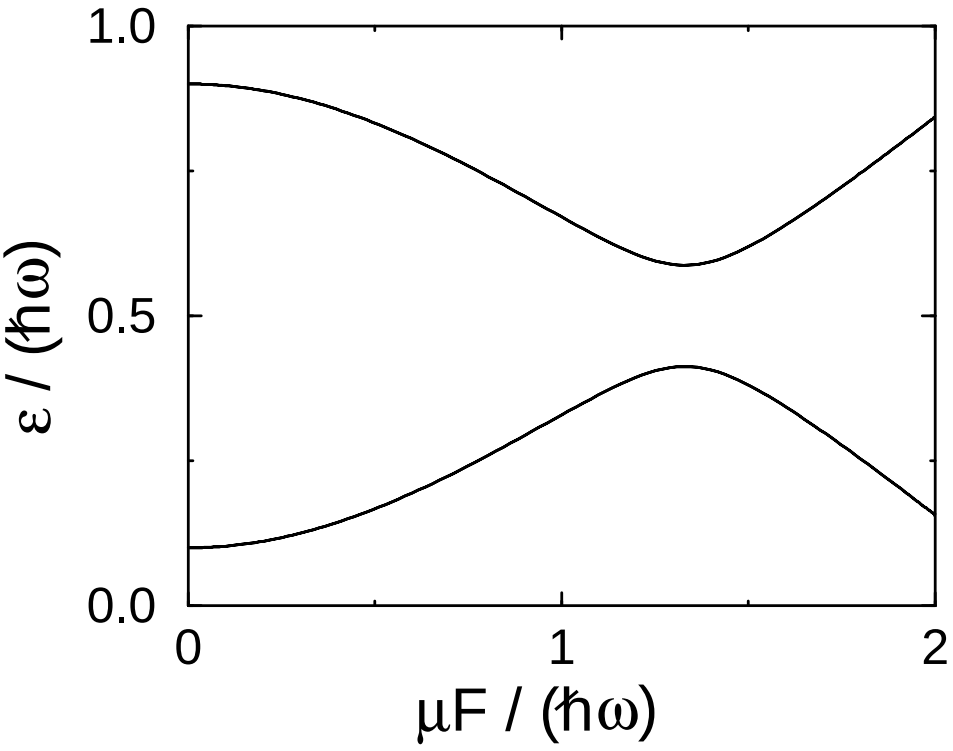

Figure 5.1: Quasienergies for the two-level system (5.22) with fixed frequency ω, and $\Delta E/(\hbar\omega) = 2.2$.

We stay clear of this resonance by choosing $\mu F_{\max}/(\hbar\omega) = 0.8$. The full line in the upper panel of figure 5.2 then shows the transition probability $|a_2(t)|^2$ obtained by numerically solving the Schrödinger equation for a pulse with a length of merely 20 cycles, $T_{\text{pulse}} = 20 \cdot 2\pi/\omega \equiv 20\,T$; the initial condition was $a_n(0) = \delta_{n,1}$. As expected from equation (5.21), the probability oscillates with period $T/2$. The lower panel depicts the absolute squares of the dominant expansion coefficients $c_{(2,m)}(t)$ in the extended Hilbert space as obtained from the $O(\hbar)$-term in equation (5.20); the dashed line in the upper panel — almost indistinguishable from the full line — shows what results from their coherent summation according to equation (5.21). Obviously, first-order adiabatic perturbation theory captures the exact transition probabilities very well, even though the pulse is by no means long, that is, the envelope $F(t)$ is not really slowly varying: it reaches its maximum amplitude already after 10 cycles. It is also interesting to see that the only significant deviation of the perturbative result from the exact one occurs in the middle of the pulse. This is due to the fact that the first derivative of the envelope function vanishes here, so that the result of the first-order calculation vanishes too (see equation (5.25) below); correcting this shortcoming requires a higher-order calculation.

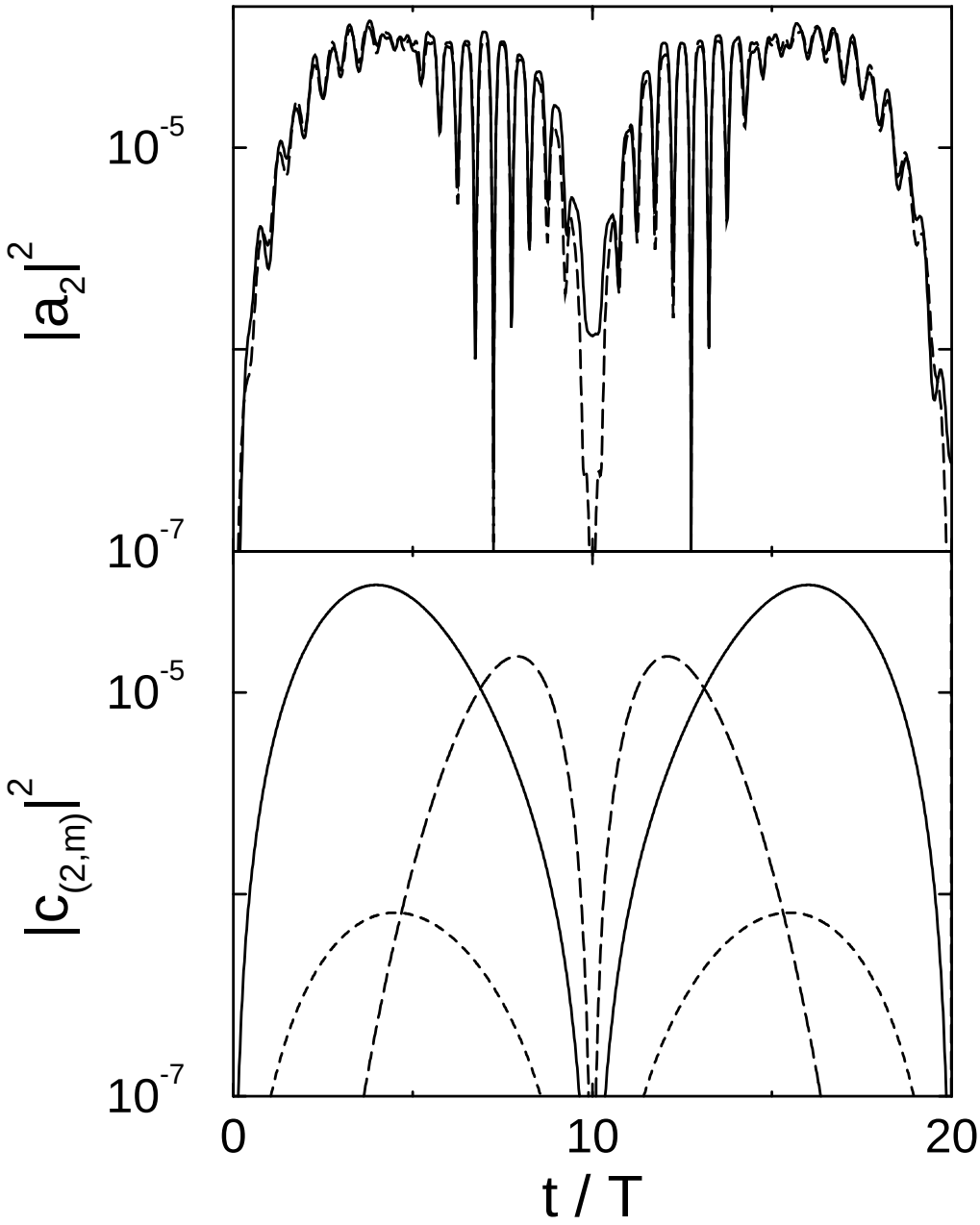

Figure 5.2: Upper panel: Numerically computed exact transition probability $|a_2(t)|^2$ (full line) for a two-level system (5.22) subjected to a pulse (5.23) with constant frequency ω; parameters are $\Delta E/(\hbar\omega) = 2.2$, $\mu F_{\max}/(\hbar\omega) = 0.8$, and $T_{\rm pulse} = 20 \cdot 2\pi/\omega \equiv 20\,T$. The dashed line results from first-oder perturbation theory; see equation (5.21). Lower panel: Dominant modes $c_{(2,m)}(t)$ for the expansion (5.17) in the extended Hilbert space.

5.2.2 Nonsmoothness at the pulse ends

We now focus on deviations from adiabaticity that are caused by some nonsmoothness at the beginning or end of the pulse. An example for this is provided already by the envelope (5.23): when continued by $F(t) \equiv 0$ for $t < 0$ and $t > T_{\rm pulse}$, it is once, but not twice, continuously

differentiable at the pulse ends. Consequences of such a roughness have been studied by Garrido and Sancho [33] and Sancho [104] in the context of merely parametrically time-dependent quantum systems, without periodic forcing.

Let us assume that the first $j-1$ derivatives of the envelope function $F(p)$ vanish at the pulse ends, and that $F^{(j)}(0+) \neq 0$ and/or $F^{(j)}(p_f-) \neq 0$. Switching again to the variable ϕ, with $\phi(t_i) = 0$ and $\phi(t_f) = \phi_f$, and starting from the first-order approximation (5.19), the leading contribution to the transition amplitude is obtained after integrating j times by parts:

$$\begin{aligned} c_\alpha(p_f) =& (-1)^j \left[\left(\frac{i\hbar\omega(p)}{\varepsilon^{R(p)}_{(1,0)} - \varepsilon^{R(p)}_\alpha} \, \partial_p \right)^{j-1} \frac{i\hbar\omega(p) \, \langle\langle u^{R(p)}_\alpha | \partial_p | u^{R(p)}_{(1,0)} \rangle\rangle}{\varepsilon^{R(p)}_{(1,0)} - \varepsilon^{R(p)}_\alpha} \right] \\ & \times \exp\left(-i \int_0^p \mathrm{d}p' \, \frac{\varepsilon^{R(p')}_{(1,0)} - \varepsilon^{R(p')}_\alpha}{\hbar\omega(p')} \right) \Bigg|_0^{p_f} \end{aligned} \tag{5.24}$$

for $\alpha \neq (1,0)$. Next, we use the identity

$$\langle\langle u^{R(p)}_\alpha | \partial_p | u^{R(p)}_\beta \rangle\rangle = \hbar\omega(p) \frac{\langle\langle u^{R(p)}_\alpha | \partial_p \mathcal{K} | u^{R(p)}_\beta \rangle\rangle}{\varepsilon^{R(p)}_\beta - \varepsilon^{R(p)}_\alpha} \qquad (\alpha \neq \beta) \; . \tag{5.25}$$

Since $\langle\langle u^{R(p)}_\alpha | \partial_p^\ell \mathcal{K} | u^{R(p)}_\beta \rangle\rangle = 0$ for $\ell < j$ and $p = 0, p_f$ by assumption, a nonvanishing contribution to $c_\alpha(p_f)$ can result only if ∂_p acts j times directly on $\mathcal{K}$. Hence, we find

$$\begin{aligned} c_\alpha(p_f) =& (-i)^j \left(\frac{\hbar\omega(p)}{\varepsilon^{R(p)}_{(1,0)} - \varepsilon^{R(p)}_\alpha} \right)^{j+1} \langle\langle u^{R(p)}_\alpha | \partial_p^j \mathcal{K} | u^{R(p)}_{(1,0)} \rangle\rangle \\ & \times \exp\left(-i \int_0^p \mathrm{d}p' \, \frac{\varepsilon^{R(p')}_{(1,0)} - \varepsilon^{R(p')}_\alpha}{\hbar\omega(p')} \right) \Bigg|_0^{p_f} \; . \end{aligned}$$

At the pulse ends $p = 0$ and $p = p_f$ we have $|u^{R(0)}_\alpha(\phi)\rangle = |n\, e^{im\phi}\rangle$, $|u^{R(p_f)}_\alpha(\phi)\rangle = |n\, e^{im\phi}\rangle e^{i\gamma_n}$, and $\varepsilon^{R(p)}_\alpha = E_n + m\hbar\omega(p)$, where $|n\rangle$ and E_n denote the eigenstates and eigenvalues of H_0, respectively. The real numbers γ_n are geometrical Berry phases [8], resulting from the parallel transport (5.13). Hence,

$$\langle\langle u^{R(0)}_\alpha | \partial_p^j \mathcal{K} | u^{R(0)}_{(1,0)} \rangle\rangle = \frac{1}{\hbar\omega(0)} \, \langle n | \widehat{\mu} | 1 \rangle \, F^{(j)}(0) \, \frac{1}{2i} \, (\delta_{m,1} - \delta_{m,-1}) \; ; \tag{5.26}$$

for $p = p_f$ one also gets a Berry phase factor $e^{i(\gamma_1 - \gamma_n)}$. Since the sinusoidal driving described by the quasienergy operator $\mathcal{K}$ connects only neighbouring modes, i.e., modes differing in m

by ± 1, the final transition probabilities $|a_n(\phi_f)|^2$ for $n \neq 1$ become

$$|a_n(\phi_f)|^2 = \frac{|\langle n|\widehat{\mu}|1\rangle|^2}{4} \left| e^{i(\gamma_1-\gamma_n)} \exp\left(-i\int_0^{\phi_f} \mathrm{d}\phi\, \frac{\varepsilon_{(1,0)}^{R(\phi)} - \varepsilon_{(n,0)}^{R(\phi)}}{\hbar\omega(\phi)}\right) \right.$$
$$\times (\hbar\omega(\phi_f))^j F^{(j)}(\phi_f -) \left[\frac{e^{i\phi_f}}{(E_n + \hbar\omega(\phi_f) - E_1)^{j+1}} - \frac{e^{-i\phi_f}}{(E_n - \hbar\omega(\phi_f) - E_1)^{j+1}}\right]$$
$$\left. - (\hbar\omega(0))^j\ F^{(j)}(0+) \left[\frac{1}{(E_n + \hbar\omega(0) - E_1)^{j+1}} - \frac{1}{(E_n - \hbar\omega(0) - E_1)^{j+1}}\right]\right|^2 \tag{5.27}$$

This formula has a transparent structure: Each of the two modes contributing to the final transition probability picks up contributions originating from the nonsmoothness at both the beginning and at the end of the pulse; the latter are accompanied by the dynamical and geometrical phases that result from evolving the wave function over the whole pulse. The dynamical phases are determined by the quasienergies, reflecting adiabatic transport of Floquet states during the pulse; the geometrical phases express the possible anholonomy of this transport [8, 110].

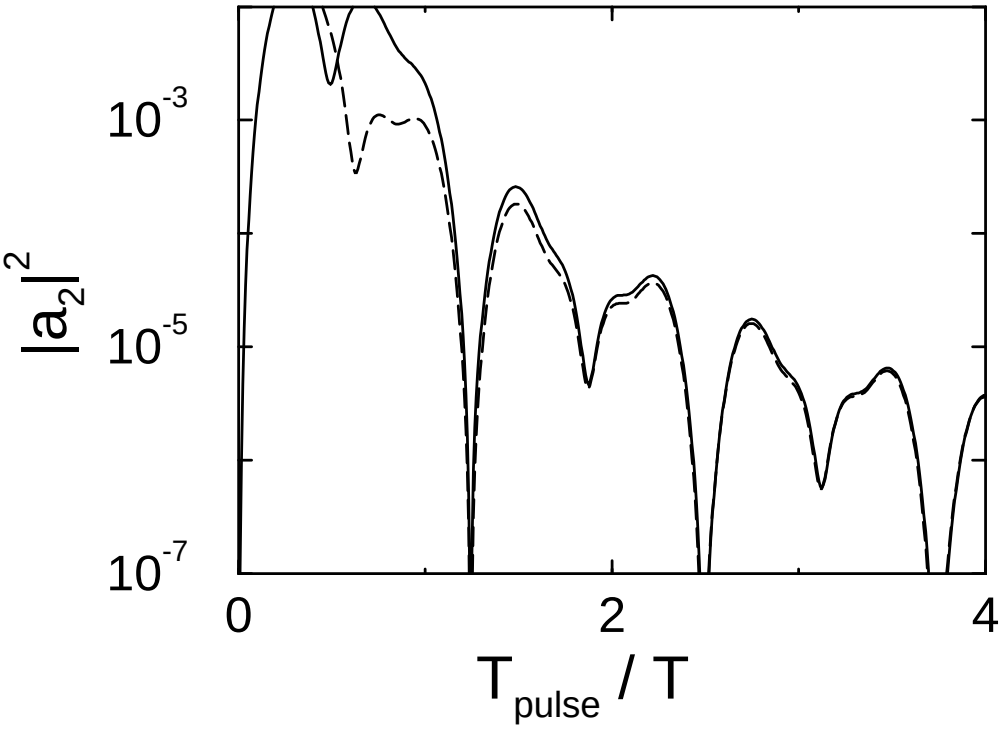

Figure 5.3: Comparison of the perturbative prediction (5.27) for the final transition probability $|a_2(T_{\mathrm{pulse}})|^2$ in a pulsed two-level system (5.22) (dashed) with exact numerical data (full line), for pulses no longer than merely 4 cycles $T = 2\pi/\omega$. The frequency ω is kept constant; the pulse shape is given by equation (5.23). Parameters are $\Delta E/(\hbar\omega) = 0.2$ and $\mu F_{\max}/(\hbar\omega) = 0.1$.

Figure 5.3 shows a comparison of the perturbative result (5.27) with exact numerical data, again for the two-level system (5.22) with the envelope function (5.23) and constant frequency ω, so that $j = 2$. In this case the geometrical phases vanish. We now have chosen $\mu F_{\max}/(\hbar\omega) = 0.1$ and $\Delta E/(\hbar\omega) = 0.2$. The analytical approximation to $|a_2(T_{\rm pulse})|^2$ starts to agree very well with the exact data already for pulses which are merely two cycles long, which again underlines the usefulness of adiabatic Floquet state perturbation theory even for really short pulses.

Evidently, the total nonadiabatic loss of probability from the initially populated state $n = 1$ that is caused by the nonsmoothness at the onset of the pulse is given by

$$\sum_{n=2}^{N} |a_n(0+)|^2 = \frac{(\hbar\omega(0))^{2j}}{4} \sum_{n=2}^{N} \left| \frac{F^{(j)}(0+)\,\langle n|\widehat{\mu}|1\rangle}{(E_n + \hbar\omega(0) - E_1)^{j+1}} - \frac{F^{(j)}(0+)\,\langle n|\widehat{\mu}|1\rangle}{(E_n - \hbar\omega(0) - E_1)^{j+1}} \right|^2 . \tag{5.28}$$

Thus, if the turn-on of the pulse is somewhat rough, a certain amount of probability is lost for the intended adiabatic transfer right from the beginning. We will return to this expression (5.28) in the following section, where we analyse pulse dynamics with the help of superadiabatic techniques.

5.2.3 Landau-Zener transitions among Floquet states

Near-degeneracies of instantaneous quasienergies during the pulse are of particular interest, since they lead to comparatively simple and robust strategies for controlling the outcome of the pulse by suitably adjusting its parameters.

We consider an avoided crossing between the quasienergy $\varepsilon^R_{(1,0)}$ originating from the energy of the initially occupied state, and some other quasienergy ε^R_α. More specifically, we assume that the variation of the instantaneous quasienergies as seen by the system in the course of time is of the Landau-Zener form [80, 124],

$$\begin{aligned} \varepsilon^{R(t)}_{(1,0)} &= \tfrac{1}{2}\sqrt{(\delta\varepsilon)^2 + \gamma^2(t-t_0)^2} && \equiv \varepsilon_+(t) \\ \varepsilon^{R(t)}_{\alpha} &= -\varepsilon^{R(t)}_{(1,0)} && \equiv \varepsilon_-(t)\ , \end{aligned}$$

so that an avoided quasienergy crossing of width $\delta\varepsilon$ is encountered at $t = t_0$; we are free to set $t_0 = 0$. Within the first-order approximation (5.19), the amplitude of the anticrossing state after the passage of the avoided crossing is then given by

$$c_\alpha(+\infty) = -\int_{-\infty}^{+\infty} {\rm d}t\, \langle\langle u^{R(t)}_\alpha | \partial_t | u^{R(t)}_{(1,0)}\rangle\rangle \exp\left(-\frac{i}{\hbar}\int_0^t {\rm d}t'\ (\varepsilon_+(t') - \varepsilon_-(t'))\right)\ , \tag{5.29}$$

apart from an irrelevant phase factor. Now we can adopt standard arguments [10, 22]: Introducing the variable

$$w(t) = \frac{1}{\hbar}\int_0^t \mathrm{d}t' \left(\varepsilon_+(t') - \varepsilon_-(t')\right)$$
$$= \frac{t}{2\hbar}\sqrt{(\delta\varepsilon)^2 + (\gamma t)^2} + \frac{(\delta\varepsilon)^2}{2\hbar\gamma}\mathrm{arsinh}\left(\frac{\gamma t}{\delta\varepsilon}\right) ,$$

the complex degeneracy point $t_c = -i\,\delta\varepsilon/\gamma$ of the quasienergies $\varepsilon_+(t)$ and $\varepsilon_-(t)$ corresponds to

$$w(t_c) \equiv w_c = -i\frac{\pi}{4}\frac{(\delta\varepsilon)^2}{\hbar\gamma} ,$$

and the expression (5.29) can be brought into the universal form [10, 22]

$$c_\alpha(+\infty) = \int_{-\infty}^{+\infty} \mathrm{d}w\, \frac{i}{6(w - w_c)} e^{-iw} .$$

Closing the contour of integration by an infinitely large semi-circle in the lower half of the complex w-plane immediately gives

$$c_\alpha(+\infty) = \frac{\pi}{3} e^{-iw_c} .$$

The prefactor $\pi/3 \approx 1.047$ appearing in the present first-order analysis is changed to unity when the perturbation series is summed to all orders [10, 22, 27], so that the correct probability for a Landau-Zener transition among the anticrossing Floquet states becomes

$$P_{LZ} = e^{-2|w_c|} = \exp\left(-\frac{\pi}{2}\frac{(\delta\varepsilon)^2}{\hbar\gamma}\right) . \tag{5.30}$$

The remarkable point here is that we are treating Landau-Zener transitions in systems of the type (5.1) that vary both parametrically and periodically in time, that is, we have what is conventionally termed "multiphoton transitions" among Floquet states, but the use of the evolution equation (5.11), which underlies the expression (5.29), has allowed us to reduce this problem entirely to the usual analysis for Landau-Zener transitions among energy eigenstates. To demonstrate the accuracy of our arguments, we resort once more to the forced two-level system (5.22), keep the field strength fixed at $\mu F/(\hbar\omega_i) = 6.089$, and consider a linear frequency chirp

$$\omega(t) = \omega_i + \frac{t - t_i}{t_f - t_i}\left(\omega_f - \omega_i\right) \tag{5.31}$$

between times t_i and t_f, with $\Delta E/(\hbar\omega_i) = 5.556$ and $\Delta E/(\hbar\omega_f) = 4.444$. Thus, we are chirping over a five-photon resonance. In figure 5.4 we depict the corresponding instantaneous quasienergies, shifted by $-\hbar\omega/2$ for graphical convenience.

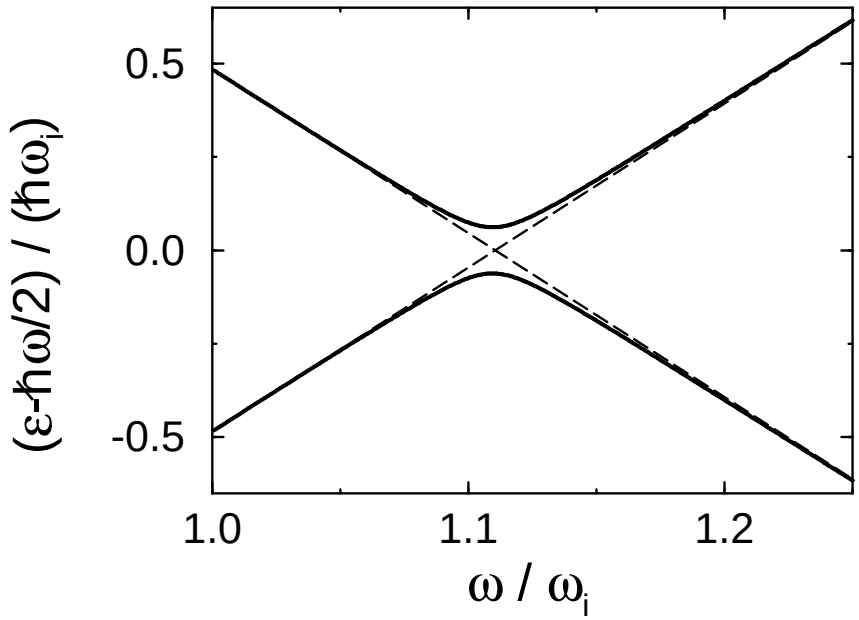

Figure 5.4: Instantaneous quasienergies (full lines) for the driven two-level system (5.22) with fixed amplitude $\mu F/(\hbar\omega_i) = 6.089$. The reference frequency ω_i is given by $\Delta E/(\hbar\omega_i) = 5.556$, so that the avoided crossing corresponds to a five-photon resonance. The width of the avoided crossing is $\delta\varepsilon/(\hbar\omega_i) = 0.1236$; the total diabatic quasienergy variation for $\omega_f/\omega_i = 1.25$ is $\Delta\varepsilon/(\hbar\omega_i) = 1.1004$. The asymptotes confirm that the five-photon transition induced by a linear frequency chirp is of the Landau-Zener type.

Choosing the initial frequency ω_i as the reference frequency, and assuming that $(t_f - t_i) = r \cdot 2\pi/\omega_i$, the Landau-Zener formula (5.30) can be written in the form

$$\frac{\ln P_{LZ}}{r} = -\frac{\pi^2}{2}\frac{(\delta\varepsilon/\hbar\omega_i)^2}{\Delta\varepsilon/\hbar\omega_i} \,,$$

where $\Delta\varepsilon$ is the *diabatic* quasienergy variation between times t_i and t_f, so that $\gamma/2 = \Delta\varepsilon/(t_f - t_i)$ in equation (5.30). From the data underlying figure 5.4 one determines $\delta\varepsilon/(\hbar\omega_i) = 0.1236$ and $\Delta\varepsilon/(\hbar\omega_i) = 1.1004$; hence one expects $\ln P_{LZ}/r = -0.0685$. On the other hand, we have solved the time-dependent Schrödinger equation for the chirped two-level system by direct numerical integration in order to determine the Landau-Zener transition probabilities without approximation; the resulting data shown in figure 5.5 give $\ln P_{LZ}/r = -0.0687$. The striking agreement with the theoretical expectation confirms that the reduction of the original Floquet-type transition problem to the usual Landau-Zener problem, which relies crucially on the evolution equation (5.11) in the extended Hilbert space, correctly captures the physics of chirp-induced multiphoton transitions.

5.3 Superadiabatic Floquet dynamics

To characterise the degree of adiabaticity when the laser pulses are short, we now replace the evolution variable p in equation (5.11) by q/η, and stipulate that q varies between 0 and

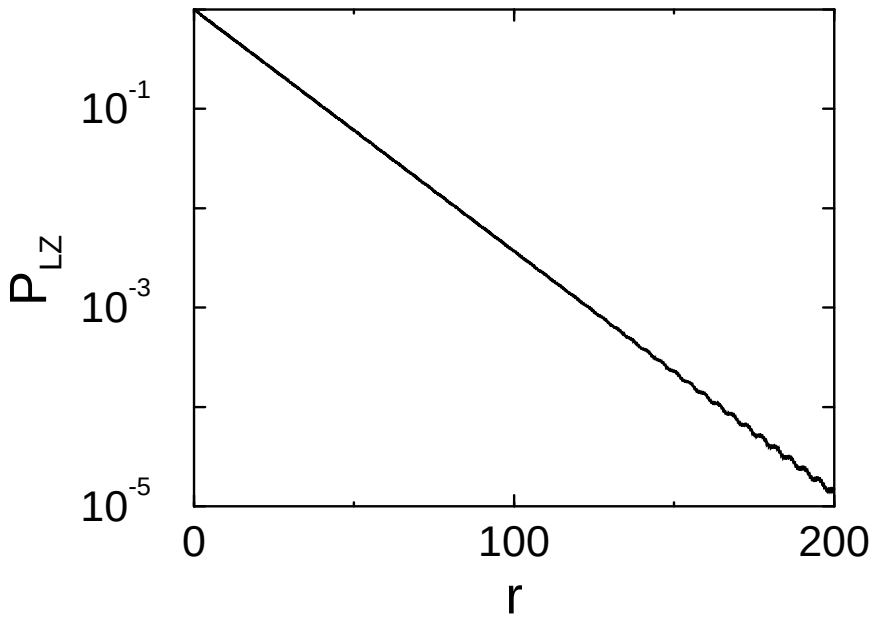

Figure 5.5: Landau-Zener transition probabilities for the two-level system (5.22) with fixed amplitude $\mu F/(\hbar\omega_i) = 6.089$ and linear frequency chirp (5.31), corresponding to the avoided quasienergy crossing displayed in figure 5.4. The data were obtained from numerical solutions of the time-dependent Schrödinger equation for chirps with duration $t_f - t_i = r \cdot 2\pi/\omega_i$. The slope of the straight line is $\ln P_{LZ}/r = -0.0687$.

1 during the pulse, so that approaching the adiabatic limit means taking the dimensionless adiabaticity parameter η to zero. The evolution equation (5.11) then takes the form

$$i\eta\frac{\partial}{\partial q}|\Psi(\phi,q)\rangle = \mathcal{K}(\phi,q)|\Psi(\phi,q)\rangle \ , \tag{5.32}$$

with $|\Psi(\phi,q)\rangle$ and $\mathcal{K}(\phi,q)$ as shorthand notation for $|\Psi(\phi,q/\eta)\rangle$, $\mathcal{K}(\phi,q/\eta)$. As a consequence, the transition amplitudes considered in sections 5.2.1 and 5.2.2 become proportional to powers of η, whereas the Landau-Zener transition probability studied in section 5.2.3 is of the order $O(\exp(-\mathrm{const.}/\eta))$. The guiding idea behind superadiabatic approaches to quantum dynamics [10, 23, 27, 66] is to provide a series of successive unitary transformations to new frames of reference that are better adapted to the actual "fast" evolution than the adiabatic basis, such that in these new bases the contributions to the transition amplitude that are merely proportional to powers of η are removed. A very transparent formulation of this idea has been given by Berry [10] for parametrically time-dependent quantum systems. In this section we generalise his approach to laser-driven systems (5.1), and show that superadiabatic transformations furnish a diagnostic tool for optimising laser pulses.

To this end, we try to represent the exact solution to equation (5.32) that emerges from the initial condition

$$|\Psi_\alpha(\phi,0)\rangle = |u_\alpha^{R(0)}(\phi)\rangle$$

by the power series

$$|\Psi_\alpha(\phi,q)\rangle = \exp\left(-\frac{i}{\eta}\int_0^q \mathrm{d}q'\,\frac{\varepsilon_\alpha^{R(q')}}{\hbar\omega(q')}\right)\sum_{s=0}^{\infty}\eta^s\,|v_\alpha^{(s)}(\phi,q)\rangle\;, \tag{5.33}$$

where the functions $|v_\alpha^{(s)}(\phi,q)\rangle$ are linear combinations of the instantaneous Floquet functions:

$$|v_\alpha^{(s)}(\phi,q)\rangle = \sum_\beta a_{\alpha\beta}^{(s)}(q)\,|u_\beta^{R(q)}(\phi)\rangle\;, \tag{5.34}$$

with initial conditions

$$a_{\alpha\beta}^{(0)}(q) = \delta_{\alpha,\beta}\;, \tag{5.35}$$

so that $|v_\alpha^{(0)}(\phi,q)\rangle = |u_\alpha^{R(q)}(\phi)\rangle$, and

$$a_{\alpha\beta}^{(s)}(0) = 0 \qquad \text{for} \quad s>0\;.$$

Inserting the ansatz (5.33) into the evolution equation (5.32) and comparing coefficients of equal powers of η, we obtain the recursive relations

$$a_{\alpha\beta}^{(s)}(q) = \frac{-i\hbar\omega(q)}{\varepsilon_\alpha^{R(q)}-\varepsilon_\beta^{R(q)}}\left[\partial_q a_{\alpha\beta}^{(s-1)}(q) + \sum_\gamma \langle\langle u_\beta^{R(q)}|\partial_q|u_\gamma^{R(q)}\rangle\rangle\, a_{\alpha\gamma}^{(s-1)}(q)\right] \quad (\alpha\neq\beta)$$

$$\partial_q a_{\alpha\alpha}^{(s)}(q) = -\sum_\beta \langle\langle u_\alpha^{R(q)}|\partial_q|u_\beta^{R(q)}\rangle\rangle a_{\alpha\beta}^{(s)}(q)$$

which are direct analogs of the corresponding relations for systems with merely a simple parametric time-dependence [27]. They allow us to determine the coefficients $a_{\alpha\beta}^{(s)}(q)$ required in equation (5.34), and hence the wave functions (5.33).

The desired sequence of superadiabatic bases $\{\,|\psi_n^{(S)}(\phi)\rangle\,\}$ ($S=0,1,2\ldots$) for monitoring the solutions to the original Schrödinger equation (5.3) is obtained by truncating the series (5.33) at $s=S$, and then returning to the physical Hilbert space by equating $q/\eta=\phi$:

$$|\psi_n^{(S)}(\phi)\rangle = \exp\left(-i\int_0^\phi \mathrm{d}\phi'\,\frac{\varepsilon_n^{R(\phi')}}{\hbar\omega(\phi')}\right)\sum_{s=0}^{S}|v_n^{(s)}(\phi,\phi)\rangle\;.$$

Because of equation (5.35), the zeroth superadiabatic basis ($S=0$) coincides with the adiabatic basis itself.

Right from the outset, it is clear that the ansatz (5.33) will, in general, be divergent: It is merely a power series in η and thus cannot account for the Landau-Zener-type contributions to the transition amplitude, since these are "beyond all orders in η". However, the series is

asymptotic [10]. Truncating at an optimal S_0, and expanding the Schrödinger wave function $|\psi(\phi)\rangle$ in that particular basis $\{\,|\psi_n^{(S_0)}(\phi)\rangle\,\}$, means disentangling the power-series contributions to the transition amplitude from the actually important Landau-Zener-type contributions, which then adopt a universal form [10]. In this way one isolates the essentials of the transition dynamics.

To explore how this works for laser-pulsed systems, we return to the two-level Hamiltonian (5.22) with pulse envelope (5.23) and fixed frequency ω. As in the situation studied in figure 5.2, we set $\Delta E/(\hbar\omega) = 2.2$ and consider a pulse with a length of merely 20 cycles, but now the peak field strength is $\mu F_{\max}/(\hbar\omega) = 1.5$, so that the avoided quasienergy crossing seen in figure 5.1 is passed twice in the course of the pulse. Figure 5.6 shows the projection

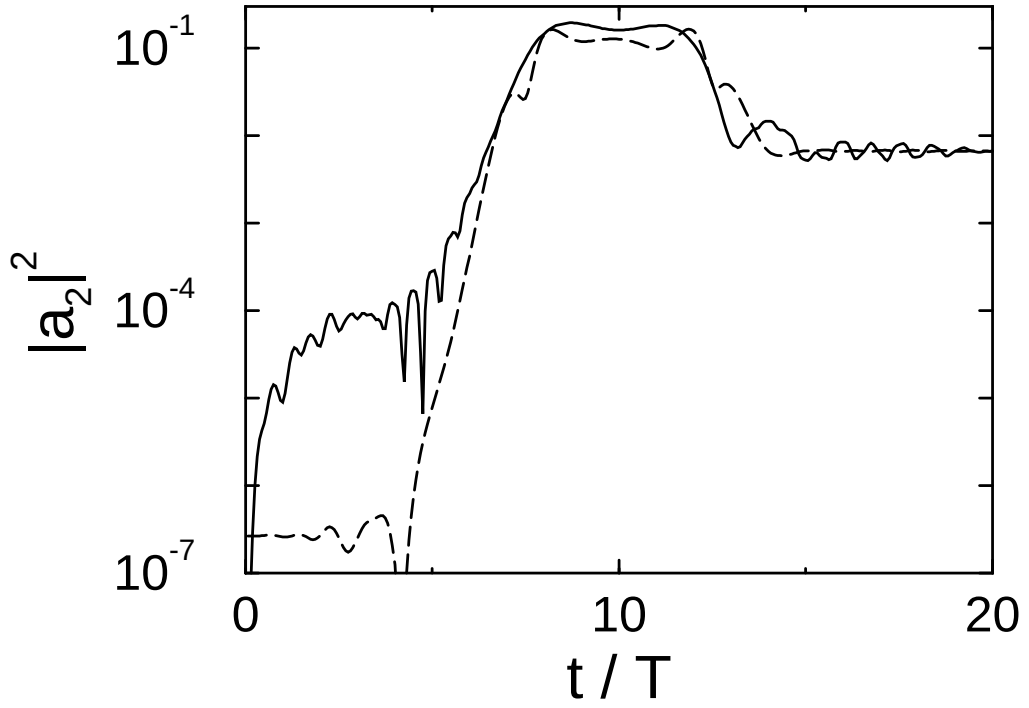

Figure 5.6: Squared projection of the Schrödinger wave function $|\psi(t)\rangle$ evolving from the initial bare state $|1\rangle$ under the influence of a pulse (5.23) with constant frequency ω onto the zeroth-order superadiabatic basis vector $|u_2^{R(t)}(t)\rangle$ (full line), and onto the second-order superadiabatic basis vector $|\psi_2^{(2)}(t)\rangle$ (dashed). Parameters are $\Delta E/(\hbar\omega) = 2.2$ and $\mu F_{\max}/(\hbar\omega) = 1.5$, so that the avoided crossing seen in figure 5.1 is passed twice during the pulse; the pulse length is $T_{\text{pulse}} = 20\,T$.

of the numerically computed solution $|\psi(t)\rangle$ to the Schrödinger equation (with bare state $|1\rangle$ as initial condition) onto the instantaneous adiabatic Floquet function $|u_2^{R(t)}(t)\rangle$ and onto the second-order superadiabatic basis vector $|\psi_2^{(2)}(t)\rangle$. A characteristic difference becomes visible at the beginning of the pulse: When measured in the adiabatic basis, the transition probability starts at zero and reaches about 10^{-4} after a few cycles. In contrast, with respect

to the second-order superadiabatic basis the probability remains initially constant at the value $2.640 \cdot 10^{-7}$. This is almost exactly equal to the value $|a_2(0+)|^2 = 2.641 \cdot 10^{-7}$ predicted by equation (5.28) as the nonadiabatic population loss due to the nonsmoothness of the pulse envelope at the beginning: Since the envelope is only once continuously differentiable, we have $j = 2$ in equation (5.28), so that the transition amplitude is affected to the order $O(\eta^2)$. The second-order superadiabatic basis is constructed such that this defect is taken out of the dynamics, so that the transition probability, viewed in this basis, initially stays constant at the value given by equation (5.28). The change of amplitude in the superadiabatic basis is caused mainly by the two passages through the avoided crossing at $t \approx 7.6\,T$ and $t \approx 12.4\,T$.

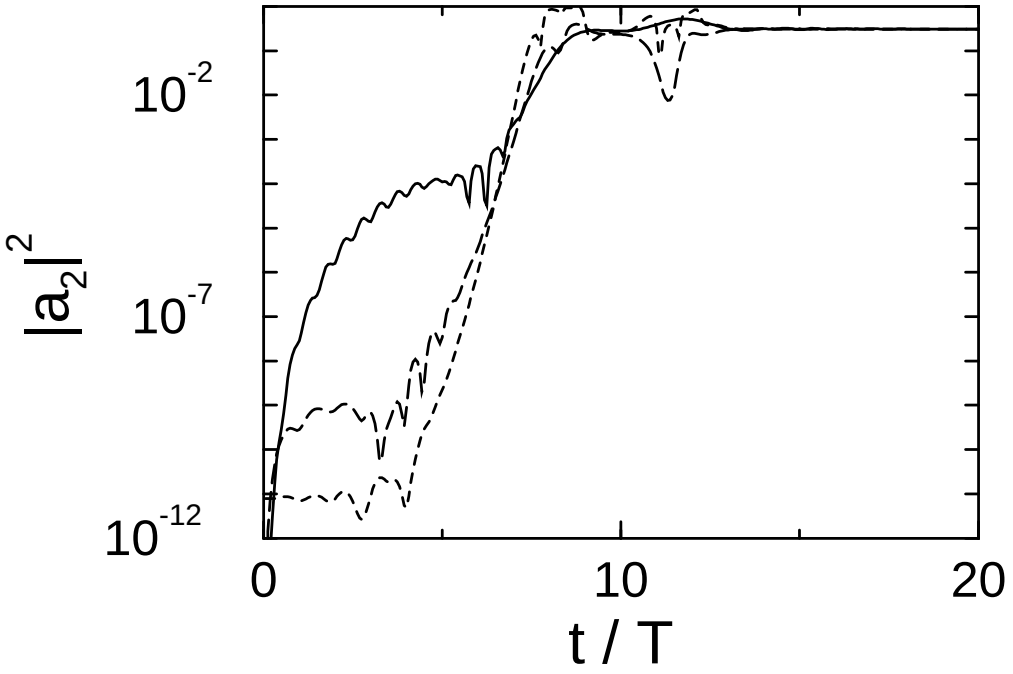

Figure 5.7: As figure 5.6, but for a pulse with the smoother envelope (5.36). The solution to the Schrödinger equation has been projected onto the adiabatic basis vector $|u_2^{R(t)}(t)\rangle$ (full line), onto the second-order superadiabatic basis vector $|\psi_2^{(2)}(t)\rangle$ (dashed), and onto the fourth-order superadiabatic basis vector $|\psi_2^{(4)}(t)\rangle$ (dotted).

When changing the pulse envelope from (5.23) to

$$F(t) = F_{\max} \sin^4\left(\frac{\pi t}{T_{\text{pulse}}}\right) \ , \qquad 0 \le t \le T_{\text{pulse}} \ , \tag{5.36}$$

while keeping the parameters fixed, the initial nonadiabatic amplitude defect becomes proportional to η^4. It is then the fourth-order superadiabatic basis that best describes the dynamics during the initial stage of the pulse. This is illustrated in figure 5.7, which compares the transition probability in the adiabatic basis to the probability viewed in the second-order and

fourth-order superadiabatic bases. Note the change of the ordinate's scale as compared to the previous figure: The smoother the onset of the pulse, the less the initial nonadiabatic loss.

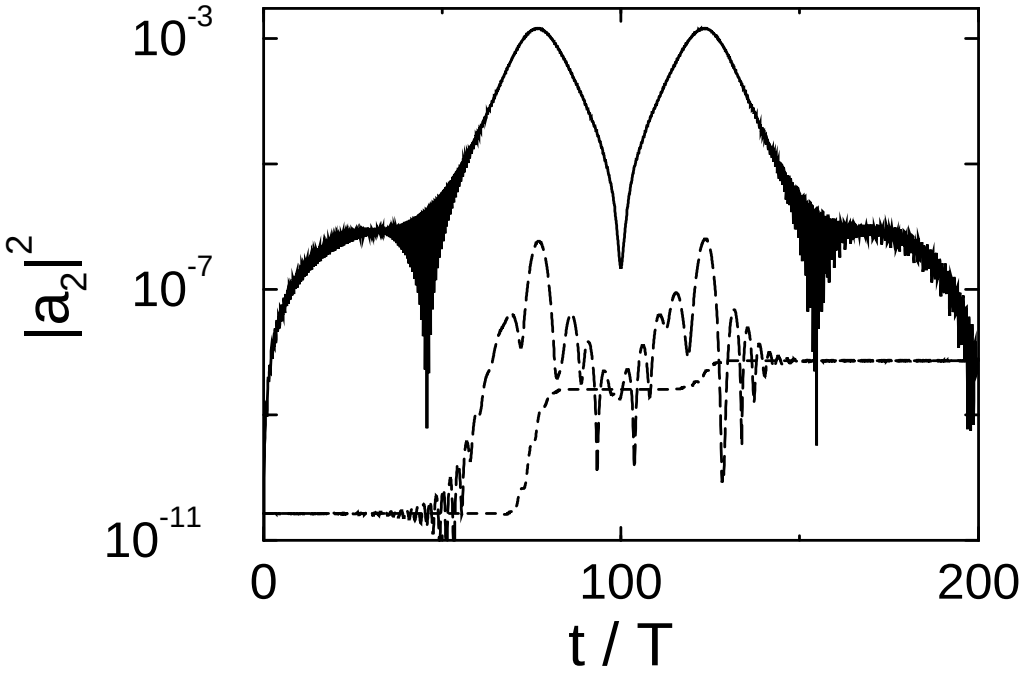

Figure 5.8: Pulse dynamics for the driven two-level system (5.22) with parameters as in figure 5.6, but for a pulse that is ten times longer, $T_{\text{pulse}} = 200\,T$. The transition probability is viewed in the adiabatic basis (full line; the black areas stem from oscillations of the type explained in figure 5.2), in the second-order superadiabatic basis (dashed), and in the tenth-order superadiabatic basis (dotted).

A striking example for the reduction to the essentials of the dynamics that can be achieved by superadiabatic transformations is displayed in figure 5.8, where we consider a $\sin^2$-pulse that is 10 times longer than the one in figure 5.6; the other parameters remain unchanged. In the adiabatic basis the final transition probability is reached after overshooting that final value by many orders of magnitude at the avoided crossings, and with the already familiar oscillations that stem from the interference of different Floquet modes, as in figure 5.2. Viewed in higher-order superadiabatic bases, the dynamics become more and more simple. For $S = 2$ one still finds oscillations of the transition probability, now caused by the interference of a "perturbative" and a "nonperturbative" component [27], but the overshooting is already substantially diminished. For $S = 10$ the transition dynamics reduces to a mere sketch: Starting with the value $2.6413 \cdot 10^{-11}$ determined by the initial roughness of the pulse envelope (for comparison: equation (5.28) gives $|a_2(0+)|^2 = 2.6412 \cdot 10^{-11}$), the probability stays constant, apart from the two steps resulting from the passages through the avoided crossing. As can be deduced from Berry's theory [10], these steps, which mark the actual Landau-Zener

induced probability loss, are universally approximated by error-functions.

As a further example for the use of superadiabatic transformations we study a chirp around the one-photon resonance of the two-level model (5.22). We choose the transition frequency $\omega_c = \Delta E/\hbar$ as reference frequency, take a $\sin^2$-envelope (5.23) with length $T_{\rm pulse} = 10\,T_c$ (where $T_c = 2\pi/\omega_c$), and chirp the instantaneous frequency according to

$$\omega(t) = \omega_c + \Delta\omega \cos\left(\frac{\pi t}{T_{\rm pulse}}\right) \tag{5.37}$$

from above to below the resonance. Figure 5.9 shows the square of the wave function's

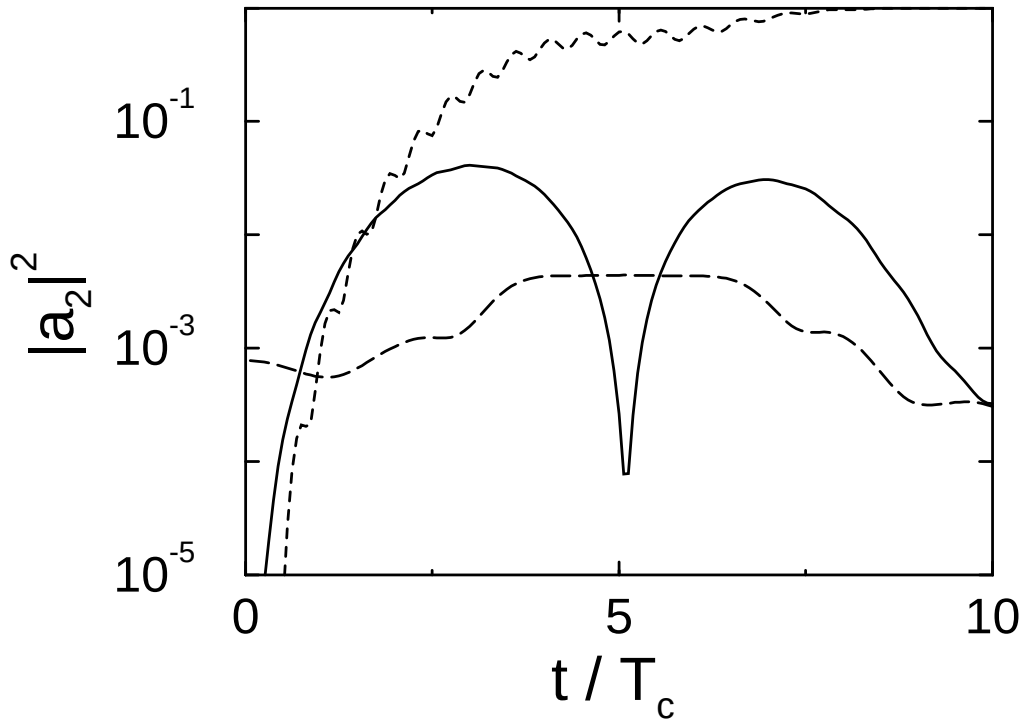

Figure 5.9: Dynamics of a chirp over the one-photon resonance of the two-level system (5.22). The instantaneous frequency of the $\sin^2$-shaped pulse is varied according to equation (5.37), with $\omega_c = \Delta E/\hbar$ and $\Delta\omega/\omega_c = 0.3$. The maximum field strength is $\mu F_{\rm max}/(\hbar\omega_c) = 0.3$; the pulse length is $T_{\rm pulse} = 10 \cdot 2\pi/\omega_c \equiv 10\,T_c$. The Schrödinger wave function $|\psi(t)\rangle$ evolving from the initial bare state $|1\rangle$ has been projected onto the bare state $|2\rangle$ (dotted), onto the instantaneous Floquet function $|u_2^{R(t)}(t)\rangle$ (full line), and onto the third-order superadiabatic basis vector $|\psi_2^{(3)}(t)\rangle$ (dashed).

projection onto the bare state $|2\rangle$, onto the adiabatic Floquet function $|u_2^{R(t)}(t)\rangle$, and onto the third-order superadiabatic basis vector $|\psi_2^{(3)}(t)\rangle$, for a pulse with $\mu F_{\rm max}/(\hbar\omega_c) = 0.3$ and $\Delta\omega/\omega_c = 0.3$. Despite the pulse's shortness, the chirp effectuates an almost complete population transfer from $|1\rangle$ to $|2\rangle$. This is made possible by the fact that the quasienergy emerging from the initial state $|1\rangle$ is adiabatically connected to the final state $|2\rangle$, as shown

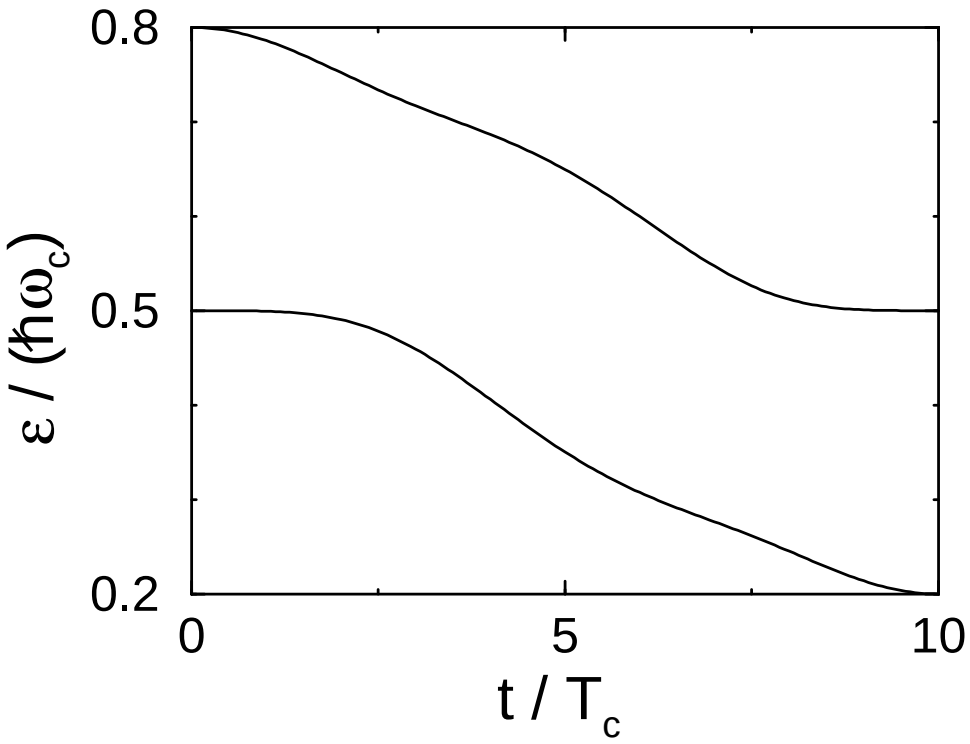

Figure 5.10: Quasienergies for the two-level system (5.22) corresponding to the chirp studied in figure 5.9. Note that the quasienergy emerging from the bare state $|1\rangle$ is continuously connected to $|2\rangle$, and vice versa.

in figure 5.10. Hence, a chirped laser pulse can induce a "transition without transition": The population can flow to the target state (almost) adiabatically. For the very short pulse considered here, the actual dynamics is more involved: The full line in figure 5.9, indicating the transition probability in the adiabatic basis, shows an overshooting of the occupation of $|u_2^{R(t)}(t)\rangle$ by about two orders of magnitude over the actual final nonadiabatic population loss. This is caused by two Landau-Zener-like transitions that occur when the instantaneous quasienergy levels approach each other slightly, comparable to the situation in figure 5.8. Unlike the case studied there, the two transition amplitudes do not add constructively, but destructively, as revealed by the transformation to the third-order superadiabatic basis. It is only this transformation which shows the actual magnitude of Landau-Zener-induced losses, and separates them from the loss due to the roughness of the pulse's edges.

5.4 Sequential ladder climbing vs. multiphoton chirp

The ideas illustrated in the previous sections with the help of the model (5.22) can be exploited in order to develop strategies for efficient population transfer in multilevel systems. As a typical example, we consider the forced Morse oscillator

$$H(t) = \frac{p^2}{2m} + D(1 - e^{-\beta x})^2 + dxF(t)\sin(\phi(t)) \tag{5.38}$$

with parameters characterising the vibrations of an HF molecule: $m = 1744.8$, $D = 0.22509$, $\beta = 1.1741$, and $d = 0.3099$ (all data in atomic units [119]). The undriven Morse oscillator then has 24 bound states with energies

$$E_n = \hbar\omega_0 \left(n + \frac{1}{2}\right) - \frac{\hbar^2\omega_0^2}{4D}\left(n + \frac{1}{2}\right)^2 , \tag{5.39}$$

where

$$\omega_0 = \sqrt{\frac{2D\beta^2}{m}}$$

is the frequency of small oscillations in the Morse potential. We restrict ourselves to the dynamics in the space spanned by the bound states, thereby excluding continuum effects.

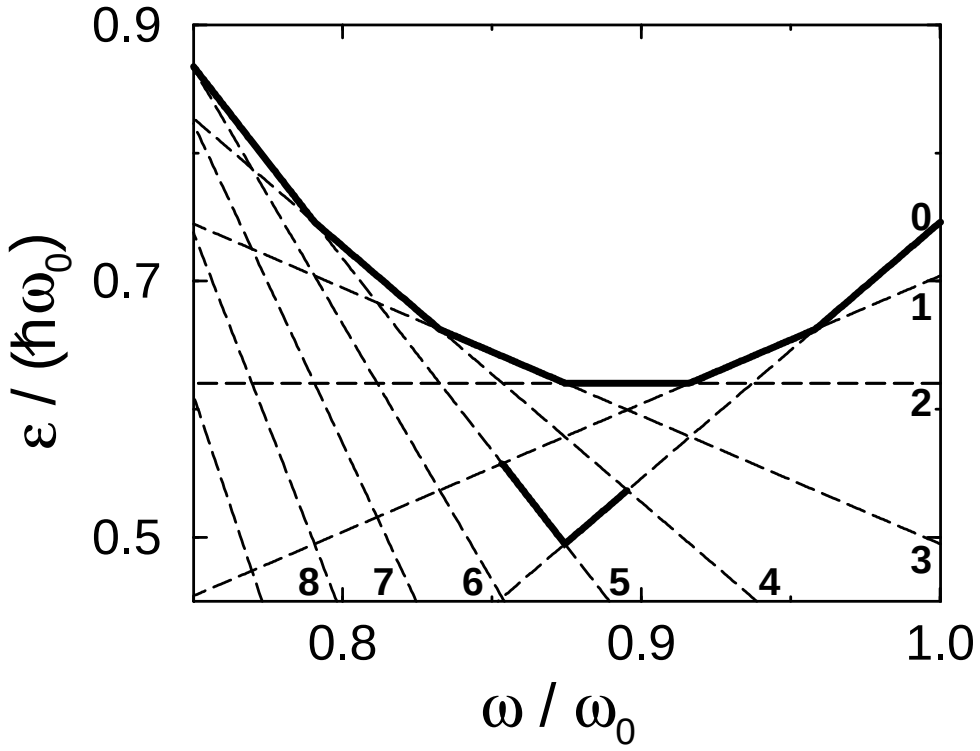

Figure 5.11: Quasienergies $\varepsilon_{(n,m)}$ for the HF-Morse oscillator (5.38), for vanishing amplitude F. The numbers correspond to the vibrational quantum number n; the slope of the lines is determined by m. For $F > 0$ the level crossings turn into anticrossings. In the case of sequential ladder climbing studied in figure 5.13, the wave function moves on the upper envelope of these lines (from right to left), whereas a multiphoton chirp exploits an individual anticrossing (with arbitrary chirp direction). The two heavy segments of the lines with $n = 0$ and $n = 5$ indicate the five-photon resonance utilised in figure 5.16.

For $F = 0$, the quasienergies $\varepsilon_{(n,m)}$ are related to the energies E_n by

$$\varepsilon_{(n,m)} = E_n + m\hbar\omega \ .$$

Hence, plotting quasienergies vs. frequency yields a web of straight lines, as in figure 5.11. For $F > 0$ the level crossings seen in this figure, indicating multiphoton resonances, turn into anticrossings, thus providing several alternative routes for adiabatic transfer schemes. For instance, if we start with the vibrational ground state $|0\rangle$ and seek to populate the fifth excited state $|5\rangle$, we may choose to move on the upper envelope of the levels in figure 5.11, beginning with a frequency ω_i that is higher than the first transition frequency $(E_1 - E_0)/\hbar$, increase the field amplitude, gradually lower the frequency and successively pass the single-photon resonances $\omega = (E_{n+1} - E_n)/\hbar$ for $n = 0, \ldots, 4$ as adiabatically as possible, and finally lower the amplitude back to zero at some frequency $(E_6 - E_5)/\hbar < \omega_f < (E_5 - E_4)/\hbar$. In this way, we successively climb the rungs of the vibrational ladder: On the individual line segments of the upper envelope in figure 5.11, the adiabatic Floquet state is closely associated with the respective Morse eigenstate.

While this scenario is well known in principle [2, 43], there is the pertinent question how to design the field amplitude $F(t)$ in order to accomplish the intended population transfer with as little loss as possible. A reasonable guideline for this purpose is varying the pulse parameters such that the difference $\Delta\varepsilon$ between the quasienergy of the transfer state and its nearest neighbour stays roughly constant during the pulse. In figure 5.12 we encode this difference in terms of shades of grey; black areas correspond to near-degeneracies that are to be circumvented. Based on this plot, we choose the pulse as indicated by the heavy line, corresponding to a cosine frequency chirp (5.37) and an envelope parametrised (somewhat arbitrarily) as

$$F(t) = F_0 \left(1 - \frac{at}{T_{\text{pulse}}}\right) \frac{4}{\pi^2} \arctan^2 \left(\frac{3\pi^2}{2} \frac{t}{T_{\text{pulse}}} \left[1 - \frac{t}{T_{\text{pulse}}}\right]\right) \tag{5.40}$$

for $0 \leq t \leq T_{\text{pulse}}$. We take an asymmetry parameter $a = 0.7$ and set $F_0 = 0.01$ a.u., $\omega_c/\omega_0 = 0.880$, and $\Delta\omega/\omega_0 = 0.109$, so that the frequency is chirped from $\omega_i/\omega_0 = 0.989 = 1.031 \cdot (E_1 - E_0)/(\hbar\omega_0)$ to $\omega_f/\omega_0 = 0.771 = 0.976 \cdot (E_5 - E_4)/(\hbar\omega_0)$, cf. figure 5.11. The upper panel of figure 5.13 then shows the population of the bare Morse eigenstates during such a pulse with length $T_{\text{pulse}} = 200 \cdot 2\pi/\omega_c$; the climbing of the vibrational ladder from $|0\rangle$ to $|5\rangle$ is quite apparent. However, the probability of a transition from the adiabatically moving Floquet state to its nearest neighbour, depicted in the lower panel, shows that the naively assumed mechanism — the adiabatic passage through five avoided crossings, corresponding to five single-photon resonances — does not quite match the reality. There are *seven*, not five, Landau-Zener-like overshootings, corresponding to fine details of the behaviour of $\Delta\varepsilon$ during the pulse (middle panel). The most interesting detail revealed by the lower panel is that the overall population loss one is left with after the pulse, about 12%, is born only on the very final stage of the pulse. Steering the pulse's path finally between the resonances $\omega = (E_5 - E_4)/\hbar$ and $\omega = (E_6 - E_5)/\hbar$ (cf. figure 5.12) requires particular care, since here the

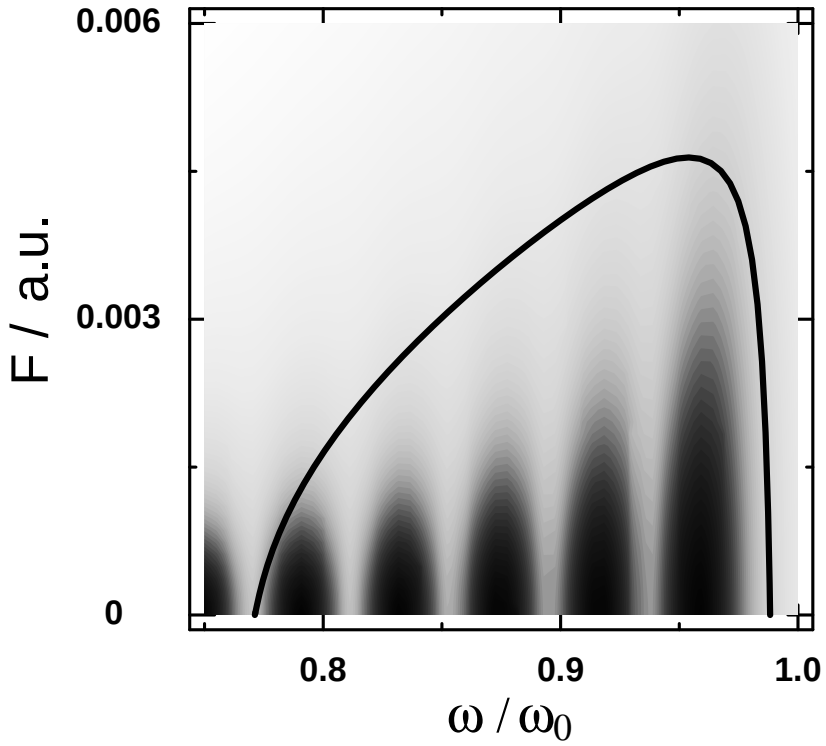

Figure 5.12: Greyscale plot encoding the difference $\Delta\varepsilon$ between the instantaneous quasienergy used for successive ladder climbing from $|0\rangle$ to $|5\rangle$ and its nearest neighbour. Black areas correspond to near-degeneracies that are to be circumvented. The heavy line is the path traversed by the pulse (5.37), (5.40).

quasienergy distances to the next and next-to-nearest neighbours necessarily become quite small. Reduction of the nonadiabatic loss thus requires optimisation of the pulse especially at its very end.

For practical purposes, one of the most important issues is the dependence of the transfer efficiency on the duration of the pulse. This is studied in figure 5.14, again for the sequential transfer from $|0\rangle$ to $|5\rangle$ and pulses with the same path (5.37), (5.40) as before, for pulse durations up to $50\,000\,T_c$. (For orientation: $1000\,T_c$ correspond to 9.16 picoseconds.) As seen in the inset, the total population loss

$$L = \sum_{n\neq 5} |a_n(T_{\text{pulse}})|^2 \,, \tag{5.41}$$

i.e., the final population of all vibrational states other than the target state $n = 5$, decreases exponentially with T_{pulse} as long as $T_{\text{pulse}} < 1000\,T_c$; we find $L < 1\%$ for $T_{\text{pulse}} > 500\,T_c$. This exponential decrease is to be expected if the loss is dominated by a single Landau-Zener-type transition. However, for substantially longer pulses the loss *increases* with T_{pulse}. This increase can be traced to a number of high-order multiphoton resonances which give

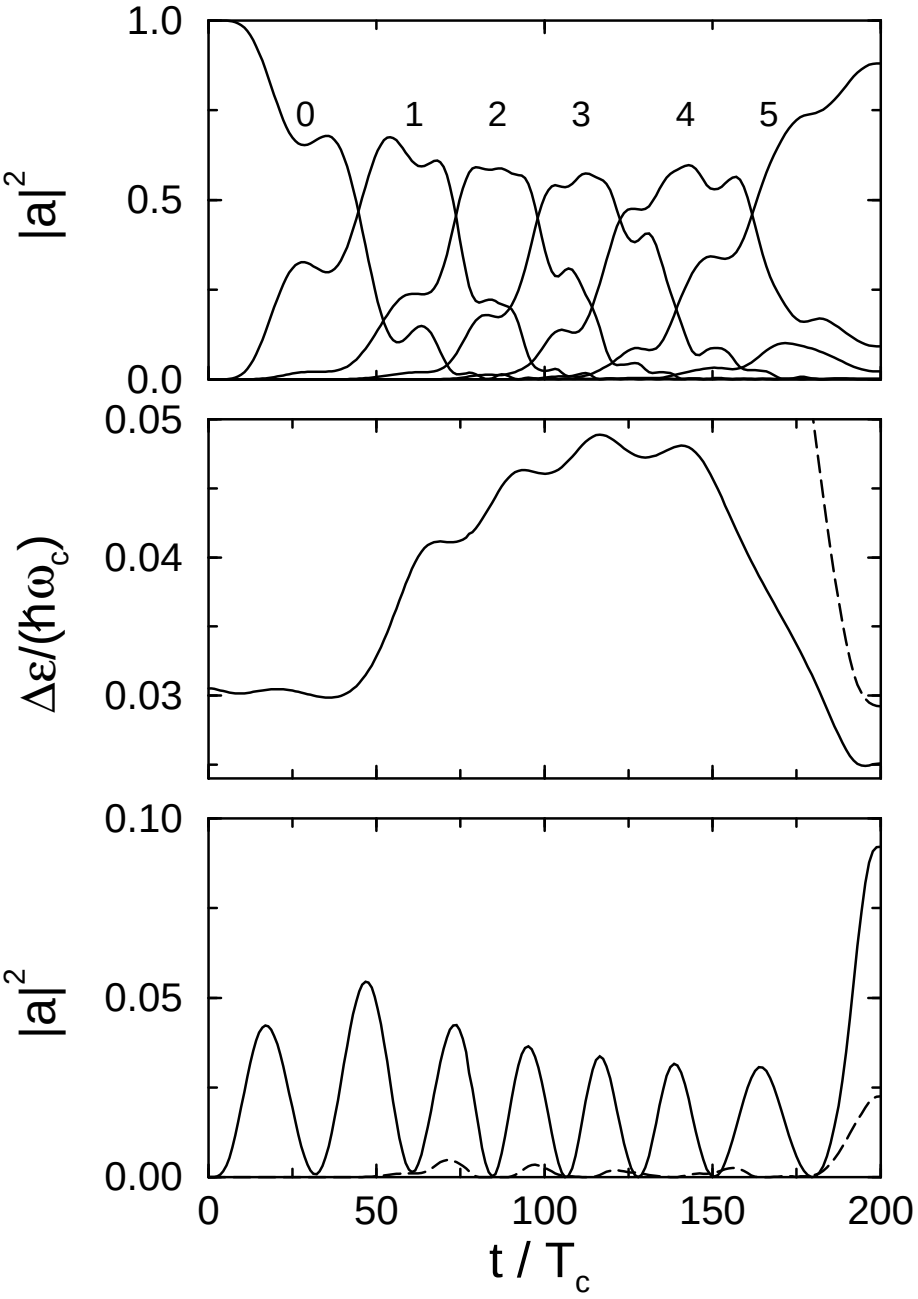

Figure 5.13: Upper panel: Population of the bare Morse eigenstates during the pulse indicated in figure 5.12, with $T_{\text{pulse}} = 200 \cdot 2\pi/\omega_c \equiv 200\,T_c$. One clearly recognises the climbing of the vibrational ladder from $|0\rangle$ to $|5\rangle$. Middle panel: Difference $\Delta\varepsilon$ between the quasienergy of the adiabatically moving Floquet state and its nearest (full line) or next-to-nearest neighbour (dashed) during the pulse. Lower panel: Population of the instantaneous Floquet state that is the nearest (full line) or next-to-nearest neighbour (dashed) of the adiabatically moving state, as determined by quasienergy difference. Note that there are seven, not five, Landau-Zener-like overshootings, as corresponding to the precise variation of $\Delta\varepsilon$. Note further that the overall population loss is induced only at the end of the pulse.

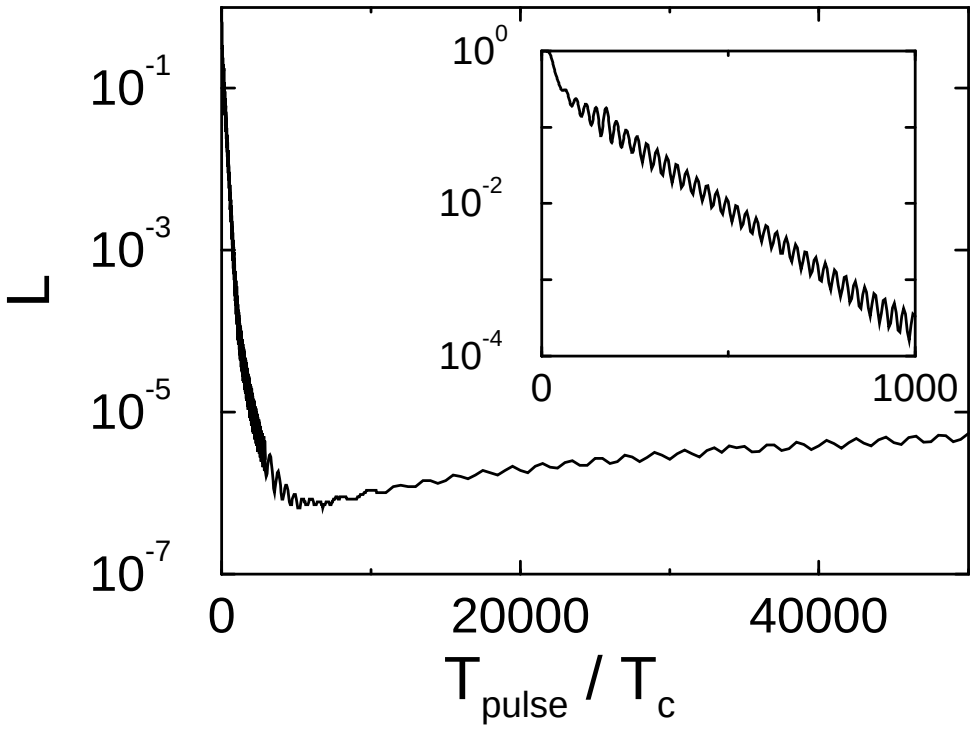

Figure 5.14: Total population loss (5.41) after sequential transfer from the vibrational ground state $|0\rangle$ to the target state $|5\rangle$, induced by chirped pulses (5.37), (5.40) with the path indicated in figure 5.12. Apart from the variation of the pulse length T_{pulse}, all parameters are the same as in figure 5.13. For $T_{\text{pulse}} > 2500\,T_c$ the oscillations are not fully resolved.

rise to tiny anticrossings with the quasienergy of the transfer state. As long as the pulse is not too long, these anticrossings are traversed practically diabatically, and therefore do not make themselves felt. For longer pulses, however, their Landau-Zener probabilities become minutely less than unity, thus directing small portions of population into unwanted channels [58]. Hence, there is an optimal pulse length that minimises the population loss; in the present example, it is about $6000\,T_c$.

As an alternative to the use of successive single-photon resonances, one may also chirp the frequency around a five-photon resonance in order to achieve the transition from $|0\rangle$ to $|5\rangle$ in a single step. This means exploiting the (anti-)crossing of the lines labelled by $n = 0$ and $n = 5$ in figure 5.11, so that the total frequency chirp $2\,\Delta\omega$ has to be much smaller than in the previous case. However, there is a trade-off: the greyscale plot of the quasienergy difference between the adiabatic state and its nearest neighbour displayed in figure 5.15 indicates that in order to circumvent the devastating near-degeneracy we now need pulse amplitudes that are about 4 times higher than the previous one. Choosing a simple $\sin^2$-envelope (5.23) with $F_{\max} = 0.02$ a.u., and a cosine chirp (5.37) with central frequency $\omega_c = (E_5 - E_0)/(5\hbar)$ exactly on five-photon resonance, $\Delta\omega/\omega_c = 0.0121$, and $T_{\text{pulse}} = 200 \cdot 2\pi/\omega_c$, we obtain the flow of population displayed in figure 5.16. In comparison with its counterpart in figure 5.13,

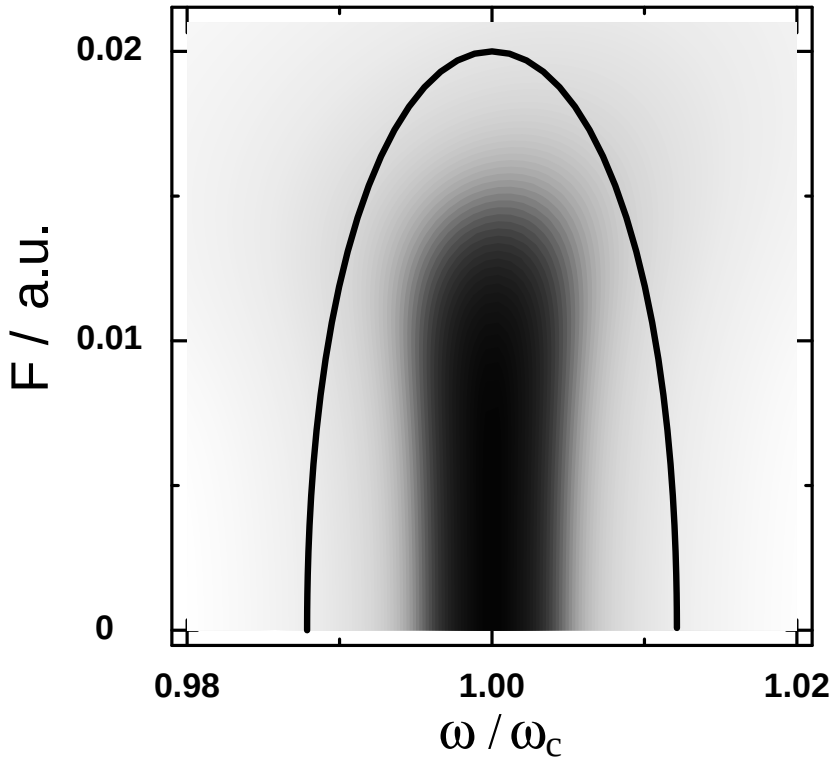

Figure 5.15: Greyscale plot visualising the quasienergy difference $\Delta\varepsilon$ between the adiabatic state and its nearest neighbour (corresponding to the full line in the middle panel of figure 5.16) for the five-photon resonance connecting the bare Morse eigenstates $|0\rangle$ and $|5\rangle$ (cf. figure 5.11). The black area marks the near-degeneracy; the heavy line is the path traversed by the pulse discussed in figure 5.16.

the bare state basis now provides hardly any information about the underlying mechanism, since the strong-field Floquet states differ substantially from the unperturbed eigenstates. In contrast, the projection to the adiabatic basis again reveals peaks corresponding to Landau-Zener dynamics, resulting from the close approaches of neighbouring quasienergies shown in the middle panel. Interestingly, there are two such peaks, instead of the naively expected one. As opposed to the sequential mechanism considered before, a similar population transfer can also be induced by chirping the frequency from red to blue over the multiphoton resonance (that is, by changing the sign of $\Delta\omega$), since one now has effectively two-level dynamics.

5.5 An application to the STIRAP process

The key principle behind population transfer by frequency chirping is to provide a quasienergy level continuously connecting the initial and the target state, as exemplified in figure 5.10. The same idea can also be realised in a different manner, namely, by exposing the system H_0 to *two* laser pulses with different, but fixed carrier frequencies ω_1 and ω_2. Instead

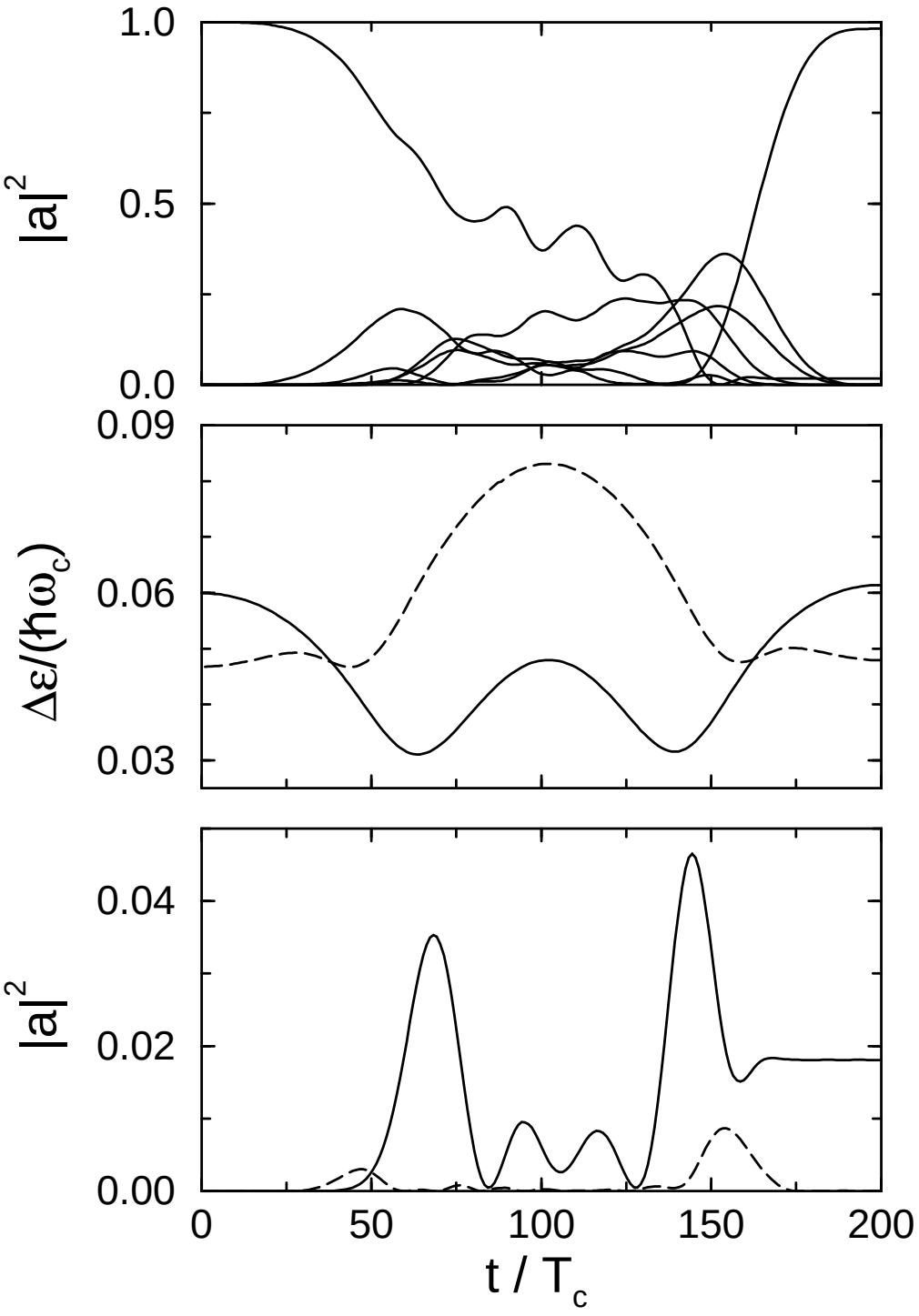

Figure 5.16: Population transfer induced by the pulse indicated in figure 5.15, for $T_{\mathrm{pulse}} = 200 \cdot 2\pi/\omega_c$. Upper panel: Population of the bare Morse eigenstates. Middle panel: Difference $\Delta\varepsilon$ between the quasienergy of the adiabatically moving Floquet state and its nearest (full line) or next-to-nearest neighbour (dashed) during the pulse. Lower panel: Population of the instantaneous Floquet state that is the nearest (full line) or next-to-nearest neighbour (dashed) of the adiabatically moving state, as determined by quasienergy difference.

of the Hamiltonian (5.1) one then has

$$H(t) = H_0 + \widehat{\mu} F_1(t) \sin(\omega_1 t) + \widehat{\mu} F_2(t) \sin(\omega_2 t + \vartheta) \ ,$$

where ϑ is a phase. If ω_1 and ω_2 are not rationally related, so that $H(t)$ becomes quasiperiodic when the amplitudes F_1 and F_2 are kept fixed, one obtains instantaneous quasienergies in the following way: Instead of the Schrödinger wave function $|\psi(t)\rangle$, consider a new function $|\Psi(t_1, t_2)\rangle$ with $|\Psi(t, t)\rangle = |\psi(t)\rangle$. Then the fixed-amplitude Schrödinger equation becomes

$$(\mathcal{H}(t_1, t_2) - i\hbar\partial_{t_1} - i\hbar\partial_{t_2}) \, |\Psi(t_1, t_2)\rangle = 0 \ ,$$

where the operator

$$\mathcal{H}(t_1, t_2) = H_0 + \widehat{\mu} F_1 \sin(\omega_1 t_1) + \widehat{\mu} F_2 \sin(\omega_2 t_2 + \vartheta)$$

is periodic in both t_1 and t_2. Hence, the Floquet theorem now suggests solutions of the form

$$|\Psi(t_1, t_2)\rangle = |u(t_1, t_2)\rangle \exp\left(-i\frac{\varepsilon_1 t_1}{\hbar} - i\frac{\varepsilon_2 t_2}{\hbar}\right)$$

with doubly periodic functions

$$|u(t_1, t_2)\rangle = |u(t_1 + T_1, t_2)\rangle = |u(t_1, t_2 + T_2)\rangle$$

for $T_k = 2\pi/\omega_k$, $k = 1, 2$. Setting $t_1 = t_2 = t$, this gives Schrödinger wave functions

$$|\psi(t)\rangle = |u(t, t)\rangle \exp\left(-i\frac{\varepsilon t}{\hbar}\right) \tag{5.42}$$

with two-colour quasienergies $\varepsilon = \varepsilon_1 + \varepsilon_2$ and quasiperiodic functions $|u(t, t)\rangle$. These states (5.42) now take over the role of the Floquet states [50]. Proceeding as in section 5.1, one can then formulate an adiabatic principle that dictates their response to changes of the amplitudes F_1 and F_2: As in the case of monochromatic driving, the wave functions evolve on "quasienergy surfaces" $\varepsilon^{(F_1, F_2)}$ in a Born-Oppenheimer-like fashion, with deviations from the ideal adiabatic behaviour that can be calculated systematically by invoking a suitably extended Hilbert space. There is, however, a mathematical subtlety: The two-colour quasienergies ε are defined $\mathrm{mod}\, \hbar\omega_1$ *and* $\mathrm{mod}\, \hbar\omega_2$, so that even an N-level system H_0 gives rise to a dense point spectrum already for vanishing amplitudes. Physically speaking, the resulting abundance of near-degeneracies counteracts adiabatic motion [58], so that substantially more care is needed than in the single-frequency case [12].

A paradigmatic example for population transfer steered by two laser pulses is provided by the STIRAP ("STImulated Raman Adiabatic Passage") mechanism for a three-level Λ-system, in which the initial bare state $|1\rangle$ is connected to the target state $|3\rangle$ only via an intermediate

state $|2\rangle$ [19, 44, 78, 105, 108]. Subjecting this system *first* to a Stokes laser pulse that couples the initially unoccupied states $|2\rangle$ and $|3\rangle$, and *then* to a pump laser pulse coupling the initial state $|1\rangle$ with $|2\rangle$, one gets almost complete population transfer from $|1\rangle$ to $|3\rangle$, provided both pulses have a sufficient overlap in time. Within the rotating wave approximation, this effect finds a transparent explanation: There exists a dressed state (an approximate two-colour Floquet state) that adiabatically connects $|1\rangle$ and $3\rangle$, and firing first the Stokes pulse, then the pump pulse amounts to adiabatically shifting the initial to the target state [79, 117, 118]. However, the use of the rotating wave approximation in conjunction with adiabatic analysis might not be uncritical, since that approximation implicitly assumes high frequencies, so that the pulses should consist of many optical cycles, which is not necessarily the case.

In this section, we show that the STIRAP principle can be extended to more complex situations even without invoking the rotating wave approximation. The proper way to avoid this approximation is to work with two-colour Floquet states [44]; the efficiency of the population transfer in a multilevel system can then be analysed with tools similar to those developed in section 5.2.

We consider again the HF-Morse oscillator (5.38) of the preceding section, and demonstrate STIRAP-like population transfer from the initial vibrational ground state $|0\rangle$ to the sixth excited state $|6\rangle$ by means of two three-photon resonances: The first pulse has the frequency $\omega_1 = (E_6 - E_3)/(3\hbar)$; the frequency of the second is $\omega_2 = (E_3 - E_0)/(3\hbar)$; they are applied in the usual counterintuitive order. Both pulses have a $\sin^2$-envelope, and the same length T_{pulse}, with separation Δt between the moments of maximum intensity. The maximum strength of the first pulse is $F_{\text{max},1} = 0.006$ a.u., that of the second is $F_{\text{max},2} = 0.009$ a.u.; the pulse separation is chosen as $\Delta t/T_{\text{pulse}} = 0.34$.

Figure 5.17 shows the most relevant instantaneous quasienergies for this configuration. Because of the particular nature of the unperturbed Morse spectrum (5.39), and taking into account the $\mathrm{mod}\,\hbar\omega_1$–$\mathrm{mod}\,\hbar\omega_2$-structure of the quasienergy spectrum, initially and finally all quasienergies adopt one of two values that are separated by $\hbar^2\omega_0^2/(2D)$. This multiple degeneracy is removed when the field amplitudes take on non-zero values, and adiabatic transfer from $|0\rangle$ to $|6\rangle$ is made possible because a representative of the quasienergy originating from E_0, indicated by the heavy line, is continuously connected to E_6. Within the usual rotating wave-approach to the STIRAP mechanism in a three-level system, the transfer state is a “dark state”, implying that its quasienergy does not depend on the field amplitudes [79]. This changes when the counterrotating components of the fields are taken into account [44]; also in the present multilevel case the quasienergy of the transfer state exhibits a pronounced amplitude-dependence.

The efficiency of this STIRAP process as function of the interaction time $T_{\text{int}} = T_{\text{pulse}} + \Delta t$,

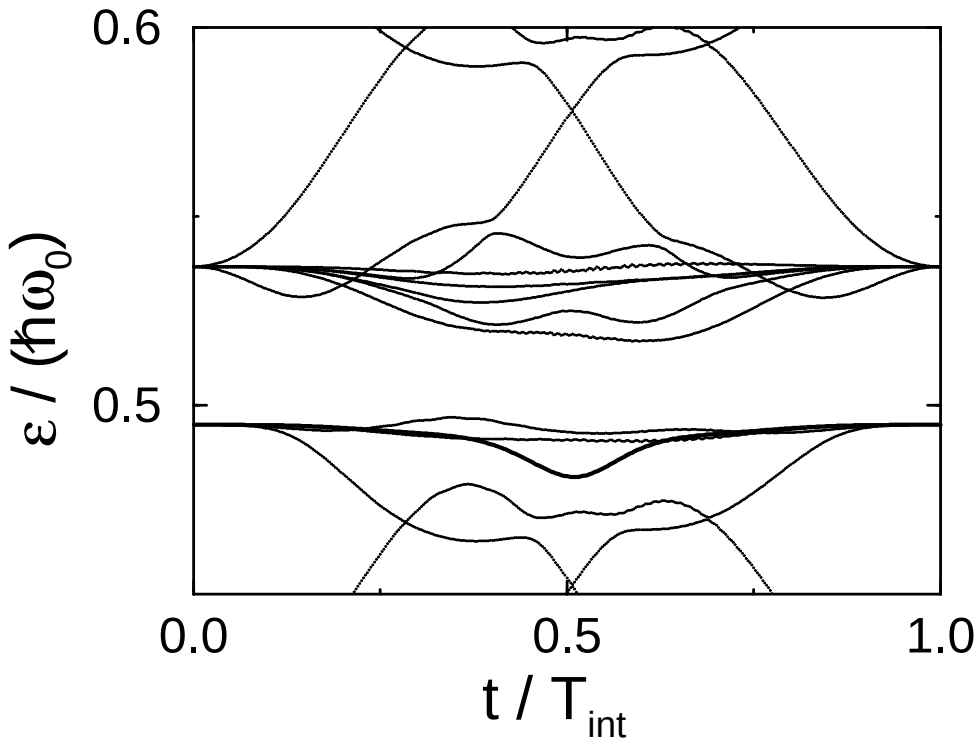

Figure 5.17: Instantaneous two-colour quasienergies for the HF-Morse oscillator driven by two partially overlapping $\sin^2$-shaped laser pulses of the same length T_{pulse}, with frequencies $\omega_1 = (E_6 - E_3)/(3\hbar)$, $\omega_2 = (E_3 - E_0)/(3\hbar)$, and maximum amplitudes $F_{\text{max},1} = 0.006$ a.u., $F_{\text{max},2} = 0.009$ a.u. The moments of maximum intensity are separated by $\Delta t/T_{\text{pulse}} = 0.34$. The quasienergy that permits adiabatic population transfer from the bare Morse eigenstate $|0\rangle$ to $|6\rangle$ is drawn as the heavy line. The total interaction time is $T_{\text{int}} = T_{\text{pulse}} + \Delta t$. (The tiny wiggles shown by some of the quasienergies are numerical artifacts.)

for fixed separation ratio $\Delta t/T_{\text{pulse}}$, is depicted in figure 5.18; the total population loss is reduced below 1% for interaction times longer than about $2750 \cdot 2\pi/\omega_0 \approx 22$ picoseconds. The population loss shows the familiar exponential decrease as long as T_{int} remains below 50 picoseconds, but then vanishes about proportionally to T_{int}^{-4}. This breakdown of the exponential behaviour should be contrasted with the breakdown of the Dykhne-Davis-Pechukas formula [22] that has recently been discussed for STIRAP systems [117, 118]. The latter stems from the initial and final degeneracy of the quasienergies and emerges even for perfectly smooth pulse envelopes [27], whereas the present T_{int}^{-4}-decay can be traced to the roughness of our $\sin^2$-envelopes. This roughness results, in the language of section 5.3, in a nonadiabatic population loss proportional to $(\eta^2)^2 = \eta^4$, with the dimensionless adiabaticity parameter η being proportional to the inverse pulse length.

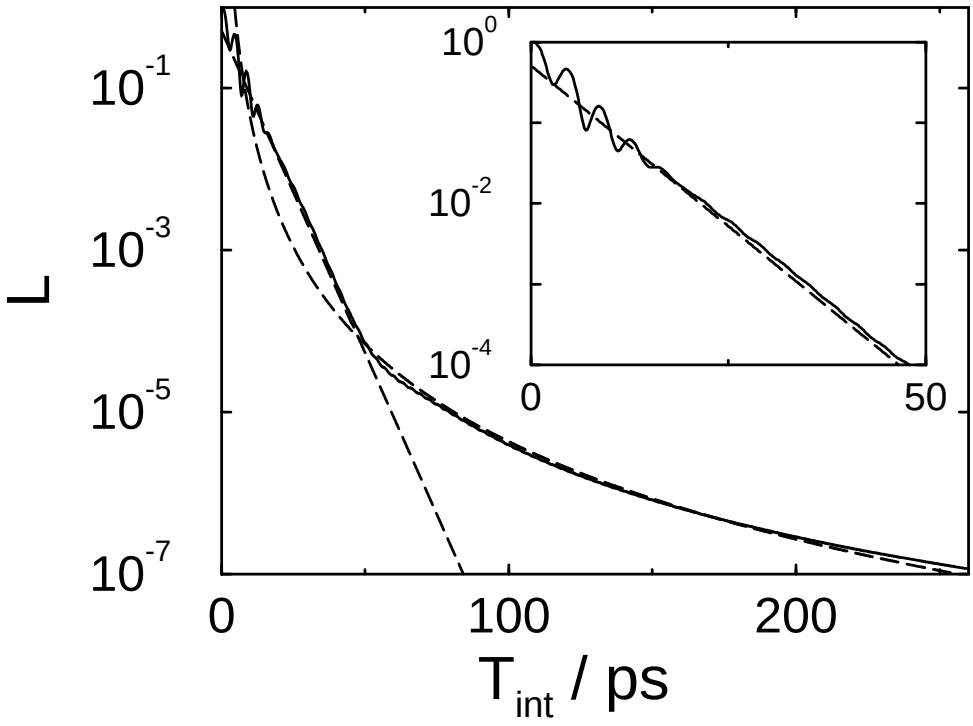

Figure 5.18: Total population loss $L = \sum_{n \neq 6} |a(T_{\rm int})|^2$ (full line) for the STIRAP configuration described in figure 5.17. For interaction times $T_{\rm int}$ less than 50 picoseconds the loss is well described by an exponential decrease, whereas for longer pulses the loss decreases approximately as $T_{\rm int}^{-4}$, as indicated by the dashed lines.

5.6 Discussion

The set of the instantaneous Floquet states provides the adiabatic basis for laser-pulsed N-level quantum systems (5.1). The investigation of the interaction with *short* laser pulses, however, necessitates to leave the adiabatic limit and to estimate nonadiabatic transition probabilities. This has been achieved in section 5.2 by applying perturbation theory to the Floquet states, after going from the original time-dependent Schrödinger equation (5.3) to the evolution equation (5.11) in the extended Hilbert space. From a technical viewpoint, this equation exploits the separation of the "fast" time scale $T = 2\pi/\omega$ and the "slow" time scale characterising the change of the pulse's envelope or frequency [14, 15]. The use of the laser phase ϕ in this equation (5.11), instead of the time t, is mandatory when the frequency $\omega(t)$ is not constant during the pulse: This is what then allows us to formulate the adiabatic principle for Floquet states in close analogy to its counterpart for adiabatically moving energy eigenstates.

When working in the extended Hilbert space, one can apply standard perturbational techniques; the Fourier modes of a Floquet state are treated like individual states. Although the process of lifting to the extended space is not unique, one always arrives at unique expres-

sions for nonadiabatic transition probabilities, since the ambiguity is removed upon projecting back to the physical space. This back-projection also reveals a peculiarity of laser-pulsed systems: The occupation probabilities of the instantaneous Floquet states exhibit oscillations that result from the interference of several modes, as expressed by equation (5.21). It should be emphasised that adiabatic Floquet state perturbation theory, set up in the way described above, cures a shortcoming of the often employed rotating wave approximation. That approximation requires high laser frequencies, and thus presupposes that many laser cycles fall into an interval during which the pulse parameters change significantly, which is at odds with short pulse durations.

The adiabatic basis, adapted to hypothetical pulses with "infinitely slowly" changing parameters, is not satisfactory for monitoring the transition dynamics induced by short pulses. As seen in figure 5.8, in the vicinity of a multiphoton resonance there is a temporary excursion of population away from the adiabatic state; the temporary population loss can exceed the actual final nonadiabatic loss by orders of magnitude. In contrast, the use of superadiabatic Floquet bases eliminates such spurious excursions and allows one to keep track of the actual losses. Again working in the extended Hilbert space, these superadiabatic bases have been constructed in section 5.3 by transferring Berry's ideas [10] to laser-pulsed systems (5.1).

Even if one is not interested in the fine details of quantum transition dynamics, but merely wishes to design laser pulses that effectuate population transfer from an initial state to some target state, the Floquet picture yields robust pulse strategies, and physical understanding, by merely inspecting the instantaneous quasienergy spectra, without the need to invoke sophisticated optimisation routines. This has been demonstrated in section 5.4 by setting up two chirped pulses for a Morse ladder system, obeying the rule to circumvent quasienergetic near-degeneracies. The final example considered in section 5.5, a STIRAP-like multiphoton process in a multilevel system, indicates how the investigation of adiabatic Floquet dynamics has to proceed in the two-colour case, including the discussion of nonadiabatic losses.

Appendix A Phase diagram for a modified Harper model

Harper's model describes a quantum particle moving on a one-dimensional tight binding lattice endowed with a potential that is incommensurate with the lattice period. Neighbouring sites are coupled by constant hopping integrals $t/2$ and the on-site energies are modulated with amplitude v, so that the stationary Schrödinger equation for the energy eigenvalues E adopts the form [109, 111] [1]

$$\frac{t}{2}\left(f_{\ell+1}+f_{\ell-1}\right)+v\cos(2\pi\alpha\ell+\beta)f_\ell = Ef_\ell\ , \tag{A.1}$$

where f_ℓ denotes the particle's amplitude at the ℓ-th site. The total number of sites is assumed to be infinite; α is an irrational and β an arbitrary real number.

This seemingly simple model is far from trivial; its properties are still the objective of rather deep mathematical investigations [64, 95]. The most notable feature of the Harper model is its self-duality [5, 111]: under the transformation

$$f_\ell = \sum_m g_m\ e^{im(2\pi\alpha\ell+\beta)+ikd\ell}\ , \tag{A.2}$$

where k is a wave vector and d the spacing between individual sites, the eigenvalue equation (A.1) becomes

$$t\cos(2\pi\alpha m+kd)g_m+\frac{v}{2}\left(g_{m+1}+g_{m-1}\right)=Eg_m\ .$$

Thus, in reciprocal space v adopts the role of t, and vice versa, but the form of the eigenvalue equation remains unchanged. With the help of this property one can show that there is a metal-insulator transition at $v=t$: the eigenstates of (A.1) are extended for $v<t$ and become exponentially localised for $v>t$ [5, 111]. At the transition point $v=t$ the eigenstates are critical, i.e., neither extended in the usual sense nor exponentially localised [77, 93], and the spectrum is a Cantor set with multifractal properties: the eigenvalues, when plotted versus the incommensurability parameter α, give rise to the famous Hofstadter butterfly [51, 102].

In chapter 3 we proposed a realisation of Harper's model with ultracold atoms in a bichromatic standing light wave. We found, however, that there is an additional term (cf.

[1] In this appendix we do not use the bracket notation of the previous chapters, not to overload the equations.

equation(3.32)), namely $w\cos(2\pi\alpha[\ell+1/2]+\beta)$, that modifies the hopping integral, so that the new hopping strength is

$$\widehat{t}_{\ell,\ell+1} = \frac{t}{2} + w\cos(2\pi\alpha[\ell+1/2]+\beta)\ . \tag{A.3}$$

For the realisation proposed in chapter 3 the new parameter w would be quite small compared to the modulation strength v of the on-site energies for an atom-optical realisation of Harper's model, and depend on v [2]. This model could also represent Bloch electrons on a rectangular lattice [46, 74], where w is the next-nearest-neighbour coupling. In this appendix, however, we will study the modified Harper model without regard to a particular laboratory realisation, and treat v and w as *independent* parameters. Without loss of generality we assume t, v, and w to be positive.

It is crucial to note that the modification (A.3) of the hopping integrals does not destroy self-duality. If $t/2$ is properly replaced by $\widehat{t}_{\ell,\ell\pm1}$ in equation (A.1), the two additional terms $w\cos(2\pi\alpha[\ell\pm1/2]+\beta)f_{\ell\pm1}$ appear on the left hand side. Under the duality transformation (A.2) these two terms become simply $w\cos(2\pi\alpha[m\pm1/2]+kd)g_{m\pm1}$: the modulation of the hopping integrals is the same for the amplitudes f_ℓ and their duals g_m, so that the eigenvalue equation for the modified Harper model still has the same form in both physical and reciprocal space.

A further essential tool for the analysis of the modified model is the relation between the distribution of energy eigenvalues and the localisation range of the eigenstates that had originally been put forward by Herbert and Jones [49] and was explored further by Thouless [112]. For a one-dimensional tight binding lattice with interactions between nearest neighbours only, the inverse fall-off distance $\lambda^{(j)}$ of an eigenstate with energy E_j is — if it exists — given by

$$\lambda^{(j)} = \lim_{N\to\infty}\left(\frac{1}{N}\sum_{i\neq j}\ln|E_i-E_j|\right) - \ln G \tag{A.4}$$

in the limit of a large number $(N+1)$ of sites, where G is the geometric mean of the hopping integrals. Hence, we have $G = t/2$ for the original Harper model, whereas

$$G = \lim_{N\to\infty}\left(w^N\prod_{\ell=0}^{N-1}\left|\frac{t}{2w}+\cos\left(2\pi\alpha\left[\ell+\frac{1}{2}\right]+\beta\right)\right|\right)^{1/N} \tag{A.5}$$

for the modified system.

[2] In the case of bichromatic standing light waves, w is by a factor of about $\exp(-\sqrt{\gamma}\pi^2/4)$ smaller than v, where γ is the depth of the optical potential created by the first (strong) wave, measured in multiples of the single-photon recoil energy. If we take $\gamma = 5$ as a typical value, we thus obtain $w/v \approx 4\cdot10^{-3}$.

For computing the product (A.5) we have to distinguish two different cases. If $t/(2w) > 1$ we set $t/(2w) = \cosh(x)$. Approximating the irrational number α by a sequence $\{Z_N/N\}$ of rationals (with Z_N and N relatively prime), and utilising the identity [38]

$$\prod_{\ell=0}^{N-1} \left| \frac{t}{2w} + \cos\left(\frac{2\pi Z_N \ell}{N} + \pi\alpha + \beta \right) \right| = 2^{(1-N)} \left| \cosh(Nx) - \cos(N[\pi\alpha + \beta + \pi]) \right| \tag{A.6}$$

one readily derives

$$G = \frac{1}{4}\left(t + \sqrt{t^2 - 4w^2} \right) \qquad \text{for} \qquad 2w < t \; . \tag{A.7}$$

If $t/(2w) < 1$, a hopping strength (A.3) may vanish. In that case the chain of sites is cut into disconnected pieces. Because of the irrationality of α, this perfect cut can occur for at most one particular link of the infinite chain. However, even if we disregard this case there remains the chance that infinitely many hopping integrals become almost zero; the spatial frequency of such almost perfect cuts depends on the number-theoretical properties of α. If we now set $t/(2w) = \cos(x)$, then the term $\cosh(Nx)$ appearing on the right hand side of equation (A.6) has to be replaced by $\cos(Nx)$ [38]. However, the possibility that infinitely many chain links may be arbitrarily weak causes a problem for the convergency of $\ln G$. We circumvent this problem with a view towards physical reality: since truly infinite coherence lengths are impossible to achieve, the separating effect of very weak links is negligible as long as the characteristic distance between them remains small compared to the particle's coherence length. With this caveat in mind, we find

$$G = \frac{w}{2} \qquad \text{for} \qquad 2w > t \; . \tag{A.8}$$

In order to obtain the geometric mean $\widetilde{G}$ for the duality-transformed system, we merely have to replace t by v:

$$\widetilde{G} = \begin{cases} \frac{1}{4}\left(v + \sqrt{v^2 - 4w^2} \right) & \text{for} \quad 2w < v \\ \frac{w}{2} & \text{for} \quad 2w > v \end{cases} \; . \tag{A.9}$$

Now we can apply some standard arguments [111]. Since the sum appearing in equation (A.4) is the same for both the original and the transformed system, the inverse localisation length $\lambda^{(j)}$ of an eigenstate of the original system is related to the corresponding inverse length $\widetilde{\lambda}^{(j)}$ pertaining to the transformed state in a simple way. Moreover, it is easy to show that if a state is exponentially localised, so that $\lambda^{(j)} > 0$, then its duality-transformed counterpart must be an extended state, $\widetilde{\lambda}^{(j)} = 0$, and vice versa [111]. Hence, there can be

only one localisation length for each system, i.e., $\lambda^{(j)} \equiv \lambda$ and $\widetilde{\lambda}^{(j)} \equiv \widetilde{\lambda}$ for all states j, and we have

$$\lambda = \widetilde{\lambda} + \ln\left(\frac{\widetilde{G}}{G}\right) \ . \tag{A.10}$$

It follows that the eigenstates of the modified Harper model must be exponentially localised if $\widetilde{G} > G$, and extended if $\widetilde{G} < G$. The expressions (A.7), (A.8), and (A.9) thus lead to the phase diagram depicted in figure A.1. All states are extended, i.e., we have a metallic

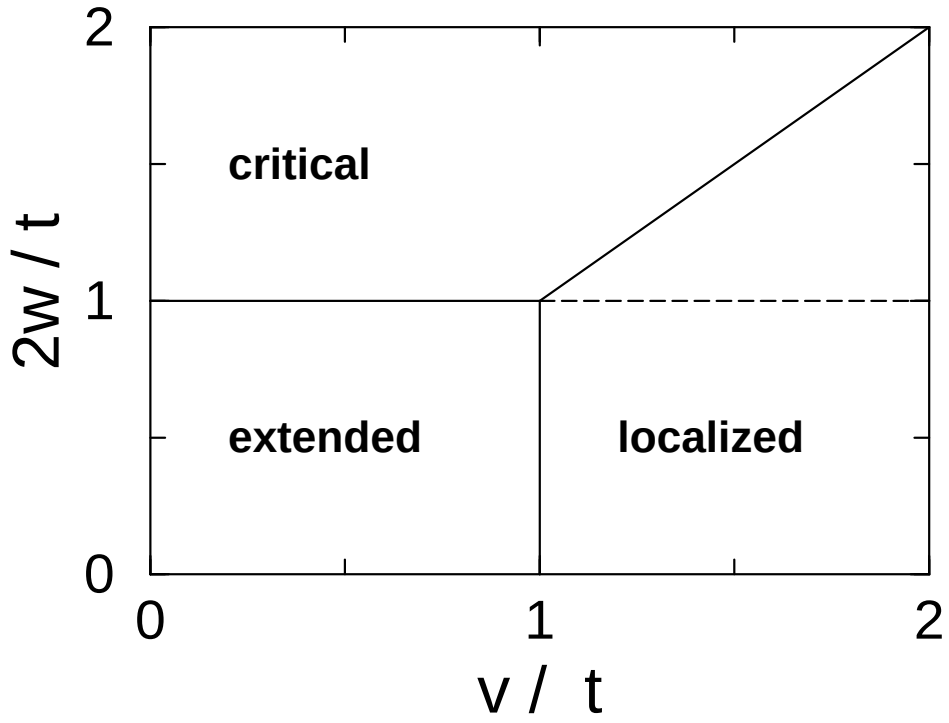

Figure A.1: Phase diagram for the modified Harper model which emerges when the constant hopping integrals $t/2$ are replaced by the site-dependent hopping integrals (A.3). The inverse fall-off length λ of exponentially localised states is given by equation (A.11) below the dashed line, and by equation (A.12) above.

phase, if both $2w/t < 1$ and $v/t < 1$. The system becomes an insulator with exponentially localised states when $2w/t < 1$ and $v/t > 1$; the inverse localisation length is then given by

$$\lambda = \ln\left(\frac{v + \sqrt{v^2 - 4w^2}}{t + \sqrt{t^2 - 4w^2}}\right) \ . \tag{A.11}$$

If $2w/t > 1$ and $2w/t < v/t$ the system remains an insulator, but the inverse fall-off distance becomes

$$\lambda = \ln\left(\frac{v + \sqrt{v^2 - 4w^2}}{2w}\right) \ . \tag{A.12}$$

Note that λ is continuous if one crosses the line $2w/t = 1$ while fixing the other parameter v/t at a constant value greater than unity. But, as shown in figure A.2, the dependency of λ on $2w/t$ exhibits a kink at $2w/t = 1$, since λ approaches that line from below with diverging slope. In the remaining region of parameter space, where $2w/t > 1$ and $2w/t > v/t$,

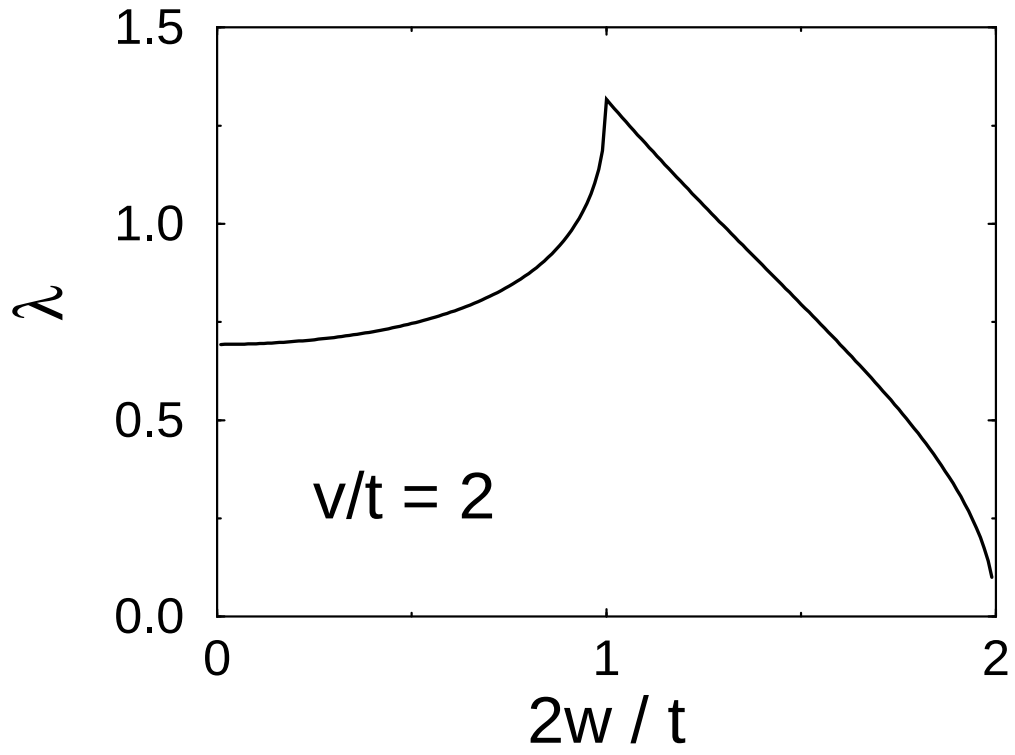

Figure A.2: Dependency of the inverse localisation length λ on the parameter $2w/t$, for $v/t = 2$. Note the kink at $2w/t = 1$, where the system crosses the dashed line drawn in figure A.1.

we have the identity $\widetilde{G} = G$: here the states are critical, which means that they cannot be characterised by a single localisation length [77, 93].

In order to illustrate the differences between the three types of states, and to check the results (A.11) and (A.12), we solve the time-dependent Schrödinger equation

$$i\hbar\partial_\tau \psi_\ell(\tau) = \sum_\ell \left\{ \widehat{t}_{\ell,\ell+1}\psi_{\ell+1}(\tau) + \widehat{t}_{\ell,\ell-1}\psi_{\ell-1}(\tau) + v\cos(2\pi\alpha\ell + \beta)\psi_\ell(\tau) \right\}$$

with the initial condition $\psi_\ell(0) = \delta_{\ell,0}$ on a lattice consisting of 10001 sites (extending from $\ell_{\min} = -5000$ to $\ell_{\max} = +5000$), with $\alpha = (\sqrt{5}+1)/2$ and $\beta = 0$. Figure A.3 shows the evolution of the standard deviation

$$\sigma(\tau) = \left\{ \sum_\ell \ell^2 |\psi_\ell(\tau)|^2 - \left(\sum_\ell \ell |\psi_\ell(\tau)|^2 \right)^2 \right\}^{1/2}$$

for three parameter combinations $(v/t,\ 2w/t)$. The parameters $(1.2,\ 0.8)$ belong to the localisation regime, so that $\sigma(\tau)$ remains bounded. For $(1.2,\ 1.4)$ we are in the regime of critical

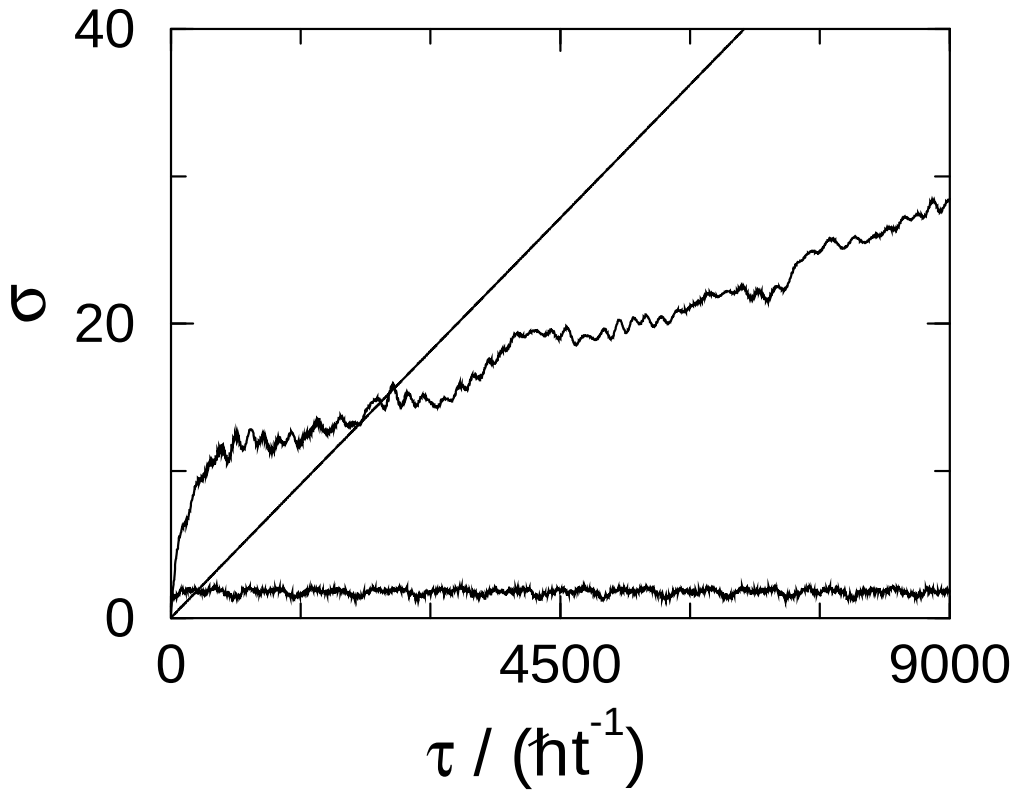

Figure A.3: Time evolution of the standard deviation σ for site-occupation probabilities of the modified Harper model with $\alpha = (\sqrt{5}+1)/2$ and $\beta = 0$; the initial condition is $\psi_\ell(0) = \delta_{\ell,0}$ for each run. For $(v/t,\ 2w/t) = (1.2,\ 0.8)$ the wave function stays localised, for $(1.2,\ 1.4)$ we find anomalous diffusion, and for $(0.6,\ 0.8)$ there is ballistic spreading with σ increasing proportional to τ. In this latter case the ordinates of the data have been scaled by a factor of $1/25$.

states, hence we encounter anomalous diffusion [42, 70, 95]. For $(0.6,\ 0.8)$ taken from the metallic regime we find the usual ballistic spreading, with σ increasing strictly proportional to τ. In this latter case the ordinates of the numerical data displayed in figure A.3 have been scaled by a factor of $1/25$.

Figure A.4 shows the corresponding site-occupation probabilities $|\psi_\ell(\tau_0)|^2$ at the moment $\tau_0 = 9000\,\hbar t^{-1}$. For the parameters belonging to the metallic phase the wave function has spread more or less homogeneously, for critical parameters the distribution over the sites remotely resembles a Gaussian, and for insulator phase-parameters there is exponential localisation, to a stunning degree of perfection. In this case we can estimate the inverse localisation length λ directly from the plot: assuming that all eigenstates of equation A.1 are exponentially localised, $f_\ell^{(j)} \propto \exp(-\lambda|\ell - j|)$, a stationary phase approximation applied to

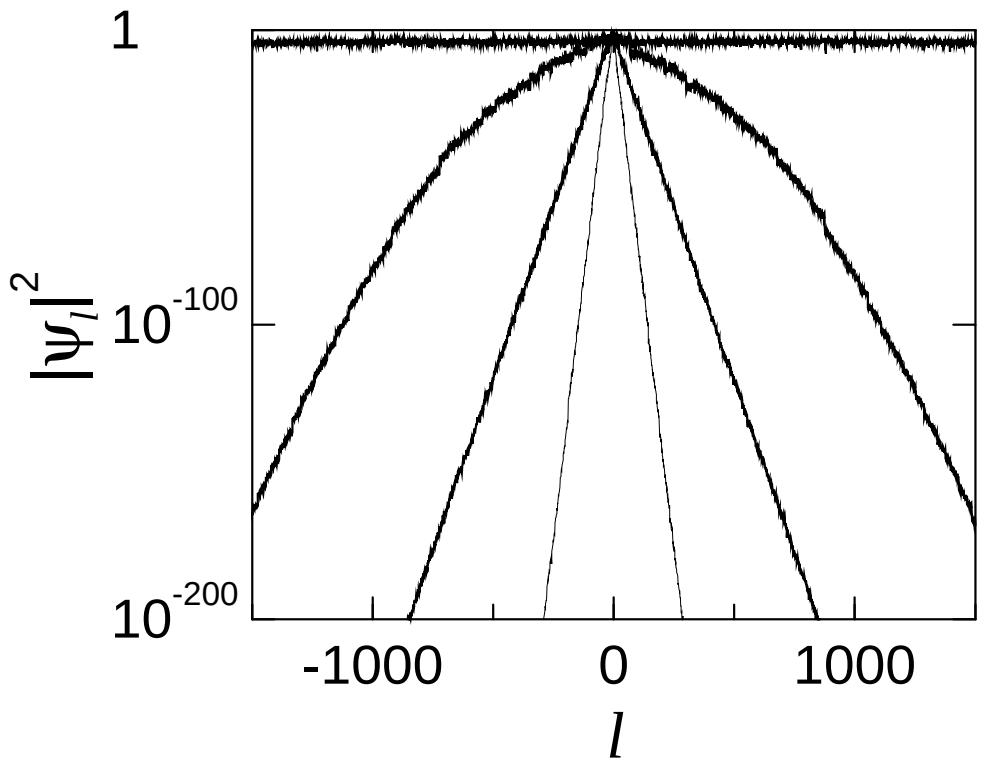

Figure A.4: Site-occupation probabilities for the modified Harper model at $\tau_0 = 9000\,\hbar t^{-1}$, cf. figure A.3. Parameters $(v/t,\ 2w/t)$ are as in figure A.3 for the heavy lines; the thin line corresponds to $(1.6,\ 1.2)$.

the time evolution operator gives

$$|\psi_\ell(\tau_0)|^2 \quad \propto \quad e^{-2\lambda|\ell|}$$

for large τ_0. In this way we find $2\lambda \approx 0.539$ for the parameters $(1.2,\ 0.8)$, compared to $2\lambda = 0.53855$ as predicted by equation (A.11). The wave function depicted by the thin line in figure A.4 belongs to $(1.6,\ 1.2)$; here we find $2\lambda \approx 1.59$ from the numerical data and $2\lambda = 1.5907$ from equation (A.12). The perfect agreement in these and other examples that we have considered confirms our line of reasoning.

To summarise, we have investigated the phase diagram of a modified Harper model with hopping integrals that are locked to the varying on-site energies. Since the modulation of the hopping integrals does not destroy the self-duality of the original Harper model, a small modulation amplitude cannot affect the metal-insulator transition, so that this transition might become visible in experiments. A particular feature of the modified model is an extended region in its two-dimensional parameter space corresponding to critical states. It should thus be an attractive candidate for the further study of spectral and dynamical properties of quasiperiodic systems.

Appendix B Numerical implementation of scheme I

The iterative scheme for constructing the superadiabatic bases (4.7) for N-level systems hinges on the solution of the recursion relations (4.10) and (4.11) for the coefficients $a_{jk}^{(m)}$. Utilising

$$\langle u_k^{(0)}|\partial_\tau|u_l^{(0)}\rangle = \frac{\langle u_k^{(0)}|\partial_\tau H^{(0)}|u_l^{(0)}\rangle}{E_l^{(0)} - E_k^{(0)}}$$

for $k \neq l$, and abbreviating $E_l^{(0)} - E_k^{(0)} \equiv \Delta E_{lk}$, we write the first of these equations in the form

$$a_{jk}^{(m)} = \frac{-i}{\Delta E_{jk}} \left\{ \partial_\tau a_{jk}^{(m-1)} + \sum_{\substack{l=1 \\ l\neq k}}^{N} a_{jl}^{(m-1)} \frac{\langle u_k^{(0)}|\partial_\tau H^{(0)}|u_l^{(0)}\rangle}{\Delta E_{lk}} \right\} . \tag{B.1}$$

Differentiating n times, one gets

$$\begin{aligned} \partial_\tau^n a_{jk}^{(m)} = -i \sum_{l_1=0}^{n} \binom{n}{l_1} \left(\partial_\tau^{l_1} \frac{1}{\Delta E_{jk}}\right) \Bigg[& \partial_\tau^{n+1-l_1} a_{jk}^{(m-1)} \\ & + \sum_{\substack{l=1 \\ l\neq k}}^{N} \sum_{l_2=0}^{n-l_1} \binom{n-l_1}{l_2} \left(\partial_\tau^{n-l_1-l_2} a_{jl}^{(m-1)}\right) \left(\partial_\tau^{l_2} \frac{\langle u_k^{(0)}|\partial_\tau H^{(0)}|u_l^{(0)}\rangle}{\Delta E_{lk}}\right) \Bigg] . \end{aligned}$$

The further processing of this equation necessitates to compute the derivatives

$$\begin{aligned} \partial_\tau^n \frac{1}{\Delta E_{jk}} = - \frac{1}{(\Delta E_{jk})^2} \Bigg[& \partial_\tau^n \Delta E_{jk} + \sum_{l_1=1}^{n-1} \binom{n-1}{l_1} \left(\partial_\tau^{n-l_1} \frac{1}{\Delta E_{jk}}\right) \\ & \times \sum_{l_2=0}^{l_1} \binom{l_1}{l_2} \left(\partial_\tau^{l_2} \Delta E_{jk}\right) \left(\partial_\tau^{l_1-l_2} \Delta E_{jk}\right) \Bigg] , \end{aligned}$$

which, in turn, demand the evaluation of

$$\partial_\tau^n E_j^{(0)} = \sum_{l_1=0}^{n-1} \binom{n-1}{l_1} \sum_{l_2=0}^{n-1-l_1} \binom{n-1-l_1}{l_2} \langle \partial_\tau^{l_1} u_j^{(0)}|\partial_\tau^{n-l_1-l_2} H^{(0)}|\partial^{l_2} u_j^{(0)}\rangle .$$

Employing

$$|\partial_\tau^n u_j^{(0)}\rangle = \sum_{\substack{k=1 \\ k\neq j}}^{N} \sum_{l=0}^{n-1} \binom{n-1}{l} |\partial_\tau^l u_k^{(0)}\rangle \left(\partial_\tau^{n-1-l} \frac{\langle u_k^{(0)}|\partial_\tau H^{(0)}|u_j^{(0)}\rangle}{\Delta E_{jk}}\right) ,$$

we are left with the derivatives

$$\partial_\tau^n \frac{\langle u_k^{(0)}|\partial_\tau H^{(0)}|u_j^{(0)}\rangle}{\Delta E_{jk}} = \sum_{l_1=0}^{n} \binom{n}{l_1} \sum_{l_2=0}^{n-l_1} \binom{n-l_1}{l_2} \sum_{l_3=0}^{n-l_1-l_2} \binom{n-l_1-l_2}{l_3} \times \langle \partial_\tau^{l_1} u_k^{(0)}|\partial_\tau^{l_2+1} H^{(0)}|\partial_\tau^{l_3} u_j^{(0)}\rangle \left(\partial_\tau^{n-l_1-l_2-l_3} \frac{1}{\Delta E_{jk}}\right) .$$

Combining these equations gives an algorithm that is well suited for determining the coefficients $a_{jk}^{(m)}$ recursively, starting from the initial conditions (4.9). It requires the instantaneous eigenvalues $E_j^{(0)}$ and eigenstates $|u_j^{(0)}\rangle$ as input, and reduces the actual calculation, apart from adding the various sums, to the computation of the matrix elements $\langle u_j^{(0)}|\partial_\tau^n H^{(0)}|u_k^{(0)}\rangle$. When employing this algorithm for stepping from the set of coefficients $a_{jk}^{(l)}$ (with $l = 1, \ldots, m-1$) to the coefficients $a_{jk}^{(m)}$, the task that remains after having solved equation (B.1) is the solution of the first-order differential equation (4.11) for the diagonal coefficients $a_{jj}^{(m)}$. This task is simplified by the fact that the knowledge of the higher derivatives $\partial_\tau^n a_{jj}^{(m)}$ can be exploited for the numerical integration.

Appendix C Prefactor renormalisation in the iterative scheme

In this appendix we sketch how the incorrect prefactor $\pi/3$ obtained in the perturbative calculation of the final Landau-Zener transition amplitude (4.22) is changed towards unity by the first step of the iterative scheme I. We start from the pole approximation to the nonadiabatic coupling,

$$\begin{aligned}\frac{\gamma^{(0)}(w)}{E^{(0)}(w)} &= \frac{i}{3(w-w_c)} - \frac{i}{3(w+w_c)} \\ &= \frac{2iw_c}{3(w^2-w_c^2)}\end{aligned}$$

with $w_c = -i\pi/2$. Inserting this into the iteration equation (4.15), we end up with

$$\frac{\gamma^{(1)}(w)}{E^{(0)}(w)} = \frac{12i\varepsilon w|w_c|}{9(w^2+|w_c|^2)^2 + 4\varepsilon^2|w_c|^2} \; .$$

The poles of this expression are located at

$$\begin{aligned}w &= \pm i|w_c|\sqrt{1 \pm \frac{2i\varepsilon}{3|w_c|}} \\ &\approx \pm i|w_c| \pm \frac{\varepsilon}{3} \; . \end{aligned} \tag{C.1}$$

We now have to evaluate the integral (4.19) for $\tau = \infty$ and $n = 1$, so that the argument of the exponential is $-(2i/\varepsilon)\int_0^\infty \mathrm{d}\tau' E^{(1)}(\tau')$, rather than $-iw/\varepsilon$, with w as given by equation (4.20). However, according to equation (4.14) the iterated eigenvalue $E^{(1)}$ differs from $E^{(0)}$ merely by an amount of order ε^2, so that the difference $(E^{(1)} - E^{(0)})/\varepsilon$ still vanishes for $\varepsilon \to 0$. Hence, we may for small ε approximate $E^{(1)}$ by $E^{(0)}$ at least in the exponential, and then change to the variable w. Closing the contour of integration in the lower complex w-plane, the residue theorem gives

$$\begin{aligned}c_{12}^{(1)}(\infty) &= \frac{\pi}{2i}\left[\exp\left(-\frac{|w_c|}{\varepsilon}\sqrt{1-\frac{2i\varepsilon}{3|w_c|}}\right) - \exp\left(-\frac{|w_c|}{\varepsilon}\sqrt{1+\frac{2i\varepsilon}{3|w_c|}}\right)\right] \\ &\approx \pi\sin(1/3)\exp\left(-\frac{|w_c|}{\varepsilon}\right)\end{aligned}$$

Thus, the prefactor reduces from $\pi/3$ to $\pi\sin(1/3)$. We emphasise that the origin for this reduction lies in the fact that the poles (C.1) are shifted by amounts of order ε with respect to $\pm w_c$. This feature is not captured when approximating all $E^{(n)}$ by $E^{(0)}$, as done in the derivation of equation (4.26).

Literaturverzeichnis

[1] M. Abramowitz and I.A. Stegun (eds.), *Handbook of Mathematical Functions* (Dover, New York, 1972) (The Mathieu equation is treated in chapter 20. The asymptotic series for the argument of the gamma function is given in equation (6.1.44)).

[2] V. M. Akulin and N. V. Karlov, *Intense Resonant Interactions in Quantum Electronics* (Springer, Berlin, 1992).

[3] P.W. Anderson, *Phys. Rev.* **109**, 1492 (1958).

[4] B.P. Anderson, T.L. Gustavson, and M.A. Kasevich, *Phys. Rev. A* **53**, R3727 (1996).

[5] S. Aubry and G. André, in *Proceedings of the Israel Physical Society*, edited by C.G. Kuper (Hilger, Bristol, 1979), Vol. 3, p. 133.

[6] P.J. Bardroff, I. Bialynicki-Birula, D.S. Krähmer, G. Kurizki, E. Mayr, P. Stifter, and W.P. Schleich, *Phys. Rev. Lett.* **74**, 3959 (1995).

[7] M. Ben Dahan, E. Peik, J. Reichel, Y. Castin, and C. Salomon, *Phys. Rev. Lett.* **76**, 4508 (1996).

[8] M. V. Berry, *Proc. R. Soc. Lond. A* **392**, 45 (1984).

[9] M.V. Berry, *Proc. R. Soc. Lond. A* **414**, 31 (1987).

[10] M.V. Berry, *Proc. R. Soc. Lond. A* **429**, 61 (1990).

[11] M.V. Berry and R. Lim, *J. Phys. A* **26**, 4737 (1993).

[12] P. M. Blekher, H. R. Jauslin, and J. L. Lebowitz, *J. Stat. Phys.* **68**, 271 (1992).

[13] M. Born and V.A. Fock, *Z. Phys.* **51**, 165 (1928).

[14] H. P. Breuer and M. Holthaus, *Z. Phys. D* **11**, 1 (1989).

[15] H. P. Breuer and M. Holthaus, *Phys. Lett. A* **140**, 507 (1989).

[16] H.P. Breuer and M. Holthaus, *Ann. Phys. (N.Y.)* **211**, (1991) 249.

[17] B.H. Bransden and C.J. Joachain, *Introduction to Quantum Mechanics* (Longman Scientific & Technical, Harlow, 1989).

[18] M. Büttiker, *J. Phys.: Condens. Matter* **5**, 9361 (1993).

[19] C.E. Carroll and F.T. Hioe, *Phys. Rev. A* **42**, 1522 (1990).

[20] D.S.F. Crothers, *Adv. Phys.* **20**, 405 (1971).

[21] S.-I Chu, *Adv. Chem. Phys.* **73**, 739 (1989).

[22] J.P. Davis and P. Pechukas, *J. Chem. Phys.* **64**, 3129 (1976).

[23] Yu N. Demkov, V. N. Ostrovskii, and E. A. Solov'ev, *Phys. Rev. A* **18**, 2089 (1978).

[24] R.B. Dingle, *Asymptotic Expansions: Their Derivation and Interpretation* (Academic Press, New York and London, 1973).

[25] K. Drese and M. Holthaus, *Phys. Rev. Lett.* **78**, 2932 (1997).

[26] K. Drese and M. Holthaus, *Chem. Phys.* **217**, 201 (1997).

[27] K. Drese and M. Holthaus, *Eur. Phys. J. D*, in press (1998).

[28] D.H. Dunlap and V.M. Kenkre, *Phys. Rev. B* **34**, 3625 (1986).

[29] A.M. Dykhne, *J. Exptl. Theoret. Phys. (U.S.S.R.)* **41**, 1324 (1961) [*Sov. Phys. JETP* **14**, 941 (1962)].

[30] M. Elk, *Phys. Rev. A* **52**, 4017 (1995).

[31] See, e.g., R.R. Freeman, P.H. Bucksbaum, W.E. Cooke, G. Gibson, T.J. McIlrath, and L.D. van Woerkom in reference [35], p. 43.

[32] H. Fukuyama, R.A. Bari and H.C. Fogedby, *Phys. Rev. B* **8**, 5579 (1973).

[33] L. M. Garrido and F. J. Sancho, *Physica* **28**, 553 (1962).

[34] B.M. Garraway and K.-A. Suominen, *Rep. Prog. Phys.* **58**, 365 (1995).

[35] A collection of review articles can be found in: *Atoms in Intense Laser Fields, Adv. At. Mol. Opt. Phys., Supplement 1*, ed. M. Gavrila (Academic Press, Boston, 1992).

[36] See, e.g., M. Gavrila in reference [35], p. 435.

[37] P.L. Gould, G.A. Ruff, and D.E. Pritchard, *Phys. Rev. Lett.* **56**, 827 (1986).

[38] I.S. Gradshteyn and I.M. Ryzhik, *Table of Integrals, Series, and Products* (Academic Press, San Diego, 1980), equations (1.395.1) and (1.395.2).

[39] R. Graham, in: *Chaos and Quantum Chaos, Lecture Notes in Physics* **411**, ed. W.D. Heiss (Springer, Berlin, 1992) p. 273.

[40] R. Graham, M. Schlautmann, and P. Zoller, *Phys. Rev. A* **45**, R19 (1992).

[41] R. Graham and S. Miyazaki, *Phys. Rev. A* **53**, 2683 (1996).

[42] I. Guarneri and G. Mantica, *Phys. Rev. Lett.* **73**, 3379 (1994).

[43] S. Guérin, *Phys. Rev. A* **56**, 1458 (1997).

[44] S. Guérin and H. R. Jauslin, *Eur. Phys. J. D*, in press (1998).

[45] P.S.S. Guimarães, B.J. Keay, J.P. Kaminski, S.J. Allen Jr., P.F. Hopkins, A.C. Gossard, L.T. Florez, and J.P. Harbison, *Phys. Rev. Lett.* **70**, 3792 (1993).

[46] J.H. Han, D.J. Thouless, H. Hiramoto, and M. Kohmoto, *Phys. Rev. B* **16**, 11365 (1994).

[47] From the mathematical viewpoint, this renormalization of the hopping integrals resembles the renormalization of atomic g-factors by oscillating magnetic fields as studied by S. Haroche, C. Cohen-Tannoudji, C. Audouin, and J.P.Schermann, *Phys. Rev. Lett.* **24**, 861 (1970).

[48] P.G. Harper, *Proc. Phys. Soc. Lond. A* **68**, 874 (1955).

[49] D.C. Herbert and R. Jones, *J. Phys. C* **4**, 1145 (1971).

[50] T.-S. Ho and S.-I Chu, *J. Phys. B* **17**, 2101 (1984).

[51] D.R. Hofstadter, *Phys. Rev. B* **14**, 2239 (1976).

[52] M. Holthaus, *Phys. Rev. Lett.* **69**, 351 (1992).

[53] M. Holthaus, in: Proceedings of the 1993 Yukawa International Seminar "Quantum and Chaos: How Incompatible?", *Prog. Theor. Phys. (Suppl.)* **116**, 417 (1994).

[54] M. Holthaus, G.H. Ristow, and D.W. Hone, *Phys. Rev. Lett.* **75**, 3914 (1995).

[55] M. Holthaus, G.H. Ristow, and D.W. Hone, *Europhys. Lett.* **32**, 241 (1995).

[56] M. Holthaus and D.W. Hone, *Phil Mag. B* **74**, 105 (1996).

[57] D.W. Hone and M. Holthaus, *Phys. Rev. B* **48**, 15123 (1993)

[58] D. W. Hone, R. Ketzmerick, and W. Kohn, *Phys. Rev. A* **56**, 4045 (1997).

[59] J.S. Howland, *Math. Ann.* **207**, 315 (1974).

[60] J. S. Howland, *Ind. Uni. Math. J.* **28**, 471 (1979).

[61] J.-T. Hwang and P. Pechukas, *J. Chem. Phys.* **67**, 4640 (1977).

[62] A.A. Ignatov, E. Schomburg, K.F. Renk, W. Schatz, J.F. Palmier, and F. Mollot, *Ann. Physik* **3**, 137 (1994).

[63] A.A. Ignatov, E. Schomburg, J. Grenzer, K.F. Renk, and E.P. Dodin, *Z. Phys. B* **98**, 187 (1995).

[64] S.Ya. Jitomirskaya and Y. Last, *Phys. Rev. Lett.* **76**, 1765 (1996).

[65] A. Joye, *J. Phys. A* **26**, 6517 (1993).

[66] A. Joye and C.-E. Pfister, *J. Math. Phys.* **34**, 454 (1993).

[67] T. Kato, *J. Phys. Soc. Japan* **5**, 435 (1950).

[68] A.P. Kazantsev, G.I. Surdutovich, V.P. Yakovlev, and D.O. Chudesnikov, *Opt. Commun.* **52**, 311 (1985).

[69] See, e.g., A.P. Kazantsev, G.I. Surdutovich, and V.P. Yakovlev, *Mechanical Action of Light on Atoms* (World Scientific, Singapore, 1990).

[70] R. Ketzmerick, G. Petschel, and T. Geisel, *Phys. Rev. Lett.* **69**, 695 (1992).

[71] B. Kramer and A. MacKinnon *Rep. Prog. Phys.* **56**, 1469 (1993).

[72] B.J. Keay, S.J. Allen, J. Galán, J.P. Kaminsky, K.L. Campman, A.C. Gossard, U. Bhattacharya, and M.J.W. Rodwell, *Phys. Rev. Lett.* **75**, 4098 (1995).

[73] B.J. Keay, S. Zeuner, S.J. Allen, K.D. Maranowski, A.C. Gossard, U. Bhattacharya, and M.J.W. Rodwell, *Phys. Rev. Lett.* **75**, 4102 (1995).

[74] J.A. Ketoja, I.I. Satija, and J.C. Chaves, *Phys. Rev. B* **52**, 3026 (1995).

[75] P.M. Koch and K.A.H. van Leeuwen, *Phys. Rep.* **255**, 289 (1995).

[76] P.M. Koch, *Physica D* **83**, 178 (1995).

[77] M. Kohmoto, L.P. Kadanoff, and C. Tang, *Phys. Rev. Lett.* **50**, 1870 (1983).

[78] A. Kuhn, S. Steuerwald, and K. Bergmann, *Eur. Phys. J. D* **1**, 57 (1998).

[79] T.A. Laine and S. Stenholm, *Phys. Rev. A* **53**, 2501 (1996).

[80] L. D. Landau, *Phys. Z. Sowjetunion* **2**, 46 (1932).

[81] R. Lim and M.V. Berry, *J. Phys. A* **24**, 3255 (1991).

[82] A.J. Lichtenberg and M.A. Lieberman, *Regular and Stochastic Motion* (Springer, New York, 1983).

[83] A. Lindner and H. Freese, *J. Phys. A* **27**, 5565 (1994).

[84] K.A. Mäder, L.W. Wang, and A. Zunger, *Phys. Rev. Lett.* **74**, 2555 (1995).

[85] J. Manz and L. Wöste (eds.), *Femtosecond Chemistry* (Verlag Chemie, Weinheim, 1995).

[86] T. Meier, G. von Plessen, P. Thomas, and S.W. Koch, *Phys. Rev. Lett.* **73**, 902 (1994).

[87] T. Meier, G. von Plessen, P. Thomas, and S.W. Koch, *Phys. Rev. B* **51**, 14490 (1995).

[88] T. Meier, F. Rossi, P. Thomas, and S.W. Koch, *Phys. Rev. Lett.* **75**, 2558 (1995).

[89] A. Messiah, *Quantum Mechanics*, vol. 2 (North-Holland, Amsterdam, 1962).

[90] N.F. Mott and W.D. Twose, *Adv. Phys.* **10**, 107 (1961).

[91] F.L. Moore, J.C. Robinson, C. Bharucha, P.E. Williams, and M.G. Raizen, *Phys. Rev. Lett.* **73**, 2974 (1994).

[92] Q. Niu, X.-G. Zhao, G.A. Georgakis, and M.G. Raizen, *Phys. Rev. Lett.* **76**, 4504 (1996).

[93] S. Ostlund, R. Pandit, D. Rand, H.J. Schellnhuber, and E.D. Siggia, *Phys. Rev. Lett.* **50**, 1873 (1983).

[94] U. Peskin and N. Moiseyev, *J. Chem. Phys.* **99**, 4590 (1993).

[95] F. Piéchon, *Phys. Rev. Lett.* **76**, 4372 (1996).

[96] G. Raithel, G. Birkl, A. Kastberg, W.D. Philips, and S.L. Rolston, *Phys. Rev. Lett.* **78**, 630 (1997).

[97] S. Raghavan, V.M. Kemkre, D.H. Dunlap, A.R. Bishop, and M.I. Salkola, *Phys. Rev. A* **54**, R1781 (1996).

[98] V.I. Ritus *Zh. Eksp. Theor. Fiz.* **51**, 1544 (1966) [*Sov. Phys. JETP* **24**, 1041 (1967)].

[99] J.C. Robinson, C. Bharucha, F.L. Moore, R. Jahnke, G.A. Georgakis, Q. Niu, and M.G. Raizen, *Phys. Rev. Lett.* **74**, 3963 (1995).

[100] J.C. Robinson, C.F. Bharucha, K.W. Madison, F.L. Moore, B. Sundaram, S.R. Wilkinson, and M.G. Raizen, *Phys. Rev. Lett.* **76**, 3304 (1996).

[101] J. Rotvig, A.P. Jauho, and H. Smith, *Phys. Rev. Lett.* **74**, 1831 (1995).

[102] A. Rüdinger and F. Piéchon, *J. Phys. A* **30**, 117 (1997).

[103] H. Sambe, *Phys. Rev. A* **7**, 2203 (1973).

[104] F. J. Sancho, *Proc. Phys. Soc.* **89**, 1 (1966).

[105] S. Schiemann, A. Kuhn, S. Steuerwald, and K. Bergmann, *Phys. Rev. Lett.* **71**, 3637 (1993).

[106] J.H. Shirley, *Phys. Rev.* **138** B979 (1965).

[107] N. Hong Shon and H.N. Nazareno, *J. Phys.: Condens. Matter* **4**, L611 (1992).

[108] B.W. Shore, K. Bergmann, and J. Oreg, *Z. Phys. D* **23**, 33 (1992).

[109] B. Simon, *Adv. Appl. Math.* **3**, 463 (1982).

[110] B. Simon, *Phys. Rev. Lett.* **51**, 2167 (1983).

[111] J.B. Sokoloff, *Phys. Rep.* **126**, 189 (1985).

[112] D.J. Thouless, *J. Phys. C* **5**, 77 (1972).

[113] D.J. Thouless, *Phys. Rep.* **13**, 93 (1974).

[114] D.J. Thouless, in: *Ill-Condensed Matter: Les Houches Session XXXI*, ed. R. Balian, R. Maynard, and G. Toulouse (Amsterdam; North Holland , 1979)

[115] K. Unterrainer, B.J. Keay, M.C. Wanke, S.J. Allen, D. Leonard, G. Medeiros-Ribeiro, U. Bhattacharya, and M.J.W. Rodwell, *Phys. Rev. Lett.* **76**, 2973 (1996).

[116] N.V. Vitanov and S. Stenholm, *Optics Commun.* **127**, 215 (1996).

[117] N.V. Vitanov and S. Stenholm, *Optics Commun.* **135**, 394 (1997).

[118] N.V. Vitanov and S. Stenholm, *Phys. Rev. A* **55**, 648 (1997).

[119] R. B. Walker and R. K. Preston, *J. Chem. Phys.* **67**, 2017 (1977).

[120] S.R. Wilkinson, C.F. Bharucha, K.W. Madison, Q. Niu, and M.G. Raizen, *Phys. Rev. Lett.* **76**, 4512 (1996).

[121] R.H. Young and W.J. Deal, *J. Math. Phys.* **11**, 3298 (1970).

[122] J. Zak, *Phys. Rev. Lett.* **71**, 2623 (1993).

[123] Ya. B. Zel'dovich, *Zh. Eksp. Theor. Fiz.* **51**, 1492 (1966) [*Sov. Phys. JETP* **24**, 1006 (1967)].

[124] C. Zener, *Proc. R. Soc. Lond. A* **137**, 696 (1932).

[125] C. Zener, *Proc. R. Soc. Lond. A* **145**, 523 (1934).

Danksagung

Es ist mir eine Freude und eine Pflicht, hier allen zu danken, die zum Entstehen dieser Arbeit direkt oder indirekt beigetragen haben.

Ein besonderer Dank geht an Priv.-Doz. Dr. Martin Holthaus, dessen Fähigkeit, auch komplizierteste physikalische Sachverhalte in kompakter und nicht nur für Spezialisten verständlicher Form darzustellen, Hilfe und Ansporn zugleich waren. Auch möchte ich ihm für die vielen fruchtbaren Diskussionen danken, die oft in einer klareren Darstellung des Sachverhaltes endeten. Mein Dank gilt einem ausgezeichneten und menschlich angenehmem Betreuer.

Auch möchte ich Prof. Dr. Siegfried Großmann für die Aufnahme in seine Arbeitsgruppe danken. Seine Art, Probleme anzugehen und Erkenntnisse darzustellen ist wohl einzigartig, nachahmenswert und sehr anregend, was sich nicht zuletzt in der ausgezeichneten Arbeitsguppenatmosphäre widerspiegelt.

Jedem einzelnen Arbeitsgruppenmitglied habe ich zu danken. Jedes hat auf seine eigene Weise durch physikalische Diskussionen oder Hilfestellungen bei Computerfragen zum Gelingen dieser Arbeit beigetragen.

Ganz besonders habe ich auch meiner „Physiker-Braut“ Sanda zu danken, die die Höhen und Tiefen dieser Arbeit miterlebt und mitgetragen und in Zweifelsfällen meinen Blick nach vorne gerichtet hat.